Министерство науки и высшего образования Российской Федерации
Федеральное государственное автономное образовательное учреждение
высшего образования «Уральский федеральный университет
имени первого Президента России Б. Н. Ельцина »

Химико -Технологический Институт
Кафедра «Технологии органического синтеза»

На правах рукописи

Абуелсоад Асмаа Мансур Ахмед

НОВЫЕ АДСОРБЕНТЫ НА ОСНОВЕ ХИТОЗАНА И ГАЛЛУАЗИТНЫХ НАНОТРУБЧАТЫХ МАТЕРИАЛОВ ДЛЯ СОРБЦИИ ИОНОВ Cu (II) И Zn (II)

Специальность 1.4.4. Физическая химия

ДИССЕРТАЦИЯ
на соискание ученой степени
кандидата химических наук

Научный руководитель:
кандидат химических наук, доцент
Елена Германовна Ковалева

Екатеринбург – 2023

Ministry of Science and Higher Education of the Russian Federation
Federal State Autonomous Educational Institution of Higher Education «Ural Federal University named after the first President of Russian federation B. N. Yeltsin»

Chemical Technology Institute

Department «Technology of organic synthesis»

As a manuscript

Abu El-Soad Asmaa Mansour Ahmed

NOVEL ADSORBENTS BASED ON CHITOSAN AND HALLOYSITE NANOTUBES FOR SORPTION OF Cu (II) AND Zn (II) METAL IONS

Specialty 1.4.4. Physical chemistry

dissertation for a degree

candidate of chemical sciences

Scientific Supervisor:

candidate of chemical sciences, associate professor

Elena Germanovna Kovaleva

Yekaterinburg – 2023

Table of Contents

INTRODUCTION

Relevance of the research topic

At present, environmental, and ecological problems take a place considerable in the world and represent one of the major challenges because they attack humans, their health, and our environment. The quality of water that is drinkable or intended for human consumption, irrigation or simply rejected in nature has become a major problem. In addition, the field of metals has become an important trade all over the world after weapons and oil are the world's third largest source of financing. To date, several countries cannot use this source of energy, manage it, and make it useful because of problems of a technical, financial or prohibition nature linked to global laws and regulations. international agreements in this area. Due to the importance of the metal industry and the pollution created by this manufacture, metals are classified into two categories according to their nature and importance. The first class includes those that are toxic to humans and the environment and require treatment severe linked to specific standards; being the subject of this research; and the second category gathers those which are valuable and necessary for several fields of industry and considered as a raw material for several technologies. Both categories require processes of recovery whose interest differs according to the importance, the profitability, the use, the price, and the toxicity. Major technologies, with varying treatment efficiency, include filtration [1], coagulation [2], ion exchange [3], activated sludge, advanced oxidation processes [4], reverse osmosis [5] and bioremediation [6]. However, higher cost of these technologies restricts their utility in pollution control. Amongst available treatment options, adsorption is usually considered as cost-effective technique with quick efficiency against wide range of pollutants, simple design, ease in operation and lower formation of toxic by-products [7]. Successful adsorption of water pollutants also offers their recovery which is especially sought for water nutrients [8, 9]. Additionally, it should be noted that regeneration of adsorbents for subsequent treatment cycles is gaining importance which would further minimize the treatment cost. Large amount of research has been devoted investigating adsorption materials such as iron minerals [8], biosorbents [10], clay minerals [11], chitosan etc. The objective of this work is to produce new materials based on chitosan and halloysite nanotubes for the treatment of a series of metallic pollutants, namely: copper and zinc. Halloysite nanotubes is a natural inorganic adsorbent due to its unique structure, reactivity and its unique features such as morphology, chemical composition, structural arrangement of functional groups designed to achieve better contaminant adsorption. Halloysite is a natural nano-sized clay mineral with tubular structure

and is a member of 1:1 kaolin group of clay minerals. Its structural formula can be written as $Al_2(OH)_4Si_2O_5 \cdot nH_2O$. Each layer of halloysite is composed of tetrahedral (Si-O) and octahedral (Al-OH) sheets and one alumina octahedron sheet, identical to those in kaolinite [12]. Compared to kaolinite, halloysite has a generally higher, but variable, water content in the interlayer spaces [13]. Owing to the smaller particle size, and higher surface area, clay minerals have shown promising adsorption potential as evident from review articles related to various clays [11, 14-17]. However, these review articles focused on other clay minerals such as bentonite, illite, montmorillonite, kaolinite etc., while ignoring the halloysite. As a matter of fact, use of halloysite for environmental remediation gained attention only during the last decade. As noted correctly by Yuan et al.[18], this previous lack of interest in halloysite was probably caused by its chemical similarity to kaolinite which is considered as a poorer adsorbent than other clay minerals having high cation exchange capacity such as montmorillonite. Better knowledge of the structure and reactivity of halloysite gradually highlighted its unique features to achieve better contaminant adsorption. For example, nano-sized tubular halloysite is characterized by porous structure and much higher surface area as compared to the non-porous micron-sized kaolinite [18]. Moreover, adsorption potential is mainly dictated by mineral structure and properties which can be easily tuned in halloysite through internal or external surface modifications. Thus, modified halloysite-based adsorbents could suppose a broad field of research, including different alternatives to be developed. On the other hand, chitosan is a biosorbent with expected high potential for the adsorption of metal ions due to its high content of amino and hydroxyl functional groups and its outstanding biological properties like biodegradability, biocompatibility, and antibacterial activity. Chitosan is usually less crystalline than chitin, which presumably makes chitosan more accessible to reagents and consequently more soluble. Most of aqueous acids dissolve chitosan. The protonation of amino groups by acids along the chitosan chain creates a multitude of cationic sites which increases its solubility by increasing the polarity. This unique property expands the potential application of chitosan including its ability to adsorb different pollutants. Modification of chitosan via different physical and chemical methods have gained attention as a promising approach for removing organic (such as dyes and pharmaceuticals) and inorganic (such as metal/metal ions) pollutants from aqueous medium. The existence of $–NH_2$ and –OH groups in its molecular structure contributes mostly to probable adsorption interfaces between chitosan and adsorbate molecules [19-22]. Chitosan is advantageous for adsorption purposes [23-27] including environmental remediation [28-30] due to its cost effectiveness, simpler

polymerization and functionalization process, and good stability [31]. The objective of this work is to produce new materials based on chitosan and halloysite nanotubes for the treatment of some metallic pollutants, namely: copper, and zinc.

The degree of the topic elaboration

Chitosan is used as adsorbent for heavy metal removal because of the presence of amounts of reactive hydroxyl (-OH) and amino ($-NH_2$) groups. Nevertheless, chitosan has some defects (i.e., low acid stability, inadequate mechanical strength, and low thermal stability) which restrict its application. Thus, some researchers have applied physical and/or chemical modification to further enhance its adsorption properties for metal ions. Although chitosan has been modified by several methods to be used for the sorption of Cu (II) and Zn (II) as reported in literature [32-39]. However, a structural search done on SciFinder databases showed that aminocarboxymethylation of chitosan and its application for sorption of Cu (II) and Zn (II) ions are practically not studied and until recently were not mentioned. On the other hand, nano-sized tubular halloysite is characterized by porous structure and much higher surface area as compared to the non-porous micron-sized kaolinite. Moreover, adsorption potential is mainly dictated by mineral structure and properties which can be easily tuned in halloysite through internal or external surface modifications. For instance, Calcined halloysite and nanotubular dehydrated halloysite grafted with diethanolamine–$(CH_2CH_2OH)_2NH$ (DEA) or triethanolamine–$(CH_2CH_2OH)_3N$ (TEA) were used for sorption of Cu (II) and Zn (II) as mentioned in literature [40, 41]. However, a structural search done on SciFinder databases showed that polyethyleneimine functionalization of halloysite nanotubes chloride derivative and its application for sorption of Cu (II) and Zn (II) ions are practically not studied, and until recently were not mentioned.

Goals and objectives of the study

The aim of this work is to compare the activity of the new created aminocarboxymethyl chitosan and halloysite nanotubes polyethyleneimine derivatives towards the adsorption of Cu (II) and Zn (II) and to determine the kinetics and thermodynamic models that control the adsorption processes.

To achieve this goal, the following tasks were solved:

- Studying the processes which involve aminocarboxymethylation of chitosan to be used as a recyclable biomaterial for adsorption of Cu (II) and Zn (II).

- Studying the effect of solvent polarity, (HNT: silane) molar ratio, time, temperature and catalyst on the development of halloysite nanotubes surface using (3-substituted propyltrimethoxy) silane derivatives to increase their degree of grafting on halloysite nanotubes surface.
- Synthesis of halloysite nanotubes polyethyleneimine derivative and studying its activity towards the adsorption of Cu (II) and Zn (II) metal ions.
- Establishing the relationship between pH factor, metal ion concentration, time of contacting between the adsorbent and the metal ions, temperature, and the sorption capacity.
- Determining the kinetics and thermodynamic models which fit with the adsorption data.
- Studying the possibility of using the created adsorbents as recyclable materials in the near future.

Scientific novelty

For the first time,

1. The activity of aminocarboxymethyl chitosan derivative towards the adsorption of Cu (II) and Zn (II) has been studied.
2. The activity of halloysite nanotubes polyethyleneimine derivative towards the adsorption of Cu (II) and Zn (II) has been studied.
3. The influence of solvent polarity, (HNT: silane) molar ratio, time, temperature and catalyst on the improvement of functionalization degree has been studied.
4. The thermal properties, crystallographic structure and the surface charge of the newly modified aminocarboxymethyl chitosan and halloysite nanotubes polyethyleneimine derivatives have been studied.
5. The optimum conditions for the adsorption of Cu (II) and Zn (II) metal ions using the newly modified aminocarboxymethyl chitosan and halloysite nanotubes polyethyleneimine derivatives have been determined, e.g. pH factor, metal ion concentration, contact time and the temperature.
6. The kinetics and thermodynamic models that fit with the adsorption data generated from the adsorption of Cu (II) and Zn (II) using the newly modified aminocarboxymethyl chitosan and halloysite nanotubes polyethyleneimine derivatives have been studied.

Theoretical and practical significance of the work

Modification of chitosan by creation of reactive -COOH groups on its surface is of great importance as it enhance its adsorption properties for metal ions. Based on Hard-Soft acid base theory, soft acids react faster and form stronger bonds with soft bases whereas hard acids react

faster and form stronger bonds with hard bases, those functional groups are expected to create great electrostatic interactions with Cu (II) and Zn (II) metal ions. Approaches to graft silanes on halloysite nanotubes surface followed by further modification of the grafted halloysite to create a new adsorbent with greatest reactive binding sites. This helps to control and adjust adsorption properties of halloysite nanotubes mineral for a specific pollutant (either polar/a polar or positively/negatively charged). The grafted materials with covalently attached organic molecules are particularly important. This relates to their stability in aqueous solutions, which makes them promising candidates for water treatment. This work discusses the possibility of using the modified aminocarboxymethyl chitosan and halloysite nanotubes polyethyleneimine derivatives for the adsorption of Cu (II) and Zn (II) from their aqueous solutions.

Methodology and methods of scientific research

When the dissertation was performed, the work used the methods of classical physical chemistry. To characterize and establish the structure of chitosan modified adsorbents, halloysite functionalized materials, a complex of physical and physicochemical methods were applied including Fourier Transform Infrared Spectroscopy (FT-IR), elemental analysis, Scanning Electron Microscopy (SEM), Differential scanning calorimetry (DSC), X-ray Diffraction Analysis (XRD) and Nitrogen adsorption/desorption isotherms.

The reliability of the results

The reliability of the results is ensured using modern methods research and good reproducibility of experimental data. All new grafted halloysite nanotubes samples as well as the new modified chitosan adsorbents are characterized by a complex of modern methods of analysis and physicochemical characteristics were measured using many devices like elemental analyzer Perkin Elmer PE 2400, Compact FT-IR Spectrometer: ALPHA II, Scanning Electron Microscope a Carl Zeiss EVO LS 10 Device, X-ray diffractometer Panalytical X 'PERT PRO MRD equipped with an anticathode of Cu Kα., The nitrogen adsorption/desorption isotherms have been computed at 77K using Micrometrics Gemini VII 2390, Thermogravimetry coupled with differential scanning calorimetry (TG-DSC) has been implemented by NETZSCH STA449F3 thermal analyzer in the air at the heating rate of 10 K/min. The specific surface area of pristine HNTs and the grafted (HN-PEI) sorbent was estimated by the Brunauer-Emmett-Teller method based on adsorption/desorption data in the partial pressure (P/P_o) ranges from 0.01 to 0.99 and the pore size

distribution was performed based on Barrett-Joyner-Halenda method. Spectrophotometric measurements were carried out by using SHIMADZU model: UV-2600 240V IVDD.

Provisions for defense

1. Data on the development of halloysite nanotubes surface using (3- substituted propyltrimethoxy) silanes with different degree of grafting based on different factors like polarity of solvent, (HNT: silane) molar ratio, time, temperature and catalyst.
2. Studying the physicochemical properties of the modified aminocarboxymethyl chitosan (CTS-CAA) and the modified halloysite nanotubes polyethyleneimine (HN-PEI) derivatives based on DSC, XRD, FT-IR and SEM analysis.
3. Estimating the pH_{PZC} for (CTS-CAA) and (HN-PEI) adsorbents to determine the surface charge within the studied pH range.
4. Determination of the adsorption mechanism for Cu (II) and Zn (II) metal ions using the (CTS-CAA) and (HN-PEI) adsorbents.
5. Modeling of the sorption data using different kinetic models and determination of the best fitting model.
6. The recycling characteristics of (CTS-CAA) and (HN-PEI) based on adsorption/ desorption cycles.

The personal contribution of the author

The author compiled, regulate, and analyze literature data on the methods of modification and characterization of the adsorbents based on halloysite nanotubes and chitosan. The author was directly involved in planning and conducting experiments, discussing, and summarizing and concluding the results obtained, writing scientific papers.

Approbation of scientific results

Thesis's materials are presented at all-Russian and international conferences**:** Problems of theoretical and experimental chemistry, XXIX Russian Youth Scientific Conference with international participation dedicated to the 150th anniversary Periodic table of chemical elements (Yekaterinburg, 23-26 April 2019). Physics, Technologies. Innovation FTI-2019, VI International Youth Scientific Conference, dedicated to the 70th anniversary of the foundation Institute of Physics and Technology Yekaterinburg, May 20-24, 2019. East-West chemistry conference Palermo, Italy, (13-15 November 2019, the campus of the university of Palermo). International Scientific Conference Actual Problems of Organic Chemistry and Biotechnology, Ministry of

Science and Higher Education of the Russian Federation “Ural Federal University named after the First President of Russia B. N. Yeltsin” (18-21 November 2020). The Eighth International Young Researchers' Conference Physics. Technologies. Innovation. PhTI-2021, Ural federal university, institute of physics and technology (May 17-21, 2021). V International conference "Modern Synthetic Methodologies For Creating Drugs And Functional Materials" (MOSM 2021), Ministry of Science and Higher Education of the Russian Federation “Ural Federal University named after the first President of Russia B. N. Yeltsin” 8 to 12 November, 2021. Abstracts of the XXXII Russian Youth Scientific Conference with International Participation "Problems of Theoretical and Experimental Chemistry", dedicated to the 110th anniversary of the birth of Professor A.A. Tager April 19-22, 2022.

Publications

Based on the materials of the dissertation, 9 articles were published in peer-reviewed scientific journals included in the list of WoS and Scopus, as well as 7 abstracts in the Conferences materials and proceedings.

The structure and scope of the thesis

The dissertation work is stated at (155) pages of type written text and consists of an introduction, a literature survey, discussion of the results, experimental part, conclusion, and application. This work contains (293) references to literary sources, (64) figures, (27) tables.

Acknowledgements

The author degenerates deep and sincere gratitude collectives of the Department of Technology for Organic Synthesis of the Ural Federal University, Yekaterinburg, Russia; Head and Junior Researcher of the Laboratory of Organic Materials of Postovsky Institute of Organic Synthesis, Ural Branch of the Russian Academy of Sciences, Yekaterinburg, Russia Dr. A. V. Pestov & Mrs. V.A. Osipova, respectively, for invaluable assistance in research; Professor of Physical Chemistry G. Lazzara,: scientific advisor from the Department of Physics and Chemistry, Università degli Studi di Palermo, Italy, This work was supported by RFBR grant 18-29- 12129mk.

CHAPTER 1 LITERATURE REVIE

Adsorption at various interfaces has concerned scientists since the beginning of this century. This phenomenon underlies a number of extremely important processes of utilitarian significance. The technological, environmental and biological importance of adsorption can never be in doubt. Its practical applications in industry and environmental protection are of paramount importance. The adsorption of substrates is the first stage in many catalytic processes. The methods for separation of mixtures on a laboratory and on an industrial scale are increasingly based on utilizing the change in concentration of components at the interface. Moreover, such vital problems as purification of water, sewages, air and soil are involved here too. On the other hand, many areas in which technological innovation has covered adsorption phenomena have been expanded more through art and craft than through science. A basic understanding of the scientific principles is far behind; in part because the study of interfaces requires extremely careful experimentation if meaningful and reproducible results are to be obtained. In recent years, however, considerable effort has been increasingly directed toward closing the gap between theory and practice. Crucial progress in theoretical description of the adsorption has been achieved, mainly through the development of new theoretical approaches formulated on a molecular level, by means of computer simulation methods and owing to new techniques which examine surface layers or interfacial regions.

Although the development of adsorption up to the 1918s has been following rather a zigzag path, this arm of surface science is now generally considered to have become a well-defined branch of physical science representing an intrinsically interdisciplinary area between chemistry, physics, biology, and engineering. The prevention of environmental pollution caused by inorganic and organic toxic (and very often cancerogenic) chemical compounds is very important. The remediation and immobilization of contaminants applies to drinking water, wastewater and soil solutions, among other substances. The potentially hazardous inorganic substances include heavy metals [42]. In turn, the organic pollutants show a variety of structures and chemical activities (eg, dyes and pigments, hydrocarbons and their chlorinated derivatives and polycyclic aromatic hydrocarbons). Many of these chemical compounds are not required for the development of living organisms and may cause serious health problems, even at low or trace concentrations. Heavy metal ions such as Pb^{2+}, Cd^{2+}, Hg^{2+}, Ni^{2+}, and Cu^{2+} are widely known for causing serious health problems in animals and humans due to their ability to bind to proteins, nucleic acids, and tiny

metabolites in living organisms The proposed remediation techniques involve precipitation of highly insoluble phases, membrane filtration and electrolytic reduction [43]. Adsorption has been recognized as one of the most popular methods due to its simplicity of operation, cost effectiveness, high efficiency, easy recovery, regeneration capacity and sludge-free operation. However, the removal of heavy metal ions from wastewater is always a challenging task for environmentalists, so some researchers have attempted to develop good performance adsorbents for the disposal of heavy metal ions. However, adsorption-based approaches are in particular applied because the materials used for treatment are of low cost and very often may be reused after appropriate regeneration [44]. The adsorbents represent a group of structurally different materials, with the most important including functionalized silica, chitosan, activated carbons, zeolites, metal oxides, biomass, polymer-based materials and raw or modified clay minerals [43-51]. On the first hand, Halloysites, especially those exhibiting nanotubular morphology, are promising as a nanomaterial used for adsorption and pollution remediation [52]. Its several derivatives are known, which are inorganic organohybrids designed on a molecular scale [40, 53, 54]. The known synthesis procedures allow to perform grafting and intercalation of several organic compounds. This helps to control and adjust adsorption properties of the clay mineral for a specific pollutant (either polar/apolar or positively/negatively charged). The grafted materials with covalently attached organic molecules and halloysite polymer nanocomposites are particularly important. This is connected with their stability in aqueous solutions, which makes them promising candidates for water treatment [55]. The first part of this chapter discusses the possibility of using halloysite and its derivatives for the remediation of polluted water and wastewater, including organic and inorganic contaminants as well as the methods of modification of halloysite nanotubes to improve its sorption properties. The second part of this chapter reviewed various chemical and physical modifications of raw chitosan and generalized the applications of these chitosan derivatives for the removal of dye pollutant and toxic heavy metal ions as well as the effects of modifications and process parameters [45, 56-61]. Babel and Kurniawan [46] summarized the application of various low-cost adsorbents (such as chitosan, zeolites, etc.) for heavy metal ion removal from contaminated water. Jayakumar et al. [62] reviewed various preparation methods for modified chitosan and outlined applications of graft copolymerized chitosan for the removal of various pollutants. Pontoni et al. [59] reviewed the removal of arsenic from aqueous solutions using chitosan and chitosan-derivatives.

1.1 Surface properties of raw halloysite and adsorption mechanisms

The reported research on halloysite confirmed that the adsorption of ions and charged molecules on pure kaolin-group minerals may be explained by two mechanisms (Figure 1.1). The first, involving ion exchange, is related to permanently charged sites present at particle faces. The generated negative charge is due to isomorphic substitutions of Al^{3+} for Si^{4+} in the tetrahedral sheet, Fe^{2+} for Al^{3+} in the octahedral sheet or both. As the substitution usually does not exceed ~1% [13, 63], this first mechanism is of minor importance in adsorption processes.

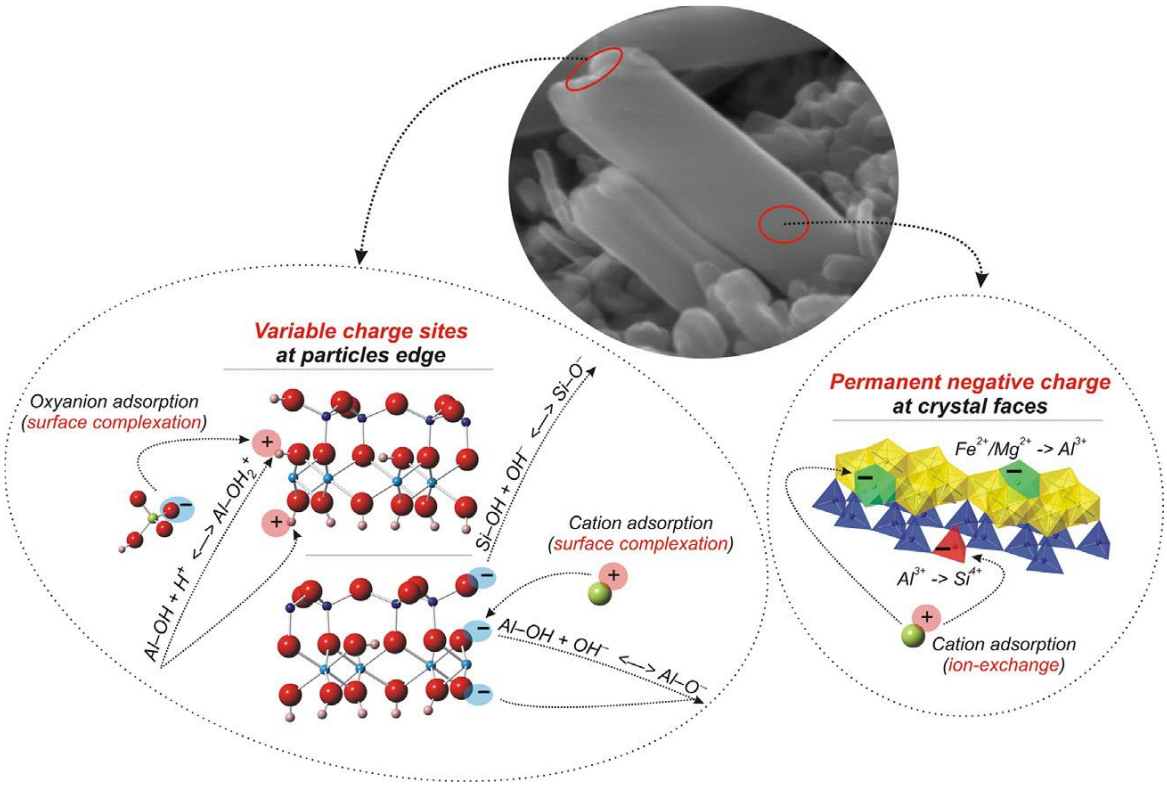

Figure 1.1 - Possible adsorption mechanisms on raw halloysite (7 A °).

The second mechanism is connected with variable charge sites found at particles edge and involves surface complexation. The nature of charge is strongly affected by the pH of solution in which the clay mineral is dispersed [64, 65]. Under acidic or alkaline conditions, the edge aluminol Al–OH and/or silanol Si–OH groups may undergo protonation or deprotonation (proton donor–acceptor reactions) which induces positive or negative charge, respectively. The interlayer space of pure, unmodified halloysite is not directly available for ions and molecules with exception of selected molecules, eg, dimethyl sulphoxide (DMSO) which has a large dipole moment and

destroys interlayer hydrogen bonding during intercalation. The typical physicochemical features of HNTs are summarized in Table 1.1.

Table 1.1 - Physico-chemical features of HNTs.

Chemical formula	**$Al_2Si_2O_5(OH)_4$. *n* H_2O**
Length	0.2–2 mm
Outer diameter	40–70 nm
Inner diameter	10–40 nm
Aspect ratio (L/D)	10–50
Elastic modulus (theoretical value)	140 GPa (130–340 GPa)
Mean particle size in aqueous solution	143 nm
Particle size range in aqueous solution	22.1–81.6 m^2/g [104]
BET surface area	50–400 nm
Pore space	22.1–46.8%
Lumen space	11–395
Density	2.14–2.59 g/cm^3
Average pore size	79.7–100.2 Å
Structural water release temperature	400–600 °C

1.2 Functionalization of halloysite structure for the improvement of adsorption properties

1.2.1 The effect of calcination and acid activation

The common, inexpensive surface modification methods of kaolin-group minerals, including halloysite, involve thermal treatment (calcination) and acid activation. Calcination of halloysite leads to structural changes similar to kaolinite [66, 67]. In the 600–850°C temperature range the structure undergoes dehydroxylation which affects largely the coordination of aluminum in the octahedral sheet. Further heating leads to formation of nanocrystalline (<5 nm) γ–Al_2O_3 (1000°C) which with increasing temperature up to 1400°C reacts with silica forming aluminum-rich mullite which is finally converted to mullite—$3Al_2O_3.2SiO_2$. From the viewpoint of

adsorption, the calcination is often performed at dehydroxylation temperature. The generation of active centers is connected with reduced coordination of aluminum.

Although thermal treatment enhances adsorption properties this is not always accompanied with an increase of specific surface area (SSA). For example, the SSA of 64 m^2/g measured for halloysite sample from Djebel Debagh, Guelma (Algeria) did not change significantly after calcination at 600°C for 2 h (60.5 m^2/g) [68, 69]. The large increase of SSA which favors adsorption can be noticed for acid-activated halloysites [69, 70]. The Algerian halloysite treated with HCl at concentrations in the 0.5–7.0 mol/L at 70°C for 4 h showed a SSA increase even up to 503.3 m^2/g [69]. In turn, a SSA increase from 47.8 to 267.1 m^2/g was noticed for halloysite from Hebei Province (China) after treatment with 3 mol/L H_2SO_4 at 90°C for 13 h [70]. However prolonged treatment times or too high acid concentration leads to aggregation of partially amorphous clay mineral particles, which lowers the SSA and overall porosity and subsequently may inhibit adsorption. The traditional use of inorganic acids in the first stage removes mineral impurities and promotes octahedral sheet dissolution with simultaneous release of Al and relative increase of SiO_2 content. Afterwards, the etching of the more stable in acidic conditions, tetrahedral sheet starts and the formed SiO_2 precipitate fills the particles lumen [71]. The affected and/or partially destroyed surface layers showed increased reactivity. The acid treatment strongly influences the zeta potential of halloysite surfaces which is crucial in adsorption phenomena [72]. The zeta potential values were found to be equal to -3.5, -32.4 and -44.8 mV at pH 2, 7 and 11, respectively. The pH and corresponding zeta potential affect the stability of halloysite particles which may agglomerate, thus lowering SSA and changing pore size distribution. The acid activation can be done selectively due to differences in chemical nature of Al and Si sheets. The H_2SO_4 acid was used for an enlargement of halloysite lumen by dissolving the octahedral sheet [73]. Such treatment increased the lumen diameter (from 15 to 25 nm) and SSA (from 40 to 250 m^2/g). As a result, a four-fold adsorption increase of benzotriazole was reported. The acid-activated halloysite shows high adsorption capacity towards methylene blue (MB) dye of 61.35 mg/g [70]. The dispersion of acid-activated halloysite in aqueous solution rapidly decreases the pH which negatively affects the cations adsorption. Thus, efficient adsorption requires the control and adjustment of pH.

1.2.2 Raw and interlayer-grafted halloysite for the removal of cations

The halloysite structure with adsorption centers and its specific morphology enable to use the clay mineral as heavy metals scavenger. A comprehensive report on Zn (II) adsorption phenomena on raw halloysites of different origin was given by Wada and Kakuto (1980)[74]. The authors underlined the high selectivity of Zn (II) ions to adsorb on halloysite active sites. The selected halloysites showed a broad range of cation-exchange capacity (CEC) from 7.7 to 56.7 meq/100 g and different Fe_2O_3 content (0.11–3.76%). A significant effect of halloysite morphology was found, that is the selectivity of Zn (II) adsorption was the highest for spherical halloysite, medium for the platy halloysite, and was found the lowest for tubular halloysites. In turn, no correlation between the adsorption and iron content was reported. It was concluded that the Zn (II) adsorbs preferentially to Ca (II) ions on halloysites and most of the adsorbed Zn (II) is present on the cation-exchange sites of the clay mineral. Moreover, the experiments indicated that charge sites show high affinity for H^+ which are mostly responsible for the attraction and binding of Zn (II). The authors discussed the role of pH-dependent cation-exchange sites at the particle's edges. The deprotonated hydroxyls may act as ligands which complex Zn (II) in preference to Ca (II). The stability of the formed Zn (II)-clay mineral monodentate or bidentate complex depends greatly on the local chemical environment in which the nature of OH groups was influenced by sterical effect of adjacent cation-exchange sites. Different Zn (II) adsorption behavior of halloysites suggested a crucial influence of the genesis and geological occurrence on the active sites. The adsorption of Zn (II) on halloysite showing nanotubular morphology was also studied by Dong et al. (2012)[75]. The authors examined the influence of solution characteristics (pH, ionic strength, temperature and competitive effect of other ions) on the adsorption. The results showed a domination of cation-exchange mechanism and outer-sphere complexation at low pH. In turn, at high pH the removal was also due to inner-sphere complexation and precipitation. The detailed analysis also showed a significant influence of the background electrolyte, i.e., competitive ions on the Zn (II) removal efficiency (Figure 1.2). The presence of Na^+, K^+, Ca^{2+} and Mg^{2+} inhibited the Zn (II) removal. The effect was much stronger when divalent cations were present which competed for binding sites with Zn (II). The authors also pointed that the decrease of Zn (II) removal in the presence of divalent cations is due to their influence on surface potential. It becomes less negative, and this hampers the Zn (II) adsorption. The anionic background electrolyte showed a much more pronounced effect on the Zn (II) removal efficiency. The Cl^- and SO_4^{2-} strongly inhibited the Zn (II) adsorption which can be attributed to the formation of soluble

Zn (II)-Cl or Zn (II)-SO_4 complexes. These being electronegative do not have the affinity to adsorb. On the other hand, CO_3^{2-} ions had a positive effect on the Zn (II) adsorption as at pH<6.5, the anion may induce the formation of ternary or multinary complexes, eg, –O–Zn–CO_3, –O–CO_3–Zn, –O–Zn–CO_3–Zn–. At higher pH values the simultaneous precipitation of $ZnCO_3$ may occur which increases the removal efficiency to 100%.

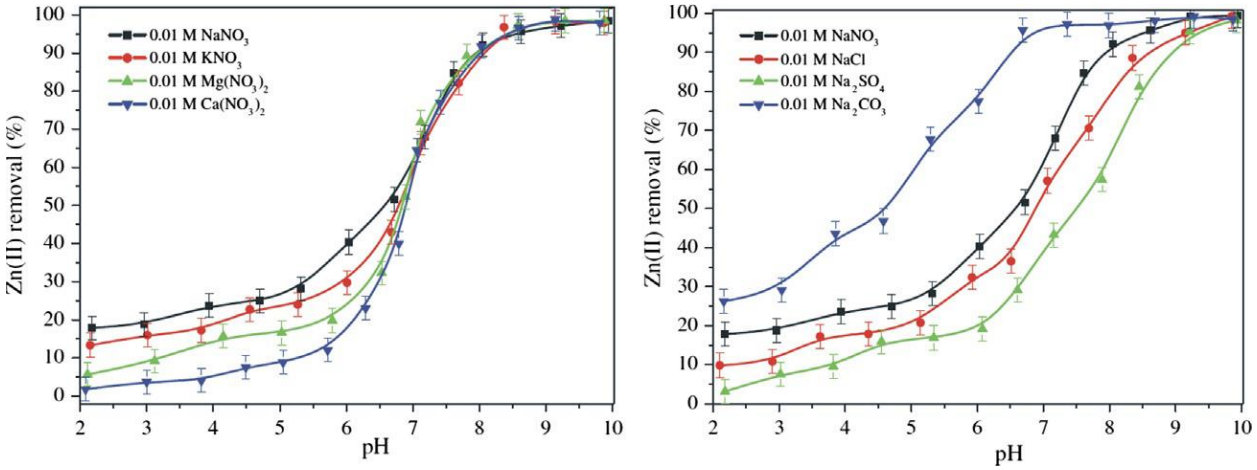

Figure 1.2 - Left: influence of coexisting electrolyte cations on the removal of Zn (II) by halloysites as a function of pH values. T=293 K, $C_{(Zn)\ initial}$=1.54^{x}10 $^{-4}$ mol/L, m/V=1.0 g/L. Right: influence of coexisting electrolyte anions on the removal of Zn (II) by halloysites as a function of pH values. T=293 K, $C_{(Zn)\ initial}$=1.54^{x}10^{-4} mol/L, m/V=1.0 g/L. Reprinted with permission from Dong et al. (2012) [75]. Copyright 2012 Springer.

The performed thermodynamic experiments, which allowed drawing temperature-dependent adsorption isotherms, showed that the adsorption process was endothermic and spontaneous. The usability of pure halloysite from New Zealand for the highly efficient removal of Ag(I) ions was also shown [76]. The experimentally obtained maximal adsorption capacity equal to 109.79 mg/g was higher than the values reported for bentonite (80.0 mg/g) and comparable to adsorption capacity of polyacrylonitrile nanofiber mats (105.7 mg/g). The investigation allowed to estimate the energy of Ag(I) adsorption on halloysite which was equal to 7.28 kJ/mol and corresponded to physical nonspecific adsorption. The binding took place mainly at the deprotonated edge sites where Ag(I) ions competed with protons especially at low pH. Due to relatively weak interaction of halloysite surface, the regeneration using HCl was very efficient and reached almost 100%, which enables the material to be reused. In other studies, a halloysite intercalated with Na^{+}, Pb^{2+} or NH^{4+} acetate was tested for the removal of Cu (II) ions [68, 77]. The nanotubular clay mineral had a CEC of 19.2 meq/100 g, SSA of 64 m^2/g and an isoelectric point

at pH 2.5. The intercalation of acetates improved the removal efficiency, and a 2.2-fold increase of adsorption capacity was noticed in contrast to the pure halloysite. The adsorption enhancement was attributed to cation exchange connected with the acetate presence and cation complexation at the particle's edges. The experimental procedures leading to the synthesis of kaolinite interlayer-grafted derivatives were shown to be effective also for halloysite due to structural similarities of the clay minerals. The exposed inner surface hydroxyls of nanotubular halloysite were reacted with diethanolamine $(CH_2CH_2OH)_2NH$ (DEA) and triethanolamine $(CH_2CH_2OH)_3N$ (TEA) which may play a role of complexing agents (Figure 1.3) [54].

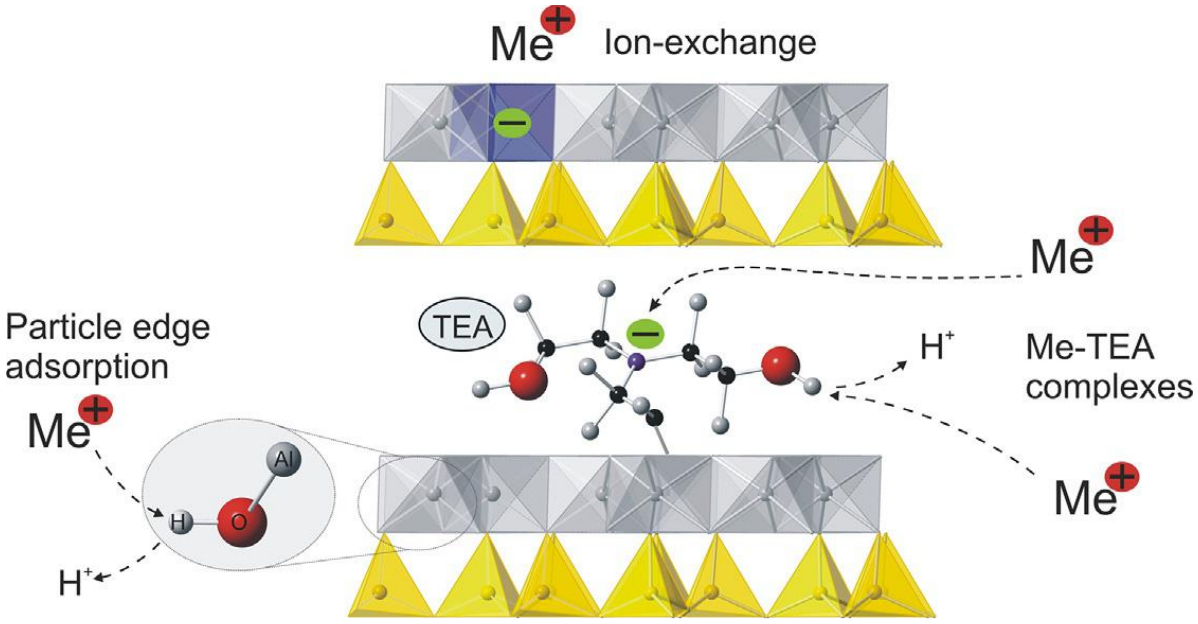

Figure 1.3 - The approximate structure of halloysite interlayer grafted with triethanolamine (TEA) and possible adsorption mechanisms in contact with aqueous solution containing cations (Me). Graphical abstract reprinted with permission from Koteja and Matusik (2015)[78]. Copyright 2015 Elsevier.

For the research a halloysite sample from Dunino deposit (SW Poland) was chosen. The synthetic route consisted of two successive steps. Firstly, an intercalation with DMSO was carried out at room temperature (22°C). Secondly, the formed intercalation compound was refluxed with DEA or TEA at 180°C under argon flow for 24 h [79]. The obtained dispersion was centrifuged, washed with isopropanol and subsequently with water and finally dried at 65°C. The extensive washing allowed to ensure that only amino alcohol molecules which are covalently attached to the octahedral sheet through Al–O–C bonds were left. The formation of Al–O–C bonds affected the dehydroxylation temperature of the halloysite due to change of the local environment of the

octahedra. The tailored materials were resistant to decomposition during prolonged washing in aqueous solutions as attested by X-ray diffraction (XRD) and Fourier transform infrared spectroscopy (FTIR) methods. Moreover, they did not show swelling properties and had a fixed interlayer space equal to 3.1 A° (DEA) or 3.6 A° (TEA). The interlayer space value was exclusively controlled by the size of the amino alcohol molecules which formed a monolayer. The introduced DEA and TEA molecules possess metal-binding properties due to presence of amine nitrogen with a lone electron pair behaving as a Lewis base in relation to metals acting as Lewis acids [54, 80-82]. The binding of metals through deprotonated OH groups which terminate the alkyl chain of amino alcohols is also possible [83]. Based on the earlier studies of Letaief and Detellier (2007) [79] it was assumed that the amino alcohols were attached through Al–O–C bonds to the octahedral sheet involving one of their OH groups. Thus, the formulas of the modified materials calculated based on nitrogen content were: $Al_2Si_2O_5(OH)_{3.93}(DEA)_{0.07}$ and $Al_2Si_2O_5(OH)_{3.90}$ $(TEA)_{0.10}$, respectively. The small content of the grafted molecules [~16% (DEA derivative) and ~25% (TEA derivative) in relation to maximal content] could be connected with the steric hindrance effect (i.e., blocking of the interlayer by DEA or TEA). The applied chemical treatment induced the formation of mesopores and macropores in the case of the TEA derivative, and in turn, part of the mesopores was blocked in the case of the DEA derivative. The textural parameters revealed the mesoporous character of the synthesized materials, with the content of micropores not exceeding 7% of the total pore volume (V_{TOT}). The grafting of TEA led to the exfoliation of particles to a small extent, in contrast to the DEA grafting, where exfoliation did not take place and probably some of the particles formed aggregates. This was attested by changes in SSA, which increased for the TEA derivative to 57.0 m^2/g and decreased to 47.37 m^2/g for the DEA derivative, in comparison to the 49.52 m^2/g initial value of raw halloysite. The applied grafting procedure did not improve the CEC and it also did not affect the point of zero charge (PZC). The performed adsorption tests revealed that the modification significantly improved the halloysite adsorption capacity with respect to Pb (II), Cd (II), Zn (II) and Cu (II). Equilibrium and kinetic experiments connected the removal enhancement with a two-step gradual migration of the cations into the halloysite interlayer space, followed by their complexation by amine nitrogen. In general, the equilibrium was achieved after about 4 min. The Weber–Morris plots enabled the identification of two stages of the process due to the presence of two linear trend lines [84]. The two-step process consisted of external mass transfer, which was followed by migration of the

cations into the interlayer space. On the other hand, in the case of pure halloysite, the adsorption took place rapidly (in the first minute of the reaction) due to surface complexation, ion exchange or both. The pH of the system increased due to the competitive behavior of protons, in contrast to a system with raw halloysite, where the pH decreased. The latter was attributed to a domination of ion-exchange and surface complexation mechanisms, and the adsorption efficiency was mainly influenced by the metals' hydrolysis constants. In the case of grafted materials, in particular, the Cu (II) ions were preferentially removed from solution, as they readily form complexes with N-donor ligands [83]. This was very visible in multielement systems where the adsorption on grafted materials followed the sequence Cu (II)>Pb (II)≫Zn (II)~Cd (II) (Figure 1.4). The Zn (II) and Cd (II) adsorption was significantly hampered. The kinetic data for these elements indicated a one-step rapid adsorption. In turn, the kinetics for Cu (II) and Pb (II) showed a gradual increase of adsorption, suggesting a binding in the interlayer space of halloysite. The formation of Cu (II)-amino alcohol complexes was confirmed using UV–vis spectroscopy. Moreover, the decomposition of grafted amino alcohol after Cu (II) took place at different temperatures and affected the shape of the exothermic peak in comparison to pure grafted derivatives. The equilibrium pH in the multielement system was always below the precipitation pH limit of metal phases. Thus, the concurrent precipitation mechanism was excluded. Experiments with the use of real wastewater showed that the materials' adsorption properties were not hampered due to the presence of organic media and other ions. Analogous to synthetic aqueous solutions, the same conclusions were drawn, including the preferential Cu (II) adsorption. The desorption experiments revealed a complex binding strength of the metal cations and showed that a complete regeneration of the materials was not possible when using ammonium acetate as a mild extractant. The mathematical description of the equilibrium adsorption data showed the best agreement when using the Langmuir model. The theoretically obtained adsorption capacity was close to the experimental data with a very high correlation coefficient. The kinetic data in the whole-time range followed the pseudo-second order equation with a high linear correlation coefficient (R^2>0.98).

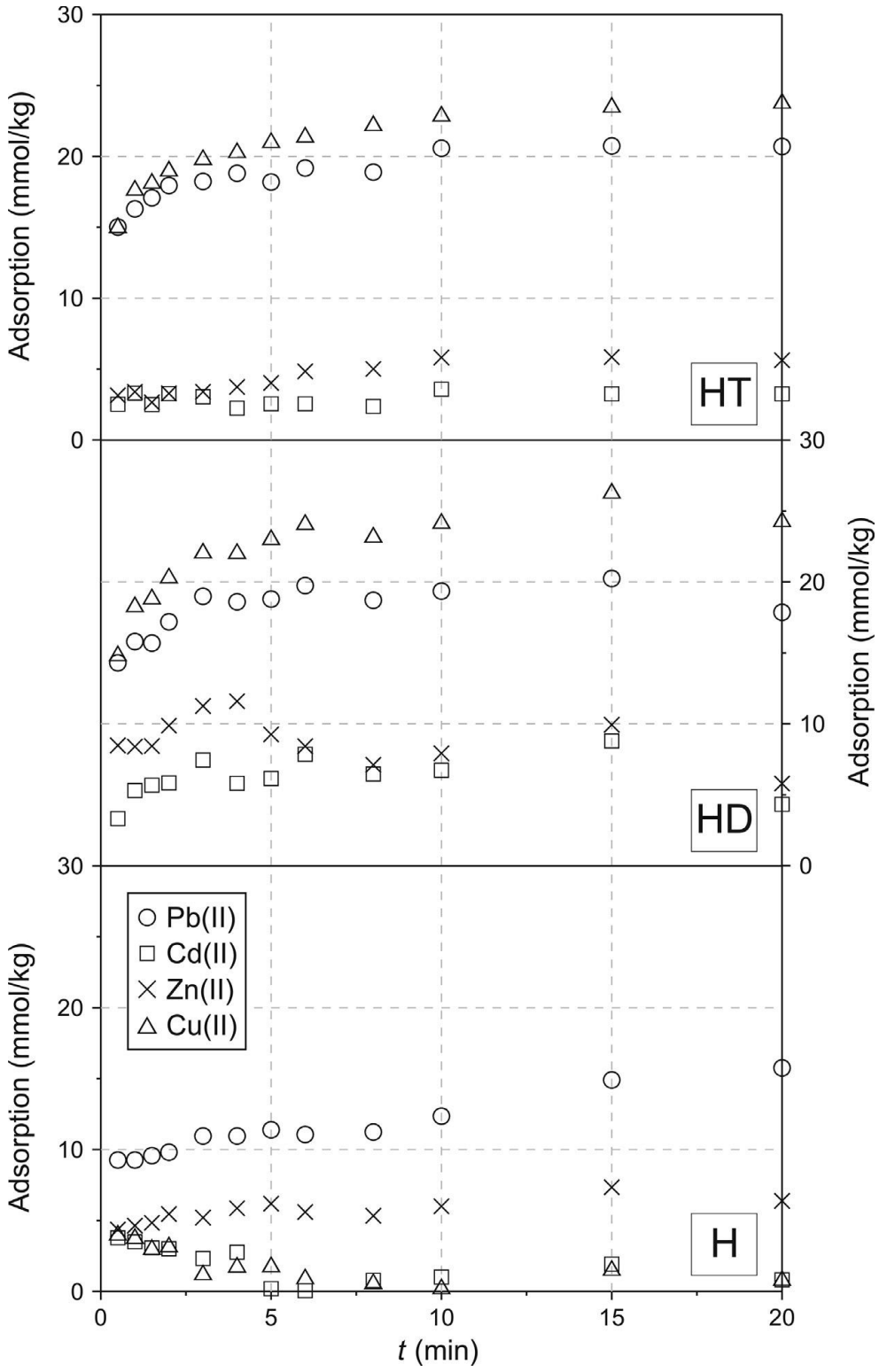

Figure 1.4 - Kinetics of Pb (II), Cd (II), Zn (II) and Cu (II) uptake in the multielement system for the H (pure halloysite), HD (DEA grafted halloysite) and HT samples (TEA-grafted halloysite). Reprinted with permission from Matusik and Ws´cisło (2014) [40]. Copyright 2014 Elsevier.

1.2.3 Surface and interlayer-modified halloysite for the removal of anions

The adsorption and removal of anions is less frequently studied due to preferential affinity of halloysite to bind cations. In theory, the surface of raw halloysite does not have the capability to attract anions in high amounts. However, the research literature reports modification procedures regarding halloysite structures that enable the enhancement of the adsorption capacity of oxyanion contaminants. One of the methods for improving oxyanion adsorption is an introduction of surfactants, which could be either intercalated or attached to the clay mineral surface [85-88]. The raw halloysite was treated with an aqueous solution of hexadecyltrimethylammonium bromide (HDTMA-Br) in different amounts in relation to its CEC [88]. In the studied experimental conditions, the HDTMA-Br was exclusively present on the clay mineral surface, as the XRD pattern of halloysite did not show changes after treatment. Moreover, the introduced molecules blocked the internal porosity, as N_2 adsorption/desorption measurements indicated a decrease in SSA from 26.5 to ~17.0 m^2/g. The presence of quaternary ammonium bromide, especially in amounts exceeding the CEC, enhanced the clay mineral's ability to remove nitrates. A twofold to threefold increase, however, was not as high as for modified bentonite (increase of more than 10-fold), where the HDTMA-Br molecules were also intercalated into the interlayer space. A similar modification approach for the halloysite in the Henan province, China, was studied by Wang et al. (2010)[89] in terms of Cr (VI) removal. The surface modification of halloysite nanotubes by HDTMA-Br increased the adsorption capacity to ~132 mmol/kg. The authors emphasized the fast kinetics of Cr(VI) uptake, with equilibrium achieved after 1 h as compared to 3–48 h equilibrium times that previously had been reported for organic polymer-modified and zeolite adsorbents [89]. The adsorption of N(V) and Cr (VI) oxyanions by HDTMA-Br modified halloysite mainly involved electrostatic interaction of the oxyanion with an adsorbed organic cation. A synthetic route leading to significant improvement in oxyanion adsorption by halloysite was based on interlayer grafting and subsequent quaternization [40, 90]. The procedure was based on the treatments reported for kaolinite, which was used as a size-selective sensor of cyanide, iodide and other anions [91-93]. The synthesis consisted of three subsequent stages. First, the halloysite from Polish Dunino deposits was pre-intercalated with DMSO. Second, the pre-intercalates were refluxed with TEA for 2 h at 180°C under argon flow. The third step included the methylation reaction with iodomethane (CH_3I) at 42°C.

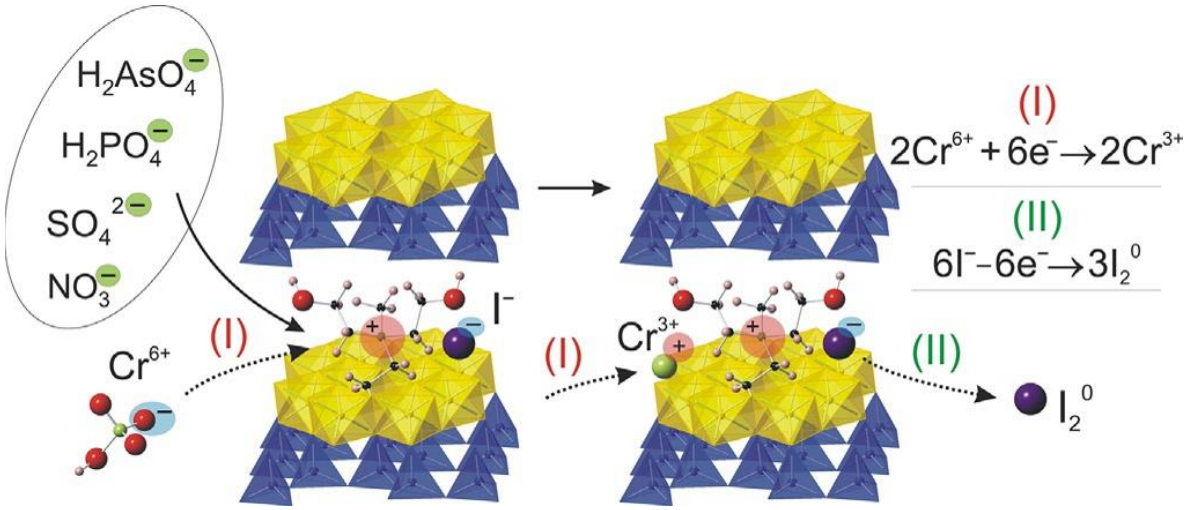

Figure 1.5 - The approximate structure of quaternized interlayer-grafted halloysite and its interaction with oxyanions involving ion exchange and Cr (VI) reduction. Reprinted with permission from Matusik and Bajda (2013) [90]. Copyright 2013 Elsevier.

The key methylation reaction involved the attachment of the CH_3 group to the interlayer-grafted TEA molecule and was confirmed by the ^{13}C CP-MAS NMR spectroscopy. This treatment was designed to form positively charged centers associated with ammonia nitrogen of ammonium salt molecules formed in the interlayer space (Figure 1.5). The generated positive charge was compensated by mobile iodide anions, which could be ion-exchanged easily. Subsequent detailed investigations indicated a significant increase in oxyanions: Cr (VI), As(V), P(V), S(VI) and N(V) adsorption capacity by the modified halloysite [54, 90]. In the case of Cr (VI) removal, the adsorption maximum (initial pH 5) for the pure halloysite (SSA: 50.6 m^2/g) reached only ~12.0 mmol/kg. In turn, the modification led to an approximately eightfold increase of the adsorption capacity of up to ~95 mmol/kg (Figure 1.6). It is worth pointing out that the chemical treatment enabled the access of the chromate to the interlayer space by increasing the d_{001} value up to ~10.8 A°. Kinetic studies confirmed that the adsorption on the interlayer-quaternized halloysite is a pseudo-second order reaction and that over 90% of the finally immobilized chromium was removed after 2 min of the reaction. The adsorption equilibrium was achieved after ~20 min, indicating that the nanotubular morphology of halloysite inhibited the adsorption rate. The analysis of solution chemistry before and after adsorption experiments, coupled with the FT-IR and X-ray photoelectron spectroscopy (XPS) analyses of solid, enabled proposing a two-step removal of Cr (VI). First, an ion exchange of Cr (VI)$\rightarrow I^-$ takes place, followed by Cr (VI) to Cr (III) reduction by iodide, which releases iodine into solution (Figure 1.5). The formation of Cr (III) is desirable

from an environmental point of view, as Cr (III) is much less toxic than Cr (VI). The pH-dependent ratio of the removed Cr (VI) to released iodide was related to the presence of either the $HCrO_4^-$ or CrO_4^{2-} ionic form and confirmed initial ion-exchange mechanism.

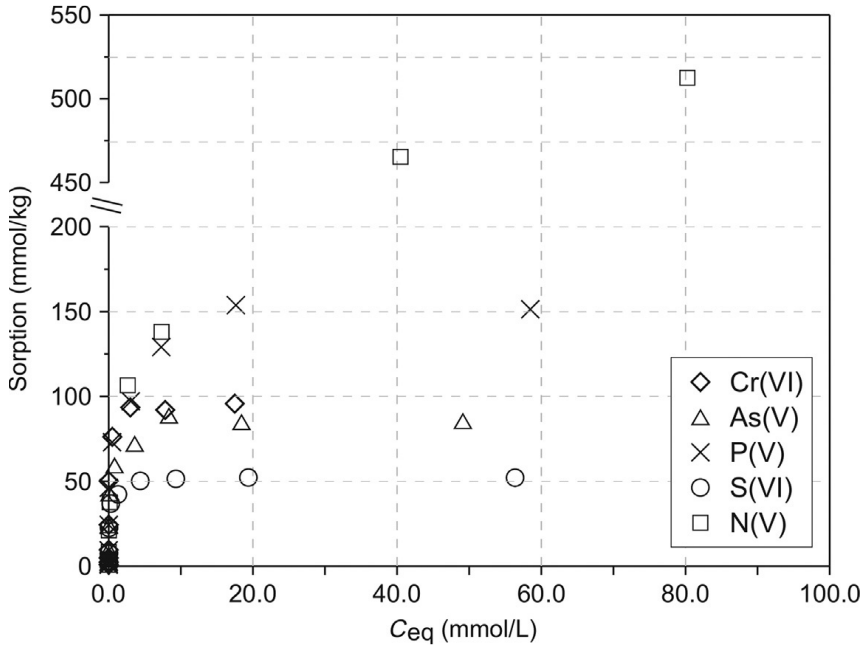

Figure 1.6 - Adsorption isotherms of selected oxyanions on the quaternized interlayer grafter halloysite. Adapted with permission from Matusik (2014) [54]. Copyright 2014 Elsevier.

The obtained interlayer-quaternized halloysite also showed improved anion adsorption properties towards As (V), P(V), S(VI) and N(V) (Figure 1.6). However, the improvement was less than for the material derived from kaolinite of high structural order [54]. The adsorption isotherms for all the anions follow the Langmuir model, with a high correlation coefficient and good fit to the experimental maximum adsorption capacity. In analogy to Cr (VI), the studied anions were mainly ion exchanged with mobile iodide ions, which was confirmed through analysis of solution chemistry and ratio of removed oxyanion to released iodide. After adsorption, the d_{001} value of the modified halloysite was unchanged, as attested by the XRD pattern confirming that swelling did not occur and only the grafted organic molecules controlled the basal spacing. Thus, the interlayer penetration by larger molecules may not be possible, giving rise to selective adsorption properties of the quaternized halloysite. Moreover, the modification does not alter or destroy the halloysite structure and morphology. Another protocol for improving Cr (VI) adsorption involved a formation of halloysite nanocomposite with polypyrrole (PPy) polymer through in situ polymerization technique [94]. Although the polymer itself is showing ion-

exchange properties, an addition of nanofiller (eg, halloysite nanotubes prevents agglomeration induced by p–p stacking). This enhances its adsorption properties and enables its usage as efficient oxyanion CPN (clay polymer nanocomposite) adsorbent. The reported maximal adsorption capacity is exceptionally high, reaching ~2870 mmol Cr (VI)/kg at pH 2 and room temperature. The performed XPS analyses showed that the Cr (VI) removal involves its reduction to Cr (III), induced by electron rich organic PPy molecules. The conducted desorption studies indicated the possibility of halloysite PPy nanocomposite regeneration and its further reuse for up to three times. Moreover, the adsorbent showed very high (~99%) Cr (VI) removal efficiency from chromium-contaminated groundwater and mine wastewater. Interestingly, the accompanying SO_4^{2-} and Cl^- ions did not hamper the Cr (VI) removal, suggesting that the material has high selectivity for chromium [94]. A CPN approach was also tested using polyethyleneimine (PEI) for the functionalization of halloysite nanotubes [55]. The procedure enabled to obtain a nanomaterial adsorbent with a relatively low SSA of 30.9 m^2/g, but again with a very high Cr (VI) adsorption capacity, equal to 1240 and 1970 mmol/kg measured at 25°C and 55°C, respectively. The reported possible removal mechanism included (i) Cr (VI) electrostatic attraction by protonated amine groups and (ii) reduction of Cr (VI) to Cr (III) through electron transfer from aldehyde and amine groups. Improvement of Cr (VI) adsorption was also achieved by using raw halloysite nanotubes grafted with the silane-coupling agent N-β-aminoethyl-γ-aminopropyl trimethoxysilane [95]. The protonated amino groups of the grafted silane attracted Cr (VI) oxyanions, and the maximum adsorption capacity reached ~716 mmol/kg (Figure 1.7). The experiments confirmed a fast removal, with 95% uptake after ~5 min. In contrast to other adsorbents, the silane-grafted halloysite showed greater removal efficiency at lower temperatures.

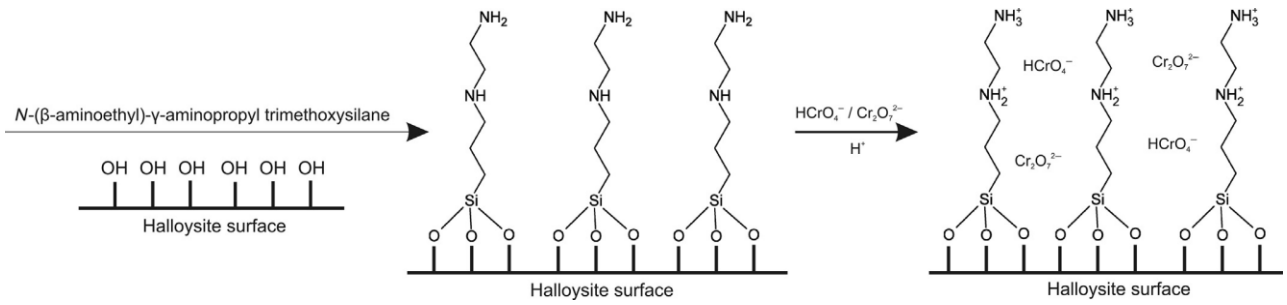

Figure 1.7 - Schematic diagram illustrating Cr (VI) adsorption onto halloysite nanotubes surface grafted with silane-coupling agent. Adapted with permission from Luo et al. (2011) [95]. Copyright 2011 American Chemical Society.

1.2.4 Raw halloysite and halloysite-based composites for the removal of organic pollutants

Apart from the common usage of nanotubular halloysite as an adsorbent of cationic and anionic inorganic species, the clay mineral is often used in the treatment of aqueous media contaminated with organic compounds. The hydrated halloysite (10 A°) has the ability to form intercalation compounds with various organic molecules [96]. The intercalation proceeds most efficiently when the molecules are polar and contain hydroxyl –OH and amine $–NH_2$ functional groups capable of forming hydrogen bonds in the halloysite interlayer space. As dehydration of halloysite (10 A°) takes place easily at room temperature in the absence of water, a halloysite (7 A°) is more often used in adsorption experiments. The nanotubular halloysite and its modifications, as well as its nanocomposites with other minerals, were used for the uptake of organic acids, dyes and simple aromatic hydrocarbons, among others. Pristine halloysite nanotubes (Hebei province, China) were tested for the removal of a commonly found cationic MB dye from aqueous solutions in batch experiments [97]. The maximal adsorption capacity reached 84.32 mg/g and was achieved after about 30 min. The removal was the highest at high pH values, which was attributed to extensive particle edge deprotonation. The thermodynamic experiments indicated that the adsorption capacity increased with decreasing temperature of the solution. The formed temporary charge attracted the cationic dye. The authors underlined the fact that the sedimentation rate of halloysite dispersion with adsorbed MB proceeds very fast. In contrast, the dispersion of pure halloysite remains stable for a much longer time. This behavior of the adsorbent is desired from the viewpoint of applications due to the simplicity of water filtration after dye removal. The same research team tested the halloysite from Hebei province for the uptake of dye used in biological research—neutral red (NR), which forms cations in aqueous solution [98]. The reported maximal dye uptake at room temperature (298 K) reached 54.85 mg/g and increased with increasing temperature to 59.24 mg/g (308 K) and to 65.45 mg/g (318 K). Thus, the observed temperature effect was the opposite of that noticed for the MB, with the adsorption being an endothermic process. The plots of adsorption capacity vs $time^{1/2}$ allowed one to distinguish the two-step nature of NR dye removal. This was connected to (i) intraparticle diffusion in the first stage and (ii) equilibrium achievement in the second stage. The reported removal of methyl violet (MV) by nanotubular halloysite from Henan province was equal to 105.26 mg/g at 298 K and reached 113.64 mg/g at 318 K [99]. The adsorption values were higher than those reported for other

substances, such as sepiolite (10.24 mg/g) and baggase fly ash (26.25 mg/g). Although the adsorption was about five times less than activated carbon (526.32 mg/g), the authors emphasized the low cost of halloysite (200$/tonne, with 4000$/tonne for activated carbon in the year 2011). This makes the inexpensive halloysite a promising candidate to use for dye removal from aqueous media. Moreover, it was shown that adsorbent regeneration was possible by calcination at 300°C. This treatment led to dye combustion without destroying the aluminum silicate framework; however, after six calcination/adsorption cycles, the regeneration efficiency decreased to 60%. Kiani et al. (2011)[100] showed that halloysite nanotubes (China Clays Ltd., New Zealand) can efficiently remove malachite green (MG) through physical adsorption, with a maximal capacity of 99.6 mg/g achieved at pH 9.5. In agreement with earlier observations, the adsorbed dye led to halloysite particle aggregation and favored adsorbent sedimentation. An interesting study showing the capability of halloysite to remove not only cationic but also anionic dyes was shown by Zhao et al. (2013) [52]. The research revealed that adsorption of rhodamine 6G (R6G) and chrome azurol S (CS) reaches 43.6 and 38.7 mg/g, respectively, and it is higher for halloysite in comparison to kaolinite. The affinity to both positively and negatively charged dyes resulted from the pH-dependent charge generated by the halloysite Al_2O_3 and SiO_2 surfaces. Such phenomenon was defined by the authors as 'bivalent adsorbancy' [52]. The regeneration of halloysite based filters was possible up to 50 times through dye combustion. The removal of R6G increased with temperature with the process being endothermic and was attributed to electrostatic dye-silanol surface interaction. In contrast, a decrease of CS adsorption was noticed, indicating an exothermic process. This was attributed to the CS hydrogen bonding through its carboxyl and hydroxyl groups to aluminol groups of the nanotube interior [52]. For the adsorption, these authors also used halloysite surfaces modified with selected surfactants and complexing agents. This treatment gave positive results in the case of CS adsorption. In particular, modification with dioctadecyldimethylammonium bromide (DODAB) led to a sixfold increase of the anionic dye adsorption. This was due to CS interaction with quaternary ammonium nitrogen showing a positive charge. The halloysite treatment with organic molecules did not improve cationic R6G removal, which was highest when a raw clay mineral was used [52]. Yuan et al. (2012a) [101] showed that grafting an organosilane γ-aminopropyltriethoxysilane (APTES) on halloysite nanotubes increased the loading of anionic acid orange II dye (AOII) (Figure 1.8). Under appropriate pH conditions, the protonated amine groups NH^{3+} of covalently bonded APTES inside halloysite lumen had strong

affinity to the AOII. An interesting approach for halloysite nanotubes used for dye adsorption was shown by Xie et al. (2011) and Duan et al. (2012) [102, 103]. The halloysite nanotubes were covered with nanocrystalline Fe_3O_4 (3–10 nm in size) through precipitation. Experimentally, the halloysite was dispersed in a solution containing iron chloride ($FeCl_3.6H_2O$) and iron sulphate ($FeSO_4.7H_2O$) at high pH (in the 9–10 range), which favored iron oxide precipitation.

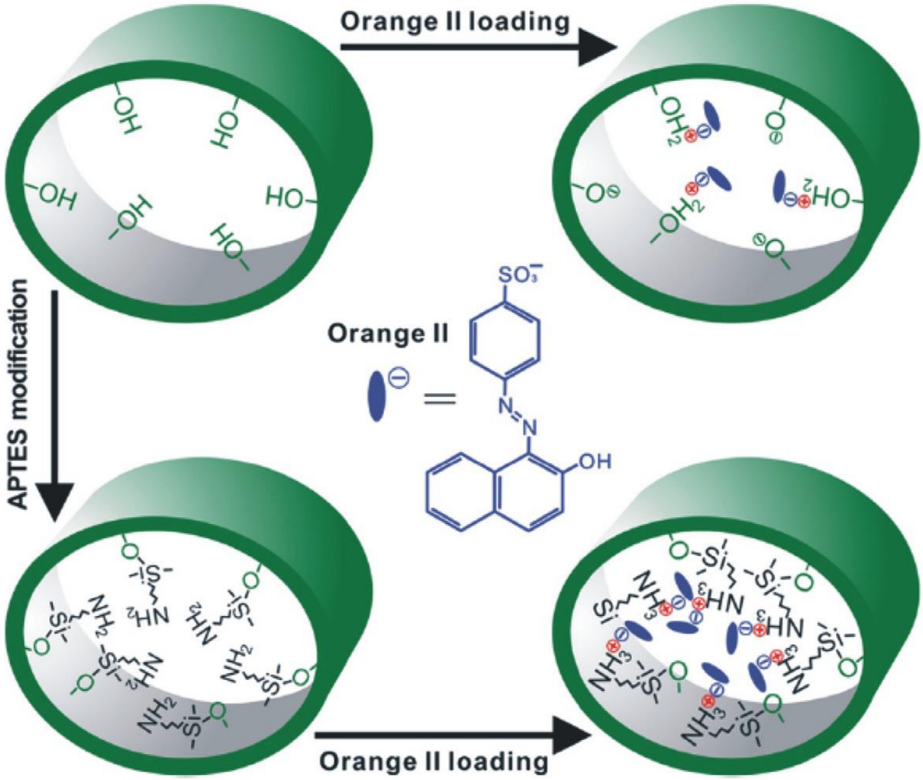

Figure 1.8 - Schematic representation of the amine modification and orange II loading of the halloysite nanotube. Reprinted with permission from Yuan et al. (2012a). Copyright 2012 ©IOP Publishing.

The formed halloysite iron nanocomposite showed high adsorption capacity towards several dyes, including MV, MB and NR, with a lower adsorption capacity towards methyl orange (MO) [102, 103]. However, the most striking feature of the used halloysite iron nanocomposite was the possibility of its simple separation from the adsorbate liquid using its magnetic properties (Figure 1.9). The external magnetic field attracted the halloysite iron nanocomposite, which could be regenerated by calcination and further used for dye adsorption. The nanocomposite composed of halloysite nanotubes and magnetic iron oxides was also used to support the preparation of sophisticated magnetic molecularly imprinted polymers (MMIP) [53]. The obtained MMIPs

showed selective recognition of a model phenolic compound: 2,4,6-trichlorophenol. The organic can be selectively removed from polluted samples with a simultaneous magnetic separation of the used adsorbent. Dye adsorption was also improved through the preparation of halloysite complexes with natural biopolymers. One of them involves the use of chitosan—a cationic polymeric carbohydrate whose adsorption properties are governed by the presence of amine and hydroxyl groups, allowing electrostatic interaction with dyes [104].

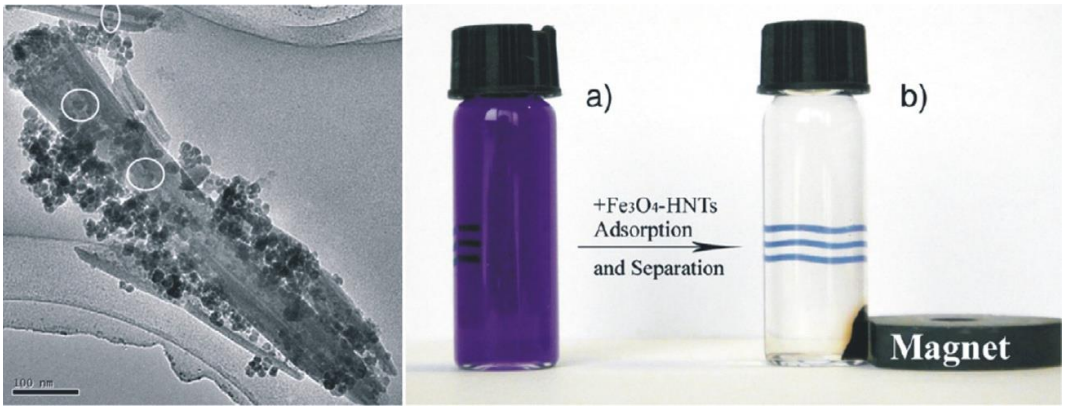

Figure 1.9 - Left: TEM micrograph of halloysite-Fe_3O_4 composite, right: magnetic separation after adsorption onto halloysite-Fe_3O_4 composite. Reprinted with permission from Xie et al. (2011); Duan et al. (2012) [102, 103]. Copyright 2012 Elsevier.

A synergetic effect of the prepared halloysite chitosan hydrogel beads (2.29–2.75 mm in diameter) was observed, and subsequently, the adsorption capacity of MB and MC dyes was enhanced. The adsorption of MB and MC equaled 217.39 and 243.90 mg/g, respectively. Meanwhile, the adsorption capacity of the best halloysite-based nanocomposites reached 270.27 mg/g (MB dye) and 294.18 mg/g (MC dye). The scanning electron microscopy (SEM) observations allowed these authors to conclude that the microstructure of halloysite-based nanocomposites was much rougher than in the case of pure chitosan. Furthermore, the loosened microstructure of hydrogel beads, which possess large SSA enables efficient molecular diffusion of adsorbate and its further immobilization. Alginate salts of alginic acid were also used to prepare the halloysite biopolymer nanocomposite. Their adsorption capacity is connected with abundant carboxyl groups having an affinity for metal binding [105]. Although pure alginate can act as an excellent adsorbent, its application is limited because of its low rigidity, low mechanical strength and dense gel layer, which hinder ion diffusion. The prepared organic/inorganic hybrid beads showed an improved MB dye adsorption capacity, with a maximum equal to 222 mg/g at 298 K.

The dynamic experiment in a column system revealed that 10 g of the hybrid beads are able to treat 29.7 L of MB aqueous solution (55 mg/L concentration) with a removal efficiency higher than 90% [105]. It is worth mentioning that hybrid morphology did not change during experiments, in contrast to pure alginate, showing its increased stability. Halloysite was used for the adsorption of selected organic molecules, e.g., aromatic naphthalene [106], 5-aminosalicylic acid [107] and chloroanilines [108]. The modification of halloysite surface by HDTMA increased naphthalene adsorption. The reported mechanism involved the organic partitioning of condensed aromatic rings in the hydrophobic environment of alkyl chains. Lee and Kim (2002) [106] proved that the amount of adsorbed HDTMA is less important than its conformation and configuration, which strongly affect the partitioning effect. The adsorption properties are often studied in the context of medical applications (i.e., drug delivery). A strong interaction between halloysite surfaces and 5-aminosalicylic acid (to cite one example) was reported [107]. Thus, the clay mineral can act as a promising support for drugs. The acid-activated halloysite has a strong affinity to remove chloroanilines such as 3-chloroaniline, 4-chloroaniline and 3,4-chloroaniline from aqueous solutions [108]. The halloysite with an adsorbed dye can serve as a functionalized nanomaterial that induces the degradation of complex organic compounds. For example, a clay mineral-based hybrid photosensitizer was obtained by surface modification of halloysite by Rose Bengal dye [109]. The hybrid material can generate singlet oxygen, which significantly enhances the photodegradation of a common pesticide 4-n-nonylphenol. The pesticide biodegradation kinetics are very slow, but the identified photodecomposition products are expected to be much more susceptible to environmental degradation with the help of bacteria.

1.3 Chitosan and its structure

Chitosan is a partially deacetylated product of chitin (a natural amino polysaccharide that serves as supporting material in crustaceans, insects, etc.) that predominantly consist of β-(1→4)-2-amino-2-deoxy-D-glucose units (deacetylated unit) and a lower percentage (usually less 20%) of β-(1→4)-2-acetamido-D-glucose (acetylated unit) [21, 110-113]. The chemical and physical characteristics of chitosan vary largely with its molecular weight, extent of deacetylation and degree of crystallinity, solubility, among others. Chitosan is of commercial interest based on its higher amount of nitrogen content in comparison with synthetic substituted cellulose [112]. Most polymers are commonly synthesized with many having lower biocompatibility and biodegradability properties. However, chitosan is considered as a suitably functionalized natural

polymer with good biocompatibility, biodegradability, adsorption properties among others. Previously, few of chitosan derivatives dissolved in common organic solvents [114] and some binary solvent systems [115]. Recently, many chemically modified chitosan structures having better solubility in common organic solvents have also been prepared [116]. Polymorphism is applicable to chitosan and chitin. This phenomenon being exhibited by chitosan gives rise to different forms of packing and as well as different degree polarity of the adjacent chains in the successive sheets. The two main polymorphs of chitosan are the hydrated form (tendon chitosan) and the anhydrous form (annealed polymorph) [117]. The uncommon functional chitosan characteristics could be determined by the chain conformation structure and the structural contacts around the domains of amino groups. The structural data of chitosan are obtained via analytical methods such as XRD, IR, NMR, thermo-physical methods, among others [111, 118-120]. The polar functional groups on chitosan have good affinity for intra-molecular and intermolecular hydrogen bonding, and in turn give rise to linear aggregates and rigid crystalline domains. It has been reported that the XRD patterns revealed orthorhombic unit cell for hydrated chitosan [118, 120]. Furthermore, 3 possible positions of water molecules in the asymmetric unit were suggested through modelling. However, polymorph density and thermogravimetric analysis data suggested two water molecules per chitosan identity period. The water molecules of the hydrated polymorph structure of chitosan stabilize it through the formation of column-like joints between the crystal layers [120].

Chitosan is of lower crystallinity than chitin, a feature that makes it to have higher accessibility to reagents. However, its decomposition prior to melting makes it a polymer without a specific melting point range like chitin. It has been reported that chitosan could exhibit different diffraction patterns to give orthorhombic and monoclinic unit cells based on its polymorphic modifications with acids such as formic, acetic, and propionic acids [121]. At times, the hydrated and anhydrous chitosan may have similar crystal structure however, transformation from hydrated form to anhydrous is irreversible and it results into loss of chitosan solubility and changes in biological properties [121]. FT-IR and NMR have also been utilized to reveal the structure of chitosan. Characteristics FT-IR absorption signals have been attributed to various stretching and bending vibrations in chitosan molecule. The stretching vibration bands around 3450–3400 cm^{-1} have been ascribed to ν(N–H) and ν(O–H). The methyl group in $NHCOCH_3$, methylene group in CH_2OH and methyne group in pyranose ring could be ascribed to stretching vibrations in the region

of 2940–2850 cm^{-1} [122]. The vibration around 1680–1620 cm^{-1} and 1550–1300 cm^{-1} could be ascribed to ν (C=O) in $NHCOCH_3$ group (Amide I band) and ν(C–N) in Amide II respectively. Furthermore, the area between 1180 and 1000 cm^{-1} is usually saturated as a result of three distinct vibrational modes of C–O–C, C–O–H and C–C ring vibrations [123]. Chitosan is soluble in most acidic solution. Formic acid and ethanoic acid are commonly utilized for chitosan dissolution. Large number of cationic sites produced on chitosan because of NH_2 protonation (via acid treatment) of the polymeric chain enhances its solubility, thereby assist in obtaining materials of higher polarity and as well enhancing the degree of electrostatic repulsion [113]. Research findings have revealed that chitosan is soluble in dimethylsulphoxide, p-toluene sulphonic acid and 10-camphorsulfonic acid [113]. Sulphuric acid is not often applied for dissolving chitosan as it generates insoluble chitosan sulphate [117]. Fatty acids medium has not been considered appropriate for dissolving chitosan [124]. In the viscometrical assessment of chitosan solutions made in ethanoic acid/sodium acetate and ethanoic acid/NaCl as revealed by Costa et al., the viscosity as well as flow rate assessment of chitosan solutions considerably dependent on the extent of deacetylation of chitosan molecules [125]. Chemical properties of chitosan depend on its functional properties. The acetylated part could associate via hydrogen bonding and as well engaged in hydrophobic relationship that considerably improve the stability of the molecule, which in turns impact certain rigidity that strengthening its structural features. The NH_2 and OH functional groups on chitosan are susceptible to modification and could in turn enhance its functional characteristics [117].

These chemical properties of chitosan allow good number possible chemical interactions with inorganic and organic compounds. Furthermore, the chemical characteristics features of chitosan relate to biological properties such as biocompatibility, biodegradability and specific interactions with various living tissues [126-129]. Findings have revealed that some properties of chitosan such as toughness and water absorption could be altered through modification with polyvinyl acetate [130]. Attachment of transition metals onto chitosan mainly involves coordination of metal with the amino group of chitosan and the coordination of divalent heavy metals with $–NH_2$ are obtained in a mole ratio of 1:1 [61].

1.4 Preparation of chitosan

In recent times, chitosan has been prepared from fungi and could be isolated from the cell walls of this organism using microwave assisted method [131], autoclave [132] and liquid

cultivation methods [133] among others. It is also obtained via enzymatic action of chitin deacetylase on chitin source. Chitosan obtained via microwave assisted extraction are better deacetylated with higher yield compared to conventional autoclave method. Although, findings revealed that both methods produced chitosan that is similar in molecular weight and crystallinity [131]. Isolation process of chitosan from fungi requires a lower number of chemical reagents as only mild conditions are employed for extraction. The processing stages required are minimal and do not involve demineralization and depigmentation, therefore it involves less toxic waste materials and could be considered as a greener process. The preparation procedure via autoclave as reported by Sebastian et al. involves suspending finely ground mycelia in 1 M NaOH and then autoclaved at 121 ◦C for 15 min. The alkali insoluble material obtained was extracted into 2% acetic acid, centrifuged and the medium pH of the supernatant was controlled to 10 and then re-centrifuged to obtain chitosan precipitate [131, 132]. The processing stages of skeletal component of crustaceans to chitosan are Demineralization via acid treatments (dil. HCl is used); deproteinisation using NaOH solution at about 100ºC (to produce Chitin); and deacetylation using NaOH solution. Chitosan is usually synthesized by deacetylating chitin with the aid of aqueous alkali solution (40–50%) at 100 ºC– 160 ºC or slightly higher to remove some or almost all the acetyl groups from the polymer for few hours (Figure 1.10). Since acidic reagents hydrolyze the polysaccharide; therefore, alkaline methods are employed for N-deacetylation of chitosan. Crabs, Shrimps, and prawns have been reported as the primary precursor of chitin required for chitosan preparation and 40–60% alkaline solution (NaOH or KOH) has utilized to obtain 65–97% deacetylation [134]. The chitosan product could be processed to have degree of deacetylation to the value of 0.95. Repeated alkaline treatment is required for complete deacetylation. Chitosan is now available in the market in various grades of degree of deacetylation. The extent of deacetylation is influenced by factors such as concentration of the alkaline solution, temperature, reaction time, treatment method of chitin adopted, particle size, and density of the chitin. The preparation conditions are monitored significantly to prepare a well deacetylated chitin required to yield a chitosan product sufficiently soluble in dilute acetic acid [124]. Deacetylation of chitin to produce chitosan is routed either heterogeneously or homogeneously. The heterogeneous process involves subjecting chitin to hot concentrated NaOH treatment for few hours to give insoluble chitosan of 85–99% deacetylated chitin. Whereas, in homogeneous transformation procedure, alkali chitin is obtained first in conc. alkali solution at 25 ◦C for 3 h and then suspended

in an ice at 0 ˚C to yield a soluble chitosan with 48–55% degree of acetylation. This method yields chitosan having homogenously distributed acetyl functionality along the polymeric chain [135]. The deacetylation of β-chitin extracted from squid pens is more rapid but could produce a heavily colored chitosan. Since β-chitin deacetylation could be achieved at lower temperature than α-chitin, reaction around 80ºC is sufficient for deacetylation and reduction of color intensity [124]. Various chemical treatments conditions reportedly yield various degree of deacetylation. Chitin treatment with 12.5 M NaOH (140 ˚C for 4 h) yielded degree of deacetylation > 80% [136]; 18 M NaOH (90 ˚C for 7 h) yielded 94.9% [137]; Chemical 50% NaOH (90 ˚C, 30 h) produced 74% [138] and ultrasound-assisted chemical method in 40% NaOH under alternate condition of irradiation (45 min) and non-irradiation (30 min) procedures yielded 77.9% [139].

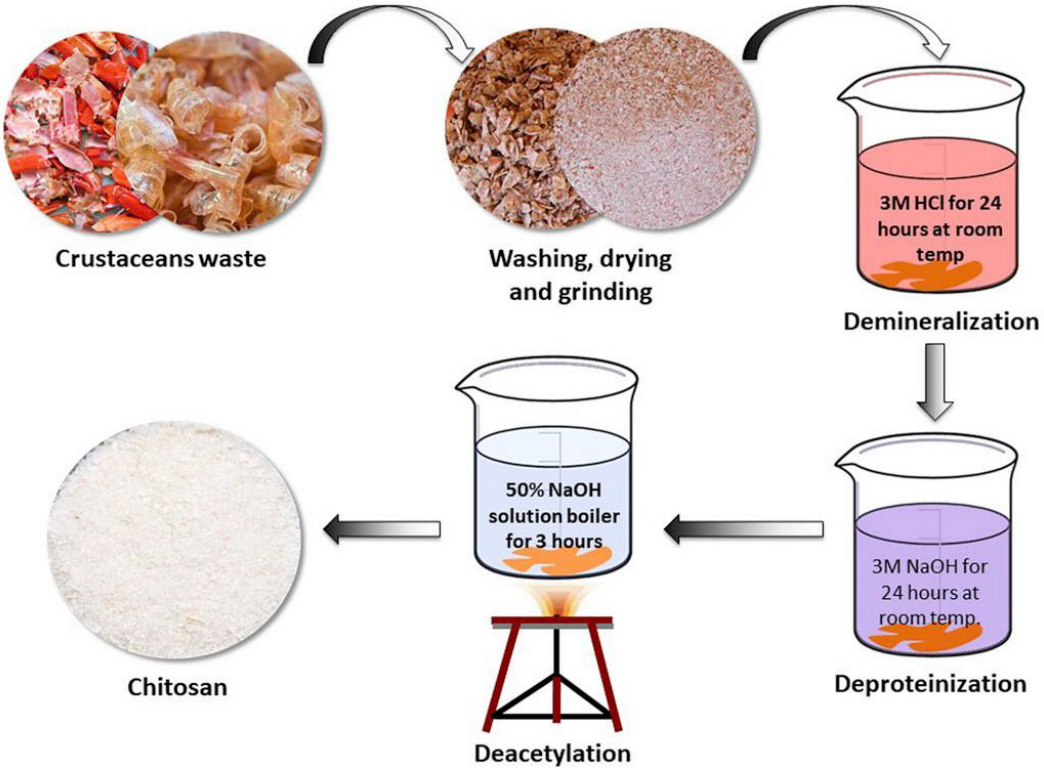

Figure 1.10 - Procedure for Chitosan Extraction from various sources.

1.5 Modification of chitosan

Modification of chitosan has been carried out through chemical or physical process, or combination of both processes. Physical modification includes blending and conversion of chitosan's forms. The physical modification of chitosan usually expands its polymer chains for

good access to the internal sorption sites and as well decreases its crystalline state. Blending of chitosan with some materials such as active carbon, graphene, Fe_3O_4, γ-Fe_2O_3 and clay [140-142] is another good method of synthesizing composites with the desired structure, which could as well enrich chitosan with better physical strength, adsorption performance, temperature sensitivity, magnetism, etc. [60, 143].

For instance, Chang and Juang prepared chitosan/activated clay composite for adsorption organic acids (tannic acid, humic acid) and dyes (methylene blue, reactive dye RR222). The adsorption capacities obtained for the chitosan/activated clay composite beads were much comparable to those with chitosan beads but larger than those obtained for the activated clay [141]. The common approaches to chitosan's modifications via chemical treatments are cross-linking and graft co-polymerization, composites preparation, and substituent incorporation among others. These methods have been applied in processing chitosan into various materials to improve its performance for various applications [141, 144, 145]. For instance, compressed porous layer of chitosan with good mechanical strength used as "buttresses" was prepared by Ladet et al., 2015[146]. Although, damage could be caused to the porous layer of chitosan-based materials in an attempt to prepare highly compressed chitosan-based materials. The porosity of chitosan-based materials is maintained and enhanced by lyophilizing a chitosan-based materials, and subsequently compresses and reacts with aqueous ammonia [146].

1.6 Chitosan cross-linking

Modification of chitosan through cross-linking has been widely applied to prepare various chitosan-based materials. Cross-linking affects some common characteristics of chitosan such as mechanical strength, stability, swelling effect, permeability, solubility among others [147]. The process of chitosan modification via cross-linking is crucial to obtain products with enhance mechanical resistance, good stability at drastic pH with reduce hydrophobicity property [60]. Different cross-linkers that favorably bonded to the readily available amino and hydroxyl groups of chitosan have been utilized for chitosan modification in various adsorption applications. The procedure employs the use of cross-linking agents (such as epichlorohydrin, tripolyphosphate (TPP), glutaraldehyde) for the modification process [148, 149]. Although cross-linking lower adsorption characteristics of chitosan, it has been used to improve mechanical strength of chitosan [150, 151]. Crosslinking of chitosan in homogeneous condition leads to enhanced metal binding capacity because of increase in hydrophilicity caused by partial destruction of crystallinity as

compared to heterogeneous cross-linking [152]. Chitosan is being reported as a cationic polymer with high sorption affinity for most dyes especially the anionic dyes [26, 153]. It has been developed into various materials via crosslinking processes for good stability and in turn a better performance on dye removal [154, 155]. The amine sites on the chitosan polymeric chain are the main reactive groups for metal ions, though hydroxyl groups may also contribute to the adsorption. These functional groups interact with metal ions through different mechanisms depending on the metal, the pH, and the matrix of the solution. The lone pair on nitrogen may bind with metal cations at pH close to neutrality [156]. Crosslinking often renders the amine site on chitosan polymer unavailable for attachment to the metal cations and dyes thereby lowering the adsorption capacity. The protonation of amine site makes the chitosan/chitosan-based polymer effective at attracting anions such as metal anions and anionic dyes [157]. Protonation is significant for the electrostatic attractions of anions. Chassary et al. reported the effectiveness of crosslinked chitosan for adsorption of metal anions (arsenate and molybdate). pH has a critical effect on metal speciation in solution. The distribution of metal species depends on pH, metal concentration and the composition of the solution, and this could strongly influence the charge of metal species present in the solution and their affinity for the sorbent [157]. The usefulness of chitosan and chitosan-based materials as a common carrier for quite a number of drugs as well in drug delivery has gained attention in recent times [158-160]. Consequently, it has been applied for detoxifying wastewater containing pharmaceuticals as pollutants [137, 161]. The cross-linking approach can be distinguished into chemical and physical cross-linking processes based on interactions between crosslinking agents and chitosan [162].

1.6.1 Chemical cross-linking

Chemical cross-linking or covalent cross-linking influences the physicochemical characteristics of chitosan and hence its application since the gelation is irreversible. Better stability that could be obtained in modified-chitosan is attributed to the binding of chitosan with the cross-linker through covalent bond. The commonly applied chemical crosslinking agents for chitosan modifications are dialdehydes (such as glutaraldehyde or glyoxal) [126-129, 163-166] and genipin [167]. A good performance of chitosan–cellulose hydrogel beads cross-linked with ethylene glycol diglycidyl ether (EGDE) as an adsorbent for Cu adsorption have also been reported by Li and Bai. The prepared hydrogel beads material was mechanically stronger with improved chemical stability and porosity of the chitosan–cellulose beads in acid solutions down to pH 1 via

crosslinking reaction using EGDE [168]. Chemical crosslinking could alter biological application characteristics of chitosan and in turn could limit its pharmaceutical applications. Furthermore, the ease of dissolving chitosan depends on pH and the amino groups in its molecule. Its higher ease of dissolution in a very much acidic environment is a major difficulty for its application various in various capacities. This effect can be managed by employing irreversible chemical crosslinking process with cross-linkers such as glutaraldehyde, formaldehyde, genipin, etc. [169]. Investigation on cross-linked chitosan prepared by microwave assisted irradiation method revealed the existence of a Schiff base (a C=N bond) between chitosan (its amino group) and vanillin (its aldehyde group) which ascertained the cross-linking process [147].

1.6.1.1 Formaldehyde cross-linked chitosan for adsorption application

Limited works are available in literature on the use of formaldehyde as a cross-linker for chitosan modification. This relates to the lower stability and mechanical strength of formaldehyde cross-linked chitosan materials. Xue et al. utilized formaldehyde as a cross-linker in the preparation of novel cross-linked chitosan resin synthesized by orthogonal procedure[170]. The prepared resin displayed good features in terms of sphericity and acid resistance under the optimal experimental conditions of 1:6 chitosan/formaldehyde at 60 $^{\circ}$C. Monier (2012) [171] also prepared cross-linked magnetic chitosan–thioglyceraldehyde resin using formaldehyde as crosslinker for the adsorption of Hg^{2+}, Cu^{2+} and Zn^{2+} ions from aqueous solution. The uptake of these ions (Hg^{2+}, Cu^{2+} and Zn^{2+}) was reported to be effective in the higher pH range and at lower temperatures. Rapid uptake reported for these ions by the prepared modified chitosan resin makes it potentially suitable for continuous flow water treatment systems [171].

1.6.1.2 Dialdehydes cross-linked chitosan for adsorption application

Dialdehydes are toxic at certain concentration [28, 172], therefore unreacted dialdehydes cross-linkers must be properly removed during preparation process. Sun et al. reported that cross-linking network is optimum at 0.51:1 aldehyde/amino mole ratio for Pb^{2+} adsorption, and it doesn't only reduce the opening of the network arrangement through additional linkages along the polymer units, but also expands the polymer network in such a way that the steric hindrance effect is minimized and in turn increases its adsorption capacity. In excess of the dialdehydes cross-linker, a more hydrophobic character could be produced. Decreasing the amount of aldehyde group through the cross-linker hinders the processing of chitosan into closely packed chain arrangements with minor influence on lowering of swelling capacity.

1.6.1.2.1 Glutaraldehyde

Glutaraldehyde is the most applied dialdehyde crosslinker in chitosan modification for adsorption of pollutants. Glutaraldehyde cross-linked with carboxymethyl-chitosan (CMC) was prepared by Sun et al. to improve the adsorption selectivity of chitosan-based materials for heavy metals [145]. Schiff's base formation that accompanies the crosslinking of glutaraldehyde with chitosan render the amine group taking part in the chemical linkages unavailable for adsorption, and thus decreases the sorption effectiveness whenever the amino group on the chitosan serves as the primary adsorption sites [145]. Glutaraldehyde was used as a cross-linker in the preparation of crosslinked N, O-carboxymethyl-chitosan resin-Pb^{2+} ions (crosslinked CMC template) developed for better adsorption selectivity for heavy metals. The fundamental point of attachment was suggested as the carboxymethyl functionality instead of the NH_2 group of CMC, and its processing into 3D structural arrangements is a property suitable for an enhanced Pb^{2+} ions adsorption[145]. Glutaraldehyde cross-linked metal-based chitosan composite has shown good performance on the removal of heavy metals from aqueous medium. A good example is the development of titanium–chitosan composite prepared by Lingfan Zhang et al. through metal-binding reaction of titanium ions with chitosan followed by crosslinking with glutaraldehyde [173]. In a similar view, Fe^{3+}-chitosan materials crosslinked with glutaraldehyde was found effective for the removal of Cr^{6+} and the mechanism of detoxification of Cr^{6+} have also been studied. In the preparation of chitosan/Fe (III) complex, chitosan would dissolve in 0.1 M $FeCl_3$, since the pH of 0.1 M $FeCl_3$ is much acidic. Therefore, chitosan/Fe (III) complex would be precipitated out from the acidic solution through the addition of ethanol and then washed with ethanol [174]. The XPS spectra revealed the role of primary alcoholic group on C-6 of the crosslinked chitosan/Fe (III) complex as an electron donor during Cr^{6+} reduction which was subsequently oxidized to a carbonyl group. Although, findings revealed an enhance Cr^{6+} reduction by glutaraldehyde cross-linked chitosan/Fe (III) complex compared with normal glutaraldehyde cross-linked chitosan.

Budnyak et al. compared the performance of chitosan-silica composite with chitosan beads partially crosslinked with glutaraldehyde on the removal of micro-quantities of V(V), Mo(VI), and Cr(VI) oxoanions from aqueous solutions with better adsorption capacities reported for the partially cross-linked chitosan beads [175]. Whereas disparity in adsorption efficiency of chitosan-silica compared to partly crosslinked chitosan has linked to the quantity of accessible adsorption sites of the chitosan-silica composite, surface area, and morphology of composite for adsorption

of V(V), Mo (VI), and Cr (VI) oxoanions. A review on Hg (II) removal using chitosan and chitosan derivatives worked on by Miretzky and Cirelli reported outstanding adsorption capacity for chitosan (1127 mg/g) at pH 6.0 and particle size 0.177 mm, 1895 mg/g for glutaraldehyde-crosslinked chitosan immobilized in polyvinyl alcohol and 1604.7 mg/g for glutaraldehyde-crosslinked chitosan grafted with cysteine [58]. Ultrasonic irradiation method can be utilized for crosslinking chitosan polymers in the presence of cross-linkers. Mallakpour and Khadem prepared cross-linked nanocomposite films using chitosan and different weight percent of N-doped graphene quantum dot through ultrasonic sound with addition of glutaraldehyde as a crosslinker for sorption of Cd(II) ions [176]. Textile reactive dyes when considered as a contaminant in an aqueous medium have been removed using cross-linked chitosan beads. Deepika et al. utilized chitosan beads modified via crosslinking (using 0.05 M glutaraldehyde and 40% glyoxal as crosslinkers) to remove acid orange-10 and direct black-22 dyes from effluents [177]. The deduction from the experimental data analyzed using Langmuir isotherm model showed that glyoxal cross-linked chitosan removed the dyes better when compared with glutaraldehyde cross-linked chitosan, and the cross-linked chitosan can be applied acidic medium that dissolved the non-crosslinked chitosan beads [177].

Mahaninia and Wilson revealed that cross-linked chitosan beads prepared with 5 wt.% glutaraldehyde and 5 wt.% epichlorohydrin cross-linkers possess good affinity for roxarsone dye in a fixed bed column [178]. Higher amorphous characteristics of the 5 wt.% glutaraldehyde and 5 wt.% epichlorohydrin cross-linked bead materials revealed through the XRD analysis indicate the disruption of the intra- and intermolecular hydrogen bonding network as a result crosslinking. Whereas the adsorption efficiency of chitosan adsorbents is reported to be inversely proportional to the degree of crystallinity. However, the 5 wt.% glutaraldehyde cross-liked chitosan was reported to have higher adsorption capacity (104 mg/g) for roxarsone dye removal compared with 5 wt.% epichlorohydrin cross-linked one 89.1 mg/g [178]. Omidi and Kakanejadifard also prepared graphene-chitosan composite using glutaraldehyde as cross-linker for dye adsorption. The adsorption experimental data evaluated give adsorption capacity of 384.62 mg/g in Langmuir isotherm model. The graphene-chitosan composite aerogel is easier to recycled [179]. In addition to the improved surface area, porosity that could be accomplished via crosslinking process, the accessibility of adsorption site of chitosan-based materials by dye molecules increases with greater amorphous character that at times emanated from cross-linking process [178]. Alkali gelation-

thermal cracking process was used to impregnate nano-Fe_3O_4 into chitosan hydrogel as reported by Bai et al. In the preparation process, the microspheres were cross-linked with 5% glutaraldehyde, before being pyrolyzed in a reactor at 350 ˚C under nitrogen. The prepared material has been found effective for the removal of doxycycline (DC) antibiotics [180]. In addition, many of the recent development involving the use of glutaraldehyde as cross-linker for chitosan modification always incorporate grafting to improve the adsorption capacity of the chitosan-based materials. In this procedure, the cross-linked process could take place as a reaction between aldehyde of the cross-linking agent (e.g glutaraldehyde) and amine of chitosan to give imine functionality. Glutaraldehyde cross-linked carboxyl-grafted chitosan (CsSUC, CsMAL, CsITA and CsTACON) using succinic anhydride (SUC), maleic anhydride (MAL), itaconic acid (ITA) and trans-aconitic acid (TACON) as grafting agents for preferential removal of diclofenac from aqueous pharmaceutical matrix have also been reported [181].

1.6.1.3 Epichlorohydrin cross-linked chitosan for adsorption application

Epichlorohydrin (ECH) is among the commonly applied chemical cross-linkers for chitosan modification for adsorption of pollutants from wastewater. ECH cross-linked-chitosan based materials offer a stable and sustainable mechanical strength even in acidic medium [182]. Chitosan–Fe^0 nanoparticles have been prepared for sorption of Cr^{6+} from wastewater. Recently, epichlorohydrin cross-linked Fe^0 nanoparticles-chitosan beads (ECH–CS–NVZI) has been prepared for reduction of Cr^{6+} from wastewater [183]. A remarkable decrease in crumpling ratios revealed a significant improvement in the mechanical strength of Fe^0-nanoparticles–chitosan beads; likewise, the thermal stability of the prepared beads was enhanced [183]. It was reported that the mean aperture size of beads that becomes smaller after crosslinking with ECH indicates favorable environment for enhancing the mechanical strength of beads. A larger porosity for better uptake of Cr^{6+} could be obtained via processing of chitosan into (ECH–CS–NVZI). Chitosan bead cross-linked with glutaraldehyde (GLA), epichlorohydrin (ECH) and ethylene glycol diglycidyl ether (EGDE) reported by Patrulea et al. was found to be stable in both acidic and alkali medium [184]. It was also reported that the application of the cross-linked chitosan beads on the uptakes of Cu(II) ions gives adsorption capacity of 59.67 mg/g for chitosan-GLA, 62.47 mg/g chitosan-ECH and 45.94 mg/g for chitosan-EGDE [184]. Nishad et al. (2017) [185] prepared nano-titania impregnated epichlorohydrin crosslinked chitosan (TA-Cts-Epi) beads for enhancing the sorption of antimony. The epichlorohydrin utilized as the crosslinker effected significant changes in

physical and sorption properties of the beads. Interestingly, crosslinking with epichlorohydrin makes the titania-chitosan beads (TA-Cts) a better sorbent for antimony with increased uptake. Epichlorohydrin doesn't act as a passive matrix component, but instead the epichlorohydrin moieties actively take part in binding process, possibly through the hydroxyl and the ether groups emanated via the crosslinking reaction [185]. The stability, swelling behavior and sorption kinetics of the beads were altered, crosslinking significantly increased the uptake of the anionic species via electrostatic interactions.

1.6.2 Physical cross-linking

Physical crosslinking process involved ionic bridge linkages between negatively charged species and positively charged chitosan chain [162]. Ionic cross-linkers such as citrate, sulphate, phosphate-bearing groups are commonly used for physical crosslinking process. Chitosan-based polyelectrolyte complexes have been obtained via physical crosslinking [159]. However, some cations (e.g., Fe(III), Pt(II)) have also been applied as ionic crosslinkers [126-129, 186]. Inorganic phosphate salts (e.g., tripolyphosphate pentasodium) have also been reported. Physical crosslinking process is a simpler modification procedure than the chemical crosslinking process. It doesn't require the presence of catalysts or the intense purification of the final product. The modification process enhances the stability of the chitosan through interaction between cationic chitosan and negatively charged ionic cross-linker. If large anionic molecules (ionic cross-linker such as polyelectrolyte complexes) are used, it buffers the solution and as well slows down the rate of chitosan hydrolysis. Chitosan cross-linked with small size ions (such as citrate and sulphate) are unstable over extended time due to the occurrence of electrolytes and pH variations when stored in solution. As such, very little work is available in the literature on the use of small-size ionic cross-linkers to strongly enhance the physicochemical stability of chitosan material [162]. The chemical stability of chitosan membrane treated with polyethylene glycol as porogen was improved via crosslinking with NaH_2PO_4 [187]. Adsorptive membranes are designed to possess reactive functional groups as active sites, improve porous structure and large surface area [187]. Furthermore, ionically cross-linked chitosan hydrogels are relatively effective in drug delivery process than the covalently cross-linked ones. Ionically crosslinking agents are utilized for controlling the discharge of pharmaceuticals in both acidic and alkaline environment [188].

1.6.2.1 Metal ions cross-linked chitosan for adsorption application

Titanium, Iron and Platinum are commonly applied metal ions for ionic cross-linking of chitosan for adsorption application. The metal-binding ability of chitosan is an important feature in ionic cross-linking. The metal-binding ability was utilized to synthesize a titanium–chitosan composite for adsorption and reduction of Cr^{6+} from aqueous medium. Zhang et al. prepared titanium–chitosan composite by contacting under stirring a chitosan solution (made in 2% (v/v) acetic acid) with titanium solution follow by precipitation of the composite in 2.0 M NaOH [173]. Zhang et al. also reported that the XRD patterns of the titanium-chitosan (Ti–CTS) revealed the conjugation of Ti^{4+} and chitosan (2θ = 19.7º shifted to 25.6º) with a decrease in the crystalline nature to some extent. It was reported that the Cr^{6+} were adsorbed and reduced to the less toxic Cr^{3+} after contacting with the titanium-chitosan composite [173]. Fixed-bed columns have also been utilized to assess the removal capacity of Cr (VI) on cross-linked copolymers and the adsorption capacity increase with bed height. Demarchi et al. reported good performance for crosslinked chitosan–Fe(III) complex (Ch–Fe) towards Cr^{6+} removal from aqueous solution using a fixed-bed column prepared with polyethylene tube that possess inner diameter of 0.75 cm and height of 5.5 cm [189]. In accordance with the report in the literature, the mechanism of Cr adsorption proves that Cr^{6+} exists as $HCrO4^{-}$ at optimum pH and could adhere to Fe^{3+} via electrostatic attraction and ion- exchange interaction. The adsorbed Cr^{6+} are partially reduced primary alcoholic function on chitosan at (C-6) while the cleavage of reduced Cr^{3+} and Fe^{3+} center take place. The free Cr^{3+} then re-adsorbed by Cr-bonding groups; also, Cr^{6+} is partly reduced to Cr^{3+} by the OH or NH_2 groups on the chitosan–Fe composite during adsorption via electrostatic attraction. Fe (III)-cross-linked chitosan beads were synthesized by Wu et al. to explore the primary mechanism of Cr^{6+} removal at lower Cr^{6+} concentration within pH of 2.0–8.0. Chitosan was dissolved in 0.1 M $FeCl_3$ and stirred at room temperature for 4 h. The beads were produced by contacting Chitosan-$FeCl_3$ solution with NaOH with the aid of syringe [25, 26]. The results obtained showed that Cr^{6+} uptake was effective within the pH range of 2.0–6.0. Furthermore, the surface area [176] and porosity [22] could be improved via crosslinking process and incorporation of zero-valent iron [190] into the chitosan's polymeric structure. This in turn increases the percentage removal of metal ions in addition to the possible coulombic attraction between the metal ions and functionality (such as OH) on the modified chitosan that could also play significant role in sorption of metals. Chitosan has better chelating ability in comparison to other natural polymers obtained from seafood wastes and natural substances like bark, activated sludge and the

synthetic polymer poly(4-aminostyrene). The ability of chitosan to bind transition metals in the presence of alkali and alkaline earth metals has also been investigated [152].

1.6.2.2 Tripolyphosphate cross-linked chitosan for adsorption application

Ionically and chemically cross-linked chitosan adsorbents with good adsorption efficiency for anionic dyes removal were prepared by Chiou et al. The cross-linked chitosan beads were reported to have better performance on the removal of the applied reactive dyes, acid dyes and direct dye than commercial activated carbon used for the study [191]. The beads formed rapidly as reported and were rigid. The rigidity was attributed to the ionic attractions between $P_3O_{10}^{5-}$(TPP) and the NH_3^+ group of chitosan in acidic medium. This improves the mechanical strength of the chitosan beads and the time required to form beads is also reduced. A literature has also reported that using sodium tripolyphosphate solution (TPP) as cross-linker makes membrane flexible but at the same time can also enhance the chemical stabilities of chitosan membrane [187].

1.7 Grafting copolymerization of chitosan

Grafting approach for modification of chitosan is often used for improving certain characteristics of chitosan-based materials featuring enhance chelation [192] or complex formation properties, antimicrobial effect [193] or improved adsorption potential [62]. Investigations on graft copolymerization of chitosan-based materials with special application as bioactive materials and biomedicine have been reported [62]. Some unique characteristics of grafted or functionalized chitosan could be broadly influenced by the molecular structure, length, and number of the side chain. These variables could affect not only the characteristics of the grafted chitosan polymers but also the graft parameters [113]. Grafting could be initiated using a chemical initiator [194, 195] system or through radiation induced process [196]. Recently, several initiators such as, ammonium persulfate, potassium persulfate, ceric ammonium nitrate, thiocarbonation-potassium bromate, potassium diperiodatocuprate (III), 2, 20-azobisisobutyronitrile and ferrous ammonium sulphate have been utilized for graft copolymerization [62]. Also, γ irradiation induced graft copolymerization and enzymes assisted method has also been reported [62, 197].

1.7.1 Graft copolymerization-free radicals-initiated process

Free radical initiated-graft copolymerization process has been used by various scientists for improving the properties of chitosan for various applications. The polyvinylics and polyacrylics are the frequently grafted materials on polysaccharides [113, 116, 198]. Vinyl grafted copolymers are obtained through the modification of pre-existing polymer chain (trunk polymer) that

composed of different structural units developed from the trunk polymer skeleton. The basic mechanism starts with the creation of free radical sites on the trunk polymer chain and then binding of the vinyl monomer with the radical to propagate into a new polymeric chain that is covalently bonded. This copolymerization process could offer the chance of preparing polymeric material that mainly combines the properties of the polymer chains [198]. Chitosan-graft-poly (vinyl acetate) copolymers were synthesized by Don et al. via grafting with a redox initiator, cerium ammonium nitrate. The chitosan molecules contributed to the reaction process and a stable dispersion solution was reported [130]. Ceric ammonium nitrate initiator has also been utilized for grafting methyl acrylate onto chitosan [199]. Liu et al. also prepared chitosan poly (methacrylate) composites through grafting of glycidyl methacrylate and α- methacrylic acid monomers on chitosan using azobisisobutyronitrile as initiator [200]. Kim et al. prepared Chitosan-g-N-isopropyl acrylamide (CS-g-NIPAAm) copolymer through grafting of NIPAAm onto chitosan initiated using ceric ammonium nitrate (CAN). The grafting of CS-g-NIPAAm was reportedly maximized at 2×10^{-3} M of CAN, 0.5 M NIPAA monomer concentration at 25°C and 2 h of reaction time. The hydrogels obtained from the crosslinked CS-g-NIPAAm possess relatively large amount of water within short period (30 min) and the swelling capacity also changes with reaction conditions like pH and temperature [201]. El-Tahlawy et al. reported work on the use of 2,2-Azobis(2-methylpropionitrile) (AMPN) initiator for grafting methacrylic acid (MAA) onto chitosan. The optimum conditions reported for the preparation are: AMPN (0.125%), material: liquor (1:30), and reaction temperature (80 °C). The resultant product could be cross-linked using epichlorohydrin as cross-linker in alkaline medium [202]. Potassium diperiodatocuprate (III) has been utilized as a redox system initiator for functionalizing chitosan using methyl acrylate (MA) in alkali medium [194]. The mechanism of radical formation for Cu (III)–chitosan system using a redox initiator was proposed in the work done by Liu et al. The single electron transferred in changing Cu (III) into Cu (II) could initiate the grafting process [194].

1.7.2 Graft copolymerization – γ-irradiation initiated process

Hydrogel of chitosan-based polyacrylamide has been prepared by ^{60}Co-γ-ray irradiation at different irradiation doses (5, 10 and 15 kGy) for induced graft polymerization [197]. High irradiation dose decreases the molecular weight of chitosan through degradation [203]. γ-irradiation up to 25 kGy may not degrade or influence any significant difference in the chemical nature or anti-inflammatory properties of chitosan [204]. In the mechanism of chitosan radiolysis

reported by Gryczka et al., species could undergo β-scission at a temperature lower than 25°C leading to ring opening (radical C5) and chain scission (radicals C1 and C4) to produce a secondary active radicals and carbonyls with active C-H bonds. Consequently, H abstraction favored by the closeness of the active centers eventually generates stable α-carbonyl terminal radical products. Furthermore, in chitosan radiolysis mechanism, nitroxyl radical signals could be observed at higher irradiation doses as secondary species obtained from the radiolysis of the NH_2 group [203].

1.7.3 Graft modified chitosan for adsorption application

Graft copolymerization, give rise to materials that can be modified to suit a specific application [205]. Grafting of chitosan permits the formation of functionalized chitosan species by covalent binding of a molecule onto the chitosan backbone [161]. Grafting procedures of some selected reagents (such as melanin, poly (1-vinyl imidazole), ethyl acrylate, methyl methacrylate, ethylenediamine, methyl alanine, polyethyleneimine and polyacrylamide) on chitosan for adsorption of metals/metal ions, dyes and pharmaceuticals are reviewed.

1.7.3.1 Procedures of selected graft modified chitosan for metal/metal ion adsorption

Chitosan modified through grafting is of great importance in metal recovery. Its derivatives have been largely prepared with the aim of removing metal ions by introducing functional groups onto the skeletal structure of chitosan [206, 207]. Functionalization of chitosan can increase the number of sorption sites, alter the pH range for metal sorption and modified the attachment sites for preferential attachment of target metal. Invariably, sorption of metal cations sometimes results into chelate formation [161]. Melamine grafted chitosan nanocomposite was synthesized by Ibrahim et al. as an effective material for ferric ions adsorption. The possibility of crosslinking using glutaraldehyde and epichlorohydrin in 0.1% nano-Montmorillonite (w/w % based on chitosan) was also reported. The preparation involved contacting chitosan (CS) solution (in 5% acetic acid) with 0.1% of nano-Montmorillonite (Nano-MMT), 0.01 mol of glutaraldehyde under refluxing at 80ºC. Under optimum conditions of the adsorption experiment, the prepared nanocomposite shows 99.97% ferric ions uptake with good reusability till third cycle [208]. The modified-chitosan's functional groups coordinate with ferric ions with the Fe^{3+} acting as the Lewis acid that take up electron pairs from NH_2 and OH groups of chitosan, OH group of MMT and amino group of Melamine [208]. Trimethoxysilyl group terminated poly(1-vinylimidazole)-modified-chitosan composite prepared by Islam et al. was developed via single-step free radical

initiated-graft polymerization of chitosan functionalized with vinyl imidazole [209]. The chitosan was modified by dissolving chitosan in 1% acetic acid followed by addition of tri-methoxysilyl group telomerized poly(1-vinylimidazole) [210]. The solution was stirred, transferred into a petri dish, dried at 50–60 °C and then heated to improve chemical coupling. The adsorbent was utilized for the uptake of Cr^{6+} ions from aqueous medium with a maximum adsorption capacity of 196.1 mg/g. Ethyl acrylate has been grafted onto chitosan as reported in the work done by Maleki et al. It could be prepared by contacting ethyl acrylate (10 equiv./NH_2 in chitosan, 0.5 mL) with chitosan solution under continuous stirring at 50 °C for 10 days. Small amount of the reaction mixture (40 mL) could be precipitated out using $NaHCO_3$. The sorption of heavy metal cations (Pb^{2+}, Cd^{2+} and Zn^{2+}) using the prepared material investigated showed good performance on decontamination of the wastewater in batch mode [211].

1.7.3.2 Procedures of selected graft modified chitosan for dye adsorption

The adsorption efficiency of grafted copolymers such as chitosan could be significantly increased through grafting/or functionalization of its side chains [212]. Singh et al. reported a poly(methyl methacrylate) grafted chitosan having an adsorption capacity for azo dyes removal to be three times that of pure chitosan as the adsorbent was also much effective for decolorizing textile industry wastewater than the chitosan alone [213]. As reported by Singh et al., the procedure of chitosan grafted with poly (methyl methacrylate) involved contacting methyl methacrylate and ascorbic acid with chitosan solution made in formic acid placed on water bath under fixed time and temperature. $K_2S_2O_8$ could be subsequently added, and graft copolymerization was allowed for 1 h to give Chitosan-graft-poly (methyl methacrylate). A biopolymer of chitosan grafted with ethylenediamine (EDA), and methyl acrylate (MA) had been applied to the removal of Congo red dye from water as reported by Tahira et al. In preparing EDA grafted-chitosan, chitosan in acetic acid solution was added to EDA/ethanol (1:1 v/v) solution to form beads. MA grafted chitosan was made by contacting MA with chitosan solution, and the mixture was subsequently transferred to NaOH solution containing propylene glycol for precipitating out the grafted chitosan [214]. Ultrasonic-assisted oxidative-radical copolymerization using ammonium persulfate as initiator has been utilized by Alshammari et al. for grafting Chitosan with methylaniline derivatives. The copolymers prepared under this condition show a better performance for dye uptake compared to non-sonicated ones [215]. Also, microwave-assisted synthesis of Polyethyleneimine-grafted-chitosan beads was reported to be effective in removing of Acid Red 27. Polyethyleneimine (PEI)

was reported as being better choice of amino-functionalized reagent for developing a potentially good adsorbent material [216]. The electrostatic potential of PEI grafted chitosan towards dyes could increase with increase in the amino group [217]. Decolorization of methylene blue (MB) and methyl orange (MO) from water using chitosan-graft-polyacrylamide have been effective as reported by Labidi et al. Desorption studies of MB and MO showed good reusability potential of the as-prepared adsorbent [218]. Therefore, availability of functional groups such as OH, NH_2, carbonyl, carboxyl on grafted-chitosan materials could increase the chance of dye molecules adhering to the surface of the grafted-chitosan based adsorbent as these functional groups serve as point of attachments. Grafting could also create more pores on chitosan-based adsorbents as adsorption sites. This could subsequently to a large extent increase the percentage of dye removal [213, 214].

1.7.3.3 Procedures of selected graft modified chitosan for pharmaceuticals adsorption

Carboxyl-grafted chitosan derivatives were reported as selective adsorbents for the uptake of diclofenac (DCF) from aqueous medium [181]. The amino groups of DCF could be protonated in acidic medium (pH = 4) and could facilitate attraction to the negatively charged carboxyl moieties ($–COO^-$) of the grafted-chitosan adsorbents. Also, a better DCF removal could be achieved when grafted chitosan is functionalized with more carboxyl moieties [181].

CHAPTER 2 EXPERIMENTAL

The second chapter is experimental, it is devoted to the presentation of the methods and reagents essential for the development of materials: parent and functionalized. It gathers the protocols preparation of adsorbents, the probable mechanisms of synthesis as well as their characterization by different physico-chemical and structural techniques such as the infrared spectroscopy, scanning electron microscopy and the point of zero charge. The positioning of these important information in this part is necessary for further work.

One of the main approaches for grafting of organosilanes on halloysite nanotubes surface is based on the condensation reaction between hydroxyl groups on HNTs surface and methoxy groups of silane and formation of covalent bond. These Si–OCH_3 groups can condense with the surface hydroxyl groups of inorganic materials by eliminating methyl alcohol molecules under proper conditions. Therefore, the organofunctional group (R) is covalently grafted onto the surface of the inorganic material and consequently modifies the surface properties. In this study, the silane coupling agents, have the general formula of X_3SiR, where R is an organofunctional group (eg, –$(CH_2)_3Cl$, —$(CH_2)_3SH$) and X is a hydrolysable group (–OCH_3), used to modify the surface properties of Halloysite nanotubes.

2.1 Grafting of (3-Mercaptopropyl) trimethoxy silane (MPTMS) on halloysite nanotubes surface

The method followed for grafting (3-Mercaptopropyl) trimethoxy silane (MPTMS) on the surface of halloysite nanotubes is illustrated in Figure 2.1.

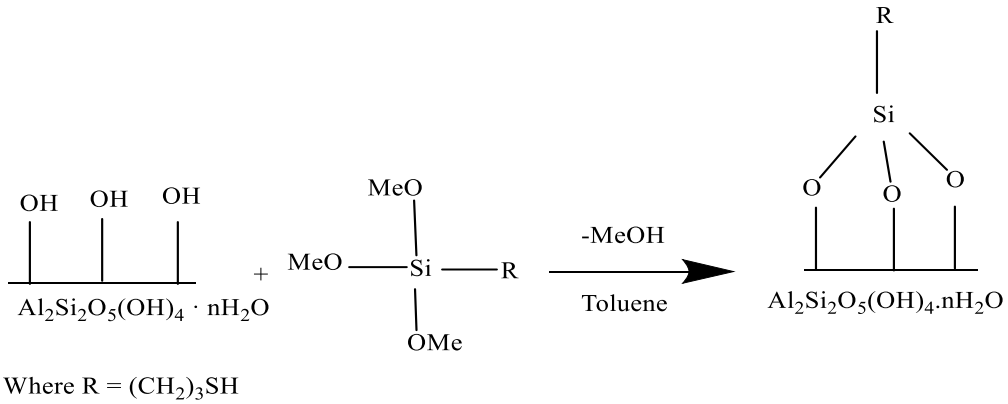

Figure 2.1 - Synthetic route that was used during the modification process. Details are provided below.

HNTs powder (1.3 g) was mixed in 20 ml of different solvents for 10 min. then different amounts of (3-Mercaptopropyl) trimethoxy silane was added as shown in Table 2.1. The mixture was dispersed ultrasonically for 60 min. then refluxed at reaction time mentioned at Table 2.1. under constant stirring and using temperature that corresponds to the boiling point of each solvent used in the experiment. The modified halloysite nanotubes were separated by centrifugation and extensively washed three times with 30 ml of the used solvent to remove the unreacted organosilanes. The separated product (HNTs-MPTMS) was finally dried at 60 °C for 12 hours. Some experiments were done in the presence of water and others were done in the presence of triethyl amine, tetraethoxy titanium and ammonia solution as mentioned at Table 2.1.

Table 2.1 - Reaction conditions of grafting (3-Mercaptopropyl) trimethoxy silane on HNTs surface.

Sample	**HNTs/MPTMS/ water/catalyst (molar ratio)**	**Solvent**	**Halloysite dispersion concentration (g/ml)**	**Temperature (°C)**	**Refluxing Time (hour)**
HNT -A1	1/1.33/0/0	Toluene	0.0325	110	4
HNT -B2	1/1.33/0/0	THF	0.0325	66	4
HNT-C3	1/1.33/3/0	Toluene	0.0325	110	4
HNT -D4	1/ 2.64/0/0	Ethanol	0.0325	79	4
HNT -E5	1/1.33/0/0	Acetonitrile	0.0325	82	4
HNT -F6	1/1.33/0/0	Acetonitrile	0.13	82	4
HNT-G7	1/1.33/0/0	Toluene	0.0325	110	48
HNT-H8	1/2/0/0	Toluene	0.0325	110	48
HNT-I9	1/1.33 /0/0	Toluene	0.13	110	4
HNT-J10	1/1.33/0/0	Toluene	0.0173	110	4
HNT-K11	4.64/6.034/0/0	n-Hexane	0.0325	69	4
HNT-L12	1/1.3/0/0	1,4-Dioxane	0.0325	100	4
HNT-M13	1/1/8.26 /0	Toluene	0.065	110	4
HNT-N14	1/1/0/0.308 $(C_2H_5)_3N$	Toluene	0.065	110	4
HNT-O15	1/ 1/0/1.027 Ti $(OC_2H_5)_4$	Toluene	0.065	110	4
HNT-P16	1/1/0/5.59 NH_4OH	Toluene	0.065	110	4

2.2 Grafting of (3-Glycidyloxypropyl) trimethoxy silane (GOPTMS) on halloysite nanotubes surface

The method followed for grafting (3-Glycidyloxypropyl) trimethoxy silane (GOPTMS) on the surface of halloysite nanotubes is illustrated in Figure 2.2.

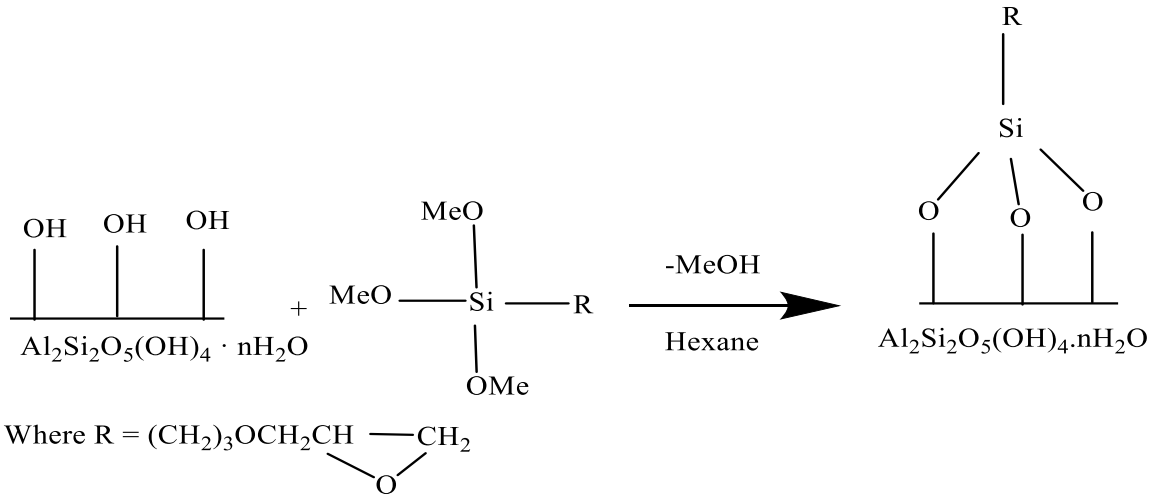

Figure 2.2 - The sketch for chemical grafting of GOPTMS on HNT surface.

In a dry flat bottom boiling flask add 1.3 g of HNT then add 10 ml of solvent and were kept in contact for 30 min. under agitation conditions to obtain good dispersion state then insert into the reaction media 6.3 mmoles of (3-Glycidyloxy propyl) trimethoxy silane and agitated for additional 30 min. at room temperature then refluxed for 2 hours. Polar protic solvents (ethanol), polar aprotic solvents (tetrahydrofuran (THF) and acetonitrile) and non-polar solvents (1,4-dioxane, toluene and n-hexane) were tested in these experiments. The grafted HNT samples were discrete by filtration, rinsed several times with 50 ml of acetone then, dehydrated in an oven for 6 hours at 78 °C as mentioned at Table 2.2.

2.3 Grafting of (3-Chloropropyl) trimethoxy silane (CPTMS) on halloysite nanotubes surface

The method followed for grafting (3-Chloropropyl) trimethoxy silane (CPTMS) on the surface of halloysite nanotubes is illustrated in Figure 2.3.

Table 2.2 - Reaction conditions of grafting (3-Glycidyloxypropyl) trimethoxy silane (GOPTMS) on HNTs surface.

Sample	Molar ratio (HNTs/ GOPTMS / H_2O)	Solvent	Halloysite dispersion concentration (g/ml)	Catalyst	(HNT/catalyst) molar ratio	Temperature (°C)	Refluxing Time (hour)
HNT- R1	(1:1.42:0)	Toluene	0.0325	-	-	110	4
HNT- R2	(1:1.42:0)	THF	0.0325	-	-	66	4
HNT- R3	(1:1.42:3.15)	Toluene	0.0325	-	-	110	4
HNT- R4	(1:1.42:0)	Ethanol	0.0325	-	-	79	4
HNT- R5	(1:1.42:0)	Toluene	0.13	-	-	110	4
HNT- R6	(1:1.42:0)	Toluene	0.0325	-	-	110	35
HNT- R7	(1:2.85:0)	Toluene	0.0325	-	-	110	4
HNT- R8	(1:4.27:0)	Toluene	0.0325	-	-	110	4
HNT- R9	(1:1.42:0)	Hexane	0.0325	-	-	69	4
HNT- R10	(1:1.42:0)	1,4 Dioxane	0.0325	-	-	100	4
HNT- R11	(1:1.42:0)	Toluene	0.0163	-	-	110	2
HNT- R12	(1:1.42:0)	Toluene	0.0325	Et_3N	(1:0.308)	110	2
HNT- R13	(1:1.42:0)	Acetonitrile	0.0325	-	-	82	4
HNT- R14	(1:1.06:8.5)	Toluene	0.0325	-	-	110	4
HNT- R15	(1:1.42:0)	Hexane	0.065	-	-	69	4
HNT- R16	(1:1.42:0)	Hexane	0.13	-	-	69	4
HNT- R17	(1:1.42:0)	Hexane	0.0163	-	-	69	4
HNT- R18	(1:1.06:8.5)	Hexane	0.0325	-	-	69	4
HNT- R19	(1:2.15:0)	Hexane	0.065	-	-	69	4
HNT- R20	(1:2.85:0)	Hexane	0.065	-	-	69	4
HNT- R21	(1:1.42:0)	Hexane	0.065	NH_4OH	(1:5.59)	69	4
HNT- R22	(1:1.42:0)	Hexane	0.065	NH_4OH	(1:11.18)	69	4
HNT- R23	(1.43:1:0)	Hexane	0.13	-	-	69	4

* (-) means no catalyst has been used.

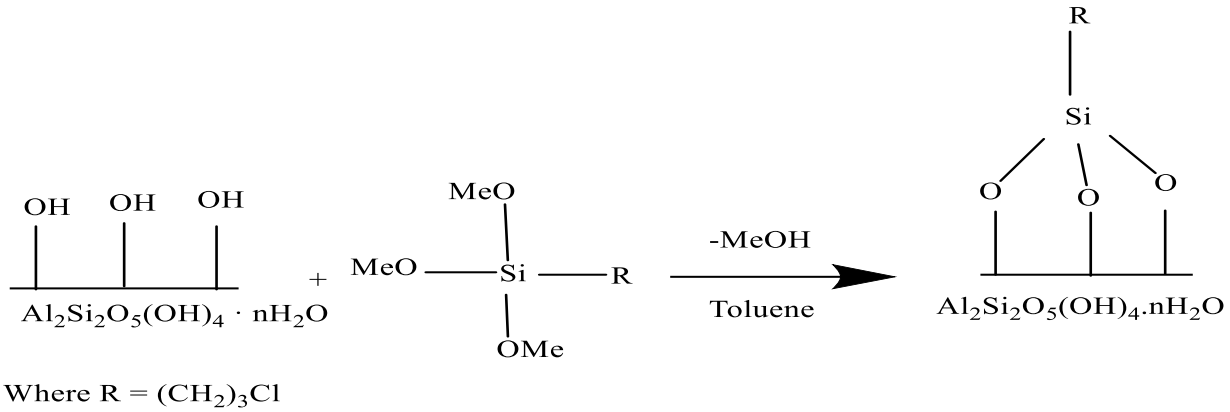

Figure 2.3 - The synthetic route that was used during the grafting of CPTMS on HNTs surface.

Halloysite nanotubes were allowed to react with (3-chloropropyl) trimethoxysilane (CPTMS) using different solvents such as toluene, tetrahydrofuran (THF), ethanol, n-hexane, 1,4 dioxane under reflux conditions for 4 hours. Triethylamine, urea, tetra-ethoxy titanium, and ammonia solution were used as catalysts and its influence on the reaction proceeding was evaluated. The effect of moistening the reaction media was tested as mentioned in Table 2.3. The resulting product was washed many times with acetone followed by ethanol and dried at 60 °c in an oven for 12 hours.

2.4 Characterization of HNTs-MPTMS, HNTs-GOPTMS and HNTs-CPTMS

Elemental analysis of carbon, hydrogen, and nitrogen (EA) for the created HNT materials which were grafted using (3-Mercaptopropyl) trimethoxy silane, (3-Glycidyloxypropyl) trimethoxy silane and (3-Chloropropyl) trimethoxy silane were carried out using an elemental analyzer Perkin Elmer PE 2400. The degree of functionalization (DF) of (HNTs-MPTMS), (HNTs-GOPTMS) and (HNTs-CPTMS) samples were computed using Eq.2.1 and 2.2:

$$DF = \frac{\%\ of\ carbon\ obtained\ from\ EA}{theoretical\ \%\ of\ carbon\ content} \quad (2.1)$$

where theoretical % of carbon content calculated using the following equation:

$$Theoretical\ \%\ of\ carbon\ content = \frac{No.of\ carbon\ atoms\ in\ silane * No.of\ moles\ of\ silane * 12}{No.of\ g\ of\ HNTs + No.of\ g\ of\ silane - No.of\ g\ of\ alcohol\ eliminated} \quad (2.2)$$

Fourier transform infrared (FT-IR) spectra were applied to confirm the presence of bands for (CH_2) group that indicate the elimination of alcohol molecules by the condensation between silane and hydroxyl groups on the surface of halloysite nanotubes. FT-IR diffuse reflectance

spectra were given using a Spectrum-One spectrometer, Perkin Elmer. The measurements were done within the wave number range (4500-500) cm^{-1} by considering 24 scans and each scan was 30 seconds. Thermogravimetric analysis (TGA) was given using a Mettler Toledo instrument for the pristine halloysite nanotubes and the best created HNTs materials (HNTs-MPTMS), (HNTs-GOPTMS) and (HNTs-CPTMS).

Table 2.3 - The different parameters which have been performed for the grafting process.

Sample	**Molar ratio (HNTs/CPTMS / H_2O)**	**Solvent**	**Halloysite dispersion concentration (g/ml)**	**Catalyst**	**(HNT/catalyst) molar ratio**	**Temperature (°C)**	**Refluxing Time (hour)**
HNT- Q1	1:1:0	Toluene	0.0325	-	-	110	4
HNT- Q2	1:1.33:0	THF	0.0325	-	-	66	4
HNT- Q3	1:1:3	Toluene	0.0325	-	-	110	4
HNT- Q4	1:1:0	Ethanol	0.0325	-	-	79	4
HNT- Q5	1:1.33:0	Toluene	0.13	-	-	110	4
HNT- Q6	1:1:0	Toluene	0.0325	-	-	110	35
HNT- Q7	1:1:0	Toluene	0.0325	-	-	110	48
HNT- Q8	1:2:0	Toluene	0.0325	-	-	110	4
HNT- Q9	1:2:0	Toluene	0.038	-	-	110	48
HNT- Q10	1:1:3	Toluene	0.0325	Et_3N	(1:0.6163)	110	7
HNT- Q11	1:1:3	Toluene	0.0325	urea	(1:0.6635)	110	4
HNT- Q12	1:1.33:0	n-Hexane	0.0325	Et_3N	(1:0.6163)	69	4
HNT- Q13	1:1.33:0	1,4 Dioxane	0.0325	Et_3N	(1:0.6163)	100	4
HNT- Q14	1:1.33:0	n-Hexane	0.0325	-	-	69	4
HNT- Q15	1:1.33:0	1,4 Dioxane	0.0325	-	-	100	4
HNT- Q16	1:1:3	Toluene	0.0325	Et_3N	(1:0.6163)	110	4
HNT- Q17	1:1:3	Toluene	0.0163	Et_3N	(1:0.6163)	110	4
HNT- Q18	1:1:3	Toluene	0.0325	Et_3N+ NH_4OH	[1: (0.6163 Et_3N+5.59 NH_4OH)]	110	4
HNT- Q19	1:1:0	Toluene	0.0325	$(EtO)_4Ti$	(1:1.027)	110	4
HNT- Q20	1:1:3	Toluene	0.0325	Et_3N + NH_4OH	[1: (0.6163 Et_3N+1.542 NH_4OH)]	110	4

* (-) means no catalyst has been used.

The mass of the created materials was measured over time as the temperature verifies from 30°C to 1000°C using a heating rate of 30 $^{\circ}$C min^{-1} under a nitrogen flow of 60 ml/min. Calibration was carried out following procedure mentioned in literature [219, 220].

Based on the rule of mixtures, the loading amount of organic moiety on the surface of HNT can be calculated using Eq. (2.3) [221]:

$$Silane\ loaded\ \ (Wt.\%) = 100\ \times [1 - \frac{MR_{\ 600\ composite} + ML_{150\ composite}}{MR_{600\ pristine} + ML_{150\ pristine}}] \qquad (2.3)$$

where $MR_{600\ composite}$ and $MR_{600\ pristine}$ is the residual matter at 600 °C for functionalized HNT and pristine HNT materials, respectively. $ML_{150\ composite}$ and $ML_{150\ pristine}$ represent the mass losses at the temperature interval 25-150 °C for the functionalized HNT and pristine HNT materials, respectively.

Scanning electron microscope (SEM) images were given using a Carl instrument Zeiss EVO LS 10. It was used to study the morphology of the pristine halloysite nanotubes and the material with the greatest functionalization efficacy (HNTs-MPTMS), (HNTs-GOPTMS) and (HNTs-CPTMS). Carbon tape was used to reduce charging effects. Minimal electron dose was used (3 kV) and the sample distance was 5.1 mm.

2.5 Synthesis of halloysite nanotubes modified with polyethyleneimine (HN-PEI)

2.5.1 Method for the modification of halloysite nanotubes with polyethyleneimine (HN-PEI)

The modification has been performed through a two-step reaction. The first step is functionalization of halloysite nanotubes surface using (3- chloropropyl) trimethoxy silane to give (HN-CPTM). The second step is further functionalization of (HN-CPTM) with branched polyethyleneimine to give (HN-PEI).

In detail, we added a mixture of halloysite nanotubes, (3- chloropropyl) trimethoxy silane, and double distilled water with molar ratio (HNTs/ H_2O/ CPTMS) equal (1: 3: 1) in a dry flat bottom flask. Then, 20 ml of toluene were dropped, and the mixture was kept under agitation at room temperature for 20 min. Afterward, 0.5 ml NH_4OH + 0.5 ml Et_3N were added to the reaction media and heated with stirring at 100°C for 4 hours under reflux conditions. The resulting product

was filtered and washed with toluene followed by acetone then dried in an oven at 60°C for 6 hours. The resulting material was referred to as (HN-CPTM).

Halloysite nanotubes functionalized by polyethyleneimine (HN-PEI) were obtained by contacting (HN-CPTM) with branched polyethyleneimine at molar ratio [(HN-CPTM) / PEI] = (1:1) in the presence of 20 ml of ethanol and the mixture was heated for 12 hours under refluxing conditions at 80°C. The resulting product was separated by filtration and was washed with hot double distilled water followed by acetone then dried at 60°C in an oven for 6 hours. The resulting material was referred to as (HN-PEI). The method followed for grafting polyethyleneimine on halloysite nanotubes which was primary grafted by (3-Chloropropyl) trimethoxy silane (HN-CPTM) is illustrated in Figure 2.4.

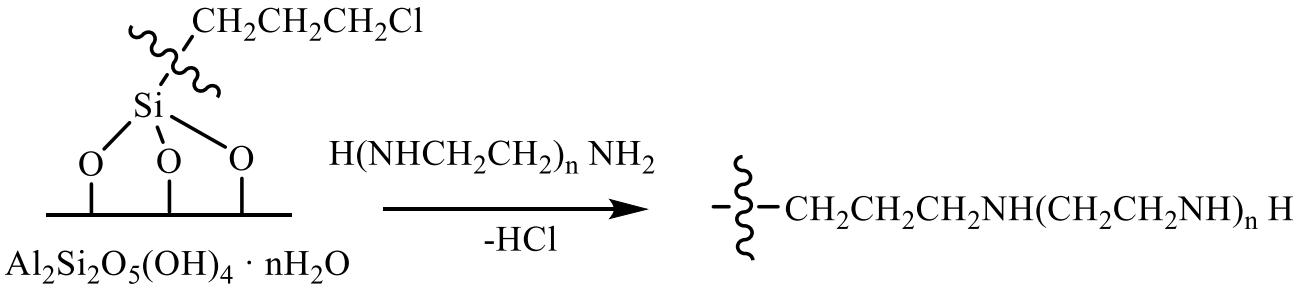

Figure 2.4 - Synthetic route that was used during the grafting of polyethyleneimine on halloysite nanotubes which was primary grafted by (3-Chloropropyl) trimethoxy silane (HN-CPTM).

2.5.2 Characterization of halloysite nanotubes modified by polyethyleneimine (HN-PEI)

(C, H, N) % was obtained for pristine HNT, (HN-CPTM), and (HN-PEI) using elemental analyzer Perkin Elmer PE 2400. Compact FT-IR Spectrometer: ALPHA II was used for FT-IR analysis within wavenumber range (4500 to 500 cm^{-1}). The morphology and surface features of pristine HNTs and (HN-PEI) were given by Scanning electron microscope a Carl Zeiss EVO LS 10 Device. The pH_{PZC} was predestined using the pH-drift method: 25 mg of (HN-PEI) were dropped into 15 ml of a 0.1 M NaCl with a variation of initial pH values (pH_0 ranging from 2.04 - 10). After 24 h of contacting, the equilibrium pH (pH_{eq}) was obtained by Mettler Toledo's pH meter. The difference between the initial and final pH values ($\Delta pH = pH_f - pH_i$) was plotted against the pH_i. The point at which $\Delta pH = 0$ is considered as pH_{PZC} [222]. Thermogravimetry

coupled with differential scanning calorimetry (TG-DSC) was implemented by NETZSCH STA449F3 thermal analyzer in the air at the heating rate of 10 K/min. The crystal structure for pristine HNTs and (HN-PEI) was analyzed by using X-ray diffractometer Panalytical X 'PERT PRO MRD, equipped with an anticathode of Cu Kα. The 2θ varies within range (10-70°) and the scanning rate was 0.09 °/s with a step size equals 0.05 °. The nitrogen adsorption/desorption isotherms have been computed at 77K using Micrometrics Gemini VII 2390. The samples were dried at 120°C for 180 min under vacuum before adsorption experiments. The specific surface area of pristine HNTs and the grafted (HN-PEI) sorbent was evaluated by the Brunauer-Emmett-Teller method based on adsorption/desorption data in the partial pressure (P/P_o) ranges from 0.01 to 0.99 and the pore size distribution was done based on Barrett-Joyner-Halenda method.

2.5.3 Sorption and desorption processes using halloysite nanotubes modified by polyethyleneimine (HN-PEI)

The adsorption efficiency of halloysite nanotubes modified by polyethyleneimine (HN-PEI) was checked by contacting 20 mg of (HN-PEI) in a conical flask, with 50 ml of copper nitrate or zinc nitrate aqueous solutions using a concentration (C_i) of 1.573 and 1.529 mmol/L for Cu (II) and Zn (II) metal ions, respectively. The pH values were within range (2 - 6) for copper nitrate and zinc nitrate solutions. The agitation (650 rpm) time was set at 110 min at 25 °C. The concentration (C_f, mmol/L) for both Cu (II) and Zn (II) metal ions was evaluated after the equilibrium using Cuprizone and Pyridylazonaphthol (PAN) spectrophotometric methods for Cu (II) and Zn (II) metal ions, respectively [223].

The method for the determination of copper in the aqueous phase using Cuprizone as a very selective method:

Reagents

Cuprizone, 0.1% solution. Dissolve 100 mg of reagent in 20 ml of hot 50% ethanol, and dilute the solution with cold 50% ethanol to 100 ml.

Standard copper solution: 1 mg/ml.

Procedure

To a solution in a 25-ml standard flask, containing not more than 70 μg of Cu, add 1-2 ml of 10% ammonium citrate solution (depending on the amount of metals in the solution which would

precipitate as the pH is increased) and adjust the solution with ammonia to pH 8-9. Add 3 ml of the cuprizone solution, dilute the solution to the mark with water, and after 10 min., measure the absorbance of the blue solution at 600 nm against water.

The spectrophotometric method for determining zinc using Pyridylazonaphthol (PAN):

Reagents

1-(2-Pyridylazo)-2-naphthol (PAN), 0.1% solution in ethanol.

Standard zinc solution: 1 mg/ml.

Tri-n-octylamine (TOA), 2% solution in benzene.

Procedure

To the alkaline solution containing not more than 25 μg of Zn, add 0.5 g of ammonium chloride, 2 ml of PAN solution, and shake with 2 portions of chloroform (shaking time 30 s). Transfer the extract to a 25-ml standard flask and dilute to the mark with $CHC1_3$. Mix well and measure the absorbance of the solution at 560 nm against a reagent blank.

Spectrophotometric measurements were carried out by using the SHIMADZU model: UV-2600 2. The greatest sorption capacity (mmol. g^{-1}) of the functionalized material (HN-PEI) was calculated by using Eq. (2.4) [224]:

$$Q_{max} = ((C_i - C_f)\, V/M \qquad (2.4)$$

where C_i, C_f are the initial and final concentration of Cu (II) and Zn (II) metal ions in the solution (mmol/L), respectively, (V) is the volume of the solution (L) and (M) is the mass of the sorbent (g).

The kinetic parameters were estimated from the data of adsorption experiments at the equilibrium with the mono-component adsorbates (copper or zinc), 20 mg of (HN-PEI) was mixed with 50 ml of metal solution [(C_i) of 1.573 and 1.529 mmol/L for Cu (II) and Zn (II) metal ions, respectively], pH = 4.5 at 25 °C and using mixing time within range (3-200) min. for Cu (II) and Zn (II) metal ions. The experiments were conducted at several temperatures, namely, 298, 308, 313, and 318 K.

The desorption experiments were accomplished after equilibration of (HN-PEI) with Cu (II) and Zn (II) metal ions in aqueous solutions using the equilibrium conditions of pH, C_i, contact

time, and temperature with sorbent dosage equal to 0.4 g/L then the loaded sorbent will be eluted by using the desired eluent. Urea, EDTA, NH_4Cl, HCl, H_2SO_4, and HNO_3 were used as eluents and were tested for the regeneration of metal ions from (HN-PEI) surface.

2.6 Synthesis of aminocarboxymethyl chitosan (CTS-CAA)

2.6.1 Method for the synthesis of aminocarboxymethyl chitosan (CTS-CAA)

The modification of chitosan was carried out in four consecutive steps as reported below.

- The cross-linking of chitosan by glutaraldehyde to get (CTS-GL). For this purpose, 4 g of chitosan powder was incorporated into a solution of acetic acid (200 ml; 5 M). The solution was agitated until it becomes homogenous. Then, we added 2 ml of glutaraldehyde solution (50%). The mixture was heated at 40°C for 2 hours. The resulting product was filtered and washed with ethanol then dried for using in the second step. The resulting product was reported as (CTS-GL) [39].
- The reaction of (CTS-GL) with epichlorohydrin to get (CTS-EC). 15 ml of epichlorohydrin were with 200 ml of (acetone/water; volume ratio 1:1). Then, we added 4 g of (CTS-GL), which were previously mixed in 150 ml of isopropanol for 30 min under agitation conditions. The resulting mixture was heated at 65 °C for 24 hours under refluxing conditions. The resulting product was filtered and washed with ethanol then dried for using in the third step. This product was mentioned as (CTS-EC) [225, 226].
- The reaction of (CTS-EC) with diethylene triamine to get (CTS-DET). For this purpose, 4 g of (CTS-EC) were mixed in 200 ml of (ethanol/water; volume ratio 1:1) under agitation at 25 °C. Then, 10 ml of diethylene triamine were incorporated into this reaction media and the mixture was kept reacting at 65 °C for 12 hours under agitation. The resulting product was filtered and washed using ethanol then dried for using in the fourth step. The resulting product was mentioned as (CTS-DET).
- The reaction of (CTS-DET) with monochloroacetic acid to get (CTS-CAA). In this step, 4 g of (CTS-DET) were mixed in 55 ml of solvent (44 ml of isopropyl alcohol and 11 ml of H_2O). Then, 6 g of monochloroacetic acid which were previously dissolved in 8 ml of isopropanol, were added to the mixture slowly and the reaction was continuously proceeded in a water bath under agitation at 60 °C for 5 hours. The reaction was stopped by adding 150 ml of diluted ethanol (60%). The resulting product was filtered and washed with ethanol

then dried for using during the sorption experiments. The product was mentioned as (CTS-CAA). The method followed for the synthesis of aminocarboxymethyl chitosan is illustrated in Figure 2.5.

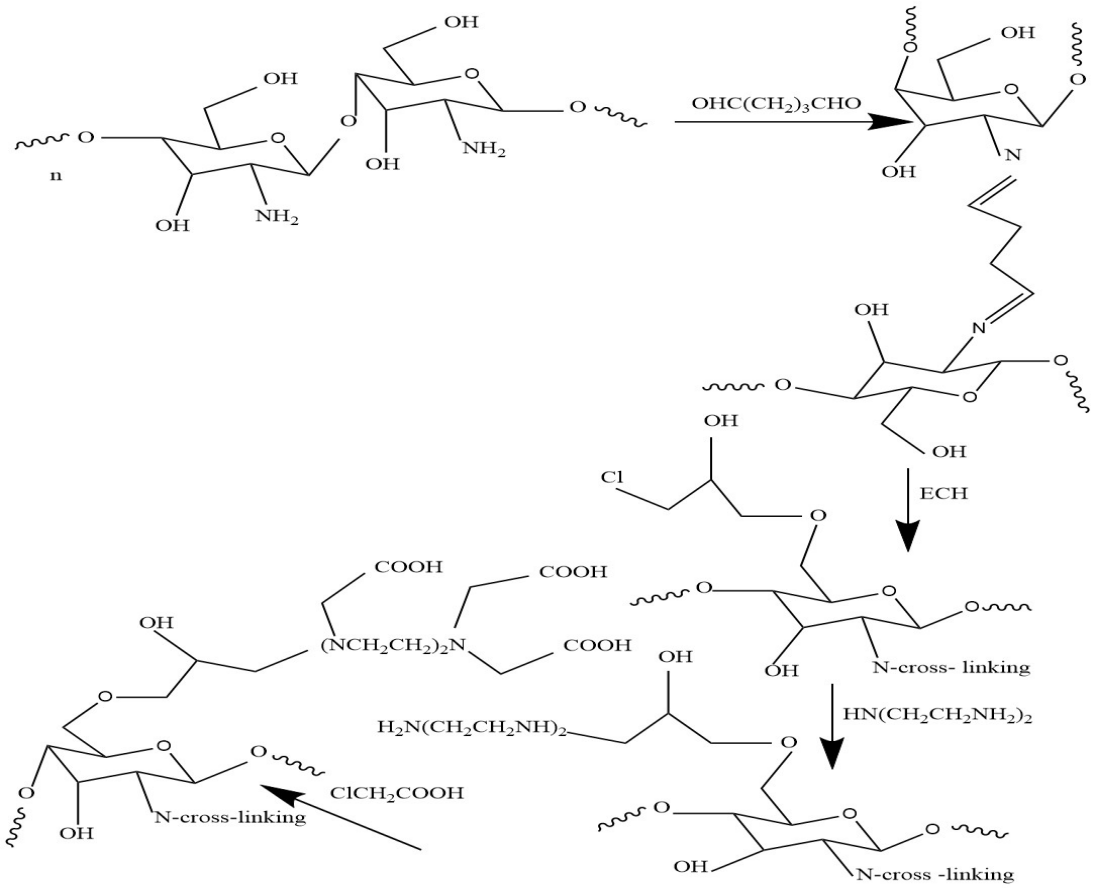

Figure 2.5 - Synthetic route that was used during the synthesis of aminocarboxymethyl chitosan.

2.6.2 Characterization of aminocarboxymethyl chitosan (CTS-CAA)

The elemental composition of unmodified chitosan and (CTS-CAA) samples was obtained by an elemental analyzer (2400 CHNS Organic Elemental Analyzer 100V) for carbon, hydrogen, and nitrogen. To evaluate the functional groups for the modified chitosan sample (CTS-CAA), Fourier transform infrared (FT-IR) spectroscopy was carried out by using the Compact FT-IR Spectrometer ALPHA II within the wavenumber range (4500-600) cm^{-1}. The pH_{PZC} was estimated based on the pH-drift method: 30 mg of (CTS-CAA) was dropped into 15 ml of a 0.1 M NaCl at different initial pH values (pH_0 within the range from 2 to 10). After 24 h of contacting, the equilibrium pH (pH_{eq}) was evaluated by using Mettler Toledo pH meter. The difference between the initial and final pH values (ΔpH =

$pH_f - pH_i$) was plotted against the pH_i. The point at which ($pH_f - pH_i$) =0 gives the value of the pH_{PZC} [227]. The morphology of the samples was investigated by scanning electron microscope by using a Carl Zeiss EVO LS 10 Device. Thermogravimetry-differential scanning calorimetry (TG-DSC) was conducted in air using NETZSCH STA449F3 thermal analyzer and the heating rate was fixed at 20/10 K/min. X-ray diffraction patterns (XRD) were obtained using X-ray diffractometer Panalytical X 'PERT PRO MRD, equipped with an anticathode of Cu Kα. The diffractograms were recorded at 2θ (10 - 70 °) using a scanning rate of 0.09 °/s and a step size equals 0.05°.

2.6.3 Sorption and desorption experiments using aminocarboxymethyl chitosan (CTS-CAA)

The adsorption of both Cu (II) and Zn (II) metal ions on the functionalized chitosan was performed by contacting 25 mg of (CTS-CAA) material with 50 ml of an aqueous solution containing Cu (II) and Zn (II) metal ions with an initial concentration (C_i) of 1.573 and 1.529 mmol/L for Cu (II) and Zn (II) metal ions, respectively. The pH of the aqueous medium was systematically varied within the range (2 - 6.2). The suspensions were kept under agitation for 120 min. Finally, the residual metal ion concentration (C_f) was estimated using Cuprizone and Pyridylazonaphthol (PAN) spectrophotometric methods for Cu (II) and Zn (II) metal ions, respectively [223]. Both Cuprizone and Pyridylazonaphthol (PAN) spectrophotometric methods were discussed in detail in section (2.5.3). The adsorption capacity (Q_{max}) expressed as mmol of metal per g of (CTS-CAA) was evaluated using Eq. (2.4) (subtitle 2.5.3).

In order to investigate the kinetics of the adsorption processes, 25 mg of (CTS-CAA) sample were kept contacting with 50 ml of an aqueous solution containing the ions (C_0 = 1.573 and 1.529 mmol/L for Cu (II) and Zn (II) metal ions, respectively) at variable times (10 – 240 minutes) using pH equals 3.5. The effect of metal ions initial concentration on the adsorption mechanism was tested by systematically changing C_0 within the range (0.393-5.507) mmol/L for Cu (II) and (0.382-5.353) mmol/L for Zn (II), (120 minutes) the contact time between the adsorbent and the solution containing the heavy metal ions. These results were used to determine the adsorption isotherms at variable temperatures (298, 304, 309, 315 K). The desorption experiments were carried out by contacting an appropriate quantity of (CTS-CAA) with sorbent dosage equal to 0.5 gL^{-1} at the equilibrium conditions then the

metals were regenerated from the sorbent using a suitable eluent. The eluent and the (CTS-CAA) sample loaded with the metal ions were kept contacting under agitation for 2 hours at room temperature. HCl, H_2SO_4, HNO_3, urea, EDTA, NH_4Cl were used as eluents and were tested for the desorption of both Cu (II) and Zn (II) metal ions from (CTS-CAA) surface. It was found that utilizing the 0.5 M of HNO_3 and 0.2 M of urea for Cu (II) and Zn (II) metal ions, respectively, can be greatly regenerate the metal ions from the modified sorbent surface.

CHAPTER 3 THE EFFECT OF DIFFERENT PARAMETERS WHICH INFLUENCE ON GRAFTING OF (3-SUBSTITUTED PROPYL) TRIMETHOXY SILANE ON HALLOYSITE NANOTUBES SURFACE

The third chapter is dedicated to the experimental results and discussion of the obtained data. It is subdivided into two parts: the first part includes discussion of different parameters which influence on grafting of (3-substituted propyl) trimethoxy silane on halloysite nanotubes surface based on the data obtained from elemental analysis and FT-IR analysis. The second part includes the estimation of the efficiency for functionalization of halloysite nanotubes by polyethyleneimine as well as the functionalization of chitosan by diethylene triamine and monochloroacetic acid based on studying the various properties of the modified materials.

3.1 Grafting of (3-Mercaptopropyl) trimethoxy silane (MPTMS) on halloysite nanotubes surface

3.1.1 Effect of polarity of solvent

Because of its role in wetting the surface of halloysite nanotubes, the solvent has a significant impact on the silanization process, which occurs as a result of the reaction between silicate-based materials and alkoxysilanes [228]. Toluene, tetrahydrofuran, ethanol, n-hexane, 1,4 dioxane, and acetonitrile were used as a solvent for the grafting process. The polarity and dielectric constant of these solvents differ. Figure 3.1 depicts the FT-IR spectra of HNTs modified with MPTMS in the presence of these solvents. The bands at 1258 cm^{-1} for HNT-A1 indicate the presence of Si-CH_2-R deformation vibration, and their intensity decreases as the aliphatic chain length increases [229].

Table 3.1 summarizes the elemental analysis data and the functionalization degree of HNTs samples grafted by MPTMS in the presence of various solvents. HNT-A1 had the highest functionalization degree. The sample HNT-A1 had the best MPTMS functionalization degree, indicating that toluene is the best solvent for grafting MPTMS on the surface of HNTs. Polar solvents such as tetrahydrofuran and ethanol had the lowest degree of functionalization, indicating that these solvents are not suitable for the grafting process due to the competition reaction between alkyl siloxane and hydroxyl groups of the solvents via H-bonding rather than hydroxyl groups of the surface [230, 231]. As shown in

Table 3.1 and Figure 3.2, increasing the number of moles of water in the reaction mixture from 13.92 mmol to 38.33 mmol resulted in a decrease in the functionalization degree from 39.78% to 33.49%. This supports the hypothesis advanced in the case of the most polar solvents.

Table 3.1 - Elemental analysis of HNT samples which have been chemically grafted in various types of solvent using (3-Mercaptopropyl) trimethoxy silane.

Sample	**Content, %**		**Degree of functionalization %**
	C	H	
HNT -A1	5.58	1.97	51.63
HNT -B2	0.95	1.80	8.79
HNT-C3	4.30	0.20	39.78
HNT -D4	1.31	1.87	8.07
HNT -E5	0.93	1.80	8.6
HNT -F6	1.96	0.42	18.13
HNT-G7	3.04	2.16	28.12
HNT-H8	3.51	1.98	25.13
HNT-I9	3.29	2.02	30.44
HNT-J10	3.77	2.12	34.88
HNT-K11	3.44	2.255	32.19
HNT-L12	3.46	1.923	32.37
HNT-M13	2.98	2.26	33.49
HNT-N14	4.76	2.39	53.53
HNT-O15	2.70	2.03	30.39
HNT-P16	8.9	3.155	99.8

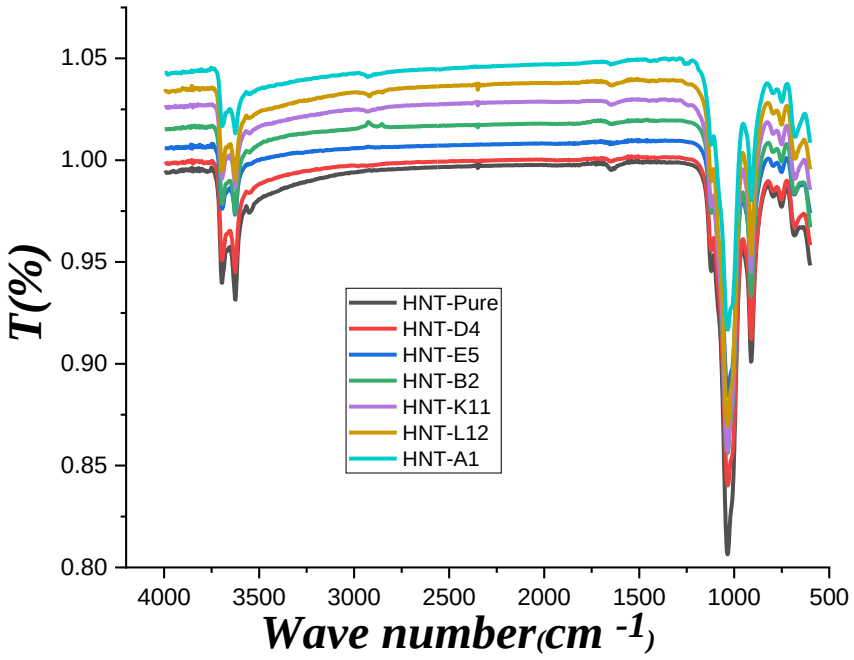

Figure 3.1 - FT-IR Spectra for the effect of solvent on grafting of MPTMS on the surface of HNTs.

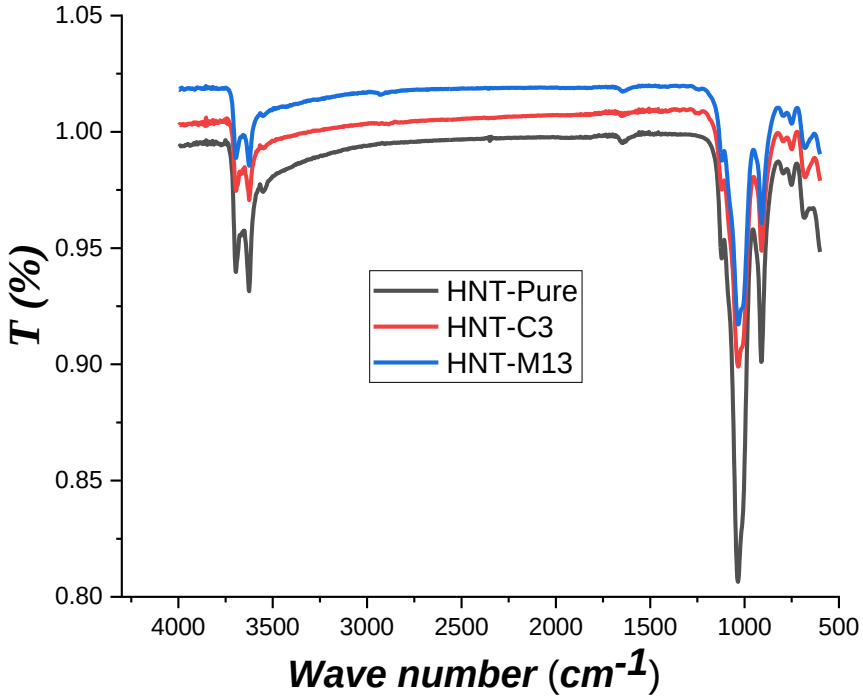

Figure 3.2 - FT-IR spectra for the effect of changing amount of water on grafting of MPTMS on HNTs surface.

3.1.2 Effect of number of moles of MPTMS

Though increasing the number of moles of silanes in the reaction media allowed more active silanol groups to interact with hydroxyl groups attached to the surface of halloysite nanotubes, elemental analysis data revealed that as the number of moles of silane increases, the functionalization degree decreases. Although many articles have discussed the effect of the amount of silane on the grafting process. There is no complete clarification why the degree of functionalization decreases as silane amount increases [232-236].

Figure 3.3 depicts new bands for HNT-N14 at 2927 cm^{-1}, 2857 cm^{-1}, corresponding to symmetric stretching of the CH_2 group [237]. This represents the condensation reaction of alkoxy silane and hydroxyl groups on the surface of HNTs. According to the results of elemental analysis and FT-IR spectra (Table 3.1 and Figure 3.3), 4.633 mmol of MPTMS was chosen as the best amount of silane for the grafting process.

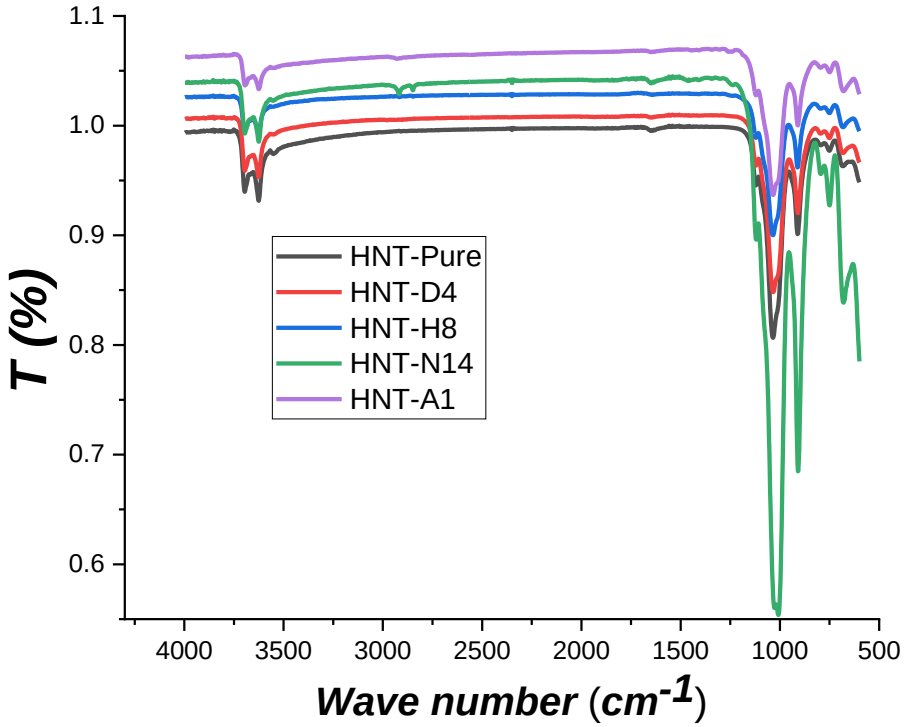

Figure 3.3 - FT-IR spectra for the effect of number of moles of MPTMS on grafting process.

3.1.3 Influence of the volume of solvent

Figure 3.4 shows the FT-IR spectra for the samples which was treated using different volumes of toluene. Table 3.1 displays the calculated functionalization degree values for these samples. The volume equals to 40 ml of toluene was chosen as the best volume of solvent for grafting MPTMS on the surface of HNTs. Figure 3.4 shows bands at 1252 cm^{-1}, 1303 cm^{-1} for HNT-M13, HNT-A1 which represents the Si-CH_2-R deformation vibration which occurs at 1250-1175 cm^{-1} and CH_2 wagging vibration which occurs near 1305 cm^{-1} respectively, and the other band at 2884 cm^{-1} for HNT-F6 which represents the C-H stretching vibrations which occurs in the region 2975-2840 cm^{-1} [238]. This indicates the formation of a condensation reaction between the hydroxyl groups on the surface of HNTs and the methoxy groups of silanes.

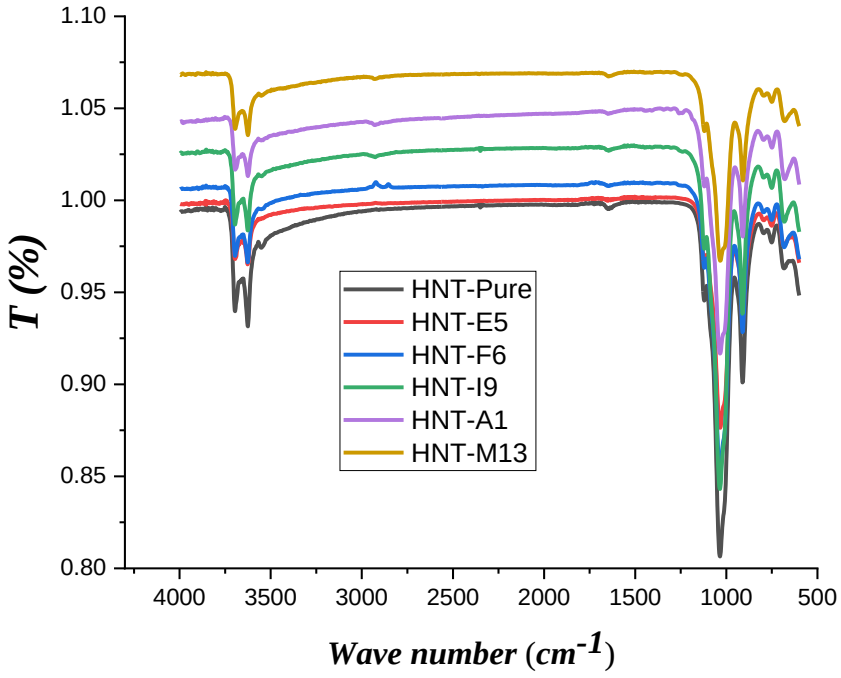

Figure 3.4 - FT-IR spectra for the effect of the volume of solvent on grafting MPTMS on HNTs surface.

3.1.4 Effect of catalyst on the grafting process

The catalyst in the investigated chemical reaction provides an alternate pathway by lowering the activation energy between reactants and products. Triethyl amine (Et_3N), ammonia solution (NH_4OH), and tetra-ethoxy titanium (Ti $(OEt)_4$) were used as catalysts for the grafting of MPTMS on the surface of halloysite nanotubes because they act as proton acceptors, facilitating

the condensation reaction between hydroxyl groups on the surface of HNTs and methoxy groups of silanes. Figure 3.5 and Table 3.1 show the FT-IR spectra and elemental analysis data for samples treated with these catalysts for grafting MPTMS on HNTs surfaces.

HNT-P16 has bands at 1239 cm^{-1}, 2849 cm^{-1}, and 2916 cm^{-1} as shown in Figure 3.5, while HNT-N14 has bands at 2925 cm^{-1}, 2832 cm^{-1}, and 1233 cm^{-1}. The medium-intensity peaks at 2849 cm^{-1}, 2832 cm^{-1}, 2916 cm^{-1}, and 2925 cm^{-1} represent C-H stretching vibrations that occur in the region 2975-2840 cm^{-1}. The peaks at 1239 cm^{-1} and 1233 cm^{-1} are very weak and represent the CH_2 wagging, rocking, and twisting vibrations that occur in the region 1430-715 cm^{-1}, and these bands are typically of weak intensity in infrared spectra and of medium intensity in Raman [239]. These peaks indicate the formation of a condensation reaction between hydroxyl groups on the surface of HNTs and methoxy groups of silanes. These results indicate that the catalyst has a positive effect on the reaction's progress.

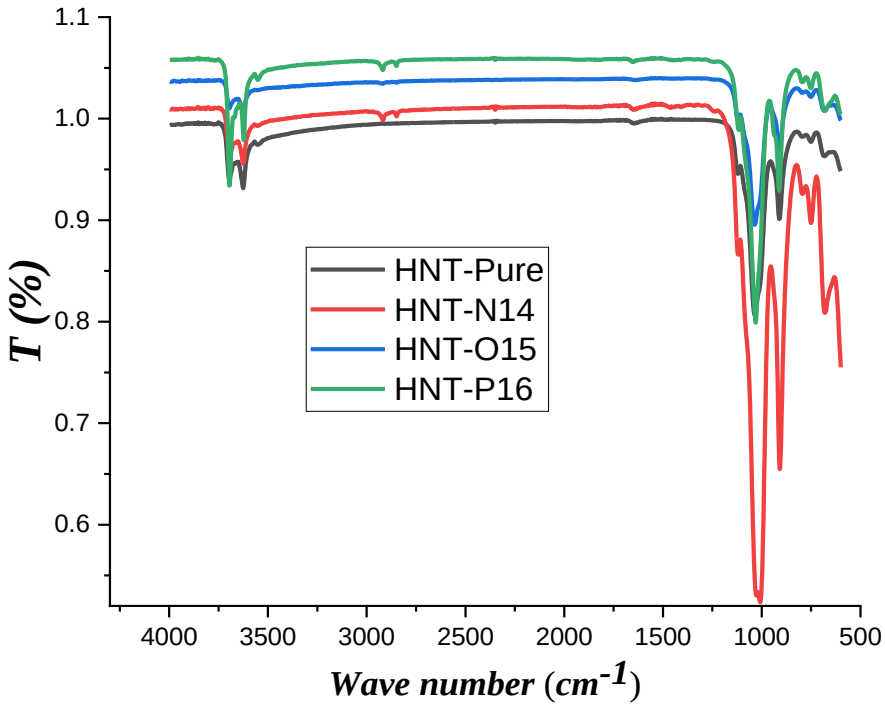

Figure 3.5 - FT-IR spectra for the effect of catalyst on grafting MPTMS on HNTs surface.

3.1.5 Characterization of the sample with the highest functionalization degree

The best modified sample was characterized by using thermogravimetric analysis (TGA), scanning electron microscope (SEM), FT-IR analysis and elemental analysis as shown in Figures 3.6, 3.7 and 3.8 and reported in Table 3.1, respectively.

According to Figure 3.6, the main mass loss for pristine HNT occurred in the temperature range (400-550 °C), which can be attributed to the dehydroxylation of structural hydroxyl groups in HNTs [240], whereas the main mass loss for (HNT-P16) occurred in the temperature range (250-500 °C). This is due to the condensation reaction between the hydroxyl groups on the surface of the HNTs and the methoxy groups of the silane, which results in the formation of a covalent bond.

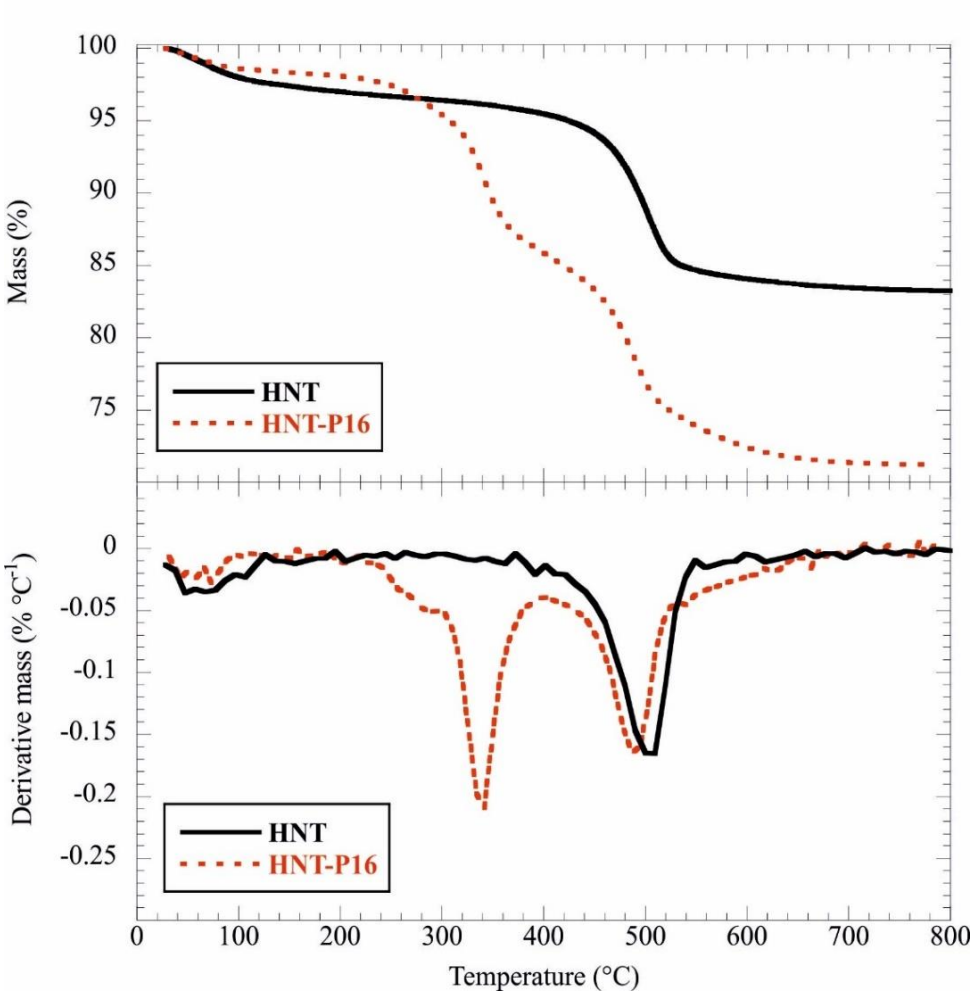

Figure 3.6 - TGA and DTG curves of pristine HNTs and the best modified HNTs sample.

Figure 3.8 depicts bands for (HNT-P16) at 1241 cm^{-1}, 2849 cm^{-1}, and 2921 cm^{-1} that are not present in pristine HNTs. The medium-intensity peaks at 2849 cm^{-1} and 2921 cm^{-1} correspond to C-H stretching vibrations that occur in the region 2975-2840 cm^{-1}. The peak at 1241 cm^{-1} is

very weak and represents the CH_2 wagging, rocking, and twisting vibrations that occur in the region 1430-715 cm^{-1}.

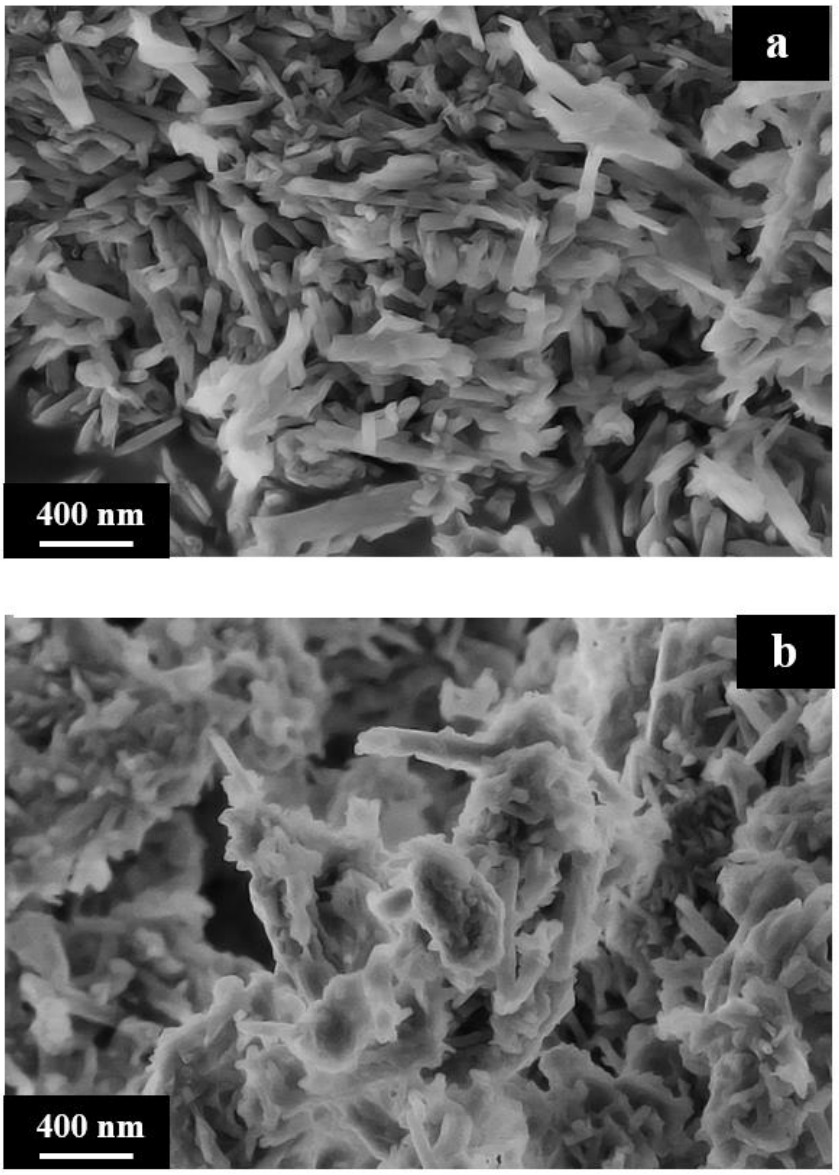

Figure 3.7 - SEM image of pristine HNTs (a) and the best modified HNTs sample (b).

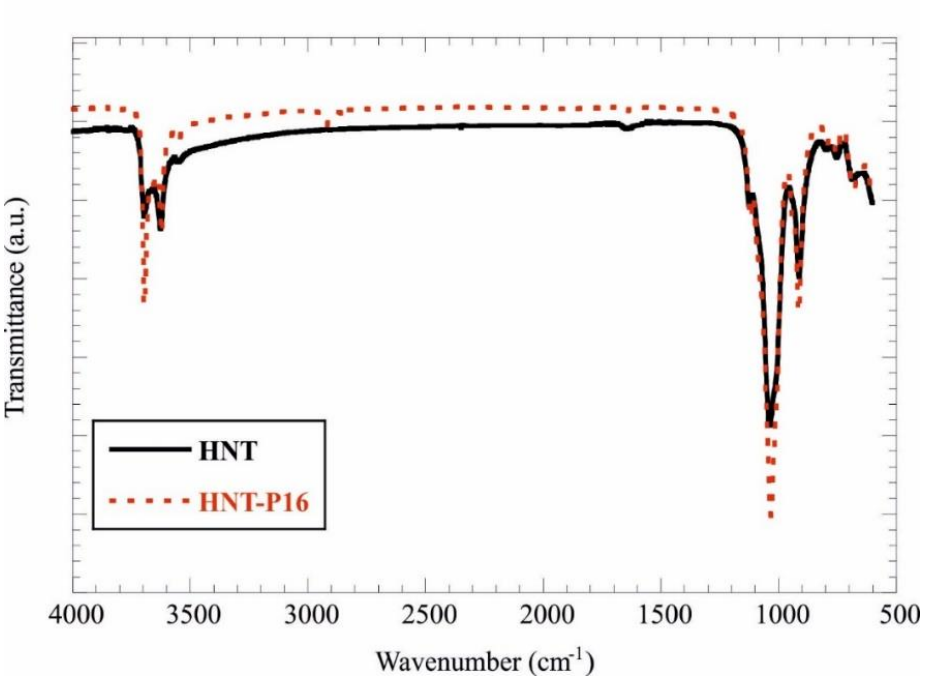

Figure 3.8 - FT-IR spectra of pristine HNTs and the best modified HNTs sample.

3.1.6 Sorption experiments using the best grafted HNT sample

The sorption capacity of both HNTs and the best modified HNTs sample was tested by contacting of a small mass (0.1 g) of (HNTs) and (HNT-P16) with a fixed volume (8 ml) of aqueous solution containing a mixture of metal ions with concentrations ca. 1500 mg/l and pH = 6.5 in a conical flask. The flasks were agitated for 24 hours. (Rotation speed, v = 700 rpm) at 25 °C. After equilibration and phase separation, the residual metal ions concentration in the aqueous phase (C_{eq}, mg/l) was measured by using an Inductively Coupled Plasma Optical Emission Spectrometer (relative error 0.08 %).

Table 3.2 - Data of the sorption capacity of both pristine HNTs and [HNT-P16] using a solution of metal acetate, at 25°C, pH= 6.5 and agitation time 24 hours.

Sample	Sorption capacity, mg/g			
	Co	Cu	Ni	Zn
HNTs	0	1	0	0
HNT-P16	0	28	0	2

Error is 5% on sorption capacity.

The mass balance equation was used to calculate the sorbent's capacity (Q_{eq} = ((C_o –C_{eq}) V/m), while C_o, C_{eq} are the initial and equilibrium concentrations of metal ions in the solution (mg/l), (V) is the volume of the solution (L), and (m) is the mass of pristine HNT or [HNT-P16] (g). The obtained results showed that the maximum sorption capacity for Cu (II) ions was changed from 1 mg/g to 28 mg/g by using pristine HNTs and HNT-P16, respectively (Table 3.2). These results indicate the effect of HNT modification on the sorption capacity of Cu (II) ions and its selectivity for Cu (II) ions.

3.2 Grafting of (3-Glycidyloxypropyl) trimethoxy silane (GOPTMS) on halloysite nanotubes surface

3.2.1 Effect of solvent

The solvent has a significant impact on the chemical modification process's rate and thermodynamic route. It can function as a base or a proton donor. Many solvents, including toluene, tetrahydrofuran, ethanol, 1,4-dioxane, acetonitrile, and n-hexane, have been tested for the silanization of halloysite nanotubes using (3-Glycidyloxypropyl) trimethoxy silane. As shown in Table 3.3, the polarity of these solvents influences the degree of functionalization of GOPTMS on the HNT surface.

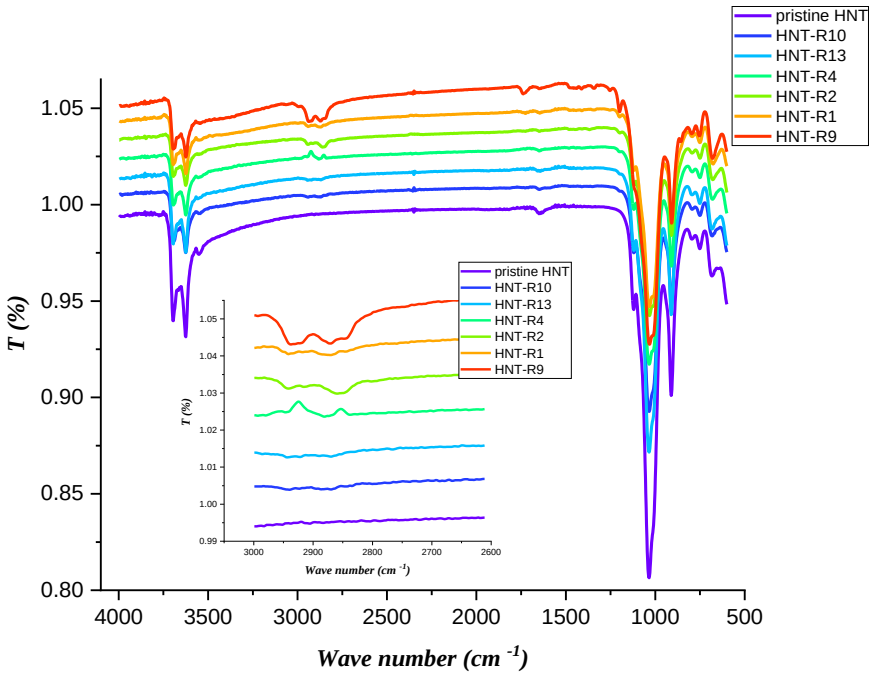

Figure 3.9 - FT-IR Spectra for the effect of solvent on grafting of GOPTMS on the surface of HNTs.

The degree of functionalization of GOPTMS onto HNTs using toluene, tetrahydrofuran, ethanol, 1,4-dioxane, acetonitrile and n-hexane was 45.6, 43.46, 23.156, 21.01, 21.015 and 93.35%, respectively. Relying on the data obtained from elemental analysis and FT-IR analysis Figure 3.9, it was found that n-hexane is the most effective solvent for the grafting of (3-Glycidyloxypropyl) trimethoxy silane onto the HNTs surface. This indicated that the solvent with low value of Dielectric constant is more appropriate for the grafting process.

Table 3.3 - Elemental analysis of HNT samples which have been chemically grafted in various types of solvent using (3-Glycidyloxypropyl) trimethoxy silane.

Sample	Content, %			Degree of grafting (%)
	C	H	N	
HNT- R1	8.98	2.73	0	45.602
HNT- R2	8.56	2.66	0	43.468
HNT- R3	9.95	3.02	0	50.527
HNT- R4	4.56	2.19	0	23.156
HNT- R5	7.35	2.66	0	37.324
HNT- R6	9.61	2.93	0	48.801
HNT- R7	6.05	2.43	0	21.476
HNT- R8	6.22	2.36	0	18.910
HNT- R9	18.31	3.9	0	93.357
HNT- R10	4.12	2.15	0	21.012
HNT- R11	4.86	2.23	0	24.761
HNT- R12	5.2	2.24	0	26.521
HNT- R13	4.12	2.12	0	21.015
HNT- R14	6.11	2.87	0	37.253
HNT- R15	17.37	4.16	0	88.589
HNT- R16	10.02	3.54	0	51.103
HNT- R17	13.83	3.36	0	70.534
HNT- R18	16.02	4.08	0	95.674
HNT- R19	4.945	2.275	0	19.880
HNT- R20	5.345	2.21	0	18.475
HNT- R21	22.575	4.645	1.325	98.427
HNT- R22	22.285	4.545	1.765	97.008
HNT- R23	4.26	2.15	0	33.593

3.2.2 Effect of HNTs: GOPTMS: H_2O molar ratio

The molar ratio (HNTs/GOPTMS/H_2O) has been varied as (1:1.42:3.15), (1:1.42:0), (1:2.85:0), (1:4.27:0) and (1:1.06:8.5). Based on the results obtained from elemental analysis (Table 3.3) and FT-IR analysis (Figure 3.10), the greatest degree of grafting was achieved by using the molar ratio (1:1.42:3.15). The degree of functionalization of GOPTMS onto HNTs using the molar ratio (HNTs/GOPTMS/H_2O) equal (1:1.42:3.15), (1:1.42:0), (1:2.85:0), (1:4.27:0) and (1:1.06:8.5) was 50.52, 45.6, 21.47, 18.91 and 37.25 %, respectively.

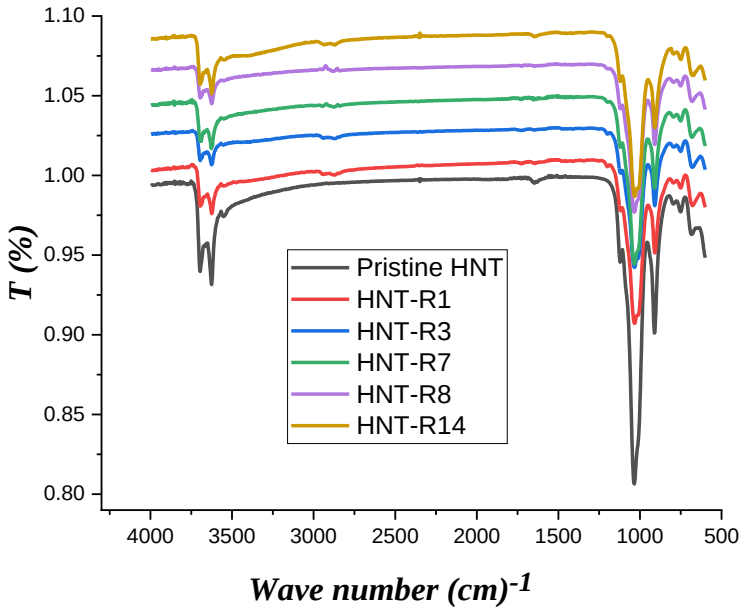

Figure 3.10 - FT-IR spectra for the effect of HNTs: GOPTMS: H_2O molar ratio on grafting process.

3.2.3 Effect of catalyst on silanization of HNTs using GOPTMS

It is known that the catalyst reduces the energy of the rate-limiting transition state and hence increases the rate of the chemical reaction. The effect of catalyst on the silanization of halloysite nanotubes using (3-Glycidyloxypropyl) trimethoxy silane was investigated using triethyl amine and ammonia solution as a base catalyst. The calculated degree of grafting using 2 ml of Et_3N, 1 ml of NH_4OH, 2 ml of NH_4OH was 26.52, 98.42, and 97.1%, respectively, based on elemental analysis data. Based on the results obtained for the calculated degree of functionalization, it was discovered that using 1 ml of NH_4OH is the best way to achieve the greatest degree of grafting of GOPTMS on the surface of HNTs. NH_4OH can function as a

Bronsted base, enhancing the proton transfer mechanism. This is clearly visible in the increased degree of grafting, as shown in Table 3.3.

3.2.4 Effect of time

The influence of time on the functionalization of halloysite nanotubes by (3-Glycidyloxypropyl) trimethoxy silane has been studied, and the functionalization degree results are shown in Table 3.3 and Figure 3.11. Three experiments were carried out with refluxing time of 2, 4, and 35 hours. Based on elemental analysis, the estimated functionalization degree values were 45.6, 48.8, and 26.52% for the experiments with refluxing time of 4, 35, and 2 hours, respectively. Based on the results, it is possible to conclude that the efficiency of functionalization of (3-Glycidyloxypropyl) trimethoxy silane on the surface of halloysite nanotubes increased as the refluxing time increased.

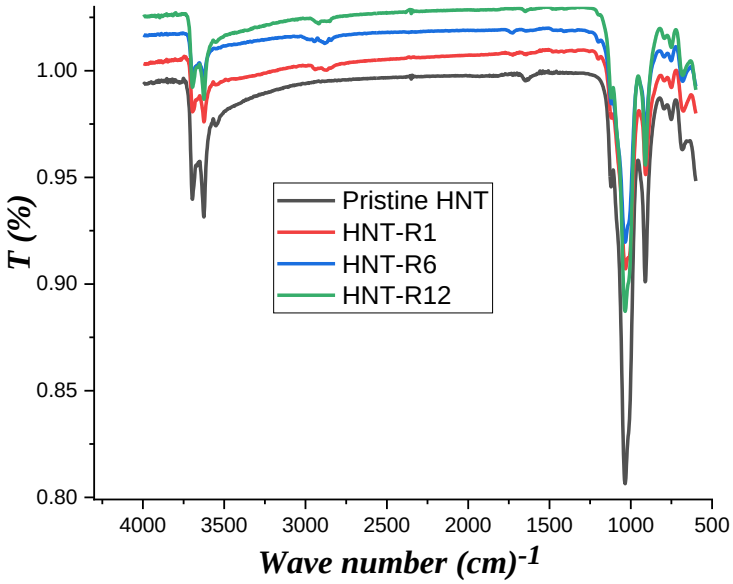

Figure 3.11 - FT-IR spectra for the effect of time on grafting GOPTMS on HNTs surface.

3.2.5 Effect of volume of n-hexane

n-Hexane has been chosen as the best solvent for functionalization of halloysite nanotubes using (3-Glycidyloxypropyl) trimethoxy silane. Four experiments were performed using 10, 20, 40, 80 mL of n-hexane. Based on elemental analysis, the estimated functionalization degree values were 93.4, 88.6, 51.1, and 70.5 % for the experiments of n-hexane volumes equal 40, 20, 10 and 80 mL, respectively. Table 3.3 and Figure 3.12 show the results.

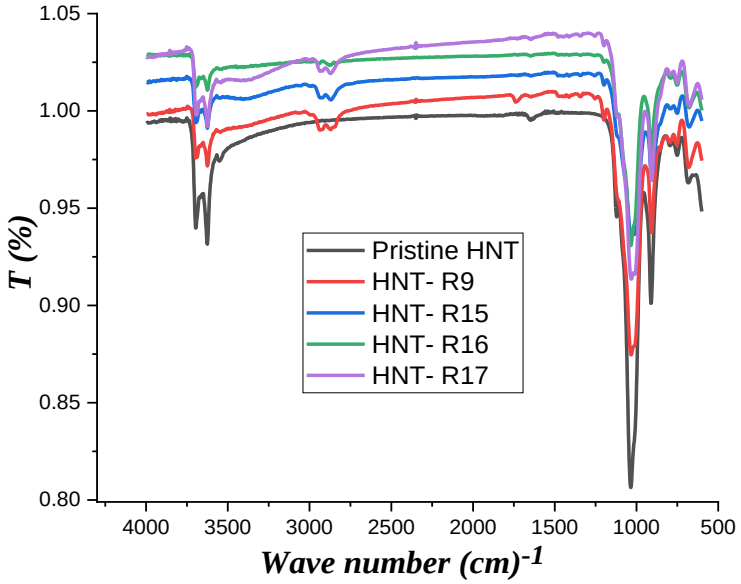

Figure 3.12 - FT-IR spectra for the effect of volume of n-hexane on grafting GOPTMS onto HNTs surface.

3.2.6 Characterization of the sample with the highest functionalization degree

Fourier transform infrared spectra of pristine HNT and the best grafted HNT with (3-Glycidyloxypropyl) trimethoxy silane are shown in Figure 3.13.

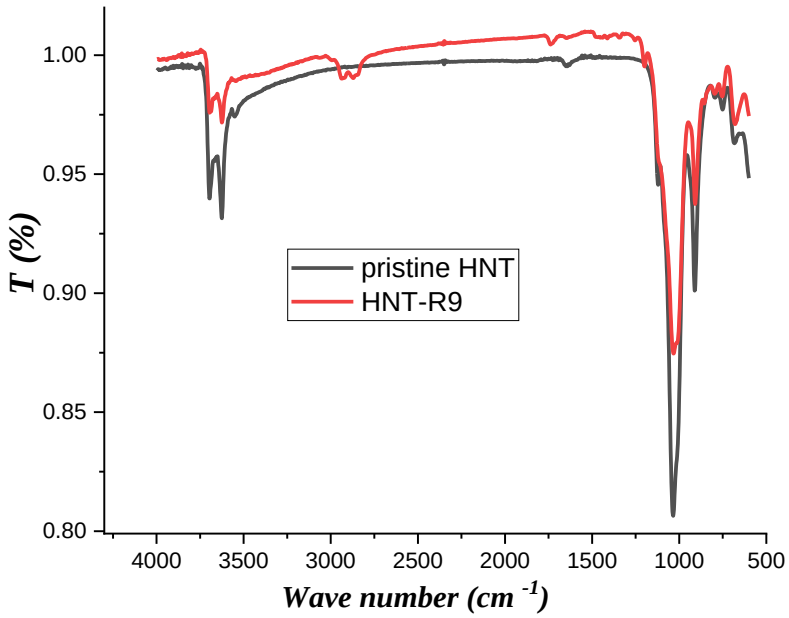

Figure 3.13 - FT-IR spectra of pristine HNTs and the best modified HNTs sample.

In comparison to pristine halloysite, some new signals were illuminated for the sample (HNT-R9) which has been done in the presence of n- hexane as a solvent. These peaks were noticed at 2930 cm^{-1}, 2860 cm^{-1}, 1725 cm^{-1} and 1200 cm^{-1}. The bands at 2930 cm^{-1} and 2860 cm^{-1} clarify symmetric stretching vibration and asymmetric stretching vibration of CH_2 groups, respectively [241]. The asymmetric deformation vibration of CH_2 groups results in a weak band near 1725 cm^{-1}. The deformation vibration of Si-CH_2-R that appears at 1175-1250 cm^{-1} was noticed by the weak band which occurs at 1200 cm^{-1} [239]. These peaks which were clarified for the sample (HNT-R9) indicate the formation of a cross-linked structure which results from the condensation of OH groups on halloysite nanotubes surface and methoxy groups of GOPTMS. Differential thermogravimetric (DTG) and thermogravimetric (TGA) curves of pristine HNT and the grafted HNT sample are shown in Figure 3.14 (a, b).

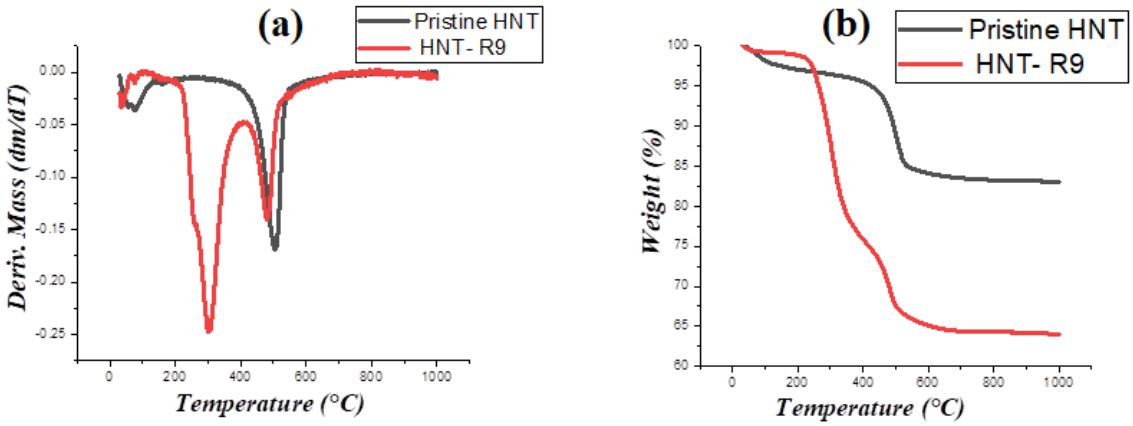

Figure 3.14 - DTG curves (a) and Thermogravimetric analysis (b) of pristine HNT and the best grafted HNT sample.

Figure 3.14 (a) shows the DTG peaks for both pristine HNT and the best grafted HNT sample. The mass loss for pristine HNT below 200°C can be attributed to the water molecules physically linked to the clay interface [242]. It was clarified that the greatest mass loss of pristine HNT occurred for temperatures ranging from 400 to 550 °C and this is imputed to the dehydroxylation of HNT's OH groups. The greatest mass loss was observed with a wider temperature variation of (200 to 500 °C) in the best grafted sample that was prepared in n- hexane. This may be attributed to the silanes physiosorbed on the HNT surface, which are covalently bonded because of the condensation reaction that occurs between the hydrolyzed silanes and the

HNT hydroxyl groups [243-245]. Table 3.4 displays the amount of the loaded silane values on HNT surface, which was calculated using Eq. 2.3 according to the rule of mixtures.

Table 3.4 - Thermogravimetric analysis of HNT samples which have been grafted in several types of solvent using (3-glycidyloxypropyl) trimethoxy silane.

Sample	Solvent	Dielectric constant	δ / $J^{1/2}$ $cm^{-3/2}$	Loaded amount (%) [a]
HNT- R1	Toluene	2.4	18.29	12.57
HNT- R2	THF	7.5	18.62	12.49
HNT- R4	Ethanol	24.5	26.43	6.28
HNT- R9	n-Hexane	2.0	14.81	23.80
HNT- R10	1, 4 dioxane	2.3	20.66	6.46
HNT- R13	Acetonitrile	37.5	24.39	6.51

[a] Determined by using Eq. (2.3)

The latter was widely used to determine the degree of functionalization of HNT modified by supramolecular and covalent interactions [246]. The silane loadings were 23.80 and 12.57 wt.% for the grafted samples which were prepared in n- hexane and toluene, respectively. The grafting efficiency was very low using ethanol as a dispersing solvent. This may be related to the ability of polar-protic solvents to solvate the silanol groups, resulting in a greater amount of GOPTMS being deposited on the halloysite surface via oligomerization. This reduces the reactivity of silane molecules towards halloysite nanotubes surface. In case of non-polar solvents, oligomerization greatly restrained, and hence the reaction proceed through the direct condensation of hydrolyzed GOPTMS and the HNT hydroxyl groups (located at the internal wall, at the edge, and at defects of the external surface) as a result of increasing the reactivity of silane molecules towards HNT surface [247, 248]. Another important fact that must be considered is the effect of dielectric constant of the solvent that was used as a dispersing media. The solvents that have great values of dielectric constant, having high strength of H-bonding. The H-bonding between GOPTMS and the OH groups will dominate in this case rather than the condensation reaction. For these reasons, n-hexane was probably the solvent providing the greatest organic content in the composite after the grafting process. To provide a predictive and semiquantitative view on the solvent polarity effect on the loading efficacy, we thought interesting to consider the Hildebrand solubility parameter that [249] are provided in Table 3.4 for all the investigated solvents. Figure 3.15 shows that there

is a correlation between the solubility parameters of the solvent and Wt. (%) of silane loaded. As the value of the solubility parameters (δ / $J^{1/2}$ $cm^{-3/2}$) increases the value of Wt. (%) of silane loaded decreases to a plateau. Interestingly a threshold limit at ca. 20 $J^{1/2}$ $cm^{-3/2}$ was observed. SEM images were collected for the sample with the greatest organic content ([HNT- R9] in n-Hexane) and compared to pristine halloysite as shown in (Figure 3.16). In agreement with the high loading of organic moieties determined by TGA, the sample [HNT- R9] shows a SEM image different from that of the pristine HNT highlighting nanotubes embedded in an organic matrix.

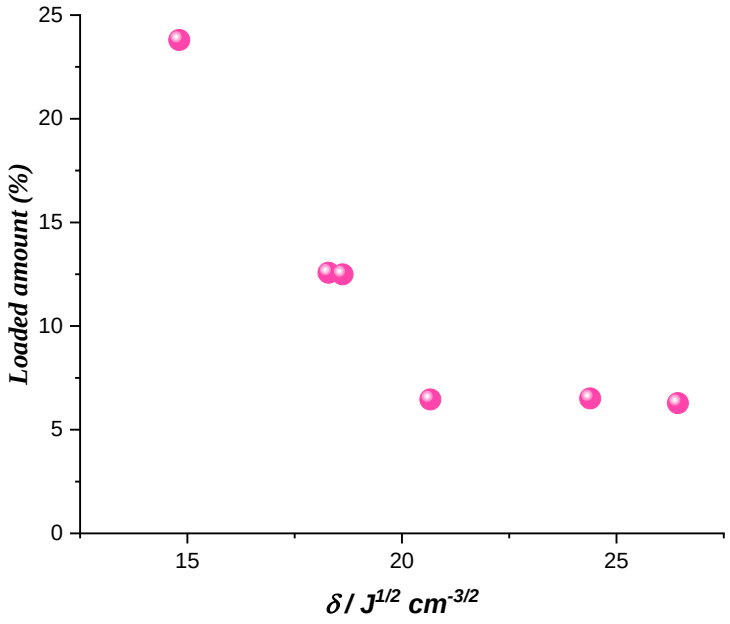

Figure 3.15 - The relation between Wt. (%) of silane loaded and the solubility parameters.

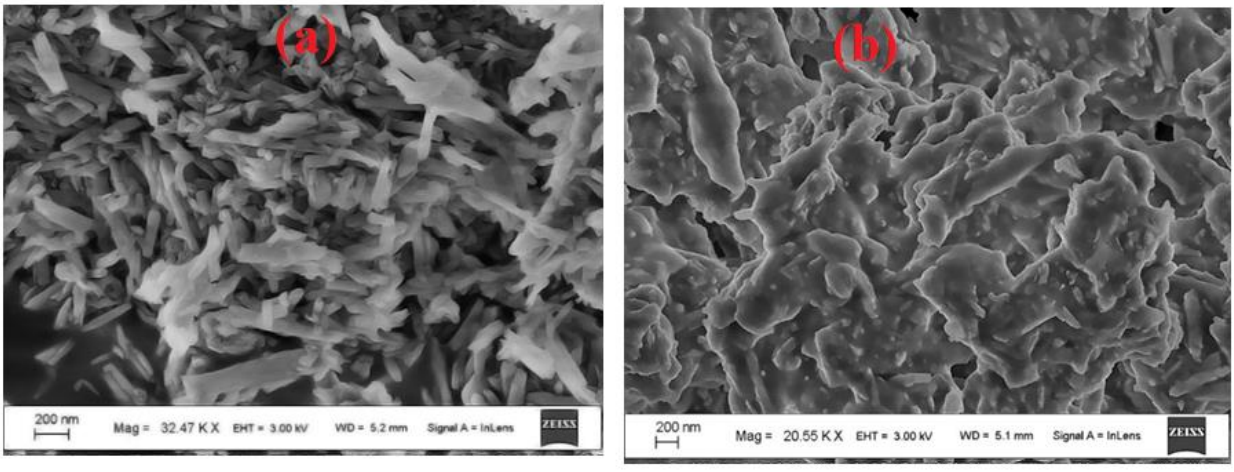

Figure 3.16 - SEM images for pristine HNT (a) and [HNT- R9] sample (b).

3.3 Grafting of (3-Chloropropyl) trimethoxy silane (CPTMS) on halloysite nanotubes surface

3.3.1 Effect of solvent

Selecting the appropriate solvent for the silanization of halloysite nanotubes using (3-chloropropyl) trimethoxy silane is critical due to the effect of solvent on both the rate and thermodynamic route of the chemical modification process. The solvent can act as a source of protons or act as a base. Furthermore, the solvation of the reactant can also be considered. In the present work, many solvents have been tested for the silanization of halloysite nanotubes using (3-chloropropyl) trimethoxy silane, such as ethanol, toluene, tetrahydrofuran, 1,4-dioxane, and n-hexane. The nature of these solvents influences the grafting degree of CPTMS onto the HNT surface as mentioned in Table 3.5. The degree of grafting of CPTMS onto HNTs using ethanol, toluene, tetrahydrofuran, 1,4-dioxane, and n-hexane was 10.75, 24.29, 11, 14.3, and 15.32%, respectively. Relying on the data obtained from elemental analysis and FT-IR analysis (Figure 3.17), it was found that toluene is the most effective solvent for the grafting of (3-chloropropyl) trimethoxy silane onto the HNT surface [250].

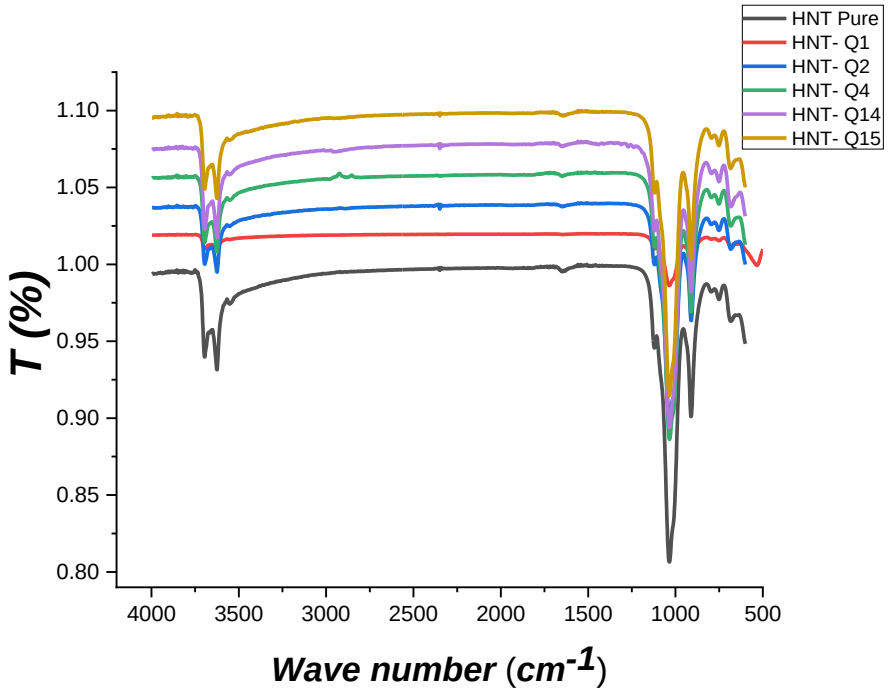

Figure 3.17 - FT-IR Spectra for the effect of solvent on grafting of CPTMS on the surface of HNTs.

Table 3.5 - Elemental analysis of HNT samples which have been chemically grafted in various types of solvent using (3-Chloropropyl) trimethoxy silane.

Sample	Content, %		Degree of grafting (%)
	C	H	
HNT- Q1	2.17	1.83	24.29
HNT- Q2	1.20	1.63	11
HNT- Q3	3.26	2.22	36.5
HNT- Q4	0.96	1.53	10.75
HNT- Q5	1.40	1.90	12.84
HNT- Q6	2.01	1.86	22.5
HNT- Q7	1.89	1.97	21.16
HNT- Q8	2.41	2.03	17.13
HNT- Q9	2.98	1.95	21.19
HNT- Q10	4.31	2.85	48.26
HNT- Q11	6.63	2.97	27.77
HNT- Q12	3.69	2.14	33.83
HNT- Q13	2.655	2.175	24.34
HNT- Q14	1.67	1.96	15.320
HNT- Q15	1.56	1.86	14.3
HNT- Q16	4.84	2.22	54.19
HNT- Q17	4.55	2.13	50.95
HNT- Q18	7.26	2.55	81.35
HNT- Q19	3.17	2.1	35.49
HNT- Q20	4.52	2.24	50.67

3.3.2 Effect of HNTs: CPTMS: H_2O molar ratio

Even though an increasing concentration of reactants results in enhancing the chance of collisions between the reactant molecules, hence speeding the rate of reaction, increasing the number of moles of CPTMS results in decreasing the degree of grafting of CPTMS onto the HNT surface. There is no clear explanation for this observation [232-234, 251]. The molar ratio HNTs/CPTMS/H_2O has been varied: 1:1:0, 1:2:0, 1:1.33:0, and 1:1:3. Based on the results obtained from elemental analysis and FT-IR analysis (Figure 3.18), the greatest degree of grafting was achieved by using the molar ratio 1:1:3. The effect of HNT/silane molar ratio on silanization of HNTs using (3-aminopropyl) triethoxy silane and (3-mercaptopropyl) trimethoxy silane was

studied in our recent work, and the results show that the degree of silane grafting onto the HNT surface decreased as the number of moles of silane increased [252, 253]. It was discovered in this study that a molar ratio of HNTs: CPTMS: H_2O equal 1:1:3 results in a high degree of grafting as shown in Table 3.5.

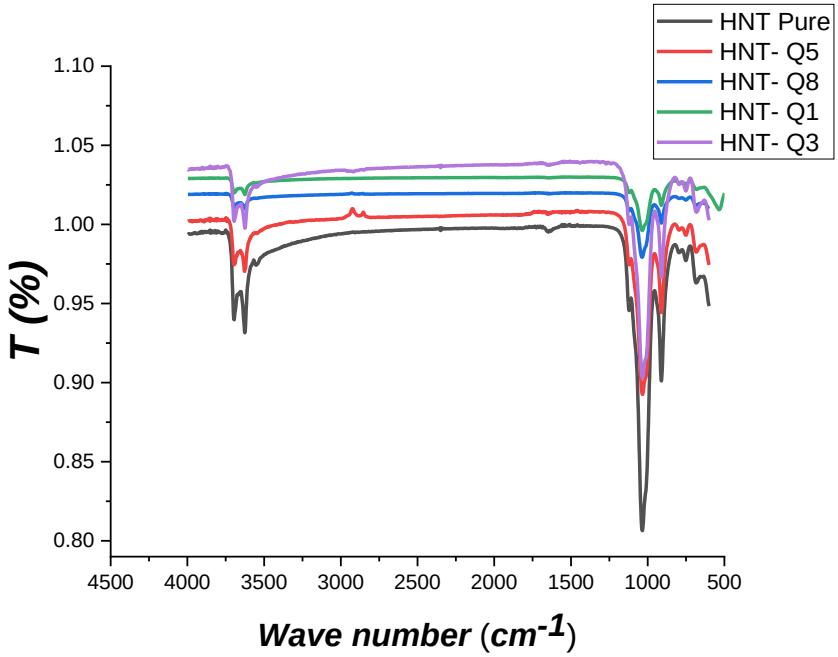

Figure 3.18 - FT-IR spectra for the effect of HNTs: CPTMS: H_2O molar ratio on grafting process.

3.3.3 Effect of catalyst on silanization of HNTs using CPTMS

Because it only works to reduce the energy of the rate-limiting transition state, a catalyst can change the rate of a chemical reaction while remaining chemically unchanged. It has no effect on the amount of product produced. To speed up the grafting of CPTMS onto the HNT surface, urea, triethylamine, ammonium hydroxide, and tetra-ethoxy titanium were used. The addition of 0.5 mL Et_3N + 0.5 mL NH_4OH as catalysts improves the condensation reaction between silane molecules and the hydroxyl groups on the surface of the halloysite mineral. This is explained relying on the fact that both NH_4OH and Et_3N act as Bronsted bases, enhancing the proton transfer mechanism. This can be clearly noticed from the enhancement of the degree of grafting, as shown in Table 3.5 and Figure 3.19.

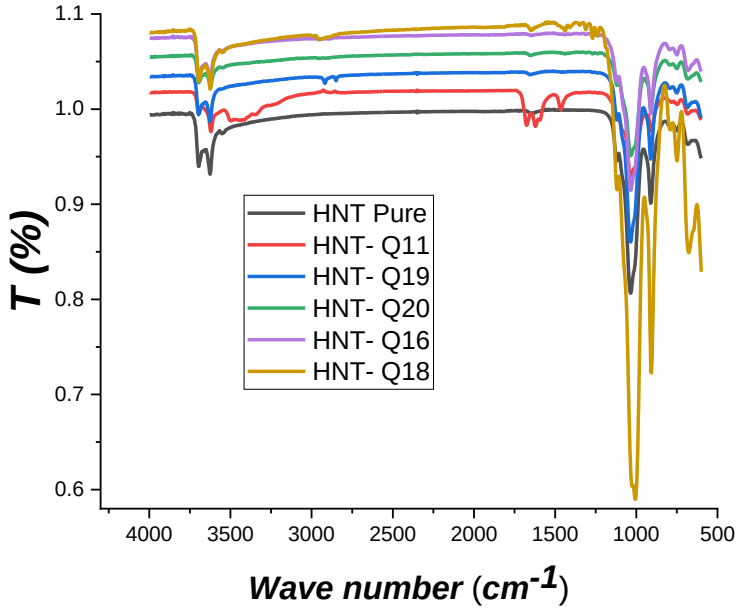

Figure 3.19 - FT-IR spectra for the effect of catalyst on grafting CPTMS on HNTs surface.

3.3.4 Effect of time

The effect of time on the degree of grafting of CPTMS onto halloysite nanotubes' surface has been discussed, and the data are reported in Table 3.5 and Figure 3.20.

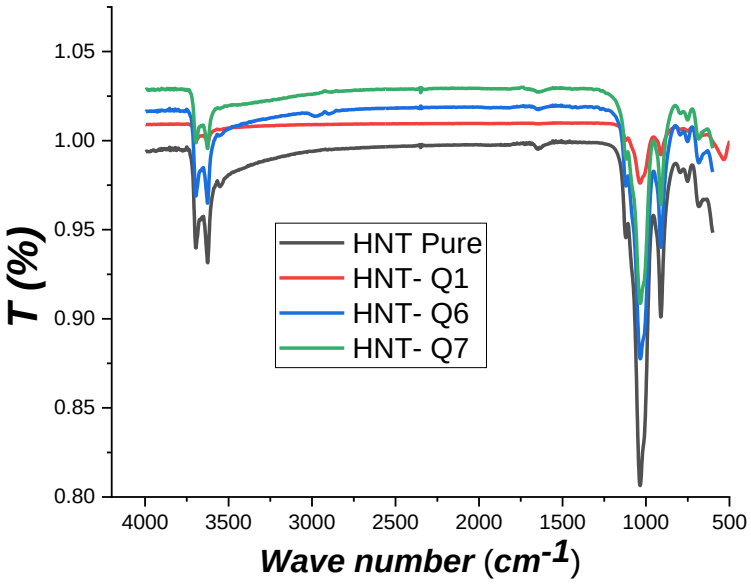

Figure 3.20 - FT-IR spectra for the effect of time on grafting CPTMS on HNTs surface.

The time was changed to be equal 4, 35, and 48 hours. The results of elemental analysis show that the degree of grafting decreased as the reaction time increased and the loss of the degree of grafting was not significant. The degree of grafting decreased in the following order: 24.29, 22.5, and 21.16 % for 4, 35, and 48 h, respectively.

3.3.5 Effect of the volume of toluene:

Toluene was chosen as the best solvent according to the elemental analysis data. The toluene volume increased from 20 to 40 mL and the degree of grafting was determined. The results show a decrement in grafting degree from 54.19 to 50.95 % when 20 and 40 mL of toluene were used, respectively. The data are reported in Table 3.5 and Figure 3.21.

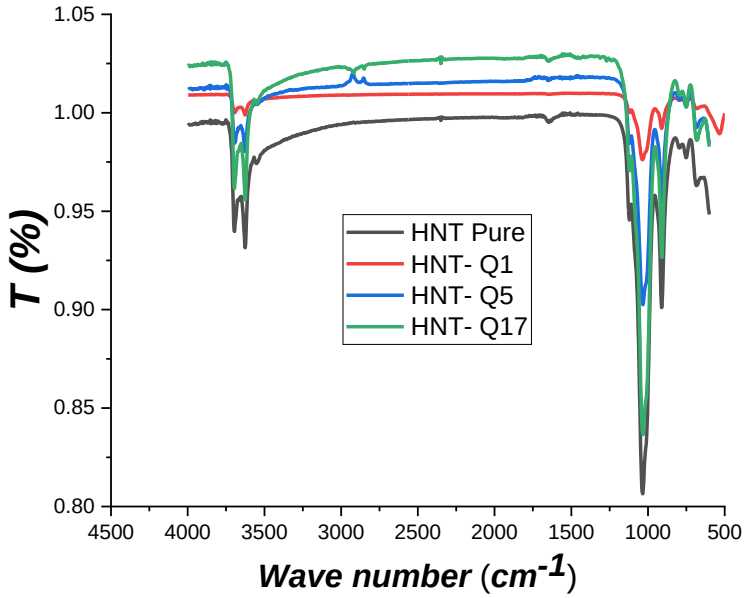

Figure 3.21 - FT-IR spectra for the effect of volume of toluene on grafting CPTMS on HNTs surface.

3.3.6 Characterization of the sample with the highest degree of grafting

FT-IR measurements (Figure 3.22), TGA (Figure 3.23), SEM (Figure 3.24) analysis, and elemental analysis for (C, H) were used to identify the sample with the highest degree of grafting using CPTMS (Table 3.5). The FT-IR measurements for pristine HNT and the best modified HNTs show the two sharp bands at 3680 cm^{-1}, 3618 cm^{-1} for HNT that represent the Hydroxyl groups O–H stretching vibrations. The band at 1652 cm^{-1} for pristine HNT represents the deformation of O–H stretching of intercalated water as shown in Figure 3.22 [254]. The presence of a new band at 2925 cm^{-1} for the best modified HNT sample represents the CH_2 stretching vibration, confirming

the formation of siloxane bonds. The presence of CH_2 groups confirms that CPTMS molecules have coated the HNTs. The TGA results of pristine HNT show that the main mass loss occurs at (400-500 °C), as previously reported for the dehydration of hydroxyl groups that are located on HNTs surface. [255]. The best modified HNT sample exhibits an additional mass loss step between 300°C and 450°C, indicating the presence of the organic moieties on the HNTs surface as shown in Figure 3.23.

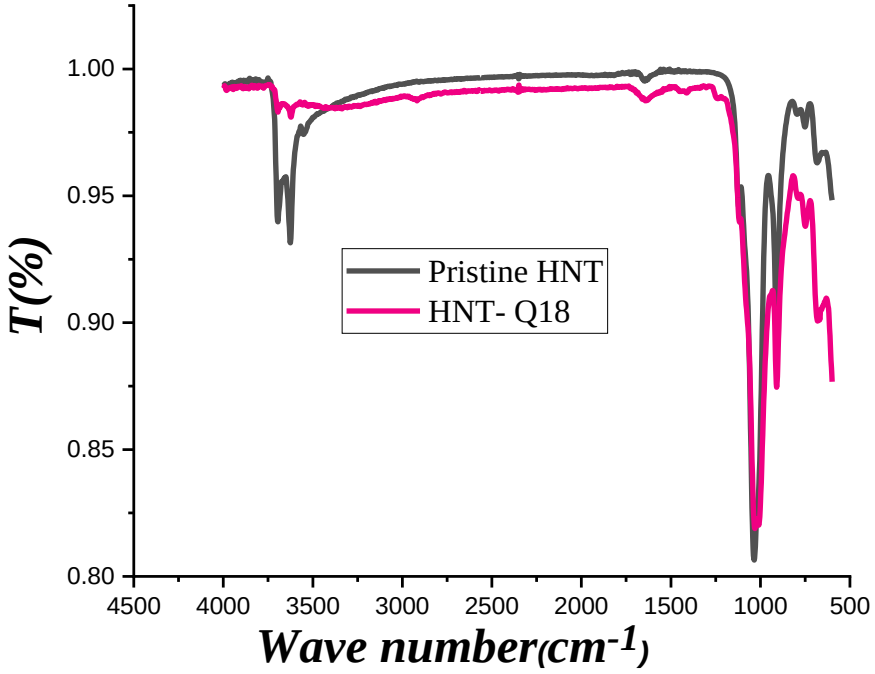

Figure 3.22 - FT-IR spectra of pristine HNTs and the best modified HNTs sample.

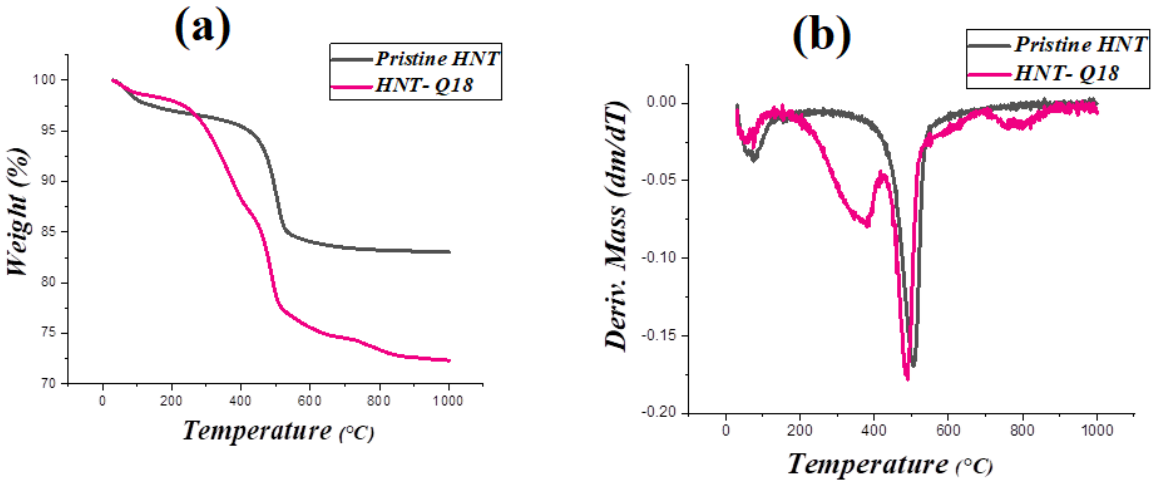

Figure 3.23 - TGA curves (a) and DTG curves (b) of pristine HNTs and the best modified HNTs sample.

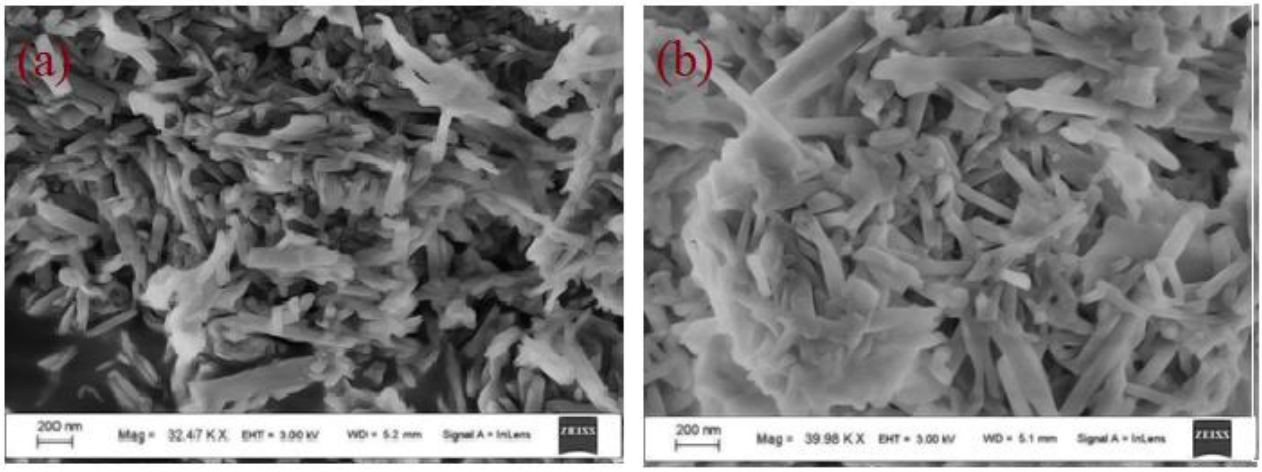

Figure 3.24 - SEM image of pristine HNTs (a) and the best modified HNTs sample (b).

Finally, the SEM morphologies confirmed that the surface modification and reaction conditions did not alter the tubular shape of the halloysite nanotubes, the halloysite nanotubes are coated with CPTMS with noticeable sticking of species together (Figure 3.24).

3.4 Characterization of halloysite nanotubes modified by polyethyleneimine (HN-PEI)

The carbon, hydrogen, and nitrogen content for pristine halloysite nanotubes, (HN-CPTM) and (HN-PEI) have been reported in Table 3.6.

Table 3.6 - Elemental analysis for pristine halloysite, (HN-CPTM) and (HN-PEI).

sample	Content (%)		
	C	H	N
Pristine halloysite	0.09	1.78	0.00
(HN-CPTM)	7.26	2.55	0.00
(HN-PEI)	12.87	9.58	4.85

The grafting of (3- chloropropyl) trimethoxy silane on halloysite nanotubes surface was emphasized due to the rising of carbon, hydrogen content (%), whereas the grafting of polyethyleneimine on (HN-CPTM) was emphasized due to the nitrogen content (%), which changed from 0.00 in case of (HN-CPTM) to 4.85 (%) for (HN-PEI). The elevation of both carbon and hydrogen content gives a notification about the significant grafting of polyethyleneimine on

HNTs surface. FT-IR spectra of pristine HNT, (HN-CPTM), and (HN-PEI) are displayed in Figure 3.25 (a, b). The bands at 3694 cm^{-1}, 3620 cm^{-1} and 1642 cm^{-1} in the spectrum of pristine HNT represent O-H stretching of inner surface hydroxyl groups and O-H deformation of water, respectively [256].

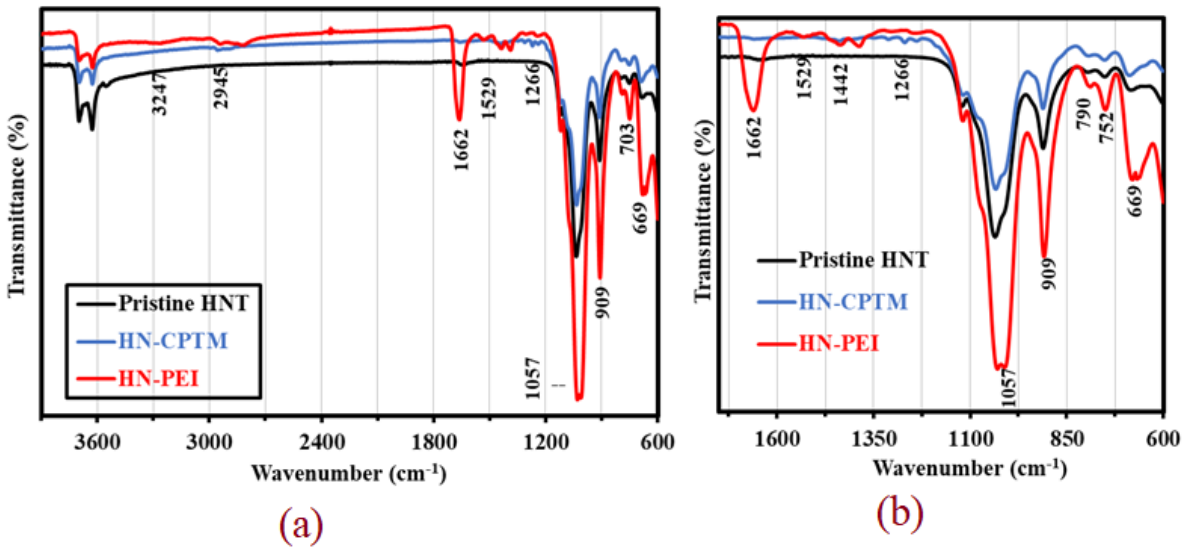

Figure 3.25 - FT-IR spectra [full wavenumber range] (a), [wavenumber range limited to 1700-600 cm^{-1}] (b) of (pristine HNT), (HN-CPTM), and (HN-PEI).

The bands at 2945 cm^{-1} and 2890 cm^{-1} in the spectrum of (HN-CPTM) represent the CH_2 stretching vibrations which can be mentioned in the wavenumber range (2975-2840) cm^{-1}. The bands at 1434 cm^{-1}, 1266 cm^{-1}, 1313 cm^{-1}, 1229 cm^{-1} display the CH_2 wagging, rocking, and twisting vibration which can be mentioned in the wavenumber range (1430-715) cm^{-1} and these bands have a low intensity in the infrared spectrum [257]. In the spectrum of (HN-PEI), the new bands appeared at the wavenumber of 3247 cm^{-1} and (1662, 1529) cm^{-1} represent the N-H stretching and scissoring absorption of NH_2 groups, respectively. The increase in the intensity of the bands at (2951, 2828) cm^{-1} represents the CH_2 stretching vibration of polyethyleneimine molecules. The new band at 669 cm^{-1} represents the out-of-plane wagging of NH_2 groups which can be mentioned at (650-900) cm^{-1}. The titration curve for pH_{PZC} assessment is provided in Figure 3.26. According to the literature, the external surface of HNT in water has a negative charge while the internal surface has a positive charge within the pH (2.5 to 8.5). It was discovered that the point of zero charges (pH_{pzc}) for (HN-PEI) occurred at pH ≈ 7 after modifying HNT with

polyethyleneimine. The surface of (HN-PEI) was positively charged in the pH range of (3 - 7) due to the protonation of amino groups, and these groups changed to be in the form of $-NH_3^+$.

Strong protonation of amino groups is expected at pH (2 - 4), which increases the difficulty of binding between the metal cations and the protonated amino groups. When the pH rises, the protonation of amino groups decreases, allowing the metal ions to bind via electrostatic attraction.

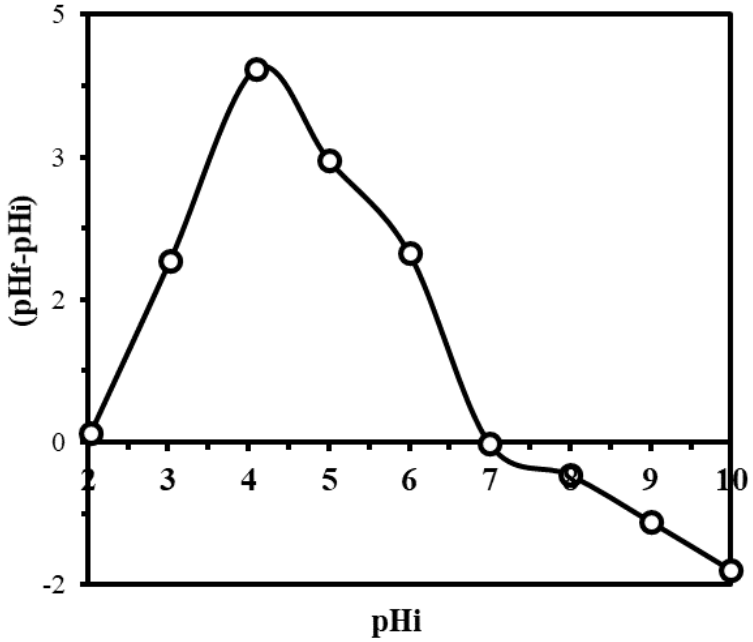

Figure 3.26 - The titration curve for pH_{PZC} estimation in case of [HN-PEI] dispersed in a solution of NaCl (0.1M) using [HN-PEI] = 25 mg /15 ml.

Figure 3.27 exhibits the morphology of pristine halloysite nanotubes, (HN-CPTM) and (HN-PEI). Pristine HNT particles exist in the form of a tubular shape with typical longitudinally cylindrical shapes with an irregular size distribution about/ around (< 200 μm); indicating that the cylinders were hollow and open-ended. The tubular structure of the halloysite nanotubes surface has been changed to be smoothed after chemical modification by polyethyleneimine. After the reaction of HNT with CPTM, the morphology of (HN-CPTM) changed by the remarkable sticking of the nanotubes together. For (HN-PEI), after further modification of (HN-CPTM) the smoothed surface and more sticking results in covering the surface of the nanotubes. It may be attributed to the chemical changes that impact the compact structure of the sorbent (disruption of hydrogen bonds between the chains due to chemical modification). Consequently, the sorbent is expected to

be slightly more open in terms of porosity and accessibility towards the metal ions. Figure 3.28 (a) exhibits the TGA curves of both halloysite nanotubes and (HN-PEI).

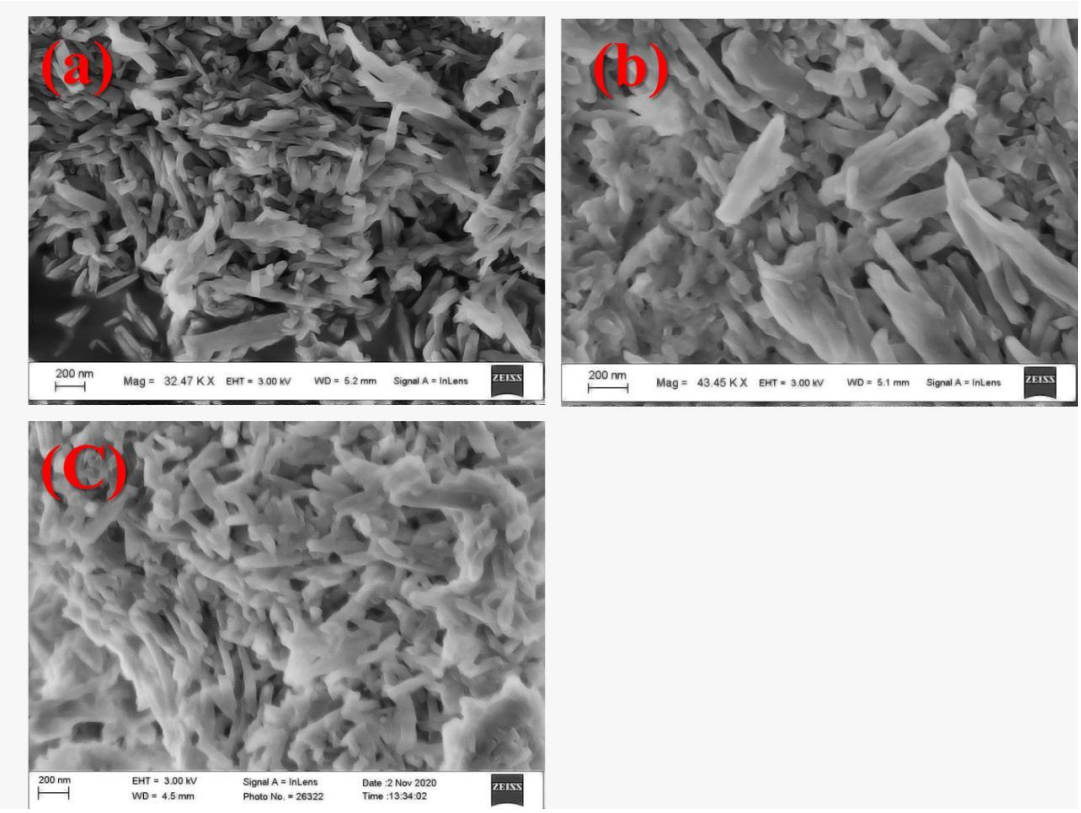

Figure 3.27 - SEM images for pristine halloysite nanotubes (a), halloysite nanotubes modified by (3- chloropropyl) trimethoxy silane (HN-CPTM) (b) and (HN-CPTM) after further modification by polyethyleneimine (HN-PEI) (C).

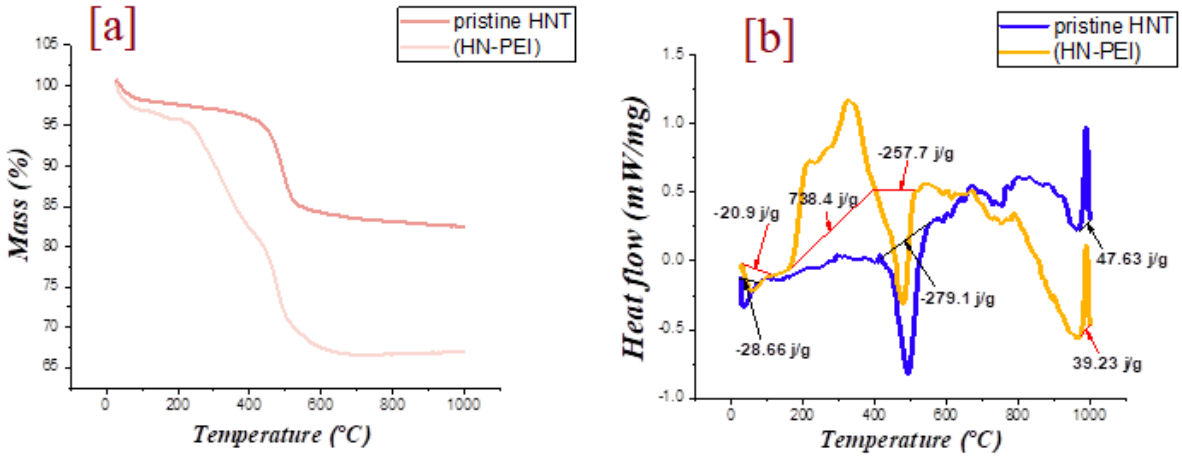

Figure 3.28 - TGA curves [a], DSC curves [b] of pristine halloysite nanotubes and (HN-PEI).

In the case of pristine halloysite nanotubes, the main loss of mass was observed in the range of (384 - 529) °C and it is caused by the dehydration of hydroxyl groups on halloysite nanotubes surface [258]. For (HN-PEI), the loss of mass was noticed within the range of (215 – 564) °C due to the degradation of polyethyleneimine moieties on the surface of the modified halloysite nanotubes. Figure 3.28 (b) exhibits the DSC curves of both pristine halloysite nanotubes and (HN-PEI). The endothermic peak that is noticed at 327 °C for (HN-PEI) represents the heat required for the dehydration process.

Figure 3.29 exhibits the comparison of the diffraction patterns in the case of pristine halloysite nanotubes and (HN-PEI). The d-Spacing [Å] was estimated for the peaks that have been changed significantly before and after modification, it is clear that the basal spacing value is slightly changed from 7.527 Å for pristine HNT to 7.203 Å for (HN-PEI) and from 3.66 Å for pristine HNT to 3.568 Å for (HN-PEI).

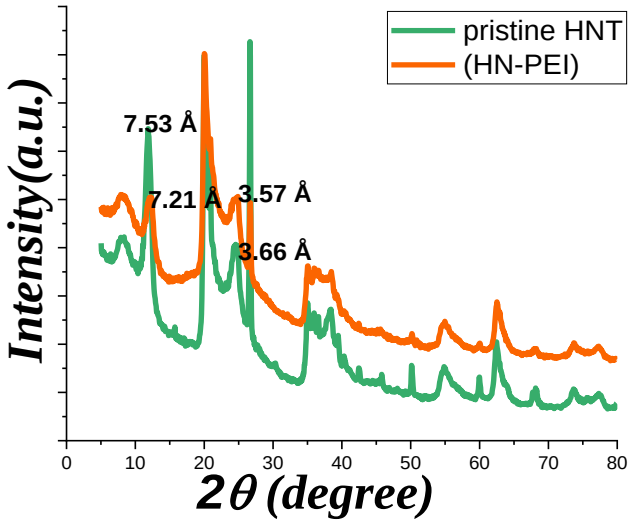

Figure 3.29 - XRD diffraction patterns of pristine halloysite nanotubes and HN-PEI.

Figure 3.30 (a) displays the nitrogen adsorption-desorption isotherms of HNT and (HN-PEI), both samples show a type IV isotherm according to IUPAC classification [259], which is a typical of a mesoporous structure. The hysteresis loop of both Pristine HNT and (HN-PEI) is similar to type H3, which is a typical of agglomerates of plate-like particles containing slit-shaped pores [260]. The quantity of N_2 adsorbed for Pristine HNT is greater than the value for (HN-PEI). The quantity of N_2 adsorbed rapidly increases at a relative partial pressure of 0.8 and more for Pristine HNT and the grafted (HN-PEI) sorbent.

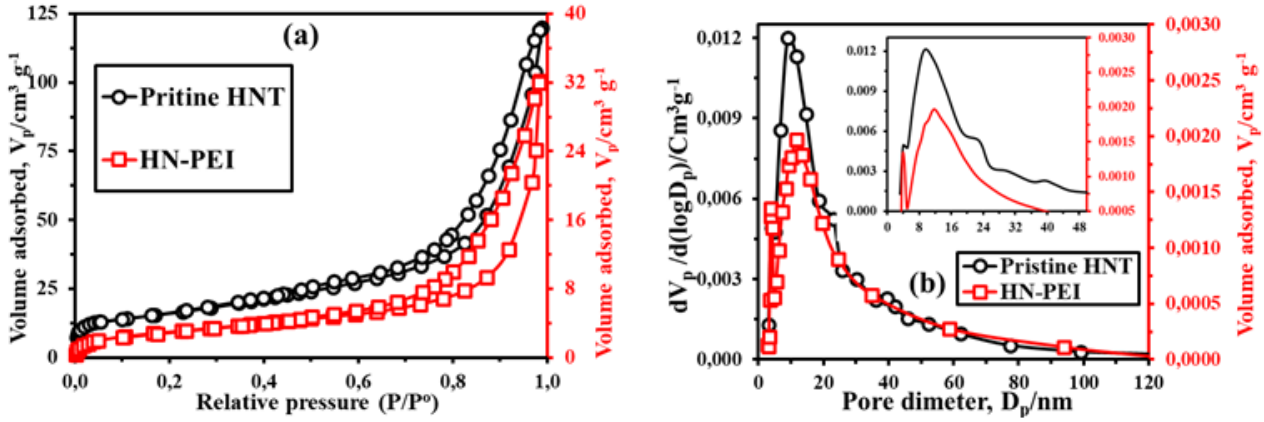

Figure 3.30 - Nitrogen adsorption/desorption models (a) and pore size distribution (b) of the Pristine HNT and the grafted (HN-PEI) sorbent.

The BET data for HNT and (HN-PEI) are shown in Table 3.7, and the pore size distribution is shown in Figure 3.30 (b). In the case of pristine HNT, the pores fall in the range of (20-50) nm, whereas in the case of (HN-PEI), the pores fall in the range of (4-15) nm. The pore volume of Pristine HNT was clearly greater than the pore volume of (HN-PEI), indicating that the grafting of polyethyleneimine on the HNT surface reduces the pore volume due to the formation of new organic coatings.

Table 3.7 - The structural characteristics of the Pristine HNT and the grafted (HN-PEI) sorbent.

Samples	BET surface area (m^2/g)	BJH pore volume (cm^3/g)	Average pore diameter (nm)
Pristine HNT	65.3	0.266	10
(HN-PEI)	10.92	0.05	18.2

3.5 Characterization of aminocarboxymethyl chitosan (CTS-CAA)

Table 3.8 reports the elemental analysis for chitosan, chitosan after its cross-linking by glutaraldehyde (CTS-GL), (CTS-GL) after its reaction with epichlorohydrin (CTS-EC), (CTS-EC) after its reaction with diethylenetriamine (CTS-DET), and (CTS-DET) after its reaction with monochloroacetic acid (CTS-CAA).

As concerns (CTS-EC), the chlorination of chitosan by Epichlorohydrin was confirmed by the decrease in carbon, hydrogen, and nitrogen contents. The significant increases in carbon, hydrogen, and nitrogen contents detected in the (CTS-DET) sample demonstrated the successful

grafting of diethylenetriamine on the (CTS-EC) sample. The significant decrease in carbon, hydrogen, and nitrogen amounts estimated in the (CTS-CAA) sample highlighted the successful grafting of monochloroacetic acid on the (CTS-DET) sample.

Table 3.8 - Elemental analysis for chitosan and modified chitosan samples.

sample	Content (%)		
	C	H	N
Chitosan	40.27	7.91	6.22
(CTS-GL)	43.01	7.23	5.81
(CTS-EC)	37.18	6.17	5.61
(CTS-DET)	43.19	7.34	8.94
(CTS-CAA)	42.54	6.98	7.38

Figure 3.31 (a, b) displays FT-IR spectra of (Unmodified chitosan), (CTS-GL), (CTS-EC), (CTS-DET), and (CTS-CAA) at a limited wavenumber range. The analysis of the FT-IR spectra provided a reliable information on the efficacy of the chitosan modification synthesis procedure.

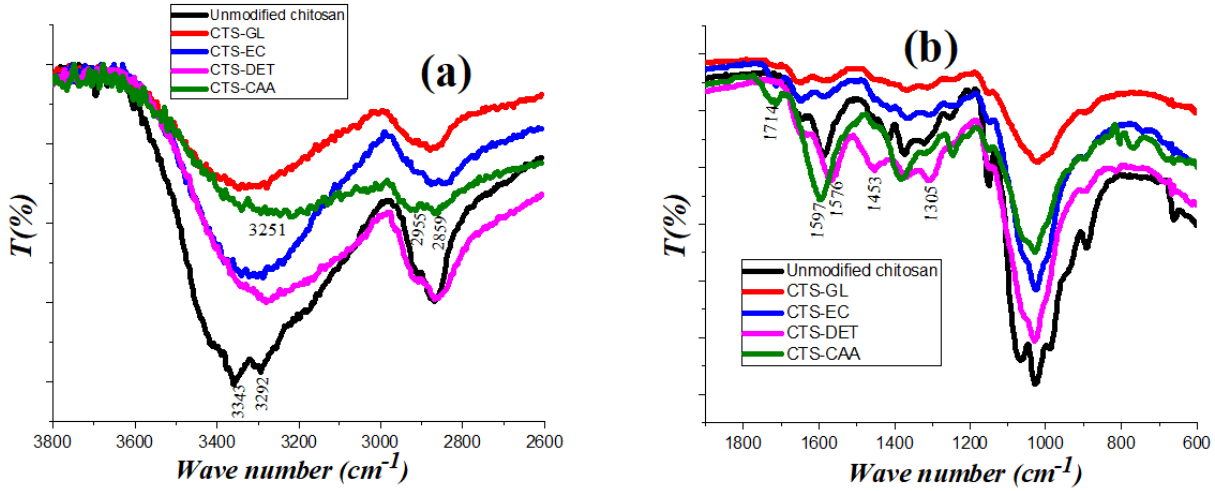

Figure 3.31 - FT-IR spectra of (Unmodified chitosan), (CTS-GL), (CTS-EC), (CTS-DET) and (CTS-CAA) [wavenumber range limited to 3800-2600 cm^{-1}] (a), [wavenumber range limited to 1900-600 cm^{-1}] (b).

The FT-IR spectrum of unmodified chitosan revealed two sharp bands centered at 3343 and 3292 cm^{-1} due to the asymmetric and the symmetric N-H stretching, respectively. These broader signals are typical of primary amines in the 3400-3250 cm^{-1} range, masking the broadband

of O-H groups. A band centered at 1564 cm^{-1} was observed which is related to the N-H bending occurring in the region 1650-1580 cm^{-1} for primary amines. A broadband at 3378 cm^{-1} was detected in the spectrum of (CTS-GLA) due to the alcohol O-H stretching in the range of 3200-3400 cm^{-1}. As a result, the two sharp bands of the N-H stretching have vanished, emphasizing the actual cross-linking of NH_2 groups by glutaraldehyde molecules. The additional bands were noticed within the area of 2951-2830 cm^{-1} because of the stretching vibration of the CH_2 groups, which are present in glutaraldehyde molecules. The spectrum of (CTS-DET) revealed the presence of sharp bands centered at 3274, 1576, and 1453 cm^{-1} (due to secondary amines N-H stretching and primary amines N-H bending, respectively), confirming the reaction between (CTS-EC) and diethylenetriamine. An additional sharp peak at 1714 cm^{-1} was detected in the spectrum of (CTS-CAA), which is related to the stretching of C=O of carboxylic acids evidencing the actual reaction between (CTS-DET) and monochloroacetic acid. Furthermore, (CTS-CAA) exhibited two weak sharp bands at 2859 and 2955 cm^{-1} (caused by the CH_2 stretching vibration of $-CH_2COOH$) and the broadband in the region between 3358 and 3171 cm^{-1}, which are generated by the stretching of N-H and O-H groups. Conjugation causes the N-H band to shift from 1576 cm^{-1} to 1597 cm^{-1}. The surface morphology of the biopolymer was affected by the chitosan modification with carboxyl groups (CTS-CAA), as displayed in SEM images (Figure 3.32).

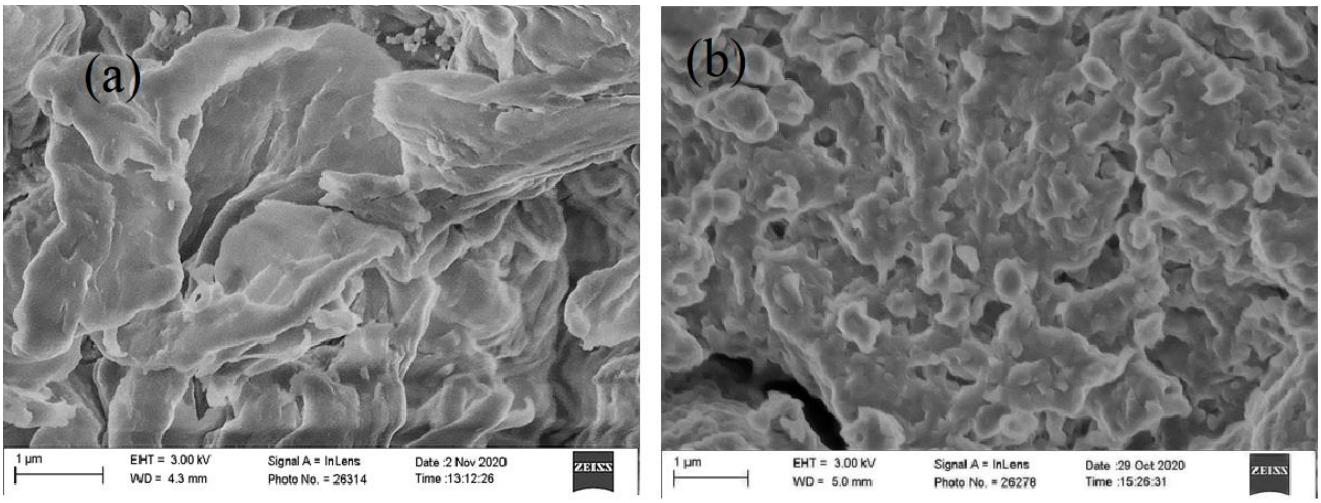

Figure 3.32 - Scanning electron microscopy images for unmodified chitosan (a) and CTS-CAA (b).

The titration curve of pH_{PZC} estimation for (CTS-CAA) sample is presented in Figure 3.33.

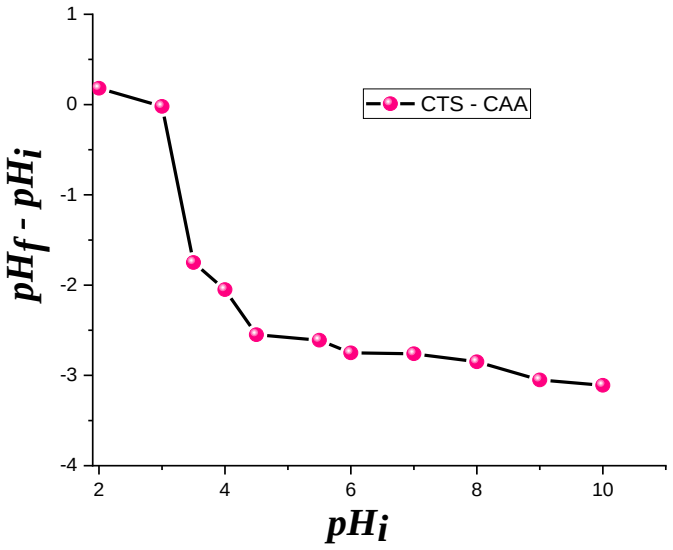

Figure 3.33 - pH_{pzc} estimation plot for (CTS-CAA) in a 0.1 M NaCl solution based on titration method.

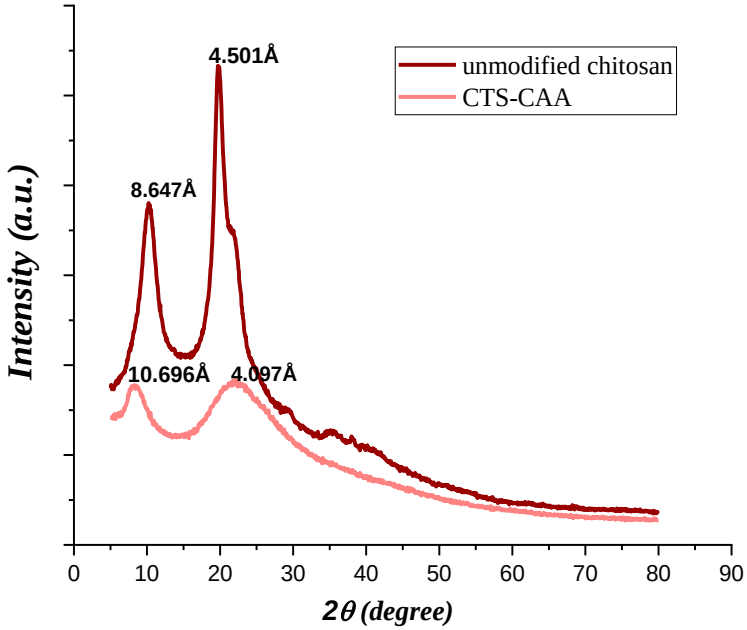

Figure 3.34 - XRD diffractograms of unmodified chitosan and (CTS-CAA).

The obtained results can be used to investigate the effect of the modification on the surface charge of chitosan. According to Figure 3.33, we estimated that the isoelectric point of (CTS-CAA) occurred at pH around 3. The surface of (CTS-CAA) was negatively charged at a pH value larger than 3 due to carboxyl groups deprotonation. As a result, chelation processes for the heavy metal adsorption can be expected within the pH range investigated. Copper and zinc cations, in

particular, can be adsorbed at pH values higher than pH_{pzc}. Figure 3.34 compares the XRD diffractograms of chitosan before and after the functionalization with carboxyl groups. Unmodified chitosan evidenced significant peaks at 2θ equals to 10.22 and 19.707°, while the main XRD peaks for the (CTS-CAA) sample were observed at 2θ equals to 8.259 and 22.145°. On this basis, it is possible to conclude that chitosan functionalization resulted in a shift of the first peak to a lower 2θ value, while the opposite effect was detected for the second peak. These findings indicate that the interplanar spacing in the chitosan polymer was significantly altered after the modification procedure. The high degree of chitosan functionalization may explain the broadening of the reflection peaks in (CTS-CAA) sample. The impact of modifying the surface on the thermal properties of chitosan was investigated by TGA and DSC methods (Figure 3.35). Figure 3.35 (a) depicts the TGA curves of both unmodified chitosan and (CTS-CAA). At around 600 °C, both materials have completely decomposed. Unmodified chitosan showed two distinct mass losses in the temperature ranges 25-120 °C and 240-580 °C. The first mass loss (12.4%) is due to the polymer's moisture content, whereas the second mass change (87.6%) could be attributed to the thermal degradation of the organic moieties.

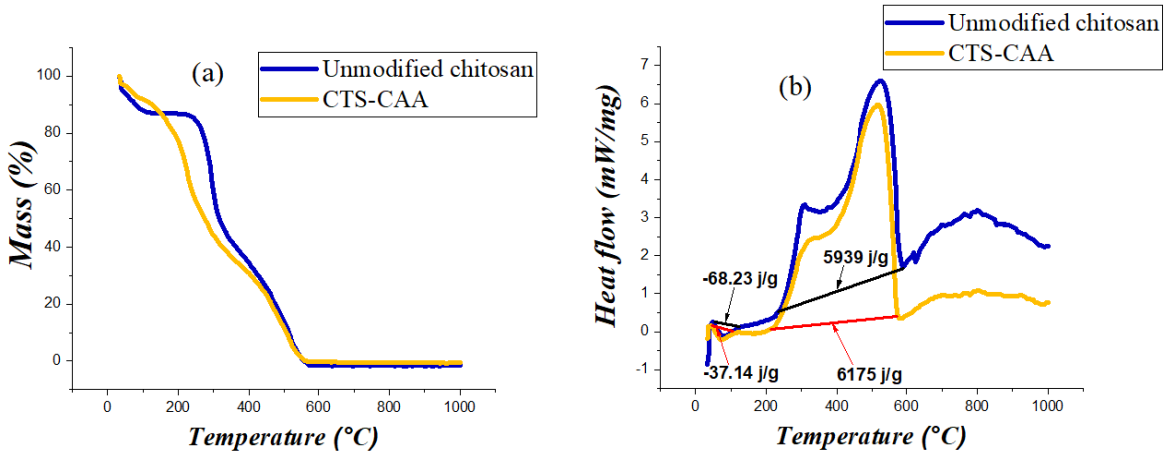

Figure 3.35 - TGA (a) and DSC (b) curves for unmodified chitosan and (CTS-CAA).

On the other hand, the estimated moisture loss of (CTS-CAA) equals 9.53 %. As a result, the chitosan modification resulted in a decrease in the hydrophilicity of the biopolymer. Because of the addition of the carboxyl moieties, the degradation of the organic moieties occurred over a wider temperature range (ca. 180 - 580 °C) than in unmodified chitosan.

As displayed in Figure 3.35 (b), the DSC curves of both unmodified chitosan and (CTS-CAA) exhibit an exothermic peak centered at approximately 76 °C which can be attributed to the

the polymeric chains degradation. The endothermic peak area of (CTS-CAA) has been significantly increased when compared to that of unmodified chitosan. This could be attributed to the fact that the hydrogen bonds between amino groups and water molecules in the case of unmodified chitosan are weaker than those formed with the terminal carboxyl groups for (CTS-CAA), so the temperature required to remove those water molecules will be higher for (CTS-CAA) than in case of unmodified chitosan.

CHAPTER 4 SORPTION EXPERIMENTS AND FITTING THE DATA USING DIFFERENT KINETIC AND THERMODYNAMIC MODELS

Chapter four includes the discussion of different parameters which influence on adsorption of Cu (II) and Zn (II) metal ions on the two modified adsorbents and desorption of Cu (II) and Zn (II) metal ions from the loaded adsorbents. Furthermore, it includes applying of the results of different sorption experiments to different kinetic and thermodynamic models.

4.1 Sorption processes using halloysite nanotubes modified with polyethyleneimine (HN-PEI)

4.1.1 Effect of pH

The concentration of hydrogen ions has a significant impact on the adsorption process because it influences the solution chemistry of contaminants as well as the state of amino-groups on the surface of (HN-PEI) [261]. The effect of $[H]^+$ ion concentration on Cu^{+2}, Zn^{+2} sorption was studied at room temperature in the pH range (2.5-6) and the results are shown in Figure 4.1.

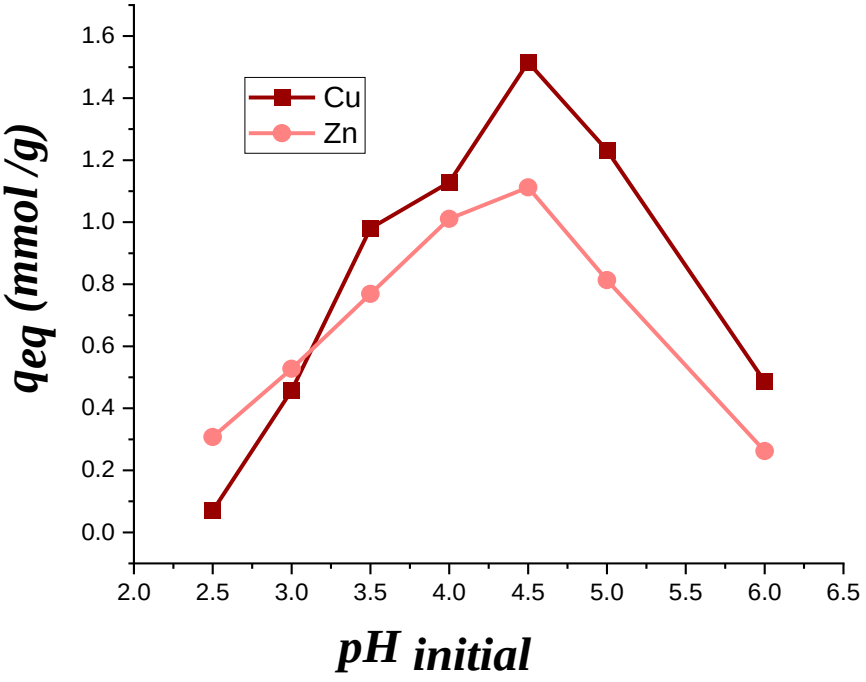

Figure 4.1 - Effect of model solution pH on the uptake of Cu^{+2} and Zn^{+2} metal ions (mmol/g).

At pH 4.5, the greatest uptake (mmol /g) of Cu (II) and Zn (II) metal ions was achieved. Despite the capability of copper and zinc to form cationic and anionic species at pH levels ranging from 1 to 14, Cu^{+2} and Zn^{+2} are the predominant species for copper and zinc at pH levels below 6.

According to the titration curve data for estimating the pH_{PZC} of (HN-PEI) (Figure 3.26), the charge on the surface of (HN-PEI) is positive at pH 4.5 due to amino groups protonation. Strong protonation of amino groups is expected at pH (2, 3) which increases the difficulty of the binding between the metal cations and the protonated amino groups. When the pH increased, the protonation of amino groups will decrease, and this facilitates the binding of metal ions by electrostatic attraction.

4.1.2 Effect of time and kinetics:

The contact time between (HN-PEI) and the metal ion solution has a significant effect on the uptake (mmol /g) of both Cu (II) and Zn (II) metal ions. The current study investigated the time of contacting between Cu^{+2}, Zn^{+2} and (HN-PEI) in the range of (3-200) min. The results are expressed in Figure 4.2, and it is clear that increasing the time increases the sorption capacity until it reaches the best value at 120 and 150 minutes for copper and zinc, respectively.

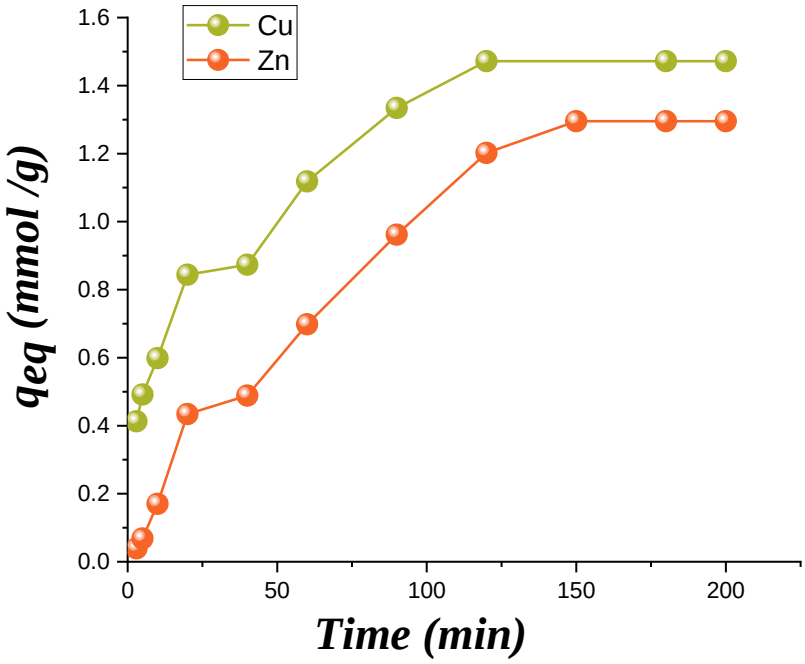

Figure 4.2 - Effect of Time (min.) on the uptake of Cu^{+2} and Zn^{+2} metal ions (mmol/g).

The experimental data was included into equations proposed by (Lagergren, Ho and Mckay, Weber Morris, Dumwald-Wagner, Elovich, and Bangham) to test the data's compliance with various kinetic models [262-265]. Table 4.1 expresses the linear equations for the proposed kinetic models [266], Where q_e, q_t (mmol $_{(Cu, Zn)}.g^{-1}$ $_{(sorbent)}$) are the amount of metal ions adsorbed experimentally at the equipoise and at a time [t] (min.), respectively, q_1, q_2 are the estimated metal

uptake as stated by the pseudo- first-order and the pseudo- second- order models, respectively, K_1 is the pseudo- first- order rate constant (min^{-1}), K_2 is the pseudo- second- order rate constant ($g.mmol^{-1}.min^{-1}$), K_i is the intraparticle diffusion rate constant ($mmol.g^{-1}.min^{-0.5}$), Z is the constant for intraparticle diffusion model (mmol. g^{-1}), K_{fd} is the Dumwald- Wagner rate constant (min^{-1}), (a, B) are Elovich's equation parameters, (K_γ, γ) are Bangham parameters, C_0 (mmol. L^{-1}) is the initial metal ion concentration, m is the weight of the (sorbent) per liter of solution ($g.L^{-1}$), V is the volume of metal ion solution (ml).

Table 4.1 - Linear equations for various kinetic models.

Kinetic model	Linear equations	Plot
Pseudo-first-order	$\log(q_e - q_t) = \log q_1 - (\frac{K_1}{2.303})t$	Log (q_e - q_t) vs. t
Pseudo-second-order	$\frac{t}{q_t} = \frac{1}{K_2 q_2^2} + \frac{1}{q_2}t$	(t/q_t) vs. t
Intraparticle diffusion	$q_t = Z + K_i t^{0.5}$	q_t vs. $t^{0.5}$
Dumwald-Wagner model	$Log(1 - F) = \left(-\frac{K_{fd}}{2.303}\right) t \ \ where\ F = (q_t / q_e)$	Log (1 -F) vs. t
Elovich's equation	$q_t = \left(\frac{1}{B}\right) \ln(aB) + \left(\frac{1}{B}\right) \ln(t)$	q_t vs. ln(t)
Bangham model	$\log\log\left(\frac{C_0}{C_0 - mq_t}\right) = \log\left(\frac{mK_\gamma}{2.303\ V}\right) + \gamma \log t$	log log (C_0 / (C_0 -mq_t) vs. log (t)

By applying the pseudo-first-order and the pseudo-second-order kinetic models to the experimental data as displayed by Figure 4.3 (a, b), the data fit the pseudo-second-order model and the pseudo-first-order model for copper and zinc, respectively. This can be explained as the following: the value of q_e obtained from the experiments brings closer to the value of q_2 and q_1 obtained by applying the pseudo-second-order model and the pseudo-first-order model for copper and zinc, respectively as described in Table 4.2. Figure 4.3 (c, e) displays Intraparticle diffusion and Dumwald-Wagner models, respectively. The experimental data for copper and zinc fit the

intraparticle diffusion model well but show poor correlation with Dumwald- Wagner model. The values of parameters for both intraparticle diffusion and Dumwald Wagner have been reported in Table 4.2. Since the data for both copper and zinc fit with the intraparticle diffusion model, Bangham kinetic model is used to describe the adsorption system for both copper and zinc as displayed by Figure 4.3 (f).

Table 4.2 - Kinetic parameters which are resulted from fitting the kinetic models with the experimental data.

Kinetic model	Model parameters	Cu (II)	Zn (II)
Equilibrium sorption capacity	q_e	1.471	1.295
Pseudo-first-order	q_1	1.125	1.301
	K_1	0.0216	0.014
	R^2	0.9604	0.9728
Pseudo-second-order	q_2	1.602	2.362
	K_2	0.035	0.003
	R^2	0.9898	0.8891
Intraparticle diffusion model	K_i	0.090	0.111
	Z	0.345	-0.144
	R^2	0.9408	0.9769
Elovich's equation	B	3.623	3.0039
	a	0.304	0.0728
	R^2	0.9609	0.9374
Dumwald-wagner	K_{fd}	0.0216	0.014
	R^2	0.9604	0.9728
Bangham kinetic model	K_γ	8.904	0.5519
	γ	0.382	0.948
	R^2	0.9816	0.9741

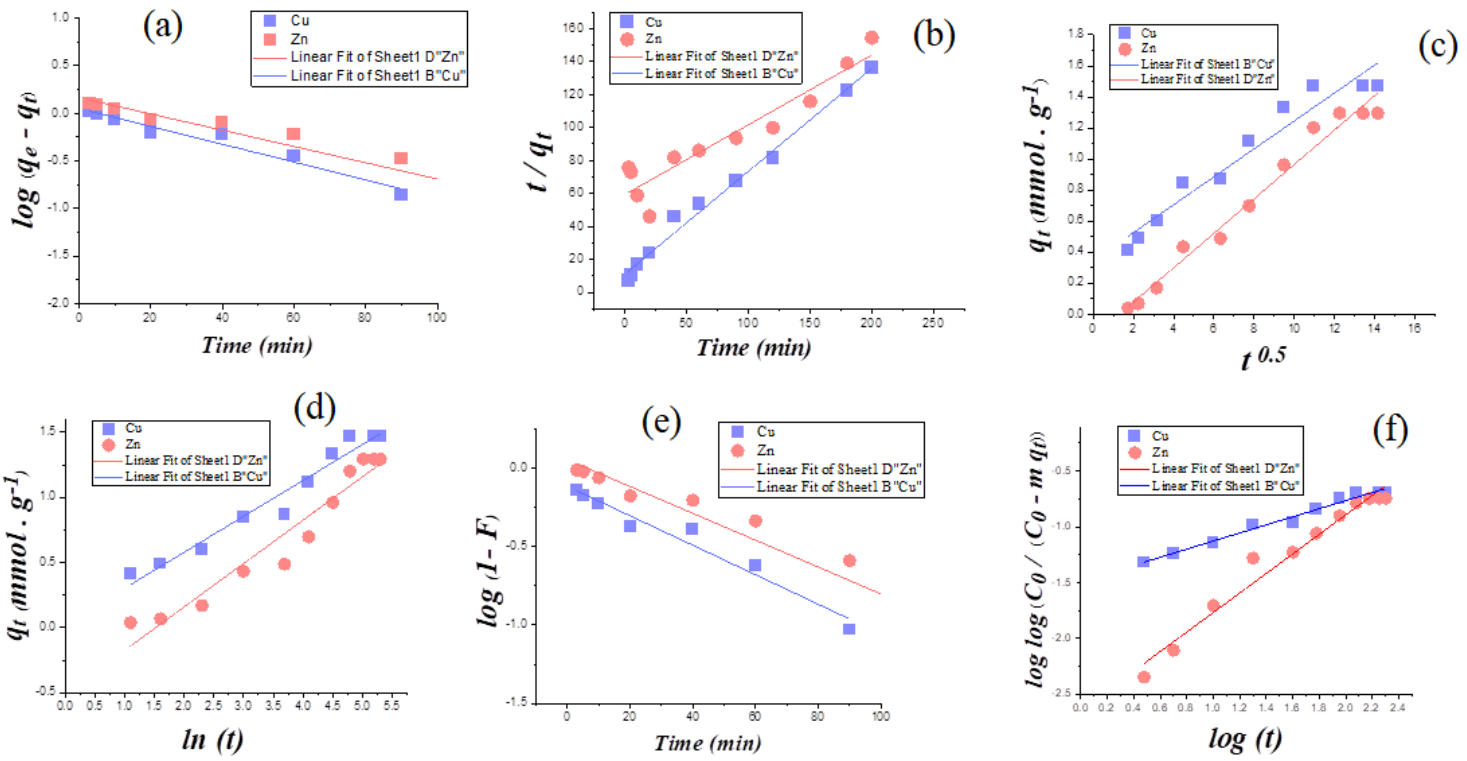

Figure 4.3 - Pseudo-first-order ***(a)***, Pseudo-second-order ***(b)***, Intraparticle diffusion ***(c)***, Elovich's equation ***(d)***, Dumwald-Wagner ***(e)***, Bangham model ***(f)***.

4.1.3 Adsorption isotherms of (HN-PEI)

C_{eq} (mmol/ L) as function of q_{eq} (mmol/g) is depicted in Figure 4.4 (a, b).

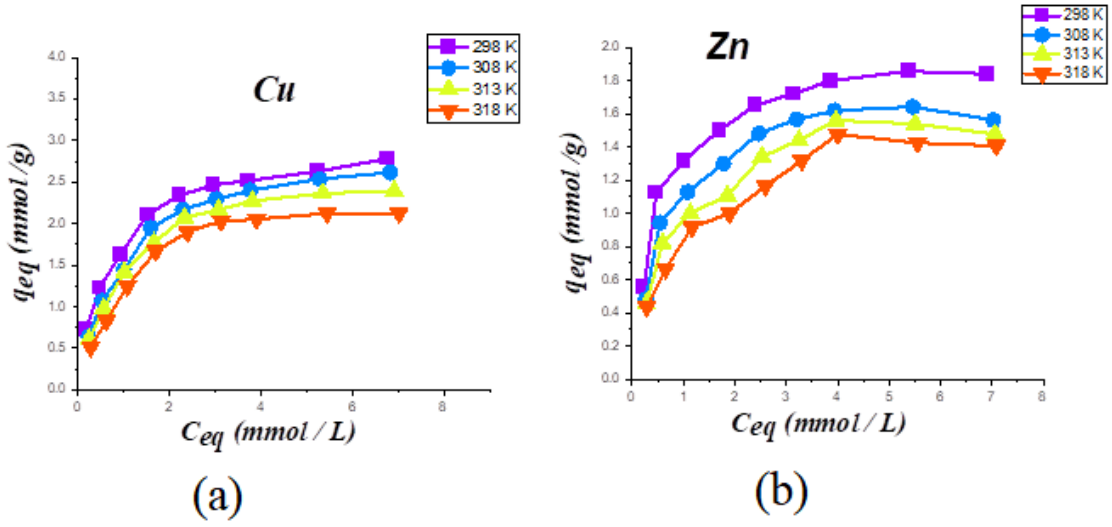

Figure 4.4 - Adsorption isotherm curves for Cu (II) (a) and Zn (II) (b).

As the value of C_{eq} increased, the value of q_{eq} increased until it reaches the equilibrium at C_{eq} ca. 6 (mmol/ L) for both Cu(II) and Zn(II) metal ions. The sorption process is described using Langmuir, Freundlich, Dubinin-Radushkevich, and Temkin isotherms [265, 267-270].
The Langmuir isotherm is described by equation (4.1):

$$\frac{C_{eq}}{q_e} = \frac{C_{eq}}{q_x} + \frac{1}{K_l q_x} \qquad (4.1)$$

where q_x (mmol/g) is the greatest sorption capacity of Cu (II) and Zn (II) on the sorbent, q_e (mmol/g) is the sorption capacity of Cu (II) and Zn (II) at the equilibrium, C_{eq} (mmol/L) is Cu (II) and Zn (II) ion concentration at the equilibrium and K_l (L/mmol) is the Langmuir binding constant.

Figure 4.5 (A, B) depicts the clear description of the sorption process as a monomolecular adsorption on energetically homogeneous surfaces of (HN-PEI). The Langmuir model fits the experimental results very well.

The value of the intercept which represents K_l can be used in equation (4.2) to predict the affinity between Cu (II) and Zn (II) metal ions and (HN-PEI) sorbent.

$$R_l = \frac{1}{1 + K_l C_0} \qquad (4.2)$$

where R_l is the dimensionless separation factor, K_l (L/mmol) is the Langmuir - binding constant, C_0 (mmol/L) is the initial Cu (II) and Zn (II) metal ions concentration.

The plot of C_0 vs R_l is shown in Figure 4.5 (C). It was noticed that the values of R_l for Cu (II) and Zn (II) metal ions are between (0.6-0.06), implying that the sorption of Cu (II) and Zn (II) metal ions on (HN-PEI) is a suitable process. The Langmuir parameters are reported in Tables 4.3 and 4.5 for Cu (II) and Zn (II) metal ions, respectively.

Table 4.3 - Langmuir and thermodynamic parameters for Cu (II).

T (K)	***Langmuir parameters***			***Thermodynamic parameters***		
	q_x	K_l	R^2	$\Delta S°$ ***J/K mol***	$\Delta H°$ ***KJ/mol***	$\Delta G°$ ***J/mol***
298	2.948	1.606	0.9988	-68.68	-21.603	-1134.3
308	2.966	1.128	0.998	-68.68	-21.603	-447.519
313	2.797	1.084	0.9979	-68.68	-21.603	-104.085

Table 4.5 - Langmuir and thermodynamic parameters for Zn (II).

T (K)	*Langmuir parameters*			*Thermodynamic parameters*		
	q_x	K_l	R^2	ΔS ° *J/K mol*	ΔH° *KJ/mol*	ΔG° *J/mol*
298	2.035	1.853	0.9982	-80.12	-25.507	-1631.24
308	1.860	1.513	0.9977	-80.12	-25.507	-830.027
313	1.803	1.166	0.9918	-80.12	-25.507	-429.42

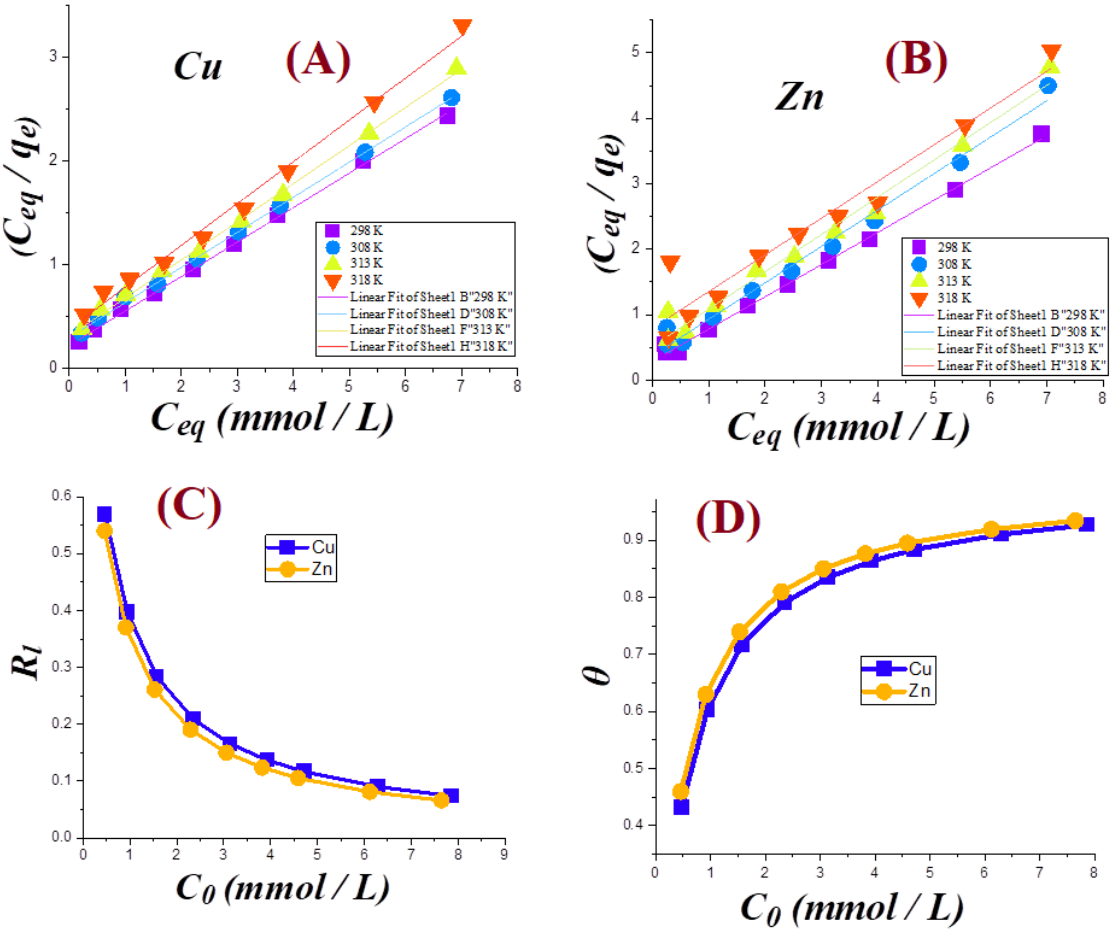

Figure 4.5 - Langmuir model for Cu (II) (A) and Zn (II) (B), Dimensionless separation factor for both Cu (II) and Zn (II) (C), Surface coverage for both Cu (II) and Zn (II) (D).

The % of surface coverage (θ) can be computed by using equation (4.3). C_0 as function of (θ) is depicted in Figure 4.5 (D).

$$\theta = \frac{k_l \ c_0}{1 + k_l \ c_0} \qquad (4.3)$$

Van't Hoff equation is represented by equation (4.4) and is used to compute the values of an enthalpy (ΔH°) and an entropy (ΔS °) changes.

$$\ln K_l = \frac{-\Delta H^\circ}{RT} + \frac{\Delta S^\circ}{R} \qquad (4.4)$$

where T is the absolute temperature (K), R is the universal gas constant (8.314 J mol^{-1} K^{-1}), ΔH°(J mol^{-1}) is the enthalpy changes and ΔS °(J mol^{-1} K^{-1}) is the entropy changes.

(1/T) as function of ln K_l is depicted in Figure 4.6. The values of Gibbs free energy (ΔG°) at the studied temeratures were determined by using equation (4.5)

$$\Delta G^\circ = \Delta H^\circ - T\Delta S^\circ \qquad (4.5)$$

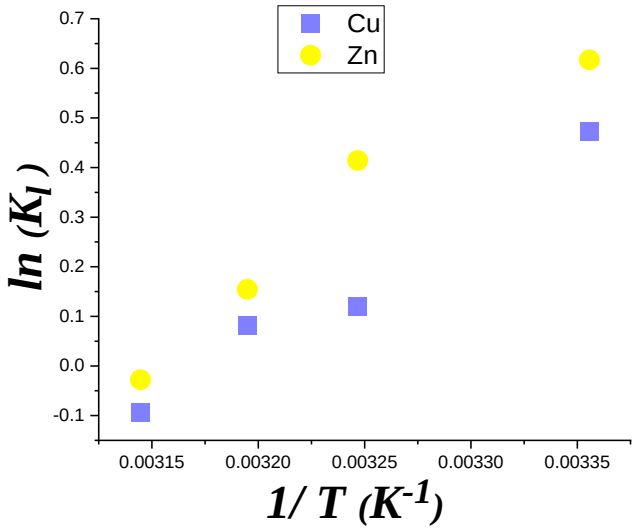

Figure 4.6 - Representation of Van't Hoff equation for both Cu (II) and Zn (II).

The values of ΔG° (J/mol) at the studied temperatures were computed and reported in Tables 4.3 and 4.5 for Cu (II) and Zn (II) metal ions, respectively. The negative values of ΔG° at the studied temperatures indicate the spontaneous nature of the sorption process. The negative values of ΔS° at the studied temperatures confirm the lower degree of randomness for the sorption of Cu (II) and Zn (II) metal ions on (HN-PEI). On the other hand, the negative values of ΔH° at the studied temperatures confirm the exothermic nature of sorption of Cu (II) and Zn (II) metal

ions on (HN-PEI). Tables 4.3 and 4.5 display the values of ΔS°, (ΔG°) and ΔH° for both Cu (II) and Zn (II) metal ions at the investigated temperatures.

Equation (4.6) describes the Freundlich isotherm [271]:

$$\log q_e = \log K_f + \frac{1}{n} \log C_{eq} \qquad (4.6)$$

where C_{eq} (mmol/ L) is the concentration of Cu (II) and Zn (II) metal ions at the equilibrium, q_e (mmol/g) is the equilibrium sorption capacity and (K_f, n) are the Freundlich constants.

As shown in Tables 4.4 and 4.6 and Figure 4.7 (a, b), the estimated values of (n) are greater than one for both copper and zinc sorption processes, indicating that the experimental results do not fit the Freundlich model.

Equation (4.7) describes Dubinin–Radushkevich (D–R) model:

$$\ln q_e = \ln Q_S - K_{DR} \varepsilon^2 \qquad (4.7)$$

where K_{DR} ($mol^2\ K\ J^{-2}$) refers to the free energy change of sorption per mole of adsorbate, Q_s is related to the theoretical saturation capacity (mmol/g) derived by Dubinin–Radushkevich, q_e (mmol/g) is the sorption capacity at the saturation stage and Ɛ is the Polanyi potential.

The Polanyi potential can be estimated from equation (4.8)

$$\varepsilon = RT \ln \left[1 + \left(\frac{1}{Ceq}\right)\right] \qquad (4.8)$$

where T refers to the absolute temperature (K) and R refers to the ideal gas constant (8.314 J $mol^{-1}\ K^{-1}$).

Equation (4.9) can be used to calculate the mean free energy (E) (kJ mol^{-1}) required to transfer one mole of Cu (II) and Zn (II) metal ions from the bulk of the solution to the solid surface of the sorbent:

$$E = \frac{1}{(2K_{DR})^{0.5}} \qquad (4.9)$$

ε^2 as function of ln q_e is depicted by Figure 4.7 (c, d). Dubinin–Radushkevich parameters for Cu (II) and Zn (II) metal ions are reported in Tables 4.4 and 4.6, respectively. The computed values of (E) at the studied temperatures were in the range of (2.88-2.67) and (2.67-2.5) (kJ/mol) for Cu (II) and Zn (II) metal ions, respectively. It is clear that the values of E were less than 8

kJ/mol, so the sorption of both Cu (II) and Zn (II) metal ions on (HN-PEI) is controlled by physical sorption. Equation (4.10) describes Temkin isotherm model:

$$q_e = B \ln C_{eq} + B \ln A_T \qquad (4.10)$$

where A_T is the equilibrium binding constant equivalent to the maximum binding energy and B is a constant describes the heterogeneity of the sorbent surface.

According to this model, the heat of adsorption decreases linearly with the surface coverage and the distribution of binding energies is the most important feature for the sorption process. The value of B can be calculated from Temkin isotherm constant (b) using the relationship (B = RT/b). The values of A_T, B and b for Cu (II) and Zn (II) metal ions sorption are listed in Tables 4.4 and 4.6, respectively. ln C_{eq} as function of q_e for Cu (II) and Zn (II) metal ions is depicted in Figure 4.7 (e, f), respectively.

Table 4.4 - Freundlich, Dubinin-Radushkevich and Temkin parameters for Cu (II).

T (K)	***Freundlich parameters***			***Dubinin-Radushkevich parameters***				***Temkin parameters***			
	N	***K_f***	***R^2***	***Q_S***	***K_{DR}***	***E (kJ/mol)***	***R^2***	***B (kJ/mol)***	***A_T (L/g)***	***$b*10^{-3}$***	***R^2***
298	2.74	1.577	0.9457	2.436	6.00E-08	2.88	0.9251	0.587	19.598	4.220	0.9845
308	2.42	1.383	0.9503	2.290	7.00E-08	2.67	0.9129	0.612	12.667	4.182	0.9839
313	2.41	1.281	0.9438	2.144	7.00E-08	2.67	0.9103	0.575	12.219	4.524	0.9769

Table 4.6 - Freundlich, Dubinin-Radushkevich and Temkin parameters for Zn (II).

T (K)	***Freundlich parameters***			***Dubinin-Radushkevich parameters***				***Temkin parameters***			
	N	***K_f***	***R^2***	***Q_S***	***K_{DR}***	***E (kJ/mol)***	***R^2***	***B (kJ/mol)***	***A_T (L/g)***	***$b*10^{-3}$***	***R^2***
298	3.18	1.169	0.8513	1.775	7.00E-08	2.67	0.9741	0.366	31.89	6.76	0.9449
308	2.96	0.990	0.8629	1.563	7.00E-08	2.67	0.975	0.344	23.06	7.43	0.9326
313	2.77	0.880	0.911	1.423	8.00E-08	2.5	0.9402	0.345	16.15	7.538	0.9482

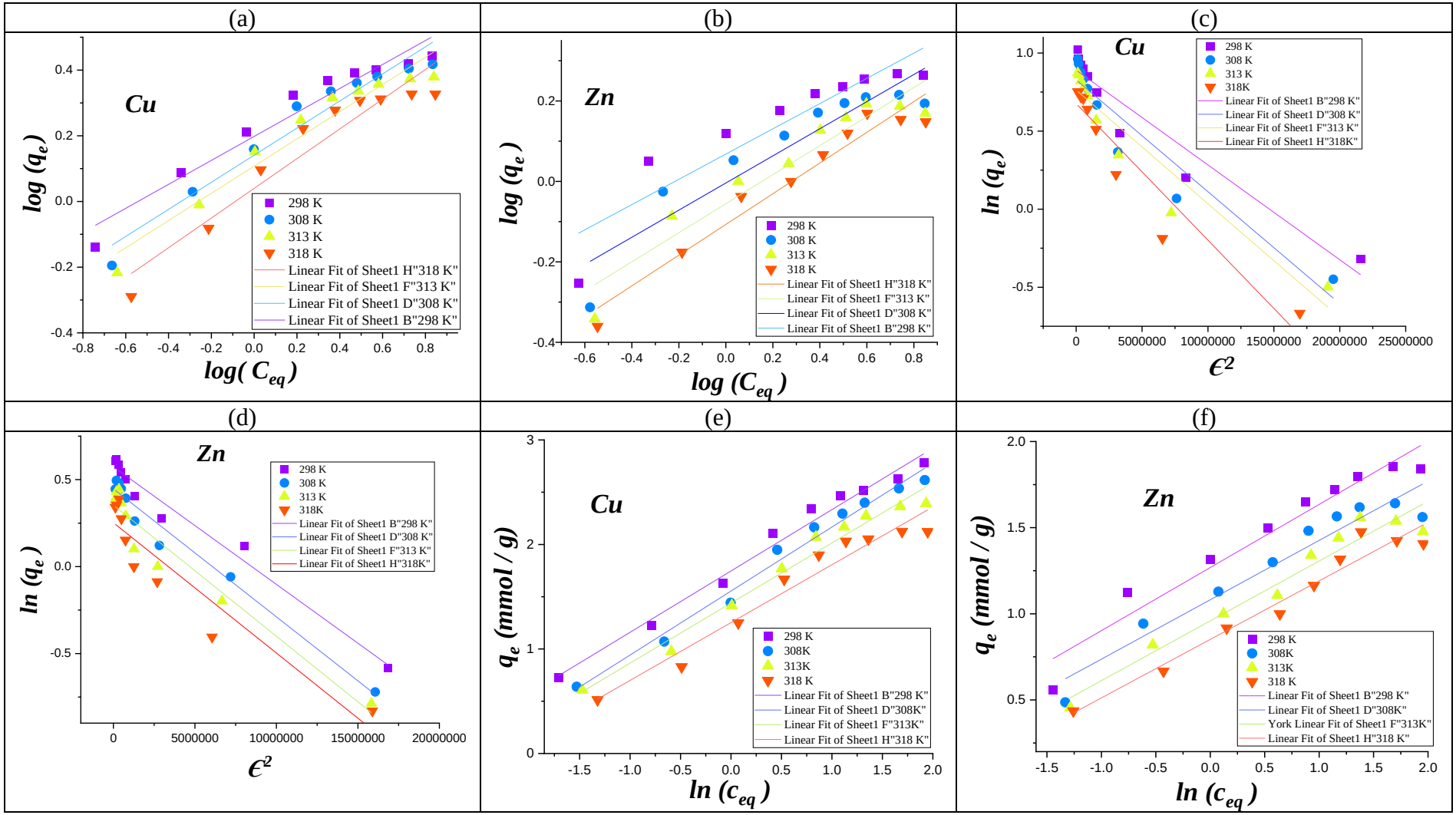

Figure 4.7 - Freundlich model for Cu (II) (a) and Zn (II) (b), Dubinin-Radushkevich model for Cu (II) (c) and Zn (II) (d), Temkin model for Cu (II) (e) and Zn (II) (f).

4.1.4 Metal desorption and (HN-PEI) recycling

Metal desorption from the loaded (HN-PEI) sorbent was evaluated as a key parameter for assessing the sorbent's potential for large-scale application. For the regeneration process, various eluents were used, including 1M HNO_3, 1 M HCl, 1.5 M H_2SO_4, 0.4 M EDTA, 0.4 M Urea and 0.6 M NH_4Cl. For the desorption steps, the contact time was set to 110 minutes and the sorbent dosage was set to 0.4 g/L.

Equation (4.11) was used to calculate the desorption efficiency:

$$\text{Desorption efficiency} = \frac{C \times V}{q_e \times m} \times 100\% \qquad (4.11)$$

where C (mmol/L) is the concentration of Cu (II) and Zn (II) metal ions in the desorption solution after using the eluent, V is set as 50 ml and it represents the volume of desorption solution, q_e (mmol/ g) is the quantity of Cu^{+2} or Zn^{+2} ions adsorbed on the sorbent before doing the desorption processes and m is the mass of the sorbent loaded by the metal ions.

The results showed that 1 M HCl and 1.5 M H_2SO_4 were used to desorb Cu (II) and Zn (II) metal ions, respectively. For each sorption and desorption step, the sorbent (HN-PEI) must be washed. The efficiency of recycling of the sorbent was tested by doing three cycles of sorption, the desorption was done after each sorption cycle and the data obtained for the desorption tests were displayed in Table 4.7. The sorption efficiency for both Cu (II) and Zn (II) metal ions is represented as 100% in the first cycle as a reference value, and the sorption capacities for the other cycles are computed relative to the first cycle. Table 4.8 displays the adsorption capacity of various adsorbents for the separation of Cu (II) and Zn (II) ions from the aqueous solutions.

Table 4.7 - Data of three cycles of metal desorption.

Cycle	1		2		3	
Metal	Sorption (%)	Desorption (%)	Sorption (%)	Desorption (%)	Sorption (%)	Desorption (%)
Copper	100	88.5	98.64	86.91	96.87	84.76
Zinc	100	90	97.25	88.07	94.38	84.94

Table 4.8 - Comparison of adsorption capacity of various adsorbents for the separation of Cu (II), Zn (II) ions from the aqueous solutions.

Metal	Material	pH_{in}	Initial inlet concentration C_i (mmol/L)	Maximum adsorption capacity Q_{max} (mmol g^{-1})	Ref.
Cu (II)	Halloysite nanotube–alginate hybrid beads	-	1.573	1.166	[272]
Cu (II)	Chitosan/Halloysite Beads (Dragonite)*	-	1.573	0.2234	[273]
Cu (II)	Chitosan/Halloysite Beads (Matauri Bay) *	-	1.573	0.166	[273]
Cu (II) and Zn (II)	Illite	7	-	Q_{max} (Cu) = 0.0639 Q_{max} (Zn) = 0.075	[274]
Cu(II)	Attapulgite	7	0.3147	0.834×10^{-4}	[275]
Cu (II) and Zn (II)	Raw halloysite from Polish Dunino deposit	5	1	Q_{max} (Cu) = 17.67×10^{-3} Q_{max} (Zn) = 2.16×10^{-3}	[40]
Cu (II) and Zn (II)	Nanotubular dehydrated halloysite grafted with diethanolamine–$(CH_2CH_2OH)_2NH$ (DEA)	5	1	Q_{max} (Cu) = 64.10×10^{-3} Q_{max} (Zn) = 52.91×10^{-3}	[40]
Cu (II) and Zn (II)	Nanotubular dehydrated halloysite grafted with triethanolamine–$(CH_2CH_2OH)_3N$ (TEA)	5	1	Q_{max} (Cu) = 75.18×10^{-3} Q_{max} (Zn) = 42.91×10^{-3}	[40]
Cu (II)	Acid-activated kaolinite adsorbent	7	1.573	0.6469	[276]
Cu (II)	Ion-imprinted montmorillonite nanosheets/chitosan (IIMNC) gel bead	(3.5-4)	0.7868	1.879	[277]
Zn (II)	Natural halloysite nanotubes	6	1.54×10^{-1}	1.51×10^{-1}	[75]
Zn (II)	Calcined halloysite	5	5	203.2×10^{-3}	[41]
Zn (II)	Coumarin-anchored halloysite nanotubes	-	5×10^{-3} (M)	0.2447	[278]
Cu (II) and Zn (II)	(HN-PEI)	4.5	C_i (Cu) = 1.573 C_i (Zn)= 1.529	Q_{max} (Cu) = 2.78 Q_{max} (Zn) =1.84	This work

*Sources of Halloysite nanotubes.

4.2 Sorption processes using aminocarboxymethyl chitosan (CTS-CAA)

4.2.1 Effect of pH

According to the data in Figure 3.33, we discovered that (CTS-CAA) has a negative surface charge at pH greater than 3. As a result, the modified chitosan is negatively charged for the pH (3.5 - 6). Within the studied pH range, the carboxylate groups on the surface of (CTS-CAA) are deprotonated, whereas the metal ions are positively charged. Based on this, we can predict electrostatic attractions between metal ions and the negatively charged surface of the modified chitosan at pH values ranging from 3.5 to 6. The adsorption capacity can be attributed to the chelation mechanism between Cu (II) and Zn (II) metal ions and the $-(COO)^-$ of (CTS-CAA). Oppositely, the protonation of amino groups of (CTS-CAA) is expected at pH < 2.5 reducing the adsorption capacity of the modified chitosan towards the heavy metals. The experimental results on the uptake capacity of the (CTS-CAA) sample towards both Cu (II) and Zn (II) metal ions confirmed these considerations (Figure 4.8). We estimated that the greatest uptake for both metal ions occurred at pH =3.5. In particular, the uptake values are 1.96 mmol/g and 1.505 mmol/g for Cu (II) and Zn (II) metal ions, respectively.

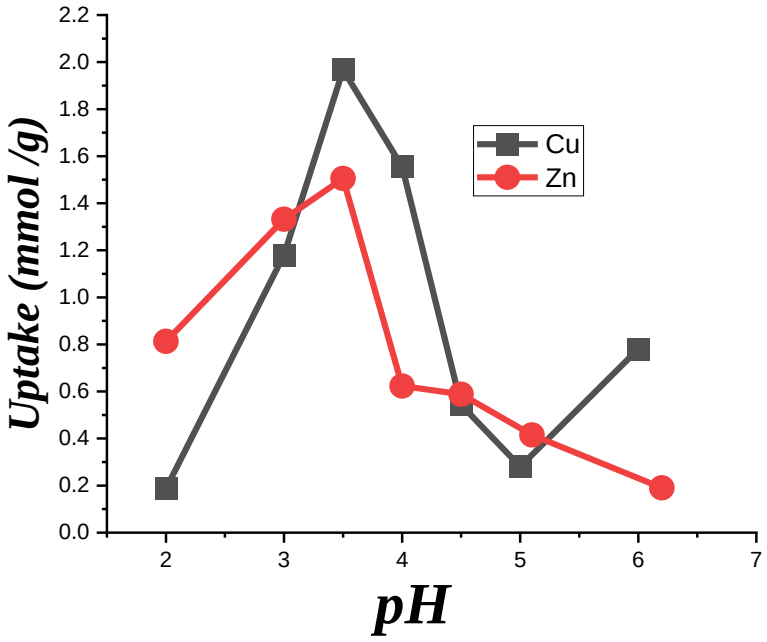

Figure 4.8 - Effect of pH on the uptake capacity of (CTS-CAA) sample towards both Cu (II) and Zn (II) metal ions.

4.2.2 Effect of time and kinetics

In order to evaluate the kinetic aspects of the adsorption processes, the uptake capacity of (CTS-CAA) sample towards the heavy metal ions was determined at a variable time within the range (10 – 240) minutes. The adsorption experiments were carried out under isothermal conditions (temperature = 25 °C) and pH = 3.5. Figure 4.9 depicts the dependences of metal ions uptake on time.

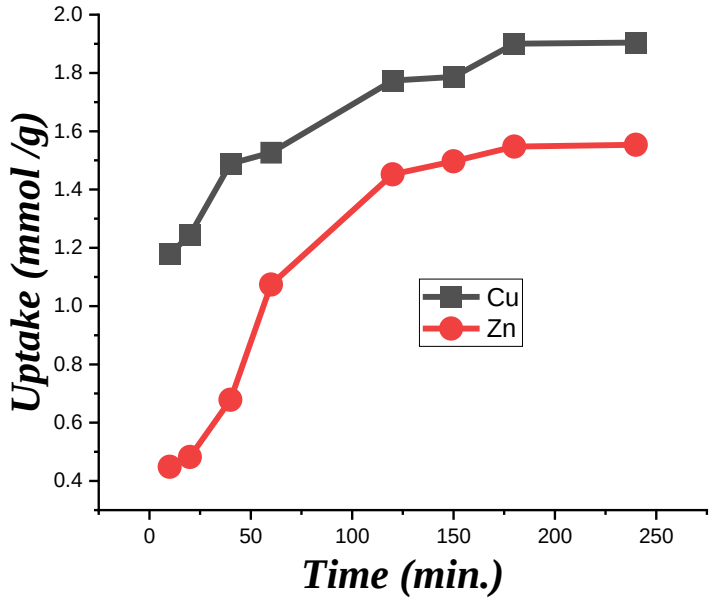

Figure 4.9 - Effect of time on the uptake capacity of (CTS-CAA) sample towards both Cu (II) and Zn (II) metal ions.

It was observed that the modified chitosan exhibited an efficient adsorption capacity (greater than 60% of the uptake at the saturation) after 40 and 60 minutes for Cu (II) and Zn (II) metal ions, respectively. The saturation of the adsorption sites of the (CTS-CAA) sample resulted in uptake values of approximately 1.9 and 1.5 mmol/g for Cu (II) and Zn (II) metal ions, respectively. The profiles shown in Figure 4.9 were analyzed using a variety of kinetic models in order to determine the rate-limiting step for the adsorption processes. Specifically, we employed Lagergren, Ho and Mckay, Weber Morris, Dumwald-Wagner, Elovich, and Bangham models to test the obeying of the data with the various kinetic models [262-265]. The linear equations for the proposed kinetic models are expressed in Table 4.1.

Figure 4.10 depicts the fitting plots for the described kinetic models. Based on the data obtained using the current plots, we could determine the adsorption parameters, which are reported in Table 4.9.

Based on the R^2 values (Table 4.9), we can state that the pseudo-second-order and Elovich's equation are the more accurate fitting procedures in the analysis of the adsorption results for both Cu (II) and Zn (II) metal ions. On the other hand, the Dumwald-Wagner model didn't provide reliable fitting parameters.

Table 4.9 - Kinetic parameters have been estimated by fitting the kinetic models with the experimental results.

Kinetic model	Model parameters	Cu (II)	Zn (II)
Equilibrium sorption capacity	q_e	1.904	1.553
Pseudo -first- order	q_1	1.282	2.166
	K_1	0.024	0.028
	R^2	0.7825	0.9433
Pseudo-second-order	q_2	1.991	1.948
	K_2	0.0393	0.0099
	R^2	0.9977	0.9753
Weber Morris diffusion model	K_i	0.0627	0.1056
	Z	1.022	0.1169
	R^2	0.9578	0.9275
Elovich's equation	B	4.0064	2.385
	a	2.291	0.0854
	R^2	0.9786	0.9409
Dumwald-Wagner	K_{fd}	0.024	0.028
	R^2	0.7825	0.9433
Bangham kinetic model	K_γ	26.479	4.038
	γ	0.212	0.533
	R^2	0.9818	0.9496

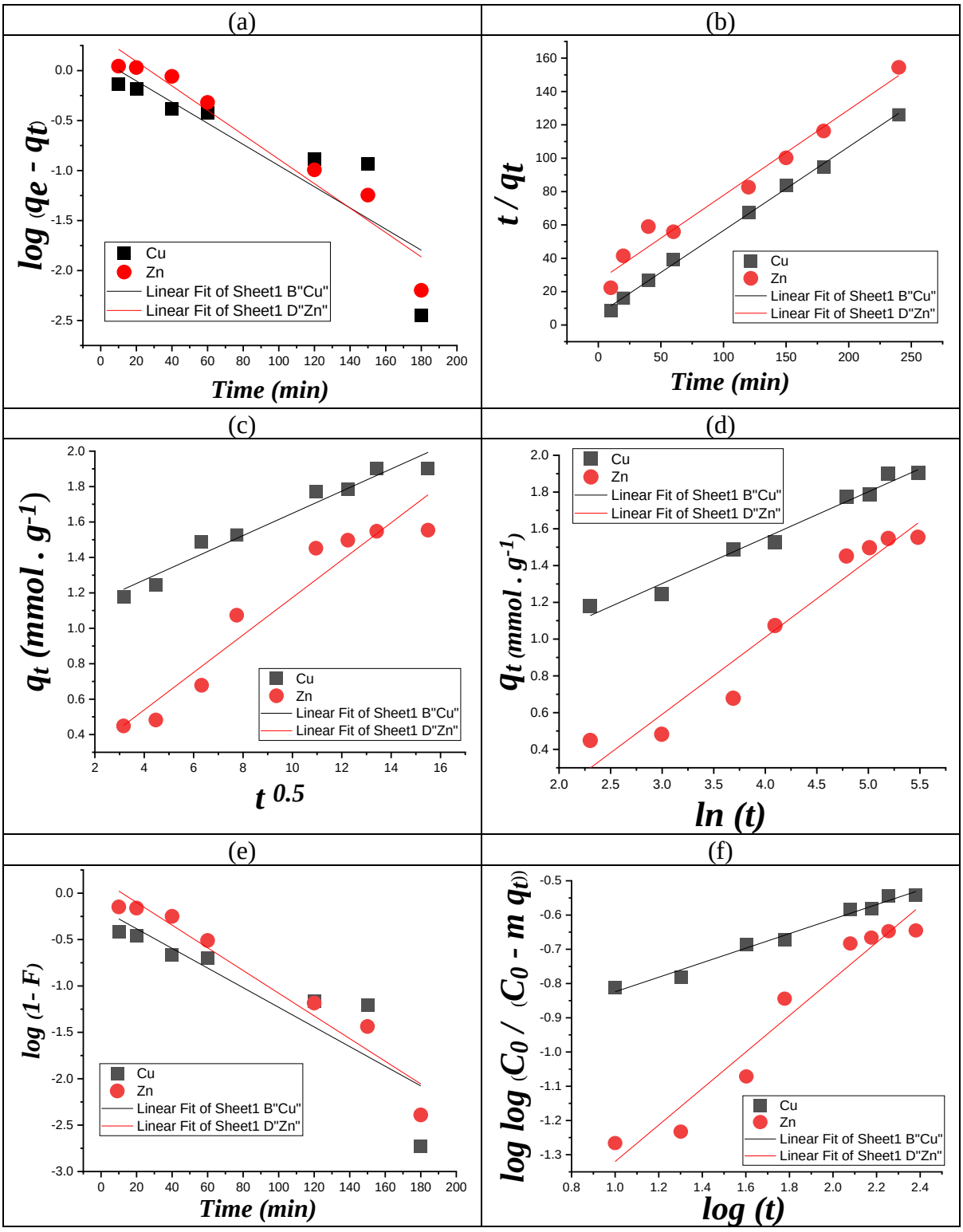

Figure 4.10 - Pseudo-first-order (a), Pseudo-second-order (b), Intraparticle diffusion (c), Elovich's equation (d), Dumwald-Wagner (e), Bangham model (f).

4.2.3 Adsorption isotherms of (CTS-CAA)

Figure 4.11 displays the adsorption isotherms of Cu (II) and Zn (II) metal ions on modified chitosan at variable temperatures.

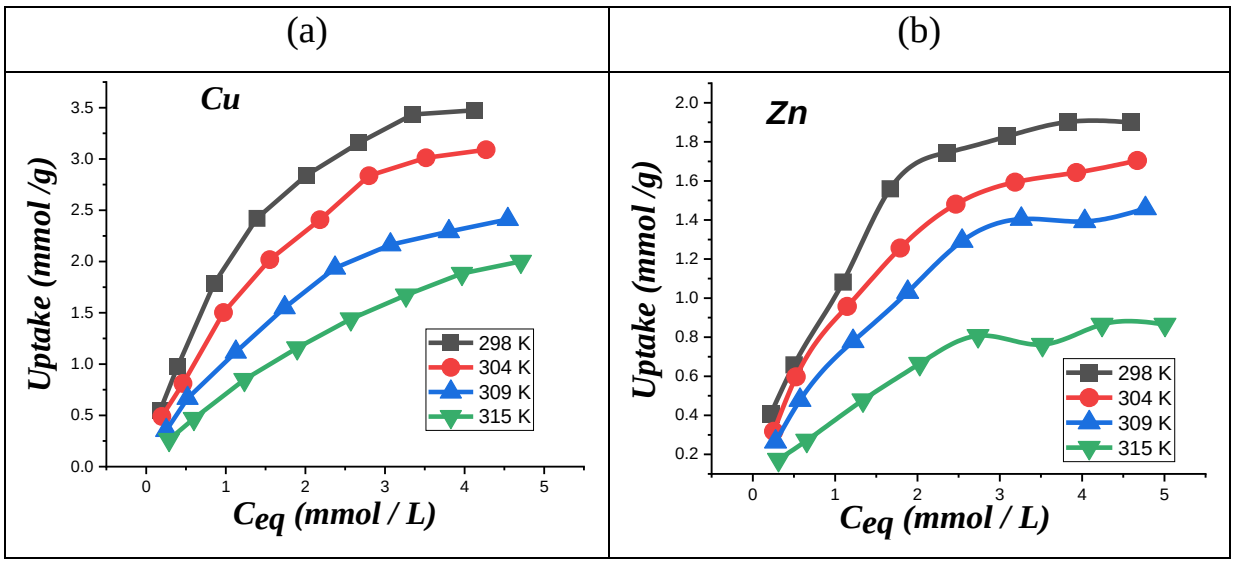

Figure 4.11 - Adsorption isotherms for Cu (II) (a) and Zn (II) (b).

As a general result, increasing the temperature reduced the metal ions uptake on the modified chitosan (Figure 4.11). Several fitting models, including Langmuir, Freundlich, Dubinin-Radushkevich, and Temkin were used to analyze the adsorption isotherms at different temperatures. Equation (4.1) describes the Langmuir isotherm [279], subtitle (4.1.3).

The linearity predicted by equation (4.1) was observed in the (C_{eq}/q_e) vs C_{eq} plots [Figure 4.12 (a, b)] for both Cu (II) and Zn (II) metal ions at the various investigated temperatures. On this basis, we can assert that the Langmuir model is appropriate for describing the adsorption process. As a result, we can conclude that (CTS-CAA) possesses a homogeneous surface with energetically equal adsorption sites.

The estimated K_l values were used in equation (4.2) (subtitle 4.1.3) to calculate the dimensionless separation factor (R_l), which indicates the affinity between Cu (II) and Zn (II) metal ions and the surface of (CTS-CAA) sorbent.

Figure 4.12 (c) displays C_0 vs R_l plots for both Cu (II) and Zn (II) metal ions. We observed exponential decreasing trends with R_l ranging between 0.8 and 0.1. In particular, the R_l intervals are 0.78 - 0.20 and 0.75 - 0.18 for Cu (II) and Zn (II) metal ions, respectively. These results highlight the suitability of (CTS-CAA) as an adsorbent material for both metals. The K_l values

were used to calculate the surface coverage percentage (θ) of (CTS-CAA) sorbent by using equation (4.3) (subtitle 4.1.3).

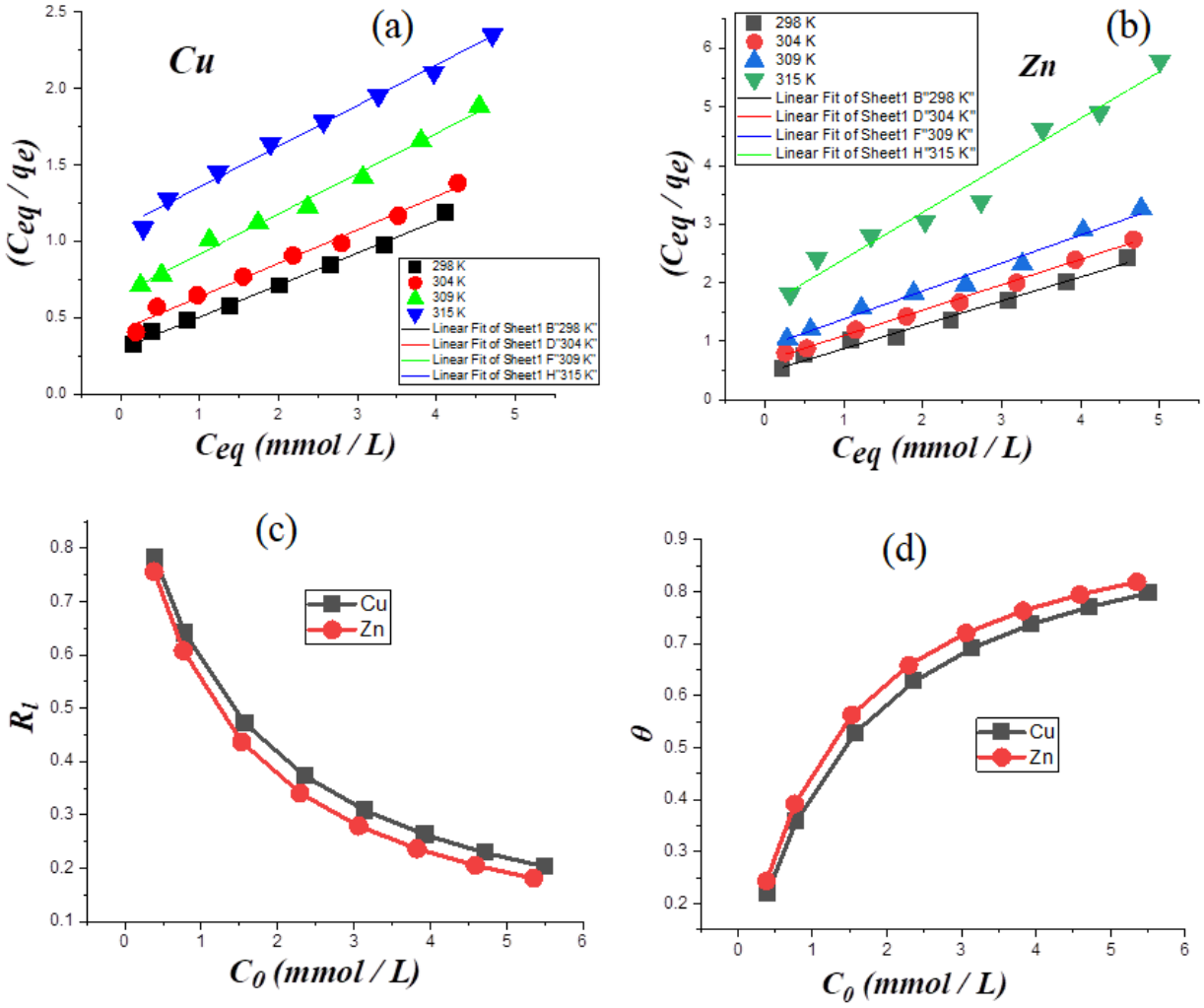

Figure 4.12 - Langmuir model for Cu (II) (a) and Zn (II) (b). Dimensionless separation factor (c) and surface coverage (d) for the adsorption of both Cu (II) and Zn (II) metal ions on modified chitosan.

As shown in Figure 4.12 (d), we detected an increasing θ vs C_0 relation for both Cu (II) and Zn (II) metal ions. We estimate θ equals ca. 0.8 at the highest C_0 for both metals. The Langmuir fitting parameters obtained for the adsorption experiments at various temperatures are collected in Tables 4.10, 4.11.

Table 4.10 - Langmuir and thermodynamic parameters for Cu (II).

T (K)	*Langmuir parameters*			*Thermodynamic parameters*		
	q_x	K_l	R^2	ΔS° *J/K mol*	ΔH° *KJ/mol*	ΔG° *J/mol*
298	4.77	0.713	0.996	-164.44	-48.28	719.51
304	4.56	0.525	0.987	-164.44	-48.28	1706.16
309	3.79	0.404	0.992	-164.44	-48.28	2528.37
315	3.75	0.245	0.991	-164.44	-48.28	3515.03

Table 4.11 - Langmuir and thermodynamic parameters for Zn (II).

T (K)	*Langmuir parameters*			*Thermodynamic parameters*		
	q_x	K_l	R^2	ΔS° *J/K mol*	ΔH° *KJ/mol*	ΔG° *J/mol*
298	2.47	0.843	0.987	-88.327	-25.82	493.45
304	2.30	0.66	0.996	-88.327	-25.82	1023.42
309	2.09	0.528	0.986	-88.327	-25.82	1465.06
315	1.26	0.489	0.972	-88.327	-25.82	1995.03

Based on the Van't Hoff approach [268] we calculated the thermodynamic parameters for the adsorption process of the metal ions on (CTS-CAA) sorbent. In detail, the K_l values at different temperatures are related to the enthalpy (ΔH°) and entropy (ΔS°) variations according to Eq. (4.4) (subtitle 4.1.3) [280].

As shown in Figure 4.13, the experimental ln K_l vs (1/T) plots show linear increasing trends that can be analyzed by equation (4.4) to determine ΔH° and ΔS° of the adsorption processes. The calculated ΔH° values are - 48.28 and -25.83 (kJ/mol) for Cu (II) and Zn (II) metal ions, respectively. On the other hand, we determined ΔS° values equal to -164.44 and -88.33 (J/K.mol) for Cu (II) and Zn (II) metal ions, respectively. Equation (4.5) can be used to determine the corresponding Gibbs free energies (ΔG°) at different temperatures (subtitle 4.1.3). Tables 4.10, 4.11 show the obtained ΔG° values. The values of ΔG° (KJ/mol) lie in the range of (0.719- 3.515) and (0.493- 1.995) for Cu (II) and Zn (II) metal ions, respectively at temperature ranges (298- 315 K).

At all studied temperatures, it was noticed that the value of $|\Delta H^\circ| < |T\Delta S^\circ|$. This indicates that the adsorption process is dominated by entropic rather than enthalpic changes. The negative values of ΔS° at different temperatures indicate less degree of randomness for the

sorption of Cu (II) and Zn (II) metal ions on (CTS-CAA), whereas the negative values of ΔH° at various temperatures indicate the exothermic nature of sorption of Cu (II) and Zn (II) metal ions on (CTS-CAA). Tables 4.10, 4.11 show the values of ΔS °, (ΔG°), and ΔH° for both Cu (II) and Zn (II) metal ions at various temperatures.

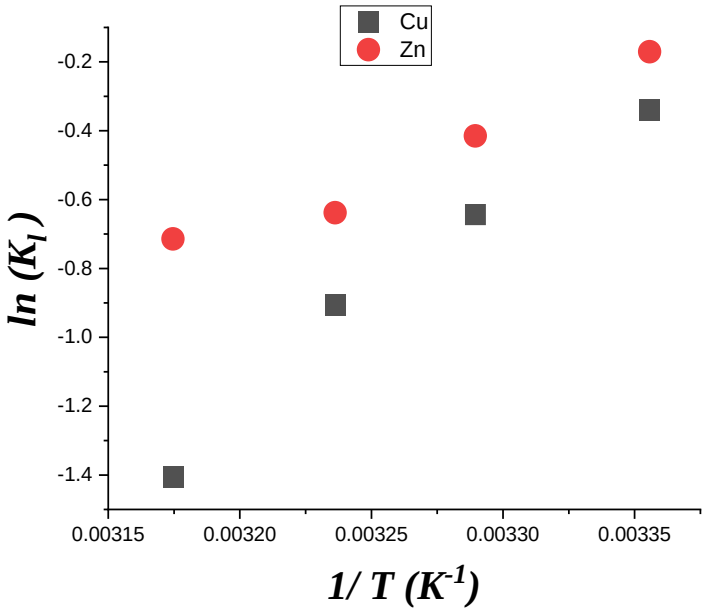

Figure 4.13 - Representation of Van't Hoff equation for the adsorption of Cu (II) and Zn (II) metal ions on (CTS-CAA).

Furthermore, the adsorption isotherms were analyzed through the Freundlich model [269, 281] using equation (4.6) (subtitle 4.1.3).

The Freundlich plots are presented in Figure 4.14 (a, b), while the obtained fitting parameters are reported in Tables 4.12, 4.13. It should be noted that the Freundlich approach is only applicable for n values between 0 and 1. According to the data in Tables 4.12, 4.13, we calculated n values larger than 1 for both metals. As a result, we can conclude that the Freundlich model is unsuitable for describing the adsorption process of Cu (II) and Zn (II) metal ions on (CTS-CAA).

Other approaches, such as Dubinin–Radushkevich (D–R) and Temkin models, were used to fit the adsorption isotherms. Equation (4.7) can be used to express the Dubinin–Radushkevich (D–R) model (subtitle 4.1.3) [265].

The Polanyi potential can be related to the temperature as described by equation (4.8) (subtitle 4.1.3).

Table 4.12 - Freundlich, Dubinin-Radushkevich and Temkin parameters for Cu (II).

T (K)	***Freundlich parameters***			***Dubinin-Radushkevich parameters***				***Temkin parameters***			
	n	***K_f***	***R^2***	***Q_S***	***K_{DR}***	***E (kJ/mol)***	***R^2***	***B (kJ/mol)***	***A_T (L/g)***	***$b*10^{-3}$***	***R^2***
298	1.66	1.737	0.9758	3.555	2.00E-07	1.581	0.9812	2.318	2.476	1.068	0.9859
304	1.58	1.407	0.9871	3.166	2.00E-07	1.581	0.963	2.129	2.25	1.186	0.971
309	1.48	0.988	0.9854	2.511	3.00E-07	1.29	0.987	1.739	2.031	1.477	0.9768
315	1.35	0.6908	0.9961	1.983	4.00E-07	1.118	0.9571	1.487	1.809	1.76	0.9591

Table 4.13 - Freundlich, Dubinin-Radushkevich and Temkin parameters for Zn (II).

T (K)	***Freundlich parameters***			***Dubinin-Radushkevich parameters***				***Temkin parameters***			
	n	***K_f***	***R^2***	***Q_S***	***K_{DR}***	***E (kJ/mol)***	***R^2***	***B (kJ/mol)***	***A_T (L/g)***	***$b*10^{-3}$***	***R^2***
298	1.86	0.989	0.9642	2.094	2.00E-07	1.58	0.9874	1.267	2.502	1.955	0.9687
304	1.73	0.807	0.9686	1.775	3.00E-07	1.29	0.9935	1.161	2.287	2.175	0.9912
309	1.63	0.647	0.9745	1.566	3.00E-07	1.29	0.9773	1.046	2.11	2.455	0.9772
315	1.63	0.373	0.9675	0.935	3.00E-07	1.29	0.959	0.634	2.024	4.125	0.9661

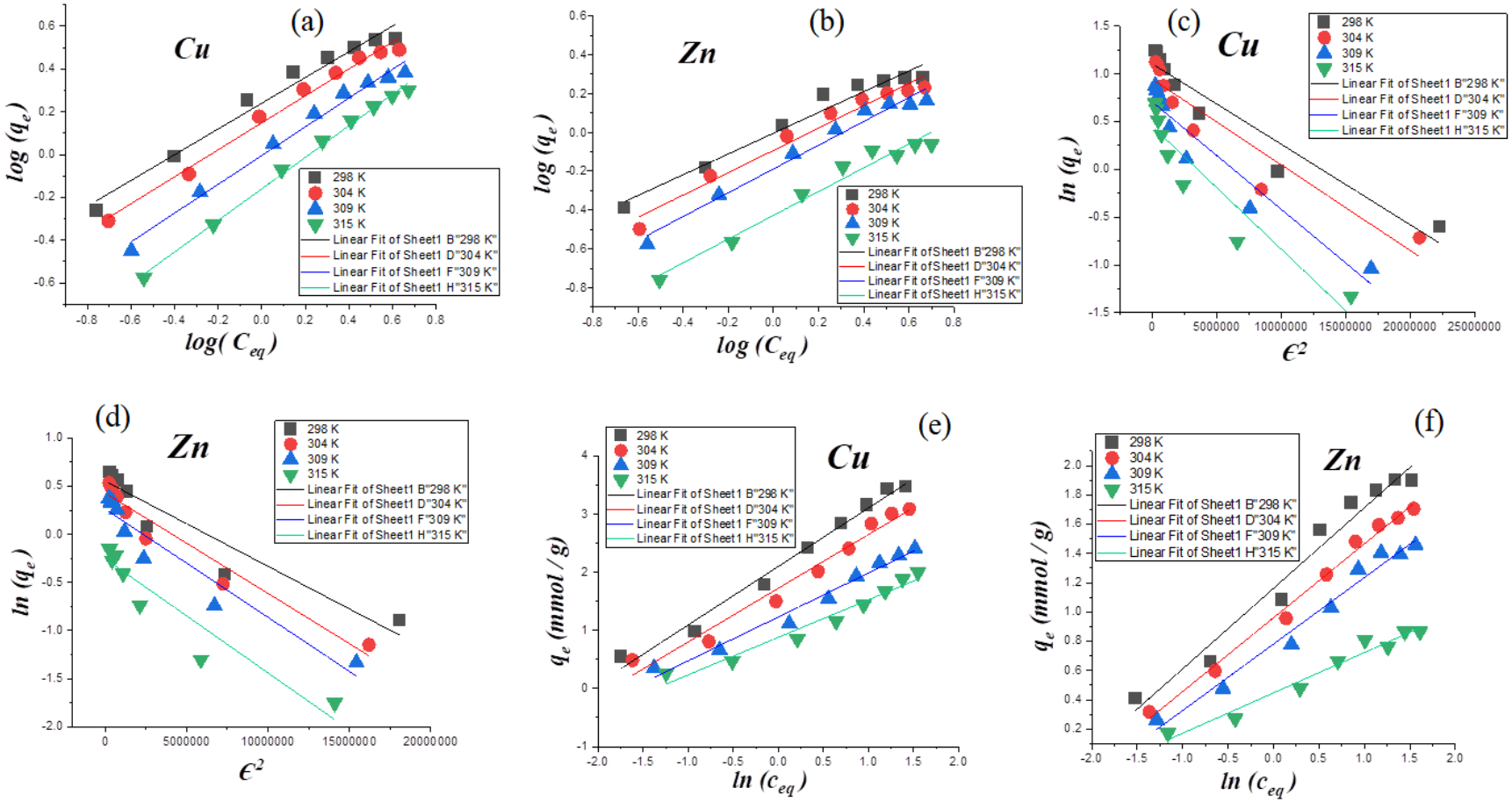

Figure 4.14 - Freundlich plots for Cu (II) (a) and Zn (II) (b). Dubinin-Radushkevich plots for Cu (II) (c) and Zn (II) (d). Temkin plots for Cu (II) (e) and Zn (II) (f).

The mean free energy (E) (kJ mol^{-1}) required to transfer one mole of ions from the solution to the solid surface of (CTS-CAA) can be calculated based on K_{DR} using equation (4.9) (subtitle 4.1.3).

Figure 4.14 (c, d) shows ε^2 vs. ln q_e plots as a representation of the Dubinin–Radushkevich model for the adsorption of both Cu (II) and Zn (II) metal ions on (CTS-CAA), while the fitting parameters are presented in Tables 4.12, 4.13 for Cu (II) and Zn (II) metal ions, respectively. As a general result, the obtained E values decrease with the temperature. The interval for the E values is (1.58-1.11) and (1.58-1.29) kJ/mol for Cu (II) and Zn (II) metal ions, respectively. Being that E values are lower than 8 kJ/mol, we can state that the adsorption of both metals on (CTS-CAA) can be attributed only to the physical sorption mechanism. As concerns the Temkin isotherm model, q_e and C_{eq} are related by the equation (4.10) (subtitle 4.1.3) [282].

The linear plots predicted by the Temkin model are displayed in Figure 4.14 (e, f), while the fitting parameters are listed in Tables 4.12, 4.13.

4.2.4 Desorption and regeneration processes

The regeneration of (CTS-CAA) sorbent from the samples loaded by the metal ions was investigated by performing desorption experiments using various eluents, including 0.5 M HNO_3, 0.5 M HCl, 0.5 M H_2SO_4, 0.2 M EDTA, 0.2 M Urea and 0.2M NH_4Cl. For the desorption steps, the contact time was set to 120 minutes and the sorbent dosage was set to 0.5 g/L.

Equation (4.11) was used to evaluate the desorption efficiency (subtitle 4.1.4).

We discovered that using 0.5 M HNO_3 and 0.2 M urea for Cu (II) and Zn (II) metal ions, respectively, resulted in a successful desorption process.

After the first desorption experiments, the (CTS-CAA) material was washed with distilled water and was applied for the second cycle of desorption. Three successful cycles were completed, and the results of the desorption tests are reported in Table 4.14. The sorption efficiency for both Cu (II) and Zn (II) metal ions is represented as 100 % as a reference value in the first cycle, and the sorption capacities for the other cycles are estimated relative to the first cycle. The adsorption capacity of various adsorbents for the separation of Cu (II), Zn (II) from the aqueous solution is shown in Table 4.15.

Table 4.14 - Data of three cycles of metal desorption.

Cycle	1		2		3	
Metal	Adsorption (%)	Desorption (%)	Adsorption (%)	Desorption (%)	Adsorption (%)	Desorption (%)
Copper	100	80.23	91.56	76.54	88.47	74.36
Zinc	100	84.21	93.42	79.89	89.74	78.89

Table 4.15 - Comparison of adsorption capacity of various adsorbents for the separation of Cu (II), Zn (II) from the aqueous solution.

adsorbent	Adsorption capacity (mg/g)		
	Cu (II)	Zn (II)	references
Sugar beet pulp	21.10	17.80	[283-285]
A biomatrix derived from rice husk	10.80	7.47	[286]
Chitosan–cellulose beads	53.20	-	[287]
Pyromellitic dianhydride modified SCB	77.40	65.00	[288]
Polyaniline graft chitosan	83.30	-	[289]
PEI-RCSA	177.10	110.20	[290]
Waste activated sludge biosolid	-	36.88	[291]
Lewatit SP 112	40.32	64.10	[292]
Lewatit TP 207	68.50	73.00	[293]
CTS-CAA	220.50	124.30	The current study

CONCLUSION

- The surface of halloysite nanotubes has been developed and functionalized with (3-chloropropyl) trimethoxysilane CPTMS, (3-glycidyloxypropyl) trimethoxysilane GOPTMS and (3-mercaptopropyl) trimethoxysilane MPTMS, the degree of functionalization (DF) was equal to 81%, 93% and 99% for grafting the above-mentioned silanes on halloysite nanotubes surface, respectively.
- The obtained data showed that toluene is the best solvent for grafting MPTMS and CPTMS on HNTs surface, while n-hexane is the best solvent for grafting GOPTMS on HNTs surface because the non-polar solvents are free of hydroxyl groups and hence there is no competition reaction between alkyl siloxane and hydroxyl groups of the solvents through H-bonding rather than hydroxyl groups of the surface
- The surface of halloysite nanotubes was functionalized with polyethyleneimine, and the affinities of Cu (II) and Zn (II) towards the modified material HN-PEI are the largest at pH 4.5 due to the deprotonation of amino groups with increasing the pH value. The pseudo-second-order and pseudo-first-order models are used to describe the data, because the q_e value obtained from the experiments brings closer to the q_2 and q_1 values for Cu (II) and for Zn (II), respectively. The data for both metal ions fit with the intraparticle diffusion model.
- For HN-PEI adsorbent, the negative $\Delta G°$ values at the studied temperatures indicate the spontaneous nature of the sorption process. The less degree of randomness for the sorption of Cu (II) (a) and Zn (II) on HN-PEI is confirmed by the negative $\Delta S°$ values at the studied temperatures.
- The modified aminocarboxymethyl chitosan CTS-CAA has been synthesized. The largest affinities of Cu (II) and Zn (II) towards CTS-CAA were reached at pH =3.5, where the strong electrostatic attractions occur. The binding between Cu (II) and Zn (II) metal ions and ($-COO^-$) on the surface of CTS-CAA within the pH range of 3.1-10 is due to the negative charge of the surface within the mentioned pH range. The pseudo-second-order and Elovich's equation are more accurate fitting procedures in the analysis of the adsorption results for both Cu (II) and Zn (II) while the Dumwald-Wagner model do not provide reliable fitting parameters.
- For CTS-CAA adsorbent, the negative $\Delta H°$ values indicate the exothermic nature for the sorption of Cu (II) and Zn (II). Since $E < 8$ kJ/mol so we can state that the adsorption of both metal ions on CTS-CAA is controlled by physical sorption mechanism.

- The uptake kinetics for Cu (II) and Zn (II) metal ions using the modified aminocarboxymethyl chitosan derivative is faster than that for the same metal ions using the modified halloysite nanotubes polyethyleneimine derivative and this is due to the greater adsorption characteristics of chitosan.
- The high potential of CTS-CAA for adsorption of Cu (II) and Zn (II) metal ions can be attributed to the presence of numerous carboxyl groups on chitosan surface after its modification plus its high content of amino and hydroxyl functional groups. In this regard, the sorption capacity of CTS-CAA and HN-PEI materials were 3.47 mmol Cu g^{-1} and 1.89 mmol Zn g^{-1}, and 2.78 mmol Cu g^{-1} and 1.84 mmol Zn g^{-1}, respectively.
- Chitosan as adsorbent is better than halloysite nanotubes because chitosan has high content of functional groups in addition that it can be easily modified using additional functional groups.

Prospects for further development of the research topic

Halloysite nanotubes modified with (3-chloropropyl)trimethoxysilane (CPTMS), (3-glycidyloxypropyl)trimethoxysilane (GOPTMS), and (3-mercaptopropyl)trimethoxysilane (MPTMS) can be further modified to create a surface terminated in -COOH, -PR3, or SO3H . These new modified materials are expected to be suitable for the recovery of many metals such as vanadium, zirconium, arsenic and gallium.

The extracted metals are valuable from an economic point of view and are used in many areas.

REFERENCES

1. Verma S. Slow sand filtration for water and wastewater treatment – a review / Verma S., Daverey A., Sharma A. // Environmental Technology Reviews. – 2017. – V. 6, № 1. – P. 47-58. https://doi.org/10.1080/21622515.2016.1278278

2. Teh C. Y. Recent Advancement of Coagulation–Flocculation and Its Application in Wastewater Treatment / Teh C. Y., Budiman P. M., Shak K. P. Y., Wu T. Y. // Industrial & Engineering Chemistry Research. – 2016. – V. 55, № 16. – P. 4363-4389. https://doi.org/10.1021/acs.iecr.5b04703

3. Levchuk I. Removal of natural organic matter (NOM) from water by ion exchange – A review / Levchuk I., Rueda Márquez J. J., Sillanpää M. // Chemosphere. – 2018. – V. 192, №. – P. 90-104. https://doi.org/10.1016/j.chemosphere.2017.10.101

4. Kanakaraju D. Advanced oxidation process-mediated removal of pharmaceuticals from water: A review / Kanakaraju D., Glass B. D., Oelgemöller M. // Journal of Environmental Management. – 2018. – V. 219, №. – P. 189-207. https://doi.org/10.1016/j.jenvman.2018.04.103

5. Malaeb L. Reverse osmosis technology for water treatment: State of the art review / Malaeb L., Ayoub G. M. // Desalination. – 2011. – V. 267, № 1. – P. 1-8. https://doi.org/10.1016/j.desal.2010.09.001

6. Sevda S. Bioelectroremediation of perchlorate and nitrate contaminated water: A review / Sevda S., Sreekishnan T. R., Pous N., Puig S., Pant D. // Bioresource Technology. – 2018. – V. 255, №. – P. 331-339. https://doi.org/10.1016/j.biortech.2018.02.005

7. Bhatnagar A. Adsorptive removal of bisphenol A (BPA) from aqueous solution: A review / Bhatnagar A., Anastopoulos I. // Chemosphere. – 2017. – V. 168, №. – P. 885-902. https://doi.org/10.1016/j.chemosphere.2016.10.121

8. Magnetite and Green Rust: Synthesis, Properties, and Environmental Applications of Mixed-Valent Iron Minerals / Usman M., Byrne J. M., Chaudhary A., Orsetti S., Hanna K., Ruby C., Kappler A., Haderlein S. B. // Chemical Reviews. – 2018. – V. 118, № 7. – P. 3251-3304. https://doi.org/10.1021/acs.chemrev.7b00224

9. Phosphate removal from aqueous solution using iron oxides: Adsorption, desorption and regeneration characteristics / Ajmal Z., Muhmood A., Usman M., Kizito S., Lu J., Dong R., Wu S. // Journal of Colloid and Interface Science. – 2018. – V. 528, №. – P. 145-155. https://doi.org/10.1016/j.jcis.2018.05.084

10. Anastopoulos I. A review on waste-derived adsorbents from sugar industry for pollutant removal in water and wastewater / Anastopoulos I., Bhatnagar A., Hameed B. H., Ok Y. S., Omirou M. // Journal of Molecular Liquids. – 2017. – V. 240, №. – P. 179-188. https://doi.org/10.1016/j.molliq.2017.05.063

11. Dyes adsorption using clay and modified clay: A review / Kausar A., Iqbal M., Javed A., Aftab K., Nazli Z.-i.-H., Bhatti H. N., Nouren S. // Journal of Molecular Liquids. – 2018. – V. 256, №. – P. 395-407. https://doi.org/10.1016/j.molliq.2018.02.034

12. Szczepanik B. Photocatalytic degradation of organic contaminants over clay-TiO2 nanocomposites: A review / Szczepanik B. // Applied Clay Science. – 2017. – V. 141, №. – P. 227-239. https://doi.org/10.1016/j.clay.2017.02.029

13. Halloysite clay minerals — a review / Joussein E., Petit S., Churchman J., Theng B., Righi D., Delvaux B. // Clay Minerals. – 2005. – V. 40, № 4. – P. 383-426. https://doi.org/10.1180/0009855054040180

14. Uddin M. K. A review on the adsorption of heavy metals by clay minerals, with special focus on the past decade / Uddin M. K. // Chemical Engineering Journal. – 2017. – V. 308, №. – P. 438-462. https://doi.org/10.1016/j.cej.2016.09.029

15. Sen Gupta S. Adsorption of heavy metals on kaolinite and montmorillonite: a review / Sen Gupta S., Bhattacharyya K. G. // Physical Chemistry Chemical Physics. – 2012. – V. 14, № 19. – P. 6698-6723. https://doi.org/10.1039/C2CP40093F

16. Adsorption of proteins and nucleic acids on clay minerals and their interactions: A review / Yu W. H., Li N., Tong D. S., Zhou C. H., Lin C. X., Xu C. Y. // Applied Clay Science. – 2013. – V. 80-81, №. – P. 443-452. https://doi.org/10.1016/j.clay.2013.06.003

17. Adeyemo A. A. Adsorption of dyes using different types of clay: a review / Adeyemo A. A., Adeoye I. O., Bello O. S. // Applied Water Science. – 2017. – V. 7, № 2. – P. 543-568. https://doi.org/10.1007/s13201-015-0322-y

18. Yuan P. Properties and applications of halloysite nanotubes: recent research advances and future prospects / Yuan P., Tan D., Annabi-Bergaya F. // Applied Clay Science. – 2015. – V. 112-113, №. – P. 75-93. https://doi.org/10.1016/j.clay.2015.05.001

19. Chang Y.-C. Preparation and adsorption properties of monodisperse chitosan-bound Fe3O4 magnetic nanoparticles for removal of Cu(II) ions / Chang Y.-C., Chen D.-H. // Journal of Colloid and Interface Science. – 2005. – V. 283, № 2. – P. 446-451. https://doi.org/10.1016/j.jcis.2004.09.010

20. A New Ion-Imprinted Chitosan-Based Membrane with an Azo-Derivative Ligand for the Efficient Removal of Pd(II) / Di Bello M. P., Lazzoi M. R., Mele G., Scorrano S., Mergola L., Del Sole R. // Materials (Basel). – 2017. – V. 10, № 10. –. https://doi.org/10.3390/ma10101133

21. Kyzas G. Z. Recent modifications of chitosan for adsorption applications: a critical and systematic review / Kyzas G. Z., Bikiaris D. N. // Mar Drugs. – 2015. – V. 13, № 1. – P. 312-37. https://doi.org/10.3390/md13010312

22. Li N. Copper adsorption on chitosan–cellulose hydrogel beads: behaviors and mechanisms / Li N., Bai R. // Separation and Purification Technology. – 2005. – V. 42, № 3. – P. 237-247. https://doi.org/10.1016/j.seppur.2004.08.002

23. Naseeruteen F. Adsorption of malachite green from aqueous solution by using novel chitosan ionic liquid beads / Naseeruteen F., Hamid N. S. A., Suah F. B. M., Ngah W. S. W., Mehamod F. S. // Int J Biol Macromol. – 2018. – V. 107, № Pt A. – P. 1270-1277. https://doi.org/10.1016/j.ijbiomac.2017.09.111

24. Regeneration of chitosan-based adsorbents used in heavy metal adsorption: A review / Vakili M., Deng S., Cagnetta G., Wang W., Meng P., Liu D., Yu G. // Separation and Purification Technology. – 2019. – V. 224, №. – P. 373-387. https://doi.org/10.1016/j.seppur.2019.05.040

25. An exploratory study on low-concentration hexavalent chromium adsorption by Fe(III)-cross-linked chitosan beads / Wu Y., Zhang Y., Qian J., Xin X., Hu S., Zhang S., Wei J. // R Soc Open Sci. – 2017. – V. 4, № 11. – P. 170905. https://doi.org/10.1098/rsos.170905

26. Production of thick uniform-coating films containing rectorite on nanofibers through the use of an automated coating machine / Wu Y., Li X., Shi X., Zhan Y., Tu H., Du Y., Deng H., Jiang L. // Colloids and Surfaces B: Biointerfaces. – 2017. – V. 149, №. – P. 271-279. https://doi.org/10.1016/j.colsurfb.2016.10.030

27. Yang D. Efficient Adsorption of Methyl Orange Using a Modified Chitosan Magnetic Composite Adsorbent / Yang D., Qiu L., Yang Y. // Journal of Chemical & Engineering Data. – 2016. – V. 61, № 11. – P. 3933-3940. https://doi.org/10.1021/acs.jced.6b00706

28. An environment-friendly and multi-functional absorbent from chitosan for organic pollutants and heavy metal ion / Li A., Lin R., Lin C., He B., Zheng T., Lu L., Cao Y. // Carbohydr Polym. – 2016. – V. 148, №. – P. 272-80. https://doi.org/10.1016/j.carbpol.2016.04.070

29. Jawad A. H. Cross-linked chitosan thin film coated onto glass plate as an effective adsorbent for adsorption of reactive orange 16 / Jawad A. H., Azharul Islam M., Hameed B. H. // International Journal of Biological Macromolecules. – 2017. – V. 95, №. – P. 743-749. https://doi.org/10.1016/j.ijbiomac.2016.11.087

30. Development of drug-loaded chitosan-vanillin nanoparticles and its cytotoxicity against HT-29 cells / Li P. W., Wang G., Yang Z. M., Duan W., Peng Z., Kong L. X., Wang Q. H. // Drug Delivery. – 2016. – V. 23, № 1. – P. 30-35. https://doi.org/10.3109/10717544.2014.900590

31. Yang Z. Enhanced Formaldehyde Removal from Air Using Fully Biodegradable Chitosan Grafted β-Cyclodextrin Adsorbent with Weak Chemical Interaction / Yang Z., Miao H., Rui Z., Ji H. // Polymers. – 2019. – V. 11, № 2. –. https://doi.org/10.3390/polym11020276

32. Spherical polystyrene-supported chitosan thin film of fast kinetics and high capacity for copper removal / Jiang W., Chen X., Pan B., Zhang Q., Teng L., Chen Y., Liu L. // Journal of Hazardous Materials. – 2014. – V. 276, №. – P. 295-301. https://doi.org/10.1016/j.jhazmat.2014.05.032

33. Negm N. A. Treatment of industrial wastewater containing copper and cobalt ions using modified chitosan / Negm N. A., El Sheikh R., El-Farargy A. F., Hefni H. H. H., Bekhit M. // Journal of Industrial and Engineering Chemistry. – 2015. – V. 21, №. – P. 526-534. https://doi.org/10.1016/j.jiec.2014.03.015
34. Preparation and characterization of chitosan–caboxymethyl-β-cyclodextrin entrapped nanozero-valent iron composite for Cu (II) and Cr (IV) removal from wastewater / Sikder M. T., Mihara Y., Islam M. S., Saito T., Tanaka S., Kurasaki M. // Chemical Engineering Journal. – 2014. – V. 236, №. – P. 378-387. https://doi.org/10.1016/j.cej.2013.09.093
35. Wan Ngah W. S. Comparative study on adsorption and desorption of Cu(II) ions by three types of chitosan–zeolite composites / Wan Ngah W. S., Teong L. C., Toh R. H., Hanafiah M. A. K. M. // Chemical Engineering Journal. – 2013. – V. 223, №. – P. 231-238. https://doi.org/10.1016/j.cej.2013.02.090
36. Kyzas G. Z. Synthesis and adsorption application of succinyl-grafted chitosan for the simultaneous removal of zinc and cationic dye from binary hazardous mixtures / Kyzas G. Z., Siafaka P. I., Pavlidou E. G., Chrissafis K. J., Bikiaris D. N. // Chemical Engineering Journal. – 2015. – V. 259, №. – P. 438-448. https://doi.org/10.1016/j.cej.2014.08.019
37. Sorption of zinc by novel pH-sensitive hydrogels based on chitosan, itaconic acid and methacrylic acid / Milosavljević N. B., Ristić M. Đ., Perić-Grujić A. A., Filipović J. M., Štrbac S. B., Rakočević Z. L., Kalagasidis Krušić M. T. // Journal of Hazardous Materials. – 2011. – V. 192, № 2. – P. 846-854. https://doi.org/10.1016/j.jhazmat.2011.05.093
38. Morsi R. E. Chitosan/MCM-41 nanocomposites for efficient beryllium separation / Morsi R. E., Elsherief M. A., Shabaan M., Elsabee M. Z. // Journal of Applied Polymer Science. – 2018. – V. 135, № 13. – P. 46040. https://doi.org/10.1002/app.46040
39. Abd El-Magied M. O. Biosorption of beryllium from aqueous solutions onto modified chitosan resin: Equilibrium, kinetic and thermodynamic study / Abd El-Magied M. O., Mansour A., Alsayed F. A. A. G., Atrees M. S., Abd Eldayem S. // Journal of Dispersion Science and Technology. – 2018. – V. 39, № 11. – P. 1597-1605. https://doi.org/10.1016/10.1080/01932691.2018.1452757
40. Matusik J. Enhanced heavy metal adsorption on functionalized nanotubular halloysite interlayer grafted with aminoalcohols / Matusik J., Wścisło A. // Applied Clay Science. – 2014. – V. 100, №. – P. 50-59. https://doi.org/10.1016/j.clay.2014.06.034
41. Maziarz P. The effect of acid activation and calcination of halloysite on the efficiency and selectivity of Pb(II), Cd(II), Zn(II) and As(V) uptake / Maziarz P., Matusik J. // Clay Minerals. – 2016. – V. 51, № 3. – P. 385-394. https://doi.org/10.1180/claymin.2016.051.3.06
42. Alloway B. J. Heavy metals in soils: trace metals and metalloids in soils and their bioavailability. / Alloway B. J.: Springer Science & Business Media, 2012. – 22.

43. Wang Y.-H. Removal of heavy metal ions from aqueous solutions using various low-cost adsorbents / Wang Y.-H., Lin S.-H., Juang R.-S. // Journal of Hazardous Materials. – 2003. – V. 102, № 2. – P. 291-302. https://doi.org/10.1016/S0304-3894(03)00218-8

44. Heavy metal removal from water/wastewater by nanosized metal oxides: A review / Hua M., Zhang S., Pan B., Zhang W., Lv L., Zhang Q. // Journal of Hazardous Materials. – 2012. – V. 211-212, №. – P. 317-331. https://doi.org/10.1016/j.jhazmat.2011.10.016

45. Bailey S. E. A review of potentially low-cost sorbents for heavy metals / Bailey S. E., Olin T. J., Bricka R. M., Adrian D. D. // Water Research. – 1999. – V. 33, № 11. – P. 2469-2479. https://doi.org/10.1016/S0043-1354(98)00475-8

46. Babel S. Low-cost adsorbents for heavy metals uptake from contaminated water: a review / Babel S., Kurniawan T. A. // Journal of Hazardous Materials. – 2003. – V. 97, № 1. – P. 219-243. https://doi.org/10.1016/S0304-3894(02)00263-7

47. Saad R. Adsorption of phosphate and nitrate anions on ammonium-functionalized MCM-48: Effects of experimental conditions / Saad R., Belkacemi K., Hamoudi S. // Journal of Colloid and Interface Science. – 2007. – V. 311, № 2. – P. 375-381. https://doi.org/10.1016/j.jcis.2007.03.025

48. Abou Taleb M. F. Adsorption and desorption of phosphate and nitrate ions using quaternary (polypropylene-g-N,N-dimethylamino ethylmethacrylate) graft copolymer / Abou Taleb M. F., Mahmoud G. A., Elsigeny S. M., Hegazy E.-S. A. // Journal of Hazardous Materials. – 2008. – V. 159, № 2. – P. 372-379. https://doi.org/10.1016/j.jhazmat.2008.02.028

49. Bhattacharyya K. G. Adsorption of a few heavy metals on natural and modified kaolinite and montmorillonite: A review / Bhattacharyya K. G., Gupta S. S. // Advances in Colloid and Interface Science. – 2008. – V. 140, № 2. – P. 114-131. https://doi.org/10.1016/j.cis.2007.12.008

50. Lee S. M. Organo and inorgano-organo-modified clays in the remediation of aqueous solutions: An overview / Lee S. M., Tiwari D. // Applied Clay Science. – 2012. – V. 59-60, №. – P. 84-102. https://doi.org/10.1016/j.clay.2012.02.006

51. Qu X. Applications of nanotechnology in water and wastewater treatment / Qu X., Alvarez P. J. J., Li Q. // Water Research. – 2013. – V. 47, № 12. – P. 3931-3946. https://doi.org/10.1016/j.watres.2012.09.058

52. Zhao Y. Halloysite nanotubule clay for efficient water purification / Zhao Y., Abdullayev E., Vasiliev A., Lvov Y. // Journal of Colloid and Interface Science. – 2013. – V. 406, №. – P. 121-129. https://doi.org/10.1016/j.jcis.2013.05.072

53. Selective Recognition of 2,4,6-Trichlorophenol by Molecularly Imprinted Polymers Based on Magnetic Halloysite Nanotubes Composites / Pan J., Yao H., Xu L., Ou H., Huo P., Li X., Yan Y. // The Journal of Physical Chemistry C. – 2011. – V. 115, № 13. – P. 5440-5449. https://doi.org/10.1021/jp111120x

54. Matusik J. Arsenate, orthophosphate, sulfate, and nitrate sorption equilibria and kinetics for halloysite and kaolinites with an induced positive charge / Matusik J. // Chemical Engineering Journal. – 2014. – V. 246, №. – P. 244-253. https://doi.org/10.1016/j.cej.2014.03.004

55. Tian X. Polyethylenimine functionalized halloysite nanotubes for efficient removal and fixation of Cr (VI) / Tian X., Wang W., Wang Y., Komarneni S., Yang C. // Microporous and Mesoporous Materials. – 2015. – V. 207, №. – P. 46-52. https://doi.org/10.1016/j.micromeso.2014.12.031

56. Owlad M. Removal of Hexavalent Chromium-Contaminated Water and Wastewater: A Review / Owlad M., Aroua M. K., Daud W. A. W., Baroutian S. // Water, Air, and Soil Pollution. – 2009. – V. 200, № 1. – P. 59-77. https://doi.org/10.1007/s11270-008-9893-7

57. Bhatnagar A. Applications of chitin- and chitosan-derivatives for the detoxification of water and wastewater--a short review / Bhatnagar A., Sillanpää M. // Adv Colloid Interface Sci. – 2009. – V. 152, № 1-2. – P. 26-38. https://doi.org/10.1016/j.cis.2009.09.003

58. Miretzky P. Hg(II) removal from water by chitosan and chitosan derivatives: a review / Miretzky P., Cirelli A. F. // J Hazard Mater. – 2009. – V. 167, № 1-3. – P. 10-23. https://doi.org/10.1016/j.jhazmat.2009.01.060

59. Pontoni L. Use of chitosan and chitosan-derivatives to remove arsenic from aqueous solutions--a mini review / Pontoni L., Fabbricino M. // Carbohydr Res. – 2012. – V. 356, №. – P. 86-92. https://doi.org/10.1016/j.carres.2012.03.042

60. Wan Ngah W. S. Adsorption of dyes and heavy metal ions by chitosan composites: A review / Wan Ngah W. S., Teong L. C., Hanafiah M. A. K. M. // Carbohydrate Polymers. – 2011. – V. 83, № 4. – P. 1446-1456. https://doi.org/10.1016/j.carbpol.2010.11.004

61. Wu F. C. A review and experimental verification of using chitosan and its derivatives as adsorbents for selected heavy metals / Wu F. C., Tseng R. L., Juang R. S. // J Environ Manage. – 2010. – V. 91, № 4. – P. 798-806. https://doi.org/10.1016/j.jenvman.2009.10.018

62. Jayakumar R. Graft copolymerized chitosan—present status and applications / Jayakumar R., Prabaharan M., Reis R. L., Mano J. F. // Carbohydrate Polymers. – 2005. – V. 62, № 2. – P. 142-158. https://doi.org/10.1016/j.carbpol.2005.07.017

63. Newman R. H. Aluminium coordination and structural disorder in halloysite and kaolinite by 27Al NMR spectroscopy / Newman R. H., Childs C. W., Churchman G. J. // Clay Minerals. – 1994. – V. 29, № 3. – P. 305-312. https://doi.org/10.1180/claymin.1994.029.3.01

64. Brady P. V. Molecular Controls on Kaolinite Surface Charge / Brady P. V., Cygan R. T., Nagy K. L. // Journal of Colloid and Interface Science. – 1996. – V. 183, № 2. – P. 356-364. https://doi.org/10.1006/jcis.1996.0557

65. Tombácz E. Surface charge heterogeneity of kaolinite in aqueous suspension in comparison with montmorillonite / Tombácz E., Szekeres M. // Applied Clay Science. – 2006. – V. 34, № 1. – P. 105-124. https://doi.org/10.1016/j.clay.2006.05.009

66. Changes in Structure, Morphology, Porosity, and Surface Activity of Mesoporous Halloysite Nanotubes Under Heating / Yuan P., Tan D., Annabi-Bergaya F., Yan W., Fan M., Liu D., He H. // Clays and Clay Minerals. – 2012. – V. 60, № 6. – P. 561-573. https://doi.org/10.1346/CCMN.2012.0600602

67. Smith M. E. Structural characterization of the thermal transformation of halloysite by solid state NMR / Smith M. E., Neal G., Trigg M. B., Drennan J. // Applied Magnetic Resonance. – 1993. – V. 4, № 1. – P. 157-170. https://doi.org/10.1007/BF03162561

68. Intercalation of halloysite from Djebel Debagh (Algeria) and adsorption of copper ions / Mellouk S., Cherifi S., Sassi M., Marouf-Khelifa K., Bengueddach A., Schott J., Khelifa A. // Applied Clay Science. – 2009. – V. 44, № 3. – P. 230-236. https://doi.org/10.1016/j.clay.2009.02.008

69. Physicochemical and adsorptive properties of a heat-treated and acid-leached Algerian halloysite / Belkassa K., Bessaha F., Marouf-Khelifa K., Batonneau-Gener I., Comparot J.-d., Khelifa A. // Colloids and Surfaces A: Physicochemical and Engineering Aspects. – 2013. – V. 421, №. – P. 26-33. https://doi.org/10.1016/j.colsurfa.2012.12.048

70. Effects of acid treatment on the physico-chemical and pore characteristics of halloysite / Zhang A.-B., Pan L., Zhang H.-Y., Liu S.-T., Ye Y., Xia M.-S., Chen X.-G. // Colloids and Surfaces A: Physicochemical and Engineering Aspects. – 2012. – V. 396, №. – P. 182-188. https://doi.org/10.1016/j.colsurfa.2011.12.067

71. White R. D. The stability of halloysite nanotubes in acidic and alkaline aqueous suspensions / White R. D., Bavykin D. V., Walsh F. C. // Nanotechnology. – 2012. – V. 23, № 6. – P. 065705. https://doi.org/10.1088/0957-4484/23/6/065705

72. Joo Y. Opening and blocking the inner-pores of halloysite / Joo Y., Sim J. H., Jeon Y., Lee S. U., Sohn D. // Chemical Communications. – 2013. – V. 49, № 40. – P. 4519-4521. https://doi.org/10.1039/C3CC40465J

73. Abdullayev E. Enlargement of Halloysite Clay Nanotube Lumen by Selective Etching of Aluminum Oxide / Abdullayev E., Joshi A., Wei W., Zhao Y., Lvov Y. // ACS Nano. – 2012. – V. 6, № 8. – P. 7216-7226. https://doi.org/10.1021/nn302328x

74. Wada K. Selective Adsorption of Zinc on Halloysite / Wada K., Kakuto Y. // Clays and Clay Minerals. – 1980. – V. 28, № 5. – P. 321-327. https://doi.org/10.1346/CCMN.1980.0280501

75. Dong Y. Removal of Zn(II) from aqueous solution by natural halloysite nanotubes / Dong Y., Liu Z., Chen L. // Journal of Radioanalytical and Nuclear Chemistry. – 2012. – V. 292, № 1. – P. 435-443. https://doi.org/10.1007/s10967-011-1425-z

76. Kiani G. High removal capacity of silver ions from aqueous solution onto Halloysite nanotubes / Kiani G. // Applied Clay Science. – 2014. – V. 90, №. – P. 159-164. https://doi.org/10.1016/j.clay.2014.01.010
77. Mellouk S. Cu(II) adsorption by halloysites intercalated with sodium acetate / Mellouk S., Belhakem A., Marouf-Khelifa K., Schott J., Khelifa A. // Journal of Colloid and Interface Science. – 2011. – V. 360, № 2. – P. 716-724. https://doi.org/10.1016/j.jcis.2011.05.001
78. Koteja A. Di- and triethanolamine grafted kaolinites of different structural order as adsorbents of heavy metals / Koteja A., Matusik J. // Journal of Colloid and Interface Science. – 2015. – V. 455, №. – P. 83-92. https://doi.org/10.1016/j.jcis.2015.05.027
79. Letaief S. Functionalized nanohybrid materials obtained from the interlayer grafting of aminoalcohols on kaolinite / Letaief S., Detellier C. // Chemical Communications. – 2007. – V. https://doi.org/10.1039/B701235G № 25. – P. 2613-2615. https://doi.org/10.1039/B701235G
80. Sen B. Characterization and studies of some triethanolamine complexes of transition and representative metals / Sen B., Dotson R. L. // Journal of Inorganic and Nuclear Chemistry. – 1970. – V. 32, № 8. – P. 2707-2716. https://doi.org/10.1016/0022-1902(70)80320-7
81. Tauler R. The complex formation of Cu(II) with triethanolamine in aqueous solution / Tauler R., Casassas E., Rainer M. J. A., Rode B. M. // Inorganica Chimica Acta. – 1985. – V. 105, № 2. – P. 165-170. https://doi.org/10.1016/S0020-1693(00)90556-5
82. Karadağ A. Di- and triethanolamine complexes of Co(II), Ni(II), Cu(II) and Zn(II) with thiocyanate: synthesis, spectral and thermal studies. Crystal structure of dimeric Cu(II) complex with deprotonated diethanolamine, $[Cu_2(\mu\text{-dea})_2(NCS)_2]$ / Karadağ A., Yilmaz V. T., Thoene C. // Polyhedron. – 2001. – V. 20, №. – P. 635-641.
83. Whitmire K. H. Triethanolamine complexes of copper / Whitmire K. H., Hutchison J. C., Gardberg A., Edwards C. // Inorganica Chimica Acta. – 1999. – V. 294, № 2. – P. 153-162. https://doi.org/10.1016/S0020-1693(99)00274-1
84. Weber W. J. Kinetics of Adsorption on Carbon from Solution / Weber W. J., Morris J. C. // Journal of the Sanitary Engineering Division. – 1963. – V. 89, № 2. – P. 31-59. https://doi.org/10.1061/JSEDAI.0000430
85. Haggerty G. M. Sorption of chromate and other inorganic anions by organo-zeolite / Haggerty G. M., Bowman R. S. // Environmental Science & Technology. – 1994. – V. 28, № 3. – P. 452-458. https://doi.org/10.1021/es00052a017
86. Li Z. Retention of inorganic oxyanions by organo-kaolinite / Li Z., Bowman R. S. // Water Research. – 2001. – V. 35, № 16. – P. 3771-3776. https://doi.org/10.1016/S0043-1354(01)00120-8

87. Bowman R. S. Applications of surfactant-modified zeolites to environmental remediation / Bowman R. S. // Microporous and Mesoporous Materials. – 2003. – V. 61, № 1. – P. 43-56. https://doi.org/10.1016/S1387-1811(03)00354-8

88. Mallavarapu M. Preparation, characterization of surfactants modified clay minerals and nitrate adsorption / Xi Y., Mallavarapu M., Naidu R. // Applied Clay Science. – 2010. – V. 48, № 1. – P. 92-96. https://doi.org/10.1016/j.clay.2009.11.047

89. Rapid adsorption of Cr (VI) on modified halloysite nanotubes / Jinhua W., Xiang Z., Bing Z., Yafei Z., Rui Z., Jindun L., Rongfeng C. // Desalination. – 2010. – V. 259, № 1. – P. 22-28. https://doi.org/10.1016/j.desal.2010.04.046

90. Matusik J. Immobilization and reduction of hexavalent chromium in the interlayer space of positively charged kaolinites / Matusik J., Bajda T. // Journal of Colloid and Interface Science. – 2013. – V. 398, №. – P. 74-81. https://doi.org/10.1016/j.jcis.2013.02.015

91. Letaief S. Nanohybrid materials from interlayer functionalization of kaolinite. Application to the electrochemical preconcentration of cyanide / Letaief S., Tonle I. K., Diaco T., Detellier C. // Applied Clay Science. – 2008. – V. 42, № 1. – P. 95-101. https://doi.org/10.1016/j.clay.2007.12.007

92. Dedzo G. K. Kaolinite–ionic liquid nanohybrid materials as electrochemical sensors for size-selective detection of anions / Dedzo G. K., Letaief S., Detellier C. // Journal of Materials Chemistry. – 2012. – V. 22, № 38. – P. 20593-20601. https://doi.org/10.1039/C2JM34772E

93. Dedzo G. K. Ionic liquid-kaolinite nanohybrid materials for the amperometric detection of trace levels of iodide / Dedzo G. K., Detellier C. // Analyst. – 2013. – V. 138, № 3. – P. 767-70. https://doi.org/10.1039/c2an36618e

94. Ballav N. Polypyrrole-coated halloysite nanotube clay nanocomposite: Synthesis, characterization and Cr(VI) adsorption behaviour / Ballav N., Choi H. J., Mishra S. B., Maity A. // Applied Clay Science. – 2014. – V. 102, №. – P. 60-70. https://doi.org/10.1016/j.clay.2014.10.008

95. Preparation and Characterization of Silane Coupling Agent Modified Halloysite for Cr(VI) Removal / Luo P., Zhang J.-s., Zhang B., Wang J.-h., Zhao Y.-f., Liu J.-d. // Industrial & Engineering Chemistry Research. – 2011. – V. 50, № 17. – P. 10246-10252. https://doi.org/10.1021/ie200951n

96. Carr R. M. Complexes of halloysite with organic compounds / Carr R. M., Chih H. // Clay Minerals. – 1971. – V. 9, № 2. – P. 153-166. https://doi.org/10.1180/claymin.1971.009.2.01

97. Zhao M. Adsorption behavior of methylene blue on halloysite nanotubes / Zhao M., Liu P. // Microporous and Mesoporous Materials. – 2008. – V. 112, № 1. – P. 419-424. https://doi.org/10.1016/j.micromeso.2007.10.018

98. Study on the adsorption of Neutral Red from aqueous solution onto halloysite nanotubes / Luo P., Zhao Y., Zhang B., Liu J., Yang Y., Liu J. // Water Research. – 2010. – V. 44, № 5. – P. 1489-1497. https://doi.org/10.1016/j.watres.2009.10.042

99. Liu R. Adsorption of methyl violet from aqueous solution by halloysite nanotubes / Liu R., Zhang B., Mei D., Zhang H., Liu J. // Desalination. – 2011. – V. 268, № 1. – P. 111-116. https://doi.org/10.1016/j.desal.2010.10.006

100. Kiani G. Adsorption studies on the removal of Malachite Green from aqueous solutions onto halloysite nanotubes / Kiani G., Dostali M., Rostami A., Khataee A. R. // Applied Clay Science. – 2011. – V. 54, № 1. – P. 34-39. https://doi.org/10.1016/j.clay.2011.07.008

101. Yuan P. Organosilane functionalization of halloysite nanotubes for enhanced loading and controlled release / Yuan P., Southon P. D., Liu Z., Kepert C. J. // Nanotechnology. – 2012. – V. 23, № 37. – P. 375705. https://doi.org/10.1088/0957-4484/23/37/375705

102. Xie Y. Magnetic halloysite nanotubes/iron oxide composites for the adsorption of dyes / Xie Y., Qian D., Wu D., Ma X. // Chemical Engineering Journal. – 2011. – V. 168, № 2. – P. 959-963. https://doi.org/10.1016/j.cej.2011.02.031

103. Duan J. Halloysite nanotube-Fe_3O_4 composite for removal of methyl violet from aqueous solutions / Duan J., Liu R., Chen T., Zhang B., Liu J. // Desalination. – 2012. – V. 293, №. – P. 46-52. https://doi.org/10.1016/j.desal.2012.02.022

104. Peng Q. Adsorption of dyes in aqueous solutions by chitosan–halloysite nanotubes composite hydrogel beads / Peng Q., Liu M., Zheng J., Zhou C. // Microporous and Mesoporous Materials. – 2015. – V. 201, №. – P. 190-201. https://doi.org/10.1016/j.micromeso.2014.09.003

105. The removal of dye from aqueous solution using alginate-halloysite nanotube beads / Liu L., Wan Y., Xie Y., Zhai R., Zhang B., Liu J. // Chemical Engineering Journal. – 2012. – V. 187, №. – P. 210-216. https://doi.org/10.1016/j.cej.2012.01.136

106. Lee S. Y. Adsorption of naphthalene by HDTMA modified kaolinite and halloysite / Lee S. Y., Kim S. J. // Applied Clay Science. – 2002. – V. 22, № 1. – P. 55-63. https://doi.org/10.1016/S0169-1317(02)00113-8

107. Viseras M. T. Equilibrium and kinetics of 5-aminosalicylic acid adsorption by halloysite / Viseras M. T., Aguzzi C., Cerezo P., Viseras C., Valenzuela C. // Microporous and Mesoporous Materials. – 2008. – V. 108, № 1. – P. 112-116. https://doi.org/10.1016/j.micromeso.2007.03.033

108. Szczepanik B. Adsorption of chloroanilines from aqueous solutions on the modified halloysite / Szczepanik B., Słomkiewicz P., Garnuszek M., Czech K. // Applied Clay Science. – 2014. – V. 101, №. – P. 260-264. https://doi.org/10.1016/j.clay.2014.08.013

109. Hybrid photosensitizer based on halloysite nanotubes for phenol-based pesticide photodegradation / Bielska D., Karewicz A., Lachowicz T., Berent K., Szczubiałka K., Nowakowska M. // Chemical Engineering Journal. – 2015. – V. 262, №. – P. 125-132. https://doi.org/10.1016/j.cej.2014.09.081

110. Chokradjaroen C. Cytotoxicity against cancer cells of chitosan oligosaccharides prepared from chitosan powder degraded by electrical discharge plasma / Chokradjaroen C., Theeramunkong S., Yui H., Saito N., Rujiravanit R. // Carbohydrate Polymers. – 2018. – V. 201, №. – P. 20-30. https://doi.org/10.1016/j.carbpol.2018.08.037

111. Ibrahim M. Spectroscopic analyses of cellulose and chitosan: FTIR and modeling approach / Ibrahim M., Osman O., Mahmoud A. A. // Journal of Computational and Theoretical Nanoscience. – 2011. – V. 8, № 1. – P. 117-123. https://doi.org/10.1166/jctn.2011.1668

112. Kumar M. N. V. R. Chitosan Chemistry and Pharmaceutical Perspectives / Kumar M. N. V. R., Muzzarelli R. A. A., Muzzarelli C., Sashiwa H., Domb A. J. // Chemical Reviews. – 2004. – V. 104, № 12. – P. 6017-6084. https://doi.org/10.1021/cr030441b

113. Mourya V. K. Chitosan-modifications and applications: Opportunities galore / Mourya V. K., Inamdar N. N. // Reactive and Functional Polymers. – 2008. – V. 68, № 6. – P. 1013-1051. https://doi.org/10.1016/j.reactfunctpolym.2008.03.002

114. Knaul J. Z. Coagulation rate studies of spinnable chitosan solutions / Knaul J. Z., Creber K. A. M. // Journal of Applied Polymer Science. – 1997. – V. 66, № 1. – P. 117-127. https://doi.org/10.1002/(SICI)1097-4628(19971003)66:1<117::AID-APP14>3.0.CO;2-Z

115. Tseng H. Bromination of regenerated chitin with N-bromosuccinimide and triphenylphosphine under homogeneous conditions in lithium bromide-N,N-dimethylacetamide / Tseng H., Furuhata K.-i., Sakamoto M. // Carbohydrate Research. – 1995. – V. 270, № 2. – P. 149-161. https://doi.org/10.1016/0008-6215(95)00004-D

116. Yu C. Chapter 7 - Grafting Modification of Chitosan / Yu C., Kecen X., Xiaosai Q. // Biopolymer Grafting / Thakur V. K.Elsevier, - 2018. -V. https://doi.org/10.1016/B978-0-323-48104-5.00007-X№. – P. 295-364.

117. Lizardi-Mendoza J. Chapter 1 - Chemical Characteristics and Functional Properties of Chitosan / Lizardi-Mendoza J., Argüelles Monal W. M., Goycoolea Valencia F. M. // Chitosan in the Preservation of Agricultural Commodities / Bautista-Baños S. и др. – San Diego: Academic Press, - 2016. -V. https://doi.org/10.1016/B978-0-12-802735-6.00001-X№. – P. 3-31.

118. Clark G. L. X-ray Diffraction Studies of Chitin, Chitosan, and Derivatives / Clark G. L., Smith A. F. // The Journal of Physical Chemistry. – 1936. – V. 40, № 7. – P. 863-879. https://doi.org/10.1021/j150376a001

119. Application of spectroscopic methods for structural analysis of chitin and chitosan / Kumirska J., Czerwicka M., Kaczyński Z., Bychowska A., Brzozowski K., Thöming J., Stepnowski P. // Mar Drugs. – 2010. – V. 8, № 5. – P. 1567-636. https://doi.org/10.3390/md8051567

120. Okuyama K. Molecular and Crystal Structure of Hydrated Chitosan / Okuyama K., Noguchi K., Miyazawa T., Yui T., Ogawa K. // Macromolecules. – 1997. – V. 30, № 19. – P. 5849-5855. https://doi.org/10.1021/ma970509n

121. Polymorphic Modifications of Chitosan / Baklagina Y. G., Klechkovskaya V. V., Kononova S. V., Petrova V. A., Poshina D. N., Orekhov A. S., Skorik Y. A. // Crystallography Reports. – 2018. – V. 63, № 3. – P. 303-313. https://doi.org/10.1134/S1063774518030033

122. Kasaai M. R. Calculation of Mark–Houwink–Sakurada (MHS) equation viscometric constants for chitosan in any solvent–temperature system using experimental reported viscometric constants data / Kasaai M. R. // Carbohydrate Polymers. – 2007. – V. 68, № 3. – P. 477-488. https://doi.org/10.1016/j.carbpol.2006.11.006

123. Kolhe P. Improvement in Ductility of Chitosan through Blending and Copolymerization with PEG: FTIR Investigation of Molecular Interactions / Kolhe P., Kannan R. M. // Biomacromolecules. – 2003. – V. 4, № 1. – P. 173-180. https://doi.org/10.1021/bm025689+

124. Kurita K. Controlled functionalization of the polysaccharide chitin / Kurita K. // Progress in Polymer Science. – 2001. – V. 26, № 9. – P. 1921-1971. https://doi.org/10.1016/S0079-6700(01)00007-7

125. Costa C. N. Viscometric study of chitosan solutions in acetic acid/sodium acetate and acetic acid/sodium chloride / Costa C. N., Teixeira V. G., Delpech M. C., Souza J. V. S., Costa M. A. S. // Carbohydrate Polymers. – 2015. – V. 133, №. – P. 245-250. https://doi.org/10.1016/j.carbpol.2015.06.094

126. Synthesis of nanoscale zero-valent iron loaded chitosan for synergistically enhanced removal of U(VI) based on adsorption and reduction / Zhang Q., Zhao D., Feng S., Wang Y., Jin J., Alsaedi A., Hayat T., Chen C. // Journal of Colloid and Interface Science. – 2019. – V. 552, №. – P. 735-743. https://doi.org/10.1016/j.jcis.2019.05.109

127. Zhang W. Cross-linked chitosan microspheres: An efficient and eco-friendly adsorbent for iodide removal from waste water / Zhang W., Li Q., Mao Q., He G. // Carbohydrate Polymers. – 2019. – V. 209, №. – P. 215-222. https://doi.org/10.1016/j.carbpol.2019.01.032

128. Novel lignin–chitosan–PVA composite hydrogel for wound dressing / Zhang Y., Jiang M., Zhang Y., Cao Q., Wang X., Han Y., Sun G., Li Y., Zhou J. // Materials Science and Engineering: C. – 2019. – V. 104, №. – P. 110002. https://doi.org/10.1016/j.msec.2019.110002

129. A novel adsorbent of core-shell construction of chitosan-cellulose magnetic carbon foam: Synthesis, characterization and application to remove copper in wastewater / Zhang Z., Li H., Li J., Li X., Wang Z.,

Liu X., Zhang L. // Chemical Physics Letters. – 2019. – V. 731, №. – P. 136573. https://doi.org/10.1016/j.cplett.2019.07.001

130. Don T.-M. Preparation of Chitosan-graft-poly(vinyl acetate) Copolymers and Their Adsorption of Copper Ion / Don T.-M., King C.-F., Chiu W.-Y. // Polymer Journal. – 2002. – V. 34, № 6. – P. 418-425. https://doi.org/10.1295/polymj.34.418

131. Sebastian J. Microwave-assisted extraction of chitosan from Rhizopus oryzae NRRL 1526 biomass / Sebastian J., Rouissi T., Brar S. K., Hegde K., Verma M. // Carbohydrate Polymers. – 2019. – V. 219, №. – P. 431-440. https://doi.org/10.1016/j.carbpol.2019.05.047

132. Pochanavanich P. Fungal chitosan production and its characterization / Pochanavanich P., Suntornsuk W. // Letters in Applied Microbiology. – 2002. – V. 35, № 1. – P. 17-21. https://doi.org/10.1046/j.1472-765X.2002.01118.x

133. Streit F. Production of fungal chitosan in liquid cultivation using apple pomace as substrate / Streit F., Koch F., Laranjeira M. C. M., Ninow J. L. // Brazilian journal of microbiology : [publication of the Brazilian Society for Microbiology]. – 2009. – V. 40, № 1. – P. 20-25. https://doi.org/10.1590/S1517-83822009000100003

134. No H. K. Preparation and Characterization of Chitin and Chitosan—A Review / No H. K., Meyers S. P. // Journal of Aquatic Food Product Technology. – 1995. – V. 4, № 2. – P. 27-52. https://doi.org/10.1300/J030v04n02_03

135. Seafood waste: a source for preparation of commercially employable chitin/chitosan materials / Yadav M., Goswami P., Paritosh K., Kumar M., Pareek N., Vivekanand V. // Bioresources and Bioprocessing. – 2019. – V. 6, № 1. – P. 8. https://doi.org/10.1186/s40643-019-0243-y

136. Structural differences between chitin and chitosan extracted from three different marine sources / Hajji S., Younes I., Ghorbel-Bellaaj O., Hajji R., Rinaudo M., Nasri M., Jellouli K. // International Journal of Biological Macromolecules. – 2014. – V. 65, №. – P. 298-306. https://doi.org/10.1016/j.ijbiomac.2014.01.045

137. Ma J. Preparation, physicochemical and pharmaceutical characterization of chitosan from Catharsius molossus residue / Ma J., Xin C., Tan C. // International Journal of Biological Macromolecules. – 2015. – V. 80, №. – P. 547-556. https://doi.org/10.1016/j.ijbiomac.2015.07.027

138. Soon C. Y. Extraction and physicochemical characterization of chitin and chitosan from Zophobas morio larvae in varying sodium hydroxide concentration / Soon C. Y., Tee Y. B., Tan C. H., Rosnita A. T., Khalina A. // International Journal of Biological Macromolecules. – 2018. – V. 108, №. – P. 135-142. https://doi.org/10.1016/j.ijbiomac.2017.11.138

139. Birolli W. G. Ultrasound-assisted conversion of alpha-chitin into chitosan / Birolli W. G., Delezuk J. A. d. M., Campana-Filho S. P. // Applied Acoustics. – 2016. – V. 103, №. – P. 239-242. https://doi.org/10.1016/j.apacoust.2015.10.002

140. Badry M. D. Synthesis, characterization, and in vitro anticancer evaluation of iron oxide/chitosan nanocomposites / Badry M. D., Wahba M. A., Khaled R., Ali M. M., Farghali A. A. // Inorganic and Nano-Metal Chemistry. – 2017. – V. 47, № 3. – P. 405-411. https://doi.org/10.1080/15533174.2016.1186064

141. Chang M.-Y. Adsorption of tannic acid, humic acid, and dyes from water using the composite of chitosan and activated clay / Chang M.-Y., Juang R.-S. // Journal of Colloid and Interface Science. – 2004. – V. 278, № 1. – P. 18-25. https://doi.org/10.1016/j.jcis.2004.05.029

142. Liu Q. Simultaneous adsorption of aniline and Cu2+ from aqueous solution using activated carbon/chitosan composite / Liu Q., Yang B., Zhang L., Huang R. // Desalination and Water Treatment. – 2015. – V. 55, № 2. – P. 410-419. https://doi.org/10.1080/19443994.2014.923331

143. Wang J. Removal of various pollutants from water and wastewater by modified chitosan adsorbents / Wang J., Zhuang S. // Critical Reviews in Environmental Science and Technology. – 2017. – V. 47, № 23. – P. 2331-2386. https://doi.org/10.1080/10643389.2017.1421845

144. Barbosa P. F. P. Chemical Modifications of Cyclodextrin and Chitosan for Biological and Environmental Applications: Metals and Organic Pollutants Adsorption and Removal / Barbosa P. F. P., Cumba L. R., Andrade R. D. A., do Carmo D. R. // Journal of Polymers and the Environment. – 2019. – V. 27, № 6. – P. 1352-1366. https://doi.org/10.1007/s10924-019-01434-x

145. Sun S. Adsorption properties of crosslinked carboxymethyl-chitosan resin with Pb(II) as template ions / Sun S., Wang L., Wang A. // Journal of Hazardous Materials. – 2006. – V. 136, № 3. – P. 930-937. https://doi.org/10.1016/j.jhazmat.2006.01.033

146. Ladet S. Method for preparing a chitosan-based porous layer / Ladet S., Francois S., Claret J., Buffin M. // Book Method for preparing a chitosan-based porous layer. Editor Google Patents. - 2019.

147. Abraham S. Preparation, characterization and cross-linking of chitosan by microwave assisted synthesis / Abraham S., Rajamanickam D., Srinivasan B. // Sci. Int. – 2018. – V. 6, № 1. – P. 18-30.

148. Mojiri A. Cross-linked magnetic chitosan/activated biochar for removal of emerging micropollutants from water: Optimization by the artificial neural network / Mojiri A., Kazeroon R. A., Gholami A. // Water (Switzerland). – 2019. – V. 11, № 3. –. https://doi.org/10.3390/w11030551

149. Zhang B. Fabrication of chitosan/magnetite-graphene oxide composites as a novel bioadsorbent for adsorption and detoxification of Cr(VI) from aqueous solution / Zhang B., Hu R., Sun D., Wu T., Li Y. // Scientific Reports. – 2018. – V. 8, № 1. – P. 15397. https://doi.org/10.1038/s41598-018-33925-7

150. Chitosan Composites Synthesized Using Acetic Acid and Tetraethylorthosilicate Respond Differently to Methylene Blue Adsorption / Essel T. Y. A., Koomson A., Seniagya M.-P. O., Cobbold G. P., Kwofie

S. K., Asimeng B. O., Arthur P. K., Awandare G., Tiburu E. K. // Polymers. – 2018. – V. 10, № 5. – P. 466. https://doi.org/10.3390/polym10050466

151. Effect of beading parameters on cross-linked chitosan adsorptive properties / Vakili M., Mojiri A., Zwain H. M., Yuan J., Giwa A. S., Wang W., Gholami F., Guo X., Cagnetta G., Yu G. // Reactive and Functional Polymers. – 2019. – V. 144, №. – P. 104354. https://doi.org/10.1016/j.reactfunctpolym.2019.104354

152. Varma A. J. Metal complexation by chitosan and its derivatives: a review / Varma A. J., Deshpande S. V., Kennedy J. F. // Carbohydrate Polymers. – 2004. – V. 55, № 1. – P. 77-93. https://doi.org/10.1016/j.carbpol.2003.08.005

153. Vanamudan A. Adsorption property of Rhodamine 6G onto chitosan-g-(N-vinyl pyrrolidone)/montmorillonite composite / Vanamudan A., Bandwala K., Pamidimukkala P. // International Journal of Biological Macromolecules. – 2014. – V. 69, №. – P. 506-513. https://doi.org/10.1016/j.ijbiomac.2014.06.012

154. Preparation and characterization of chitosan/clay composite for direct Rose FRN dye removal from aqueous media: comparison of linear and non-linear regression methods / Kausar A., Naeem K., Hussain T., Nazli Z.-i.-H., Bhatti H. N., Jubeen F., Nazir A., Iqbal M. // Journal of Materials Research and Technology. – 2019. – V. 8, № 1. – P. 1161-1174. https://doi.org/10.1016/j.jmrt.2018.07.020

155. Yusoff S. M. Adsorption of malachite green onto modified chitosan– sulfuric acid beads: A preliminary study / Yusoff S. M., Ngah W. S. W., Mehamod F. S., Suah F. B. M. // Malaysian Journal of Analytical Sciences. – 2019. – V. 23, № 4. – P. 625-636. https://doi.org/10.17576/mjas-2019-2304-08

156. Aramesh N. Chitosan-based hybrid materials for adsorptive removal of dyes and underlying interaction mechanisms / Aramesh N., Bagheri A. R., Bilal M. // International Journal of Biological Macromolecules. – 2021. – V. 183, №. – P. 399-422. https://doi.org/10.1016/j.ijbiomac.2021.04.158

157. Chassary P. Metal anion sorption on chitosan and derivative materials: A strategy for polymer modification and optimum use / Chassary P., Vincent T., Guibal E. // Reactive and Functional Polymers. – 2004. – V. 60, № 1-3. – P. 137-149. https://doi.org/10.1016/j.reactfunctpolym.2004.02.018

158. Guaresti O. Synthesis of stimuli–responsive chitosan–based hydrogels by Diels–Alder cross–linking `click´ reaction as potential carriers for drug administration / Guaresti O., García-Astrain C., Aguirresarobe R. H., Eceiza A., Gabilondo N. // Carbohydrate Polymers. – 2018. – V. 183, №. – P. 278-286. https://doi.org/10.1016/j.carbpol.2017.12.034

159. Hamman J. H. Chitosan based polyelectrolyte complexes as potential carrier materials in drug delivery systems / Hamman J. H. // Marine drugs. – 2010. – V. 8, № 4. – P. 1305-1322. https://doi.org/10.3390/md8041305

160. Karimidost S. Thermodynamic and kinetic studies sorption of 5-fluorouracil onto single walled carbon nanotubes modified by chitosan / Karimidost S., Moniri E., Miralinaghi M. // Korean Journal of Chemical Engineering. – 2019. – V. 36, № 7. – P. 1115-1123. https://doi.org/10.1007/s11814-019-0292-0

161. Alves N. M. Chitosan derivatives obtained by chemical modifications for biomedical and environmental applications / Alves N. M., Mano J. F. // International Journal of Biological Macromolecules. – 2008. – V. 43, № 5. – P. 401-414. https://doi.org/10.1016/j.ijbiomac.2008.09.007

162. Szymańska E. Stability of chitosan-a challenge for pharmaceutical and biomedical applications / Szymańska E., Winnicka K. // Marine drugs. – 2015. – V. 13, № 4. – P. 1819-1846. https://doi.org/10.3390/md13041819

163. Gupta K. C. Glutaraldehyde and glyoxal cross-linked chitosan microspheres for controlled delivery of centchroman / Gupta K. C., Jabrail F. H. // Carbohydrate Research. – 2006. – V. 341, № 6. – P. 744-756. https://doi.org/10.1016/j.carres.2006.02.003

164. Synthesis, characterization, and antibacterial activity of cross-linked chitosan-glutaraldehyde / Li B., Shan C. L., Zhou Q., Fang Y., Wang Y. L., Xu F., Han L. R., Ibrahim M., Guo L. B., Xie G. L., Sun G. C. // Mar Drugs. – 2013. – V. 11, № 5. – P. 1534-52. https://doi.org/10.3390/md11051534

165. Slow delivery of a nitrification inhibitor (dicyandiamide) to soil using a biodegradable hydrogel of chitosan / Minet E. P., O'Carroll C., Rooney D., Breslin C., McCarthy C. P., Gallagher L., Richards K. G. // Chemosphere. – 2013. – V. 93, № 11. – P. 2854-2858. https://doi.org/10.1016/j.chemosphere.2013.08.043

166. Wang X. Selective removal of mercury ions using a chitosan–poly(vinyl alcohol) hydrogel adsorbent with three-dimensional network structure / Wang X., Deng W., Xie Y., Wang C. // Chemical Engineering Journal. – 2013. – V. 228, №. – P. 232-242. https://doi.org/10.1016/j.cej.2013.04.104

167. Modulation of stability and mucoadhesive properties of chitosan microspheres for therapeutic gastric application / Fernandes M., Gonçalves I. C., Nardecchia S., Amaral I. F., Barbosa M. A., Martins M. C. L. // International Journal of Pharmaceutics. – 2013. – V. 454, № 1. – P. 116-124. https://doi.org/10.1016/j.ijpharm.2013.06.068

168. Li N. Copper adsorption on chitosan-cellulose hydrogel beads: Behaviors and mechanisms / Li N., Bai R. // Separation and Purification Technology. – 2005. – V. 42, № 3. – P. 237-247. https://doi.org/10.1016/j.seppur.2004.08.002

169. Moura M. J. Rheological Study of Genipin Cross-Linked Chitosan Hydrogels / Moura M. J., Figueiredo M. M., Gil M. H. // Biomacromolecules. – 2007. – V. 8, № 12. – P. 3823-3829. https://doi.org/10.1021/bm700762w

170. Xue J. Q. Preparation and Characterization of Formaldehyde Crosslinked Chitosan / Xue J. Q., Li J. X., Wu M., Wang W., Ma D. N. // Advanced Materials Research. – 2011. – V. 239-242, №. – P. 279-282. https://doi.org/10.4028/www.scientific.net/AMR.239-242.279

171. Monier M. Adsorption of Hg^{2+}, Cu^{2+} and Zn^{2+} ions from aqueous solution using formaldehyde cross-linked modified chitosan–thioglyceraldehyde Schiff's base / Monier M. // International Journal of Biological Macromolecules. – 2012. – V. 50, № 3. – P. 773-781. https://doi.org/10.1016/j.ijbiomac.2011.11.026

172. Development of drug-loaded chitosan-vanillin nanoparticles and its cytotoxicity against HT-29 cells / Li P. W., Wang G., Yang Z. M., Duan W., Peng Z., Kong L. X., Wang Q. H. // Drug Deliv. – 2016. – V. 23, № 1. – P. 30-5. https://doi.org/10.3109/10717544.2014.900590

173. Zhang L. Synthesis of titanium cross-linked chitosan composite for efficient adsorption and detoxification of hexavalent chromium from water / Zhang L., Xia W., Liu X., Zhang W. // Journal of Materials Chemistry A. – 2015. – V. 3, № 1. – P. 331-340. https://doi.org/10.1039/C4TA05194G

174. Highly efficient detoxification of Cr(VI) by chitosan-Fe(III) complex: process and mechanism studies / Shen C., Chen H., Wu S., Wen Y., Li L., Jiang Z., Li M., Liu W. // J Hazard Mater. – 2013. – V. 244-245, №. – P. 689-97. https://doi.org/10.1016/j.jhazmat.2012.10.061

175. Budnyak T. M. Synthesis and adsorption properties of chitosan-silica nanocomposite prepared by sol-gel method / Budnyak T. M., Pylypchuk I. V., Tertykh V. A., Yanovska E. S., Kolodynska D. // Nanoscale Research Letters. – 2015. – V. 10, № 1. – P. 87. https://doi.org/10.1186/s11671-014-0722-1

176. Mallakpour S. Linear and nonlinear behavior of crosslinked chitosan/N-doped graphene quantum dot nanocomposite films in cadmium cation uptake / Mallakpour S., Khadem E. // Sci Total Environ. – 2019. – V. 690, №. – P. 1245-1253. https://doi.org/10.1016/j.scitotenv.2019.06.431

177. Deepika R. Studies on the behaviour of reactive dyes onto the cross-linked chitosan using adsorption isotherms / Deepika R., Venkateshprabhu M., Pandimdevi M. // International Journal of Environmental Sciences. – 2013. – V. 4, № 3. – P. 323.

178. Mahaninia M. H. A Kinetic Uptake Study of Roxarsone Using Cross-Linked Chitosan Beads / Mahaninia M. H., Wilson L. D. // Industrial & Engineering Chemistry Research. – 2017. – V. 56, № 7. – P. 1704-1712. https://doi.org/10.1021/acs.iecr.6b04412

179. Omidi S. Eco-friendly synthesis of graphene–chitosan composite hydrogel as efficient adsorbent for Congo red / Omidi S., Kakanejadifard A. // RSC Advances. – 2018. – V. 8, № 22. – P. 12179-12189. https://doi.org/10.1039/C8RA00510A

180. Magnetic Fe_3O_4@ chitosan carbon microbeads: removal of doxycycline from aqueous solutions through a fixed bed via sequential adsorption and heterogeneous Fenton-like regeneration / Bai B., Xu X., Li C., Xing J., Wang H., Suo Y. // Journal of Nanomaterials. – 2018. – V. 2018, №. –.

181. Chitosan Grafted Adsorbents for Diclofenac Pharmaceutical Compound Removal from Single-Component Aqueous Solutions and Mixtures / Tzereme A., Christodoulou E., Kyzas G. Z., Kostoglou M., Bikiaris D. N., Lambropoulou D. A. // Polymers. – 2019. – V. 11, № 3. – P. 497. https://doi.org/10.3390/polym11030497

182. Guo T. Y. Adsorptive separation of hemoglobin by molecularly imprinted chitosan beads / Guo T. Y., Xia Y. Q., Hao G. J., Song M. D., Zhang B. H. // Biomaterials. – 2004. – V. 25, № 27. – P. 5905-5912. https://doi.org/10.1016/j.biomaterials.2004.01.032

183. Liu T. Enhanced chitosan/Fe^0-nanoparticles beads for hexavalent chromium removal from wastewater / Liu T., Wang Z.-L., Zhao L., Yang X. // Chemical Engineering Journal. – 2012. – V. 189-190, №. – P. 196-202. https://doi.org/10.1016/j.cej.2012.02.056

184. Wan Ngah W. S. Removal of copper(II) ions from aqueous solution onto chitosan and cross-linked chitosan beads / Wan Ngah W. S., Endud C. S., Mayanar R. // Reactive and Functional Polymers. – 2002. – V. 50, № 2. – P. 181-190. https://doi.org/10.1016/S1381-5148(01)00113-4

185. Nishad P. A. Enhancing the antimony sorption properties of nano titania-chitosan beads using epichlorohydrin as the crosslinker / Nishad P. A., Bhaskarapillai A., Velmurugan S. // Journal of Hazardous Materials. – 2017. – V. 334, №. – P. 160-167. https://doi.org/10.1016/j.jhazmat.2017.04.009

186. Yu Z. Magnetic Chitosan–Iron(III) Hydrogel as a Fast and Reusable Adsorbent for Chromium(VI) Removal / Yu Z., Zhang X., Huang Y. // Industrial & Engineering Chemistry Research. – 2013. – V. 52, № 34. – P. 11956-11966. https://doi.org/10.1021/ie400781n

187. Liu C. Sodium tripolyphosphate (TPP) crosslinked chitosan membranes and application in humic acid removal / Liu C., Bai R., Nan L. // American Institute of Chemical Engineers, Proceedings of the annual meeting –, 2004. –.

188. Amouzgar P. A short review on presence of pharmaceuticals in water bodies and the potential of chitosan and chitosan derivatives for elimination of pharmaceuticals / Amouzgar P., Salamatinia B. // J. Mol. Genet. Med. – 2015. – V. 4, № 001. –.

189. Adsorption of Cr(VI) on crosslinked chitosan–Fe(III) complex in fixed-bed systems / Demarchi C. A., Debrassi A., Magro J. D., Nedelko N., Ślawska-Waniewska A., Dłużewski P., Greneche J.-M., Rodrigues C. A. // Journal of Water Process Engineering. – 2015. – V. 7, №. – P. 141-152. https://doi.org/10.1016/j.jwpe.2015.05.003

190. Liu T. Entrapment of nanoscale zero-valent iron in chitosan beads for hexavalent chromium removal from wastewater / Liu T., Zhao L., Sun D., Tan X. // Journal of Hazardous Materials. – 2010. – V. 184, № 1. – P. 724-730. https://doi.org/10.1016/j.jhazmat.2010.08.099

191. Chiou M.-S. Adsorption of anionic dyes in acid solutions using chemically cross-linked chitosan beads / Chiou M.-S., Ho P.-Y., Li H.-Y. // Dyes and Pigments. – 2004. – V. 60, № 1. – P. 69-84. https://doi.org/10.1016/S0143-7208(03)00140-2

192. Yang Z. Studies on the synthesis and properties of hydroxyl azacrown ether-grafted chitosan / Yang Z., Yuan Y. // Journal of Applied Polymer Science. – 2001. – V. 82, № 8. – P. 1838-1843. https://doi.org/10.1002/app.2026

193. Jung B.-O. Preparation of amphiphilic chitosan and their antimicrobial activities / Jung B.-O., Kim C.-H., Choi K.-S., Lee Y. M., Kim J.-J. // Journal of Applied Polymer Science. – 1999. – V. 72, № 13. – P. 1713-1719. https://doi.org/10.1002/(SICI)1097-4628(19990624)72:13<1713::AID-APP7>3.0.CO;2-T

194. Liu Z. Graft copolymerization of methyl acrylate onto chitosan initiated by potassium diperiodatoargentate (III) / Liu Z., Wu G., Liu Y. // Journal of Applied Polymer Science. – 2006. – V. 101, № 1. – P. 799-804. https://doi.org/10.1002/app.23834

195. Sun T. Graft copolymerization of methacrylic acid onto carboxymethyl chitosan / Sun T., Xu P., Liu Q., Xue J., Xie W. // European Polymer Journal. – 2003. – V. 39, № 1. – P. 189-192. https://doi.org/10.1016/S0014-3057(02)00174-X

196. Recent progress in the structural modification of chitosan for applications in diversified biomedical fields / Mittal H., Ray S. S., Kaith B. S., Bhatia J. K., Sukriti Sharma J., Alhassan S. M. // European Polymer Journal. – 2018. – V. 109, №. – P. 402-434. https://doi.org/10.1016/j.eurpolymj.2018.10.013

197. Sokker H. H. Adsorption of crude oil from aqueous solution by hydrogel of chitosan based polyacrylamide prepared by radiation induced graft polymerization / Sokker H. H., El-Sawy N. M., Hassan M. A., El-Anadouli B. E. // Journal of Hazardous Materials. – 2011. – V. 190, № 1. – P. 359-365. https://doi.org/10.1016/j.jhazmat.2011.03.055

198. Jenkins D. W. Review of Vinyl Graft Copolymerization Featuring Recent Advances toward Controlled Radical-Based Reactions and Illustrated with Chitin/Chitosan Trunk Polymers / Jenkins D. W., Hudson S. M. // Chemical Reviews. – 2001. – V. 101, № 11. – P. 3245-3274. https://doi.org/10.1021/cr000257f

199. Manoj P. Graft Copolymerization of Methyl Acrylate on Chitosan, Initiated by Ceric Ammonium Nitrate as the Initiator / Manoj P., Nayak P. // Characterization and Antimicrobial Activity. – 2012. – V. 3, № 3. – P. 1646-1654.

200. Liu D. Preparation of Chitosan Poly(methacrylate) Composites for Adsorption of Bromocresol Green / Liu D., Yuan J., Li J., Zhang G. // ACS Omega. – 2019. – V. 4, № 7. – P. 12680-12686. https://doi.org/10.1021/acsomega.9b01576

201. Kim S. Y. Thermo- and pH-responsive behaviors of graft copolymer and blend based on chitosan and N-isopropylacrylamide / Kim S. Y., Cho S. M., Lee Y. M., Kim S. J. // Journal of Applied Polymer Science.

– 2000. – V. 78, № 7. – P. 1381-1391. https://doi.org/10.1002/1097-4628(20001114)78:7<1381::AID-APP90>3.0.CO;2-M

202. El-Tahlawy K. F. Preparation and application of chitosan/poly(methacrylic acid) graft copolymer / El-Tahlawy K. F., El-Rafie S. M., Aly A. S. // Carbohydrate Polymers. – 2006. – V. 66, № 2. – P. 176-183. https://doi.org/10.1016/j.carbpol.2006.03.001

203. The mechanism of chitosan degradation by gamma and e-beam irradiation / Gryczka U., Dondi D., Chmielewski A. G., Migdal W., Buttafava A., Faucitano A. // Radiation Physics and Chemistry. – 2009. – V. 78, № 7. – P. 543-548. https://doi.org/10.1016/j.radphyschem.2009.03.081

204. Desai K. G. Study of gamma-irradiation effects on chitosan microparticles / Desai K. G., Hyun J. P. // Drug Delivery: Journal of Delivery and Targeting of Therapeutic Agents. – 2006. – V. 13, № 1. – P. 39-50. https://doi.org/10.1080/10717540500309123

205. Krajewska B. Membrane-based processes performed with use of chitin/chitosan materials / Krajewska B. // Separation and Purification Technology. – 2005. – V. 41, № 3. – P. 305-312. https://doi.org/10.1016/j.seppur.2004.03.019

206. Environmentally friendly chitosan/PEI-grafted magnetic gelatin for the highly effective removal of heavy metals from drinking water / Li B., Zhou F., Huang K., Wang Y., Mei S., Zhou Y., Jing T. // Scientific Reports. – 2017. – V. 7, № 1. – P. 43082. https://doi.org/10.1038/srep43082

207. Removal of toxic heavy metal lead (II) using chitosan oligosaccharide-graft-maleic anhydride/polyvinyl alcohol/silk fibroin composite / P A., K V., M S., T G., K R., P N. S., Sukumaran A. // Int J Biol Macromol. – 2017. – V. 104, № Pt B. – P. 1469-1482. https://doi.org/10.1016/j.ijbiomac.2017.05.111

208. Kenawy I. M. M. Melamine grafted chitosan-montmorillonite nanocomposite for ferric ions adsorption: Central composite design optimization study / Kenawy I. M. M., Eldefrawy M. M., Eltabey R. M., Zaki E. G. // Journal of Cleaner Production. – 2019. – V. 241, №. – P. 118189. https://doi.org/10.1016/j.jclepro.2019.118189

209. Islam M. N. Preparation of bio-inspired trimethoxysilyl group terminated poly (1-vinylimidazole)-modified-chitosan composite for adsorption of chromium (VI) ions / Islam M. N., Khan M. N., Mallik A. K., Rahman M. M. // Journal of hazardous materials. – 2019. – V. 379, №. – P. 120792.

210. Takafuji M. Preparation of Poly(1-vinylimidazole)-Grafted Magnetic Nanoparticles and Their Application for Removal of Metal Ions / Takafuji M., Ide S., Ihara H., Xu Z. // Chemistry of Materials. – 2004. – V. 16, № 10. – P. 1977-1983. https://doi.org/10.1021/cm030334y

211. Maleki A. Ethyl acrylate grafted chitosan for heavy metal removal from wastewater: Equilibrium, kinetic and thermodynamic studies / Maleki A., Pajootan E., Hayati B. // Journal of the Taiwan Institute of Chemical Engineers. – 2015. – V. 51, №. – P. 127-134. https://doi.org/10.1016/j.jtice.2015.01.004

212. Tsai B. Poly(Poly(Ethylene Glycol) Methyl Ether Methacrylate) Grafted Chitosan for Dye Removal from Water / Tsai B., Garcia-Valdez O., Champagne P., Cunningham M. F. // Processes. – 2017. – V. 5, № 1. –. https://doi.org/10.3390/pr5010012

213. Singh V. Poly (methylmethacrylate) grafted chitosan: An efficient adsorbent for anionic azo dyes / Singh V., Sharma A. K., Tripathi D., Sanghi R. // Journal of hazardous materials. – 2009. – V. 161, № 2-3. – P. 955-966.

214. Adsorptive removal of acidic dye onto grafted chitosan: A plausible grafting and adsorption mechanism / Tahira I., Aslam Z., Abbas A., Monim-ul-Mehboob M., Ali S., Asghar A. // International Journal of Biological Macromolecules. – 2019. – V. 136, №. – P. 1209-1218. https://doi.org/10.1016/j.ijbiomac.2019.06.173

215. Alshammari M. S. Ultrasonic-Assisted Synthesis and Characterization of Chitosan-Graft-Substituted Polyanilines: Promise Bio-Based Nanoparticles for Dye Removal and Bacterial Disinfection / Alshammari M. S., Essawy A. A., El-Nggar A. M., Sayyah S. M. // Journal of Chemistry. – 2020. – V. 2020, №. –. https://doi.org/10.1155/2020/3297184

216. Shu D. Prominent adsorption performance of amino-functionalized ultra-light graphene aerogel for methyl orange and amaranth / Shu D., Feng F., Han H., Ma Z. // Chemical Engineering Journal. – 2017. – V. 324, №. – P. 1-9. https://doi.org/10.1016/j.cej.2017.04.136

217. Microwave-Assisted Synthesis of Polyethyleneimine Grafted Chitosan Beads for the Adsorption of Acid Red 27 / Yusof N. H., Foo K. Y., Wilson L. D., Hameed B. H., Hussin M. H., Sabar S. // Journal of Polymers and the Environment. – 2020. – V. 28, № 2. – P. 542-552. https://doi.org/10.1007/s10924-019-01628-3

218. Labidi A. Functional Chitosan Derivative and Chitin as Decolorization Materials for Methylene Blue and Methyl Orange from Aqueous Solution / Labidi A., Salaberria A. M., Fernandes S. C. M., Labidi J., Abderrabba M. // Materials (Basel). – 2019. – V. 12, № 3. –. https://doi.org/10.3390/ma12030361

219. Thermal characterization of a series of lignin-based polypropylene blends / Blanco I., Cicala G., Latteri A., Saccullo G., El-Sabbagh A. M. M., Ziegmann G. // Journal of Thermal Analysis and Calorimetry. – 2017. – V. 127, № 1. – P. 147-153. https://doi.org/10.1007/s10973-016-5596-2

220. Blanco I. Thermal behaviour of a series of novel aliphatic bridged polyhedral oligomeric silsesquioxanes (POSSs)/polystyrene (PS) nanocomposites: The influence of the bridge length on the resistance to thermal degradation / Blanco I., Abate L., Bottino F. A., Bottino P. // Polymer Degradation and Stability. – 2014. – V. 102, №. – P. 132-137. https://doi.org/10.1016/j.polymdegradstab.2014.01.029

221. Functionalized halloysite nanotubes for enhanced removal of lead(II) ions from aqueous solutions / Cataldo S., Lazzara G., Massaro M., Muratore N., Pettignano A., Riela S. // Applied Clay Science. – 2018. – V. 156, №. – P. 87-95. https://doi.org/10.1016/j.clay.2018.01.028

222. Abd El-Magied M. O. Removal of nickel (II) ions from aqueous solutions using modified activated carbon: A kinetic and equilibrium study / Abd El-Magied M. O., Hassan A. M. A., Gad H. M. H., Mohammaden T. F., Youssef M. A. M. // Journal of Dispersion Science and Technology. – 2018. – V. 39, № 6. – P. 862-873. https://doi.org/10.1080/01932691.2017.1402337

223. Marczenko Z. Separation, preconcentration and spectrophotometry in inorganic analysis. / Marczenko Z., Balcerzak M.: Elsevier, 2000.

224. Halloysite nanotubes sponges with skeletons made of electrospun nanofibers as innovative dye adsorbent and catalyst support / Xu T., Zheng F., Chen Z., Ding Y., Liang Z., Liu Y., Zhu Z., Fong H. // Chemical Engineering Journal. – 2019. – V. 360, №. – P. 280-288. https://doi.org/10.1016/j.cej.2018.11.233

225. Elwakeel K. Z. Fast removal of uranium from aqueous solutions using tetraethylenepentamine modified magnetic chitosan resin / Elwakeel K. Z., Atia A. A., Guibal E. // Bioresource Technology. – 2014. – V. 160, №. – P. 107-114. https://doi.org/10.1016/j.biortech.2014.01.037

226. Elwakeel K. Z. Removal of Cr(VI) from alkaline aqueous solutions using chemically modified magnetic chitosan resins / Elwakeel K. Z. // Desalination. – 2010. – V. 250, № 1. – P. 105-112. https://doi.org/10.1016/j.desal.2009.02.063

227. Lopez-Ramon M. V. On the characterization of acidic and basic surface sites on carbons by various techniques / Lopez-Ramon M. V., Stoeckli F., Moreno-Castilla C., Carrasco-Marin F. // Carbon. – 1999. – V. 37, № 8. – P. 1215-1221. https://doi.org/10.1016/S0008-6223(98)00317-0

228. Characterization of organo-montmorillonites and comparison for Sr(II) removal: Equilibrium and kinetic studies / Wu P., Dai Y., Long H., Zhu N., Li P., Wu J., Dang Z. // Chemical Engineering Journal. – 2012. – V. 191, №. – P. 288-296. https://doi.org/10.1016/j.cej.2012.03.017

229. Socrates G. Infrared and Raman characteristic group frequencies: tables and charts. / Socrates G.: John Wiley & Sons, 2004.

230. Effect of addition of silica- and amine functionalized silica-nanoparticles on the microstructure of calcium silicate hydrate (C–S–H) gel / Monasterio M., Gaitero J. J., Erkizia E., Guerrero Bustos A. M., Miccio L. A., Dolado J. S., Cerveny S. // Journal of Colloid and Interface Science. – 2015. – V. 450, №. – P. 109-118. https://doi.org/10.1016/j.jcis.2015.02.066

231. Preparation and characterization of 3-aminopropyltriethoxysilane grafted montmorillonite and acid-activated montmorillonite / Shen W., He H., Zhu J., Yuan P., Ma Y., Liang X. // Chinese Science Bulletin. – 2009. – V. 54, № 2. – P. 265-271. https://doi.org/10.1007/s11434-008-0361-y

232. Xue A. Effective NH_2-grafting on attapulgite surfaces for adsorption of reactive dyes / Xue A., Zhou S., Zhao Y., Lu X., Han P. // J Hazard Mater. – 2011. – V. 194, №. – P. 7-14. https://doi.org/10.1016/j.jhazmat.2011.06.018

233. Application of functionalized nano HMS type mesoporous silica with N-(2-aminoethyl)-3-aminopropyl methyldimethoxysilane as a suitable adsorbent for removal of Pb (II) from aqueous media and industrial wastewater / Javadian H., Koutenaei B. B., Shekarian E., Sorkhrodi F. Z., Khatti R., Toosi M. // Journal of Saudi Chemical Society. – 2017. – V. 21, №. – P. S219-S230. https://doi.org/10.1016/j.jscs.2014.01.007

234. Preparation of multi-amine-grafted mesoporous silicas and their application to heavy metal ions adsorption / Zhang L., Yu C., Zhao W., Hua Z., Chen H., Li L., Shi J. // Journal of Non-Crystalline Solids. – 2007. – V. 353, № 44. – P. 4055-4061. https://doi.org/10.1016/j.jnoncrysol.2007.06.018

235. Jazi M. B. Kinetic and thermodynamic investigations of Pb(II) and Cd(II) adsorption on nanoscale organo-functionalized SiO_2-Al_2O_3 / Jazi M. B., Arshadi M., Amiri M. J., Gil A. // J Colloid Interface Sci. – 2014. – V. 422, №. – P. 16-24. https://doi.org/10.1016/j.jcis.2014.01.032

236. Adsorption of lead (II) on SBA-15 mesoporous molecular sieve functionalized with $–NH_2$ groups / Hernández-Morales V., Nava R., Acosta-Silva Y. J., Macías-Sánchez S. A., Pérez-Bueno J. J., Pawelec B. // Microporous and Mesoporous Materials. – 2012. – V. 160, №. – P. 133-142. https://doi.org/10.1016/j.micromeso.2012.05.004

237. Lin-Vien D. The handbook of infrared and Raman characteristic frequencies of organic molecules. / Lin-Vien D., Colthup N. B., Fateley W. G., Grasselli J. G.: Elsevier, 1991.

238. Vickers T. J. B. K. W. Book Review: Handbook of Near-Infrared Analysis. 2nd Edition, Infrared and Raman Characteristic Group Frequencies: Table and Charts. 3rd Edition, Fourier Transforms in Spectroscopy / Vickers T. J. B. K. W., Wang H., Small G. W. // Applied Spectroscopy. / UK S. P. S. – London, England, - 2002. -V. 56, № 2. – P. 52A-53A.

239. Larkin P. Infrared and Raman spectroscopy: principles and spectral interpretation. / Larkin P.: Elsevier, 2017.

240. Fu H. Synthesis of vegetable oil-based waterborne polyurethane/silver-halloysite antibacterial nanocomposites / Fu H., Wang Y., Li X., Chen W. // Composites Science and Technology. – 2016. – V. 126, №. – P. 86-93. https://doi.org/10.1016/j.compscitech.2016.02.018

241. Wang Z. Preparation and antifouling property of polyethersulfone ultrafiltration hybrid membrane containing halloysite nanotubes grafted with MPC via RATRP method / Wang Z., Wang H., Liu J., Zhang Y. // Desalination. – 2014. – V. 344, №. – P. 313-320. https://doi.org/10.1016/j.desal.2014.03.040

242. Andrini L. Halloysite nanotube and its firing products: Structural characterization of halloysite, metahalloysite, spinel type silicoaluminate and mullite / Andrini L., Toja R. M., Conconi M. S., Requejo F. G., Rendtorff N. // Journal of Electron Spectroscopy and Related Phenomena. – 2019. – V. 234, №. – P. 19-26.

243. Liu M. Recent advance in research on halloysite nanotubes-polymer nanocomposite / Liu M., Jia Z., Jia D., Zhou C. // Progress in Polymer Science. – 2014. – V. 39, № 8. – P. 1498-1525. https://doi.org/10.1016/j.progpolymsci.2014.04.004

244. Saif M. J. Pristine and γ-irradiated halloysite reinforced epoxy nanocomposites – Insight study / Saif M. J., Naveed M., Zia K. M., Asif M. // Radiation Physics and Chemistry. – 2016. – V. 127, №. – P. 115-121. https://doi.org/10.1016/j.radphyschem.2016.06.015

245. Surface chemistry of halloysite nanotubes controls the curability of low filled epoxy nanocomposites / Akbari V., Najafi F., Vahabi H., Jouyandeh M., Badawi M., Morisset S., Ganjali M. R., Saeb M. R. // Progress in Organic Coatings. – 2019. – V. 135, №. – P. 555-564. https://doi.org/10.1016/j.porgcoat.2019.06.009

246. Lisuzzo L. Why does vacuum drive to the loading of halloysite nanotubes? The key role of water confinement / Lisuzzo L., Cavallaro G., Pasbakhsh P., Milioto S., Lazzara G. // Journal of Colloid and Interface Science. – 2019. – V. 547, №. – P. 361-369. https://doi.org/10.1016/j.jcis.2019.04.012

247. Sharma K. K. Toward Efficient Nanoporous Catalysts: Controlling Site-Isolation and Concentration of Grafted Catalytic Sites on Nanoporous Materials with Solvents and Colorimetric Elucidation of Their Site-Isolation / Sharma K. K., Anan A., Buckley R. P., Ouellette W., Asefa T. // Journal of the American Chemical Society. – 2008. – V. 130, № 1. – P. 218-228. https://doi.org/10.1021/ja074128t

248. Bentley T. W. Solvent Polarity and Organic Reactivity in Mixed Solvents: Evidence Using a Reactive Molecular Probe To Assess the Role of Preferential Solvation in Aqueous Alcohols / Bentley T. W., Ebdon D. N., Kim E.-J., Koo I. S. // The Journal of Organic Chemistry. – 2005. – V. 70, № 5. – P. 1647-1653. https://doi.org/10.1021/jo048163j

249. Hildebrand and Hansen solubility parameters from molecular dynamics with applications to electronic nose polymer sensors / Belmares M., Blanco M., Goddard W. A. 3rd, Ross R. B., Caldwell G., Chou S. H., Pham J., Olofson P. M., Thomas C. // J Comput Chem. – 2004. – V. 25, № 15. – P. 1814-26. https://doi.org/10.1002/jcc.20098

250. Copper acetylacetonate anchored onto amine-functionalised clays / Pereira C., Patrício S., Silva A. R., Magalhães A. L., Carvalho A. P., Pires J., Freire C. // Journal of Colloid and Interface Science. – 2007. – V. 316, № 2. – P. 570-579. https://doi.org/10.1016/j.jcis.2007.07.053

251. Adsorption of lead (II) on SBA-15 mesoporous molecular sieve functionalized with–NH_2 groups / Hernández-Morales V., Nava R., Acosta-Silva Y., Macías-Sánchez S., Pérez-Bueno J., Pawelec B. // Microporous and Mesoporous Materials. – 2012. – V. 160, №. – P. 133-142.

252. Carli L. N. The effects of silane coupling agents on the properties of PHBV/halloysite nanocomposites / Carli L. N., Daitx T. S., Soares G. V., Crespo J. S., Mauler R. S. // Applied Clay Science. – 2014. – V. 87, №. – P. 311-319. https://doi.org/10.1016/j.clay.2013.11.032

253. Functionalization of Halloysite by 3-Aminopropyltriethoxysilane in Various Solvents / Osipova V. A., Pestov A. V., Mekhaev A. V., Abuelsoad A. M. A., Tambasova D. P., Antonov D. O., Kovaleva E. G. // Petroleum Chemistry. – 2020. – V. 60, № 5. – P. 597-600. https://doi.org/10.1134/S0965544120050072
254. Functionalization of Halloysite Clay Nanotubes by Grafting with γ-Aminopropyltriethoxysilane / Yuan P., Southon P. D., Liu Z., Green M. E. R., Hook J. M., Antill S. J., Kepert C. J. // The Journal of Physical Chemistry C. – 2008. – V. 112, № 40. – P. 15742-15751. https://doi.org/10.1021/jp805657t
255. Duce C. Thermal behavior study of pristine and modified halloysite nanotubes / Duce C., Vecchio Ciprioti S., Ghezzi L., Ierardi V., Tinè M. R. // Journal of Thermal Analysis and Calorimetry. – 2015. – V. 121, № 3. – P. 1011-1019. https://doi.org/10.1007/s10973-015-4741-7
256. Hashemifard S. A. Mixed matrix membrane incorporated with large pore size halloysite nanotubes (HNT) as filler for gas separation: Experimental / Hashemifard S. A., Ismail A. F., Matsuura T. // Journal of Colloid and Interface Science. – 2011. – V. 359, № 2. – P. 359-370. https://doi.org/10.1016/j.jcis.2011.03.077
257. Insights into grafting of (3-Mercaptopropyl) trimethoxy silane on halloysite nanotubes surface / Abu El-Soad A. M., Pestov A. V., Tambasova D. P., Osipova V. A., Martemyanov N. A., Cavallaro G., Kovaleva E. G., Lazzara G. // Journal of Organometallic Chemistry. – 2020. – V. 915, №. – P. 121224. https://doi.org/10.1016/j.jorganchem.2020.121224
258. Grafting of (3-Chloropropyl)-Trimethoxy Silane on Halloysite Nanotubes Surface / Abu El-Soad A. M., Lazzara G., Pestov A. V., Tambasova D. P., Antonov D. O., Cavallaro G., Kovaleva E. G. // Applied Sciences. – 2021. – V. 11, № 12. – P. 5534-5541. https://doi.org/10.3390/app11125534
259. Panda A. K. Effect of sulphuric acid treatment on the physico-chemical characteristics of kaolin clay / Panda A. K., Mishra B. G., Mishra D. K., Singh R. K. // Colloids and Surfaces A: Physicochemical and Engineering Aspects. – 2010. – V. 363, № 1. – P. 98-104. https://doi.org/10.1016/j.colsurfa.2010.04.022
260. Sangwichien C. Density functional theory predictions of adsorption isotherms with hysteresis loops / Sangwichien C., Aranovich G. L., Donohue M. D. // Colloids and Surfaces A: Physicochemical and Engineering Aspects. – 2002. – V. 206, № 1. – P. 313-320. https://doi.org/10.1016/S0927-7757(02)00048-1
261. Zhou Y.-T. Removal of Cu^{2+} from aqueous solution by chitosan-coated magnetic nanoparticles modified with α-ketoglutaric acid / Zhou Y.-T., Nie H.-L., Branford-White C., He Z.-Y., Zhu L.-M. // Journal of Colloid and Interface Science. – 2009. – V. 330, № 1. – P. 29-37. https://doi.org/10.1016/j.jcis.2008.10.026
262. Lagergren S. K. About the theory of so-called adsorption of soluble substances / Lagergren S. K. // Sven. Vetenskapsakad. Handingarl. – 1898. – V. 24, №. – P. 1-39.

263. Ho Y. S. Pseudo-second order model for sorption processes / Ho Y. S., McKay G. // Process Biochemistry. – 1999. – V. 34, № 5. – P. 451-465. https://doi.org/10.1016/S0032-9592(98)00112-5
264. Weber Walter J. Kinetics of Adsorption on Carbon from Solution / Weber Walter J., Morris J. C. // Journal of the Sanitary Engineering Division. – 1963. – V. 89, № 2. – P. 31-59. https://doi.org/10.1061/JSEDAI.0000430
265. Akkaya R. Adsorption isotherms, kinetics, thermodynamics and desorption studies for uranium and thorium ions from aqueous solution by novel microporous composite P(HEMA-EP) / Akkaya R., Akkaya B. // Journal of Nuclear Materials. – 2013. – V. 434, № 1. – P. 328-333. https://doi.org/10.1016/j.jnucmat.2012.11.056
266. Laus R. Adsorption and desorption of Cu(II), Cd(II) and Pb(II) ions using chitosan crosslinked with epichlorohydrin-triphosphate as the adsorbent / Laus R., Costa T. G., Szpoganicz B., Fávere V. T. // Journal of Hazardous Materials. – 2010. – V. 183, № 1. – P. 233-241. https://doi.org/10.1016/j.jhazmat.2010.07.016
267. Foo K. Y. Insights into the modeling of adsorption isotherm systems / Foo K. Y., Hameed B. H. // Chemical Engineering Journal. – 2010. – V. 156, № 1. – P. 2-10. https://doi.org/10.1016/j.cej.2009.09.013
268. Langmuir I. The adsorption of gases on plane surfaces of glass, mica and platinum / Langmuir I. // Journal of the American Chemical Society. – 1918. – V. 40, № 9. – P. 1361-1403. https://doi.org/10.1021/ja02242a004
269. Freundlich H. Über die Adsorption in Lösungen / Freundlich H. // Zeitschrift für Physikalische Chemie. – 1907. – V. 57U, № 1. – P. 385-470. https://doi.org/10.1515/zpch-1907-5723
270. Dubinin M. M. Sorption and structure of active carbons. I. Adsorption of organic vapors / Dubinin M. M., Zaverina E., Radushkevich L. // Zhurnal Fizicheskoi Khimii. – 1947. – V. 21, № 3. – P. 151-162.
271. Adsorption of chromium (VI) by ethylenediamine-modified cross-linked magnetic chitosan resin: Isotherms, kinetics and thermodynamics / Hu X.-j., Wang J.-s., Liu Y.-g., Li X., Zeng G.-m., Bao Z.-l., Zeng X.-x., Chen A.-w., Long F. // Journal of Hazardous Materials. – 2011. – V. 185, № 1. – P. 306-314. https://doi.org/10.1016/j.jhazmat.2010.09.034
272. Wang Y. Continuous fixed bed adsorption of Cu(II) by halloysite nanotube-alginate hybrid beads: an experimental and modelling study / Wang Y., Zhang X., Wang Q., Zhang B., Liu J. // Water Sci Technol. – 2014. – V. 70, № 2. – P. 192-9. https://doi.org/10.2166/wst.2014.148
273. Chitosan/halloysite beads fabricated by ultrasonic-assisted extrusion-dripping and a case study application for copper ion removal / Choo C. K., Kong X. Y., Goh T. L., Ngoh G. C., Horri B. A., Salamatinia B. // Carbohydrate Polymers. – 2016. – V. 138, №. – P. 16-26. https://doi.org/10.1016/j.carbpol.2015.11.060

274. Turan N. G. Adsorption of copper and zinc ions on illite: Determination of the optimal conditions by the statistical design of experiments / Turan N. G., Elevli S., Mesci B. // Applied Clay Science. – 2011. – V. 52, № 4. – P. 392-399. https://doi.org/10.1016/j.clay.2011.04.010

275. Falayi T. Removal of heavy metals and neutralisation of acid mine drainage with un-activated attapulgite / Falayi T., Ntuli F. // Journal of Industrial and Engineering Chemistry. – 2014. – V. 20, № 4. – P. 1285-1292. https://doi.org/10.1016/j.jiec.2013.07.007

276. Adsorption of heavy metal from industrial wastewater onto low-cost Malaysian kaolin clay-based adsorbent / Chai J. B., Au P. I., Mubarak N. M., Khalid M., Ng W. P., Jagadish P., Walvekar R., Abdullah E. C. // Environ Sci Pollut Res Int. – 2020. – V. 27, № 12. – P. 13949-13962. https://doi.org/10.1007/s11356-020-07755-y

277. Preparation of ion-imprinted montmorillonite nanosheets/chitosan gel beads for selective recovery of Cu(II) from wastewater / Qin L., Zhao Y., Wang L., Zhang L., Kang S., Wang W., Zhang T., Song S. // Chemosphere. – 2020. – V. 252, №. – P. 126560. https://doi.org/10.1016/j.chemosphere.2020.126560

278. Coumarin-anchored halloysite nanotubes for highly selective detection and removal of Zn(II) / Su Z., Zhang H., Gao Y., Huo L., Wu Y., Ba X. // Chemical Engineering Journal. – 2020. – V. 393, №. – P. 124695. https://doi.org/10.1016/j.cej.2020.124695

279. Cellulose and chitosan derivatives for enhanced sorption of erbium(III) / Abd El-Magied M. O., Galhoum A. A., Atia A. A., Tolba A. A., Maize M. S., Vincent T., Guibal E. // Colloids and Surfaces A: Physicochemical and Engineering Aspects. – 2017. – V. 529, №. – P. 580-593. https://doi.org/10.1016/j.colsurfa.2017.05.031

280. Kinetic and thermodynamic aspects of adsorption of arsenic onto granular ferric hydroxide (GFH) / Banerjee K., Amy G. L., Prevost M., Nour S., Jekel M., Gallagher P. M., Blumenschein C. D. // Water Research. – 2008. – V. 42, № 13. – P. 3371-3378. https://doi.org/10.1016/j.watres.2008.04.019

281. Abu El-Soad A. M. Synthesis and characterization of modified sulfonated chitosan for beryllium recovery / Abu El-Soad A. M., Abd El-Magied M. O., Atrees M. S., Kovaleva E. G., Lazzara G. // International Journal of Biological Macromolecules. – 2019. – V. 139, №. – P. 153-160. https://doi.org/10.1016/j.ijbiomac.2019.07.162

282. Aharoni C. Kinetics of activated chemisorption. Part 2.—Theoretical models / Aharoni C., Ungarish M. // Journal of the Chemical Society, Faraday Transactions 1: Physical Chemistry in Condensed Phases. – 1977. – V. 73, № 0. – P. 456-464. https://doi.org/10.1039/F19777300456

283. Reddad Z. Comparison of the fixation of several metal ions onto a low-cost biopolymer / Reddad Z., Gérente C., Andrès Y., Le Cloirec P. // Water Science and Technology: Water Supply. – 2002. – V. 2, № 5-6. – P. 217-224. https://doi.org/10.2166/ws.2002.0172

284. Reddad Z. Adsorption of Several Metal Ions onto a Low-Cost Biosorbent: Kinetic and Equilibrium Studies / Reddad Z., Gerente C., Andres Y., Le Cloirec P. // Environmental Science & Technology. – 2002. – V. 36, № 9. – P. 2067-2073. https://doi.org/10.1021/es0102989

285. Ni(II) and Cu(II) binding properties of native and modified sugar beet pulp / Reddad Z., Gérente C., Andrès Y., Ralet M.-C., Thibault J.-F., Cloirec P. L. // Carbohydrate Polymers. – 2002. – V. 49, № 1. – P. 23-31. https://doi.org/10.1016/S0144-8617(01)00301-0

286. Krishnani K. K. Biosorption mechanism of nine different heavy metals onto biomatrix from rice husk / Krishnani K. K., Meng X., Christodoulatos C., Boddu V. M. // Journal of Hazardous Materials. – 2008. – V. 153, № 3. – P. 1222-1234. https://doi.org/10.1016/j.jhazmat.2007.09.113

287. Competitive fixed-bed adsorption of Pb (II), Cu (II), and Ni (II) from aqueous solution using chitosan-coated bentonite / Tsai W.-C., de Luna M. D. G., Bermillo-Arriesgado H. L. P., Futalan C. M., Colades J. I., Wan M.-W. // International Journal of Polymer Science. – 2016. – V. 2016, №. –.

288. Bagasse Cellulose Grafted with an Amino-Terminated Hyperbranched Polymer for the Removal of Cr(VI) from Aqueous Solution / Xia L., Huang Z., Zhong L., Xie F., Tang C. Y., Tsui C. P. // Polymers. – 2018. – V. 10, № 8. – P. 931.

289. Igberase E. The adsorption of copper (II) ions by polyaniline graft chitosan beads from aqueous solution: Equilibrium, kinetic and desorption studies / Igberase E., Osifo P., Ofomaja A. // Journal of Environmental Chemical Engineering. – 2014. – V. 2, № 1. – P. 362-369. https://doi.org/10.1016/j.jece.2014.01.008

290. Adsorption of Cu(II), Zn(II), and Pb(II) from aqueous single and binary metal solutions by regenerated cellulose and sodium alginate chemically modified with polyethyleneimine / Zhan W., Xu C., Qian G., Huang G., Tang X., Lin B. // RSC Advances. – 2018. – V. 8, № 33. – P. 18723-18733. https://doi.org/10.1039/C8RA02055H

291. Norton L. Biosorption of zinc from aqueous solutions using biosolids / Norton L., Baskaran K., McKenzie T. // Advances in Environmental Research. – 2004. – V. 8, № 3. – P. 629-635. https://doi.org/10.1016/S1093-0191(03)00035-2

292. Hubicki Z. The effect of the presence of metatartaric acid on removal effectiveness of heavy metal ions on chelating ion exchangers / Hubicki Z., Gęca M., Kołodyńska D. // Environmental Technology. – 2011. – V. 32, № 8. – P. 805-816. https://doi.org/10.1080/09593330.2010.514291

293. Morcali M. H. Adsorption of copper and zinc from sulfate media on a commercial sorbent / Morcali M. H., Zeytuncu B., Baysal A., Akman S., Yucel O. // Journal of Environmental Chemical Engineering. – 2014. – V. 2, № 3. – P. 1655-1662. https://doi.org/10.1016/j.jece.2014.07.013